Nuclear Science

ISBN 978-92-64-99137-8
NEA/NSC/DOC(2010)11

NEA Nuclear Science Committee
NEA Committee on the Safety of Nuclear Installations
US Nuclear Regulatory Commission

Boiling Water Reactor Turbine Trip (TT) Benchmark

Volume IV: Summary Results of Exercise 3

Bedirhan Akdeniz, Kostadin N. Ivanov
Pennsylvania State University

Andy M. Olson
Exelon Nuclear

© OECD 2010
NEA No. 6050

NUCLEAR ENERGY AGENCY
Organisation for Economic Co-operation and Development

ORGANISATION FOR ECONOMIC CO-OPERATION AND DEVELOPMENT

The OECD is a unique forum where the governments of 33 democracies work together to address the economic, social and environmental challenges of globalisation. The OECD is also at the forefront of efforts to understand and to help governments respond to new developments and concerns, such as corporate governance, the information economy and the challenges of an ageing population. The Organisation provides a setting where governments can compare policy experiences, seek answers to common problems, identify good practice and work to co-ordinate domestic and international policies.

The OECD member countries are: Australia, Austria, Belgium, Canada, Chile, the Czech Republic, Denmark, Finland, France, Germany, Greece, Hungary, Iceland, Ireland, Israel, Italy, Japan, Korea, Luxembourg, Mexico, the Netherlands, New Zealand, Norway, Poland, Portugal, the Slovak Republic, Slovenia, Spain, Sweden, Switzerland, Turkey, the United Kingdom and the United States. The European Commission takes part in the work of the OECD.

OECD Publishing disseminates widely the results of the Organisation's statistics gathering and research on economic, social and environmental issues, as well as the conventions, guidelines and standards agreed by its members.

This work is published on the responsibility of the Secretary-General of the OECD. The opinions expressed and arguments employed herein do not necessarily reflect the official views of the Organisation or of the governments of its member countries.

NUCLEAR ENERGY AGENCY

The OECD Nuclear Energy Agency (NEA) was established on 1st February 1958 under the name of the OEEC European Nuclear Energy Agency. It received its present designation on 20th April 1972, when Japan became its first non-European full member. NEA membership today consists of 28 OECD member countries: Australia, Austria, Belgium, Canada, the Czech Republic, Denmark, Finland, France, Germany, Greece, Hungary, Iceland, Ireland, Italy, Japan, Korea, Luxembourg, Mexico, the Netherlands, Norway, Portugal, the Slovak Republic, Spain, Sweden, Switzerland, Turkey, the United Kingdom and the United States. The European Commission also takes part in the work of the Agency.

The mission of the NEA is:

- to assist its member countries in maintaining and further developing, through international co-operation, the scientific, technological and legal bases required for a safe, environmentally friendly and economical use of nuclear energy for peaceful purposes, as well as
- to provide authoritative assessments and to forge common understandings on key issues, as input to government decisions on nuclear energy policy and to broader OECD policy analyses in areas such as energy and sustainable development.

Specific areas of competence of the NEA include safety and regulation of nuclear activities, radioactive waste management, radiological protection, nuclear science, economic and technical analyses of the nuclear fuel cycle, nuclear law and liability, and public information.

The NEA Data Bank provides nuclear data and computer program services for participating countries. In these and related tasks, the NEA works in close collaboration with the International Atomic Energy Agency in Vienna, with which it has a Co-operation Agreement, as well as with other international organisations in the nuclear field.

Corrigenda to OECD publications may be found online at: *www.oecd.org/publishing/corrigenda*.
© OECD 2010

You can copy, download or print OECD content for your own use, and you can include excerpts from OECD publications, databases and multimedia products in your own documents, presentations, blogs, websites and teaching materials, provided that suitable acknowledgment of OECD as source and copyright owner is given. All requests for public or commercial use and translation rights should be submitted to *rights@oecd.org*. Requests for permission to photocopy portions of this material for public or commercial use shall be addressed directly to the Copyright Clearance Center (CCC) at *info@copyright.com* or the Centre français d'exploitation du droit de copie (CFC) *contact@cfcopies.com*.

Cover photos: Exelon Corporation.

Foreword

The OECD Nuclear Energy Agency (NEA) completed under US Nuclear Regulatory Commission (NRC) sponsorship a PWR main steam line break (MSLB) benchmark against coupled system three-dimensional (3-D) neutron kinetics and thermal-hydraulic codes. Another NEA/NRC coupled-code benchmark was completed for a BWR turbine trip (TT) transient and is the object of the present report. Turbine trip transients in a BWR are pressurisation events in which the coupling between core space-dependent neutronics phenomena and system dynamics plays an important role. The data made available from actual experiments carried out at the Peach Bottom 2 reactor make the present benchmark particularly valuable. While defining and co-ordinating the BWR TT benchmark, a systematic approach and multi-level methodology was developed, which not only allowed for a consistent and comprehensive validation process, but also contributed to the study of key parameters of pressurisation transients. The benchmark consists of three separate exercises, two steady states and five transient scenarios.

The benchmark team – Pennsylvania State University (PSU) in co-operation with Exelon Nuclear and the OECD/NEA – was responsible for co-ordinating benchmark activities, answering participants' questions and assisting participants in developing their models, as well as analysing submitted solutions and providing reports summarising the results for each phase. The benchmark team was also involved in the technical aspects of the benchmark, including sensitivity studies for the different exercises. In performing these tasks, the PSU team has been collaborating with Andy M. Olson and Kenneth W. Hunt of Exelon Nuclear. Lance J. Agee, of the Electric Power Research Institute (EPRI), also provided technical assistance for this international benchmark project.

The BWR TT benchmark is being published in four volumes as OECD/NEA reports. A CD-ROM will also be prepared and will include the four reports and the transient boundary conditions, decay heat values as a function of time, cross-section libraries and supplementary tables and graphs not published in the paper version.

BWR TT Benchmark – Volume I: Final Specifications was issued in 2001 [NEA/NSC/DOC(2001)1]. The definitions of the benchmark exercises and technical specifications including thermal-hydraulics, core and neutronics data were provided in this volume.

BWR TT Benchmark – Volume II: Summary Results of Exercise 1 was published in 2004 [NEA/NSC/DOC(2004)21]. It summarised the results for Exercise 1 of the benchmark and identified the key parameters and important issues concerning the thermal-hydraulic system modelling of the TT transient with specified core average axial power distribution and fission power (or reactivity) time transient history. Exercise 1 helped the participants initialise and test their system code models for use in Exercise 2 and Exercise 3 on coupled 3-D kinetics/system thermal-hydraulics simulations.

BWR TT Benchmark – Volume III: Summary Results of Exercise 2 was published in 2006 [NEA/NSC/DOC(2006)23]. Volume III summarised the results for Exercise 2 of the benchmark and identified key parameters and important issues concerning the coupled neutronics/thermal-hydraulic core modelling with provided core inlet and outlet boundary conditions. Exercise 2 helped the participants initialise and test their core models for further use in Exercise 3 on coupled 3-D kinetics/system thermal-hydraulics simulations.

The final volume of the BWR TT benchmark, Volume IV, summarises the results for Exercise 3 of the benchmark and identifies the key parameters and important issues of this exercise which comprises the best-estimate coupled neutronics/thermal-hydraulic system modelling and four different extreme scenarios. Exercise 3 helped the participants to verify the capabilities of the coupled codes to analyse complex transients with coupled core-plant interactions.

Acknowledgements

The authors would like to thank Professor J. Aragonés from the Polytechnic University of Madrid (UPM), Professor F. D'Auria from the University of Pisa, Dr. S. Langenbuch from the Gesellschaft für Anlagen- und Reaktorsicherheit (GRS) and Dr. F. Eltawila of US Nuclear Regulatory Commission (NRC), whose support and encouragement in establishing this benchmark have been invaluable.

This report is the sum of many efforts made by the participants, the funding agencies and their staff, and notably the US Nuclear Regulatory Commission and the OECD Nuclear Energy Agency (NEA). Special appreciation is due to: E. Royer, Commissariat à l'énergie atomique (CEA-Saclay); Professor T. Downar, Purdue University; R. Velten, AREVA NP GmbH; Dr. B. Aktas, Information Systems Laboratories (ISL Inc.); Dr. G. Gose and Dr. C. Peterson, Computer Simulation and Analysis (CSA); Dr. A. Hotta, TEPCO System Corporation; Dr. P. Coddington, Paul Scherrer Institute (PSI); and Dr. U. Grundmann, Forschungszentrum Dresden-Rossendorf (FZD). Their technical assistance, comments and suggestions have been very valuable. We would like to thank them for the effort and time involved.

Of particular note are the efforts of Dr. F. Eltawila assisted by Drs. J. Han, J. Uhle and T. Ulses of the US Nuclear Regulatory Commission. Through their efforts, funding was secured for this project. We also thank them for their outstanding technical advice and assistance.

The authors wish to express their sincere appreciation for the outstanding support offered by Dr. E. Sartori, who provided efficient administration, organisation and valuable technical advice.

The authors wish to particularly thank all the OECD/NEA BWR Turbine Trip Benchmark participants for their valuable support, comments and feedback during this study.

Finally, the authors are grateful to Amanda Costa for having devoted her competence and skills to the editing of this report.

Table of contents

Foreword ... 3
List of figures ... 7
List of tables ... 11
List of abbreviations ... 13
Chapter 1 Introduction ... 15
Chapter 2 Description of Exercise 3 ... 19
2.1 General ... 19
2.2 Core and neutronics data ... 21
2.3 Thermal-hydraulic data ... 46
2.4 Initial steady-state conditions ... 47
2.5 Transient calculations ... 49
Chapter 3 Methodologies to quantify the accuracy of the calculations ... 51
3.1 Standard techniques for the comparison of results ... 51
3.1.1 Integral parameter values ... 51
3.1.2 One-dimensional (1-D) steady-state axial distributions ... 53
3.1.3 Two-dimensional (2-D) steady-state radial distributions ... 53
3.2 Time histories ... 54
3.2.1 ACAP analysis ... 54
3.3 Statistical analysis of normalised parameters from transient calculations ... 56
3.3.1 Two-dimensional (2-D) core-averaged radial power distribution ... 57
3.3.2 One-dimensional (1-D) core-averaged axial power distribution ... 58
3.3.3 One-dimensional (1-D) relative axial power distribution for FA 75 and 367 ... 59
3.4 Multiple code dependencies ... 59
Chapter 4 Results and discussion ... 61
4.1 Steady-state results ... 62
4.2 Transient results of best-estimate case ... 72
4.2.1 Time histories (best-estimate case) ... 73
4.2.2 Snapshot at the time of maximum power (best-estimate case) ... 100
4.2.3 Snapshot at the end of the transient (best-estimate case) ... 111
4.3 Transient results of Extreme Scenario 1 ... 120
4.4 Transient results of Extreme Scenario 2 ... 142
4.5 Transient results of Extreme Scenario 3 ... 164
4.6 Transient results of Extreme Scenario 4 ... 185

Chapter 5 Conclusions 205

References 209

Appendix A Description of the computer codes used for analysis in Exercise 3 of the NEA-NRC BWR TT benchmark 211

CATHARE/CRONOS2/FLICA4 (CEA, France) 211

S-RELAP5/RAMONA5-2.1 (FANP, Germany) 212

DYN3D/ATHLET (FZD, Germany) 214

QUABOX/CUBBOX-ATHLET (GRS, Germany) 218

TRAC-BF1/COS3D (NFI, Japan) 219

TRAC-BF1/SKETCH-INS (NUPEC, Japan) 220

RETRAN-3D and CORETRAN (PSI, Switzerland) 221

TRAC-M/PARCS (PSU/PURDUE/NRC, United States) 222

TRAC-BF1/ENTRÉE (TEPSYS, Japan) 224

RELAP5/PARCS (UPISA, Italy) 225

POLCA-T (Westinghouse, Sweden) 226

Appendix B Questionnaire for Exercise 3 of the NEA-NRC BWR TT benchmark 229

CATHARE/CRONOS2/FLICA4 (CEA, France) 231

S-RELAP5/RAMONA5-2.1 (FANP, Germany) 234

DYN3D/ATHLET (FZD, Germany) 238

QUABOX/CUBBOX-ATHLET (GRS, Germany) 242

TRAC-BF1/SKETCH-INS (NUPEC, Japan) 246

RETRAN-3D (PSI, Switzerland) 250

TRAC-M/PARCS (PSU/PURDUE/NRC, United States) 259

TRAC-BF1/ENTRÉE (TEPSYS, Japan) 265

RELAP5/PARCS (UPISA, Italy) 268

POLCA-T (Westinghouse, Sweden) 272

Available on CD-ROM upon request

Appendix C Reference results

Appendix D1 Participant deviations integral parameters

Appendix D2 Participant deviations axial parameters

Appendix D3 Participant deviations 2-D radial parameters

Appendix D4 Participant deviations time histories

List of figures

2-1 Key elements of Exercise 3 best-estimate case and extreme scenarios 20
2-2 Reactor core cross-sectional view 37
2-3 PB2 initial fuel assembly lattice 38
2-4 PB2 reload fuel assembly lattice for 100 mil channels 39
2-5 PB2 reload fuel assembly lattice for 120 mil channels 40
2-6 PB2 reload fuel assembly lattice for LTA assemblies 41
2-7 PSU control rod grouping 42
2-8 Radial distribution of assembly types 42
2-9 Fuel assembly orientation for ADF assignment 43
2-10 Core orificing and TIP system arrangement 44
2-11 Elevation of core components 45
2-12 Reactor core thermal-hydraulic channel radial map 46
2-13 PB2 HZP control rod pattern 47
2-14 PB2 HP control rod pattern 48
2-15 PB2 TT2 initial core axial relative power from P1 edit 49
3-1 FOM configuration in ACAP 55
4-1 Steady-state k_{eff} 64
4-2 Steady-state core average axial void fraction distribution (Group 1) 65
4-3 Steady-state core average axial void fraction distribution (Group 2) 65
4-4 Steady-state core average axial void fraction (mean and standard deviation) 66
4-5 Steady-state core average normalised axial power distribution (Group 1) 66
4-6 Steady-state core average normalised axial power distribution (Group 2) 67
4-7 Steady-state core average normalised axial power distribution (measured vs. mean and standard deviations) 67
4-8 Steady-state axial power distribution for FA 75 (Group 1) 68
4-9 Steady-state axial power distribution for FA 75 (Group 2) 68
4-10 Steady-state axial power distribution for FA 75 (mean and standard deviation) 69
4-11 Steady-state axial power distribution for FA 367 (Group 1) 69
4-12 Steady-state axial power distribution for FA 367 (Group 2) 70
4-13 Steady-state axial power distribution for FA 367 (mean and standard deviation) 70
4-14 Steady-state radial power distribution (average of participants) 71
4-15 Standard deviation of steady-state radial power distribution 71
4-16 Best-estimate case – transient power (fission) 76
4-17 Best-estimate case – transient power (fission – zoom) 76
4-18 Best-estimate case – transient power (total) 77
4-19 Best-estimate case – transient power (total – zoom) 77
4-20 Best-estimate case – transient fission power comparison (average vs. measured) 78
4-21 Best-estimate case – transient fission power comparison (average vs. measured – zoom) 78
4-22 Best-estimate case – transient dome pressure (Group 1) 79
4-23 Best-estimate case – transient dome pressure (Group 2) 80
4-24 Best-estimate case – transient dome pressure (average vs. measured) 80
4-25 Best-estimate case – transient core exit pressure (Group 1) 81
4-26 Best-estimate case – transient core exit pressure (Group 2) 82
4-27 Best-estimate case – transient total core flow rate (Group 1) 83
4-28 Best-estimate case – transient total core flow rate (Group 2) 83
4-29 Best-estimate case – total reactivity (Group 1) 84
4-30 Best-estimate case – total reactivity (Group 1 – zoom) 85
4-31 Best-estimate case – total reactivity (Group 2) 85
4-32 Best-estimate case – total reactivity (Group 2 – zoom) 86
4-33 Best-estimate case – Doppler reactivity 87
4-34 Best-estimate case – Doppler reactivity (zoom) 87
4-35 Best-estimate case – void reactivity 88
4-36 Best-estimate case – void reactivity (zoom) 89
4-37 Best-estimate case – maximum cladding temperature 90
4-38 Best-estimate case – maximum cladding temperature (zoom) 90
4-39 Best-estimate case – radial power peaking factors 91
4-40 Best-estimate case – LPRM-A 92

4-41 Best-estimate case – LPRM-A (zoom) 92
4-42 Best-estimate case – LPRM-A (average vs. measured) 93
4-43 Best-estimate case – LPRM-B 94
4-44 Best-estimate case – LPRM-B (zoom) 94
4-45 Best-estimate case – LPRM-B (average vs. measured) 95
4-46 Best-estimate case – LPRM-C 96
4-47 Best-estimate case – LPRM-C (zoom) 96
4-48 Best-estimate case – LPRM-C (average vs. measured) 97
4-49 Best-estimate case – LPRM-D 98
4-50 Best-estimate case – LPRM-D (zoom) 98
4-51 Best-estimate case – LPRM-D (average vs. measured) 99
4-52 Best-estimate case – time of maximum power 101
4-53 Best-estimate case – time of maximum power 101
4-54 Core axial power profile at maximum power (participants submitted fission power) 103
4-55 Core axial power profile at maximum power (participants submitted total power) 103
4-56 Core axial power profile at maximum power (participants submitted fission power) – mean and deviation 104
4-57 Core axial power profile at maximum power (participants submitted total power) – mean and deviation 104
4-58 Relative power of FA 75 at maximum power (participants submitted fission power) 105
4-59 Relative power of FA 75 at maximum power (participants submitted total power) 105
4-60 Relative power of FA 75 at maximum power (participants submitted fission power) – mean and deviation 106
4-61 Relative power of FA 75 at maximum power (participants submitted total power) – mean and deviation 106
4-62 Relative power of FA 367 at maximum power (participants submitted fission power) 107
4-63 Relative power of FA 367 at maximum power (participants submitted total power) 107
4-64 Relative power of FA 367 at maximum power (participants submitted fission power) – mean and deviation 108
4-65 Relative power of FA 367 at maximum power (participants submitted total power) – mean and deviation 108
4-66 Mean radial power distribution at maximum power (participants submitted fission power) 109
4-67 Mean radial power distribution at maximum power (participants submitted total power) 109
4-68 Standard deviation of radial power distribution at maximum power (participants submitted fission power) 110
4-69 Standard deviation of radial power distribution at maximum power (participants submitted total power) 110
4-70 Core axial power profile at the end of the transient (participants submitted fission power) 112
4-71 Core axial power profile at the end of the transient (participants submitted total power) 112
4-72 Core axial power profile at the end of the transient (participants submitted fission power) – mean and deviation 113
4-73 Core axial power profile at the end of the transient (participants submitted total power) – mean and deviation 113
4-74 Relative power of FA 75 at the end of the transient (participants submitted fission power) 114
4-75 Relative power of FA 75 at the end of the transient (participants submitted total power) 114
4-76 Relative power of FA 75 at the end of the transient (participants submitted fission power) – mean and deviation 115
4-77 Relative power of FA 75 at the end of the transient (participants submitted total power) – mean and deviation 115
4-78 Relative power of FA 367 at the end of the transient (participants submitted fission power) 116
4-79 Relative power of FA 367 at the end of the transient (participants submitted total power) 116

4-80 Relative power of FA 367 at the end of the transient (participants submitted fission power) – mean and deviation 117
4-81 Relative power of FA 367 at the end of the transient (participants submitted total power) – mean and deviation 117
4-82 Mean radial power distribution at the end of the transient (participants submitted fission power) 118
4-83 Mean radial power distribution at the end of the transient (participants submitted total power) 118
4-84 Standard deviation of radial power distribution at the end of the transient (participants submitted fission power) 119
4-85 Standard deviation of radial power distribution at the end of the transient (participants submitted total power) 119
4-86 Extreme Scenario 1 – transient power (fission) 123
4-87 Extreme Scenario 1 – transient power (fission – zoom) 123
4-88 Extreme Scenario 1 – transient power (total) 124
4-89 Extreme Scenario 1 – transient power (total – zoom) 124
4-90 Extreme Scenario 1 – transient dome pressure (Group 1) 125
4-91 Extreme Scenario 1 – transient dome pressure (Group 2) 126
4-92 Extreme Scenario 1 – transient core exit pressure (Group 1) 127
4-93 Extreme Scenario 1 – transient core exit pressure (Group 2) 127
4-94 Extreme Scenario 1 – transient S/RV pressure (Group 1) 128
4-95 Extreme Scenario 1 – transient S/RV pressure (Group 2) 129
4-96 Extreme Scenario 1 – total reactivity (Group 1) 130
4-97 Extreme Scenario 1 – total reactivity (Group 1 – zoom) 130
4-98 Extreme Scenario 1 – total reactivity (Group 2) 131
4-99 Extreme Scenario 1 – total reactivity (Group 2 – zoom) 131
4-100 Extreme Scenario 1 – Doppler reactivity 132
4-101 Extreme Scenario 1 – Doppler reactivity (zoom) 133
4-102 Extreme Scenario 1 – void reactivity 134
4-103 Extreme Scenario 1 – void reactivity (zoom) 134
4-104 Extreme Scenario 1 – LPRM-A 135
4-105 Extreme Scenario 1 – LPRM-A (zoom) 136
4-106 Extreme Scenario 1 – LPRM-B 137
4-107 Extreme Scenario 1 – LPRM-B (zoom) 137
4-108 Extreme Scenario 1 – LPRM-C 138
4-109 Extreme Scenario 1 – LPRM-C (zoom) 139
4-110 Extreme Scenario 1 – LPRM-D 140
4-111 Extreme Scenario 1 – LPRM-D (zoom) 140
4-112 Extreme Scenario 2 – transient power (fission) 145
4-113 Extreme Scenario 2 – transient power (fission – zoom) 145
4-114 Extreme Scenario 2 – transient power (total) 146
4-115 Extreme Scenario 2 – transient power (total – zoom) 146
4-116 Extreme Scenario 2 – transient dome pressure (Group 1) 147
4-117 Extreme Scenario 2 – transient dome pressure (Group 2) 148
4-118 Extreme Scenario 2 – transient core exit pressure (Group 1) 149
4-119 Extreme Scenario 2 – transient core exit pressure (Group 2) 149
4-120 Extreme Scenario 2 – transient S/RV pressure (Group 1) 150
4-121 Extreme Scenario 2 – transient S/RV pressure (Group 2) 151
4-122 Extreme Scenario 2 – total reactivity (Group 1) 152
4-123 Extreme Scenario 2 – total reactivity (Group 1 – zoom) 152
4-124 Extreme Scenario 2 – total reactivity (Group 2) 153
4-125 Extreme Scenario 2 – total reactivity (Group 2 – zoom) 153
4-126 Extreme Scenario 2 – Doppler reactivity 154
4-127 Extreme Scenario 2 – Doppler reactivity (zoom) 155
4-128 Extreme Scenario 2 – void reactivity 156
4-129 Extreme Scenario 2 – void reactivity (zoom) 156
4-130 Extreme Scenario 2 – LPRM-A 157
4-131 Extreme Scenario 2 – LPRM-A (zoom) 158
4-132 Extreme Scenario 2 – LPRM-B 159

4-133 Extreme Scenario 2 – LPRM-B (zoom) 159
4-134 Extreme Scenario 2 – LPRM-C 160
4-135 Extreme Scenario 2 – LPRM-C (zoom) 161
4-136 Extreme Scenario 2 – LPRM-D 162
4-137 Extreme Scenario 2 – LPRM-D (zoom) 162
4-138 Extreme Scenario 3 – transient power (fission) 166
4-139 Extreme Scenario 3 – transient power (fission – zoom) 167
4-140 Extreme Scenario 3 – transient power (total) 167
4-141 Extreme Scenario 3 – transient power (total – zoom) 168
4-142 Extreme Scenario 3 – transient dome pressure (Group 1) 169
4-143 Extreme Scenario 3 – transient dome pressure (Group 2) 169
4-144 Extreme Scenario 3 – transient core exit pressure (Group 1) 170
4-145 Extreme Scenario 3 – transient core exit pressure (Group 2) 171
4-146 Extreme Scenario 3 – transient S/RV pressure (Group 1) 172
4-147 Extreme Scenario 3 – transient S/RV pressure (Group 2) 172
4-148 Extreme Scenario 3 – total reactivity (Group 1) 173
4-149 Extreme Scenario 3 – total reactivity (Group 1 – zoom) 174
4-150 Extreme Scenario 3 – total reactivity (Group 2) 174
4-151 Extreme Scenario 3 – total reactivity (Group 2 – zoom) 175
4-152 Extreme Scenario 3 – Doppler reactivity 176
4-153 Extreme Scenario 3 – Doppler reactivity (zoom) 176
4-154 Extreme Scenario 3 – void reactivity 177
4-155 Extreme Scenario 3 – void reactivity (zoom) 178
4-156 Extreme Scenario 3 – LPRM-A 179
4-157 Extreme Scenario 3 – LPRM-A (zoom) 179
4-158 Extreme Scenario 3 – LPRM-B 180
4-159 Extreme Scenario 3 – LPRM-B (zoom) 181
4-160 Extreme Scenario 3 – LPRM-C 182
4-161 Extreme Scenario 3 – LPRM-C (zoom) 182
4-162 Extreme Scenario 3 – LPRM-D 183
4-163 Extreme Scenario 3 – LPRM-D (zoom) 184
4-164 Extreme Scenario 4 – transient power (fission) 188
4-165 Extreme Scenario 4 – transient power (fission – zoom) 188
4-166 Extreme Scenario 4 – transient power (total) 189
4-167 Extreme Scenario 4 – transient power (total – zoom) 189
4-168 Extreme Scenario 4 – transient dome pressure (Group 1) 190
4-169 Extreme Scenario 4 – transient dome pressure (Group 2) 191
4-170 Extreme Scenario 4 – transient core exit pressure (Group 1) 192
4-171 Extreme Scenario 4 – transient core exit pressure (Group 2) 192
4-172 Extreme Scenario 4 – total reactivity (Group 1) 193
4-173 Extreme Scenario 4 – total reactivity (Group 1 – zoom) 194
4-174 Extreme Scenario 4 – total reactivity (Group 2) 194
4-175 Extreme Scenario 4 – total reactivity (Group 2 – zoom) 195
4-176 Extreme Scenario 4 – Doppler reactivity 196
4-177 Extreme Scenario 4 – Doppler reactivity (zoom) 196
4-178 Extreme Scenario 4 – void reactivity 197
4-179 Extreme Scenario 4 – void reactivity (zoom) 198
4-180 Extreme Scenario 4 – LPRM-A 199
4-181 Extreme Scenario 4 – LPRM-A (zoom) 199
4-182 Extreme Scenario 4 – LPRM-B 200
4-183 Extreme Scenario 4 – LPRM-B (zoom) 201
4-184 Extreme Scenario 4 – LPRM-C 202
4-185 Extreme Scenario 4 – LPRM-C (zoom) 202
4-186 Extreme Scenario 4 – LPRM-D 203
4-187 Extreme Scenario 4 – LPRM-D (zoom) 204

List of tables

1-1 List of participants in Exercise 3 – best-estimate case 16
1-2 List of participants in Exercise 3 – extreme scenarios 17
2-1 PB2 fuel assembly data 23
2-2 Assembly design 1 23
2-3 Assembly design 2 23
2-4 Assembly design 3 24
2-5 Assembly design 4 24
2-6 Assembly design 5 24
2-7 Assembly design 6 25
2-8 Decay constant and fractions of delayed neutrons 25
2-9 Heavy element decay heat constants 25
2-10 Assembly design for Type 1 initial fuel 26
2-11 Assembly design for Type 2 initial fuel 27
2-12 Assembly design for Type 3 initial fuel 28
2-13 Assembly design for Type 4, 8×8 UO_2 reload 29
2-14 Assembly design for Type 5, 8×8 UO_2 reload 30
2-15 Assembly design for Type 6, 8×8 UO_2 reload, LTA 31
2-16 Control rod data (movable control rods) 32
2-17 Definition of assembly types 32
2-18 Composition numbers in axial layer for each assembly type 33
2-19 Range of variables 34
2-20 Key to macroscopic cross-section tables 35
2-21 Macroscopic cross-section tables' structure 35
2-22 PB2 HZP initial conditions 47
2-23 PB2 TT2 initial conditions from process computer P1 edit 48
2-24 PB2 TT2 initial core axial relative power from P1 edit 49
2-25 PB2 TT2 event timing (time in ms) 50
2-26 PB2 TT2 scram characteristics 50
2-27 CRD position after scram vs. time 50
2-28 Nuclear system safety and relief valves 50
3-1 Exercise 3 parameters for statistical comparisons in steady-state analysis 52
3-2 Parameters for statistical comparisons in Exercise 3 transient analysis – best-estimate case 52
3-3 Parameters for statistical comparisons in Exercise 3 transient analysis – Extreme Scenarios 1, 2, 3 and 4 53
4-1 Number of channels used and power submitted by the participants – best-estimate case 63
4-2 Models used at initial HP steady state 63
4-3 Steady-state k_{eff} 64
4-4 Sequence of events in best-estimate case 73
4-5 Models used in transient – best-estimate case 74
4-6 Best-estimate case – transient power, figure of merit 79
4-7 Best-estimate case – transient dome pressure, figure of merit 81
4-8 Best-estimate case – transient core exit pressure, figure of merit 82
4-9 Best-estimate case – transient total core flow rate, figure of merit 84
4-10 Best-estimate case – total reactivity, figure of merit 86
4-11 Best-estimate case – Doppler reactivity, figure of merit 88
4-12 Best-estimate case – void reactivity, figure of merit 89
4-13 Best-estimate case – maximum cladding initial (time = 0 s) temperature 91
4-14 Best-estimate case – maximum cladding temperature, figure of merit 91
4-15 Best-estimate case – normalised LPRM-A power, figure of merit 93
4-16 Best-estimate case – normalised LPRM-B power, figure of merit 95
4-17 Best-estimate case – normalised LPRM-C power, figure of merit 97
4-18 Best-estimate case – normalised LPRM-D power, figure of merit 99
4-19 Best-estimate case – time of maximum transient power and deviation 102
4-20 Best-estimate case – maximum transient power and deviation 102
4-21 Best-estimate case – power at the end of the transient (5 s) and deviation 111

4-22 Number of channels used and power submitted by the participants – Extreme Scenario 1 120
4-23 Models used in Extreme Scenario 1 121
4-24 Sequence of events in Extreme Scenario 1 122
4-25 Extreme Scenario 1 – transient power, figure of merit 125
4-26 Extreme Scenario 1 – transient dome pressure, figure of merit 126
4-27 Extreme Scenario 1 – transient core exit pressure, figure of merit 128
4-28 Extreme Scenario 1 – transient S/RV pressure, figure of merit 129
4-29 Extreme Scenario 1 – total reactivity, figure of merit 132
4-30 Extreme Scenario 1 – Doppler reactivity, figure of merit 133
4-31 Extreme Scenario 1 – void reactivity, figure of merit 135
4-32 Extreme Scenario 1 – normalised LPRM-A power, figure of merit 136
4-33 Extreme Scenario 1 – normalised LPRM-B power, figure of merit 138
4-34 Extreme Scenario 1 – normalised LPRM-C power, figure of merit 139
4-35 Extreme Scenario 1 – normalised LPRM-D power, figure of merit 141
4-36 Number of channels used and power submitted by the participants – Extreme Scenario 2 142
4-37 Models used in Extreme Scenario 2 143
4-38 Sequence of events in Extreme Scenario 2 144
4-39 Extreme Scenario 2 – transient power, figure of merit 147
4-40 Extreme Scenario 2 – transient dome pressure, figure of merit 148
4-41 Extreme Scenario 2 – transient core exit pressure, figure of merit 150
4-42 Extreme Scenario 2 – transient S/RV pressure, figure of merit 151
4-43 Extreme Scenario 2 – total reactivity, figure of merit 154
4-44 Extreme Scenario 2 – Doppler reactivity, figure of merit 155
4-45 Extreme Scenario 2 – void reactivity, figure of merit 157
4-46 Extreme Scenario 2 – normalised LPRM-A power, figure of merit 158
4-47 Extreme Scenario 2 – normalised LPRM-B power, figure of merit 160
4-48 Extreme Scenario 2 – normalised LPRM-C power, figure of merit 161
4-49 Extreme Scenario 2 – normalised LPRM-D power, figure of merit 163
4-50 Number of channels used and power submitted by the participants – Extreme Scenario 3 164
4-51 Models used in Extreme Scenario 3 165
4-52 Sequence of events in Extreme Scenario 3 166
4-53 Extreme Scenario 3 – transient power, figure of merit 168
4-54 Extreme Scenario 3 – transient dome pressure, figure of merit 170
4-55 Extreme Scenario 3 – transient core exit pressure, figure of merit 171
4-56 Extreme Scenario 3 – transient S/RV pressure, figure of merit 173
4-57 Extreme Scenario 3 – total reactivity, figure of merit 175
4-58 Extreme Scenario 3 – Doppler reactivity, figure of merit 177
4-59 Extreme Scenario 3 – void reactivity, figure of merit 178
4-60 Extreme Scenario 3 – normalised LPRM-A power, figure of merit 180
4-61 Extreme Scenario 3 – normalised LPRM-B power, figure of merit 181
4-62 Extreme Scenario 3 – normalised LPRM-C power, figure of merit 183
4-63 Extreme Scenario 3 – normalised LPRM-D power, figure of merit 184
4-64 Number of channels used and power submitted by the participants – Extreme Scenario 4 185
4-65 Models used in Extreme Scenario 4 186
4-66 Sequence of events in Extreme Scenario 4 187
4-67 Extreme Scenario 4 – transient power, figure of merit 190
4-68 Extreme Scenario 4 – transient dome pressure, figure of merit 191
4-69 Extreme Scenario 4 – transient core exit pressure, figure of merit 193
4-70 Extreme Scenario 4 – total reactivity, figure of merit 195
4-71 Extreme Scenario 4 – Doppler reactivity, figure of merit 197
4-72 Extreme Scenario 4 – void reactivity, figure of merit 198
4-73 Extreme Scenario 4 – normalised LPRM-A power, figure of merit 200
4-74 Extreme Scenario 4 – normalised LPRM-B power, figure of merit 201
4-75 Extreme Scenario 4 – normalised LPRM-C power, figure of merit 203
4-76 Extreme Scenario 4 – normalised LPRM-D power, figure of merit 204

List of abbreviations

1-D	One-dimensional
2-D	Two-dimensional
3-D	Three-dimensional
ACAP	Automated Code Assessment Program
ADF	Assembly discontinuity factor
APRM	Average range power monitor
AVZ	Above vessel zero
BC	Boundary conditions
BE	British Energy
BOC	Beginning of cycle
BP	Burnable poison
BPV	Bypass valve
BVBO	Bypass valve begins opening
BVFO	Bypass valve full open
BWR	Boiling water reactor
CA	Control assembly
CEA	Commissariat à l'énergie atomique
CEA-33	CEA results with 33-channel model
CEA-764	CEA results with 764-channel model
CEPIR	Core exit pressure initial response
DPIR	Dome pressure initial response
EOC	End of cycle
EOT	End of transient
EPRI	Electric Power Research Institute
EXELON	Exelon Corporation
FA	Fuel assembly
FANP	Framatome ANP
FFT	Fast Fourier transform
FOM	Figure of merit
FZD	Forschungszentrum Dresden-Rossendorf
GE	General Electric
GRS	Gesellschaft für Anlagen- und Reaktorsicherheit mbH
HFP	Hot full power
HZP	Hot zero power
LPRM	Local power range monitor

LWR	Light water reactor
ME	Mean error
MSIV	Main steam isolation valve
MSLB	Main steam line break
MVCEP	Maximum value per cent initial value of core exit pressure
NEA	Nuclear Energy Agency
NEM	Nodal expansion method
NFI	Nuclear Fuel Industries, Ltd.
NP	Normalised power
NPP	Nuclear power plant
NRC	Nuclear Regulatory Commission
NRS	Nuclear reactor systems
NSC	Nuclear Science Committee
NSSS	Nuclear steam supply system
NUPEC	Nuclear Power Engineering Corporation
OECD	Organisation for Economic Co-operation and Development
PB	Peach Bottom Atomic Power Station
PB2	Peach Bottom Atomic Power Station Unit 2
PECo	Philadelphia Electric Company
PSI	Paul Scherrer Institute
PSU	Pennsylvania State University
PWR	Pressurised water reactor
PUR	Purdue University
S/RV	Safety/relief valve
S/RVO	First S/RV opening (refer to valve with lowest opening set-point)
S/RVC	Last S/RV closing (refer to valve with lowest closing set-point)
TEPSYS	TEPCO Systems Corporation
T-H	Thermal-hydraulic
TSV	Turbine stop valve
TSVC	Turbine stop valve closing
TT	Turbine trip
TT2	Turbine trip test 2
UPISA	University of Pisa
UPV	Universidad Politecnica de Valencia
UPV-1	UPV results from MODKIN code
UPV-2	UPV results from NOKIN-3D code
VBA	Visual basic for applications
WES	Westinghouse Electric Company

Chapter 1: Introduction

Modern nuclear reactor designs depend heavily on the simulation of the reactor core behaviour and plant dynamics as well their mutual interactions. This simulation is possible by utilising digital computer programs or so-called "codes" in which various mathematical models are included. Prediction of a nuclear power plant's behaviour under both normal and abnormal conditions has an important effect on its safety and economic operation. Incorporation of full three-dimensional (3-D) models of the reactor core into system transient codes allows for a "best-estimate" calculation of interactions between the core behaviour and plant dynamics. Recent progress in computer technology has made the development of such coupled system thermal-hydraulic and neutron kinetics code systems feasible. Considerable efforts have been made in various countries and organisations in this direction. To verify the capability of the coupled codes to analyse complex transients with coupled core-plant interactions and to fully test thermal-hydraulic coupling, appropriate light water reactor (LWR) transient benchmarks need to be developed on a higher "best-estimate" level. The previous sets of transient benchmark problems separately addressed system transients (designed mainly for thermal-hydraulic system codes with point kinetics models) and core transients (designed for thermal-hydraulic core boundary conditions models coupled with a 3-D neutron kinetics model).

The Nuclear Energy Agency (NEA) of the Organisation for Economic Co-operation and Development (OECD) has completed – under the sponsorship of the US Nuclear Regulatory Commission (NRC) – a pressurised water reactor (PWR) main steam line break (MSLB) benchmark (NEA, 1999) against coupled thermal-hydraulic and neutron kinetics codes. The success of the PWR MSLB benchmark yielded a similar benchmark based on a turbine trip (TT) scenario for a boiling water reactor (BWR) plant transient which was also established as an OECD/NRC activity (NEA, 2001). TT transients in a BWR are pressurisation events in which the coupling between core space-dependent neutronics phenomena and system dynamics plays an important role. In addition, the available real plant experimental data (Larsen, 1978; Carmichael, 1978) makes this benchmark problem very valuable. The NEA, OECD and US NRC have approved the BWR TT benchmark for the purpose of validating advanced system best-estimate analysis codes. Over the course of defining and co-ordinating the BWR TT benchmark a systematic approach has been established by the Pennsylvania State University (PSU) in order to validate best-estimate coupled codes. This approach employs a multi-level methodology that not only allows for a consistent and comprehensive validation process but also contributes to the study of key parameters of pressurisation transients. PSU has defined three exercises of BWR TT benchmark within the framework of this methodology.

Further background information on this benchmark with complete lists of participants can be found in the summaries of the five workshops held in Philadelphia, PA, USA [NEA/NSC/DOC(2000)22], Villigen, Switzerland [NEA/NSC/DOC(2001)20], Dresden, Germany [NEA/NSC/DOC(2002)11], Seoul, Republic of Korea [NEA/NSC/DOC(2002)15] and Barcelona, Spain [NEA/NSC/DOC(2003)1]. The BWR TT benchmark is sponsored by the US NRC, the OECD/NEA and the Nuclear Engineering Program (NEP) of PSU. Exelon Nuclear and EPRI, USA, assist in the analysis of the benchmark.

The BWR TT benchmark project was designed to test the coupled system thermal-hydraulic/ neutron kinetics codes for simulation of the Peach Bottom 2 (PB2 – a General Electric designed BWR/4) turbine trip transient with a sudden closure of the turbine stop valve. Three turbine trip transients at different power levels were performed at the PB2 nuclear power plant (NPP) prior to shutdown for refuelling at the end of Cycle 2 in April 1977. The second test (TT2) was selected for the benchmark problem to investigate the effect of the pressurisation transient (following the sudden closure of the turbine stop valve) on the neutron flux in the reactor core. In a best-estimate manner the test conditions approached the design basis conditions as closely as possible. The actual data were collected, including a compilation of reactor design and operating data for Cycles 1 and 2 of PB2 and the plant transient experimental data. The transient selected for this benchmark is a dynamically

complex event and it constitutes a good problem to test the coupled codes on both levels: neutronics/thermal-hydraulics coupling, and core/plant system coupling. In the TT2 test, the thermal-hydraulic feedback alone limited the power peak and initiated the power reduction. The void feedback plays the major role while the Doppler feedback plays a subordinate role. The reactor scram then inserted additional negative reactivity and completed the power reduction and eventual core shutdown.

The purposes of this benchmark are met through the application of the three exercises, which are described in *BWR TT Benchmark – Volume I: Final Specifications* (NEA, 2001). In addition to the definitions of the benchmark exercises, technical specifications including thermal-hydraulics, core and neutronics data are provided in the Volume I.

The purpose of the first exercise is to test the thermal-hydraulic system response and to initialise the participants' system models for use in Exercise 3 on coupled 3-D kinetics/system thermal-hydraulics simulations. Core power response is provided to reproduce the actual test results utilising either power or reactivity versus time data. A comprehensive analysis of Exercise 1 is provided in *BWR TT Benchmark – Volume II: Summary Results of Exercise 1* (NEA, 2004).

Comparative analysis of the submitted results for Exercise 2 is given in *BWR TT Benchmark – Volume III: Summary Results of Exercise 2* (NEA, 2006). The purpose of Exercise 2 is to provide a clean initialisation of the coupled core models since the core thermal-hydraulic boundary conditions are provided. The second exercise has two steady-state conditions: hot zero power (HZP) conditions and the initial hot power (HP) conditions of TT2. Thus, Exercise 2 provides the opportunity to initialise and test participants' core models for use in Exercise 3.

The concluding exercise, Exercise 3, primarily comprises the best-estimate coupled 3-D core/thermal-hydraulic system modelling. This exercise combines elements of the first two exercises of this benchmark and is an analysis of the transient in its entirety. Exercise 3 also has four extreme scenarios which allow participants to test their code capabilities in terms of coupling and feedback modelling. Comparative analysis of the participants' results for Exercise 3 has been performed and it is summarised in this report. In total, fourteen sets of best-estimate case results have been submitted by the participants. Fourteen organisations from eight different countries have been involved in this exercise. All the participants from the best-estimate case also submitted a total of forty-eight sets of results for the four extreme scenarios.

The list of participants who have submitted results to the PSU benchmark team for the third exercise best-estimate case is given in Table 1-1, while the list of extreme scenario participants is given in Table 1-2.

Table 1-1: List of participants in Exercise 3 – best-estimate case

#	Participant*	Codes	Country
1	CEA-33 (33-channel)	CATHARE/CRONOS2/FLICA4	France
2	CEA-764 (764-channel)	CATHARE/CRONOS2/FLICA4	France
3	FANP	S-RELAP5/RAMONA5-2.1	Germany
4	FZD	DYN3D/ATHLET	Germany
5	GRS	QUABOX/CUBBOX-ATHLET	Germany
6	NFI	TRAC-BF1/COS3D	Japan
7	NUPEC	TRAC-BF1/SKETCH-INS	Japan
8	PSI	RETRAN-3D MOD 003.1	Switzerland
9	PSU/PURDUE/NRC	TRAC-M/PARCS	USA
10	TEPSYS	TRAC-BF1/ENTRÉE	Japan
11	UPISA	RELAP5/PARCS	Italy
12	UPV-1 (MODKIN)	TRAC-BF1 MODKIN	Spain
13	UPV-2 (NOKIN)	TRAC-BF1 NOKIN-3D	Spain
14	WESTINGHOUSE	POLCA-T	Sweden

* Participants' full names can be found in the list of abbreviations at the beginning of this work.

Table 1-2: List of participants in Exercise 3 – extreme scenarios

#	Participant*	Codes	Country
1	CEA (33-channel)	CATHARE/CRONOS2/FLICA4	France
2	FANP	S-RELAP5/RAMONA5-2.1	Germany
3	FZD	DYN3D-ATHLET	Germany
4	GRS	ATHLET-QUABOX/CUBBOX	Germany
5	NFI	TRAC-BF1/COS3D	Japan
6	NUPEC	TRAC-BF1/SKETCH-INS	Japan
7	PSI	RETRAN-3D MOD 003.1	Switzerland
8	PSU/PURDUE/NRC	TRAC-M/PARCS	USA
9	TEPSYS	TRAC-BF1/ENTRÉE	Japan
10	UPISA	RELAP5/PARCS	Italy
11	UPV (NOKIN)	TRAC-BF1 NOKIN-3D	Spain
12	WESTINGHOUSE	POLCA-T	Sweden

* Participants' full names can be found in the list of abbreviations at the beginning of this work.

Chapter 2 of this report contains the description of Exercise 3 best-estimate case and extreme scenarios. The data regarding core, neutronics, thermal-hydraulics, steady-state and transient conditions are also provided in the second chapter. Chapter 3 mainly discusses the utilised statistical methodologies which quantify the accuracy of the results submitted by the participants. Chapter 4 presents comparative analysis of the final results for Exercise 3 while the final chapter, Chapter 5, summarises the conclusions drawn from the analysis of this exercise.

Participants' detailed code descriptions can be found in Appendix A. In addition, the modelling assumptions made by each participant are given in Appendix B.

Chapter 2: Description of Exercise 3

2.1 General

A TT transient in a BWR-type reactor is considered one of the most complex events to be analysed because it involves the reactor core, the high pressure coolant boundary, associated valves and piping in highly complex interactions with variables changing very rapidly. The PB2 TT2 test starts with a sudden closure of the turbine stop valve (TSV) and then the turbine bypass valve begins to open. From a fluid flow phenomena point of view, pressure and flow waves play an important role during the early phase of the transient (of about 1.5 seconds) because rapid valve actions cause sonic waves, as well as secondary waves, generated in the pressure vessel. The pressure oscillation generated in the main steam piping propagates with relatively little attenuation into the reactor core. The induced core pressure oscillation results in changes of the core void distribution and fluid flow. The magnitude of the neutron flux transient taking place in the BWR core is affected by the initial rate of pressure rise caused by the pressure oscillation and has a spatial variation. The simulation of the power response to the pressure pulse and subsequent void collapse requires a 3-D core modelling supplemented by 1-D simulation of the remainder of the reactor coolant system.

The reference design for the BWR is derived from real reactor, plant and operation data for the PB2 NPP and it is based on the information provided in EPRI reports (Carmichael, 1978; Hornyik, 1979; Larsen, 1978; Moberg, 1981) and some additional sources such as the PECo Energy Topical report (Olson, 1988). Although a complete set of core/neutronics and thermal-hydraulics input specifications are provided in Volume I (NEA, 2001) and Volume II (NEA, 2006), the data relevant to Exercise 3 are also given in this chapter for the convenience of the reader.

The previous exercises of this benchmark, Exercise 1 and Exercise 2, have provided participants with an opportunity to initialise their core and system models, and also to test their code capabilities for coupling of thermal-hydraulic and neutronics phenomena. Measured core power has been used as a boundary condition in the first exercise, and only core calculations have been performed using specified boundary conditions in the second exercise. The successes of Exercises 1 and 2 allowed participants to perform the third exercise which combines elements of the first two exercises of this benchmark and is an analysis of the transient in its entirety.

Exercise 3 consists of a base case (the so-called best-estimate case) and hypothetical cases (the so-called extreme scenarios). The purpose of the Exercise 3 best-estimate case is to provide a comprehensive assessment of all the participating codes in analysing complex transients with 3-D coupled core and system calculations. In order to validate such assessments, available measured plant data are utilised for this case during the comparative analyses presented in this report. In addition to the base case, the analysis of the extreme scenarios provides a further understanding of the reactor behaviour, which is the result of the dynamic coupling of the whole system, *i.e.* the interaction between the steam line and vessel flows, the pressure, the Doppler, void and control reactivity and power. The following four extreme scenarios are analysed by the participants over the course of this exercise:

- *Extreme Scenario 1*: Turbine trip (TT) with steam bypass relief system failure.
- *Extreme Scenario 2*: TT without reactor scram.
- *Extreme Scenario 3*: TT with steam bypass relief system failure and without reactor scram.
- *Extreme Scenario 4*: Combined scenario – turbine trip with steam bypass system failure, without scram and without safety relief valves opening.

The key elements of Exercise 3 are illustrated in the simple BWR schematic given in Figure 2-1. Extreme Scenario 1 (TT without bypass system relief opening) and Extreme Scenario 2 (TT without scram) can be considered as single failures and therefore provide information from the perspective of the safety of the plant. Extreme Scenario 3 (combination of 1 and 2), which considers the coincidence of two independent failures, and Extreme Scenario 4 (in addition to 3 no opening of safety relief valves), which considers the coincidence of three independent failures are extremely unlikely from a safety perspective, while they help with the understanding of the short-time dynamics of the reactor system. In the base case, SRV are not opening during the transient while this happens in the Extreme Scenarios 1, 2 and 3. In hypothetical cases, the dynamical response of the system due to the interaction of the flow in the steam line with the dynamics of the safety relief valves (SRV) happens to be more challenging for the coupled codes. Hence, Extreme Scenario 4 provides clear comparison of physical models of the participants' codes. It should be noted that no comparison with measured data is possible for the extreme cases since they are hypothetical scenarios. Therefore, submitted extreme scenario results are compared with an ''average'' of the results of the benchmark participants in this report.

Figure 2-1: Key elements of Exercise 3 best-estimate case and extreme scenarios

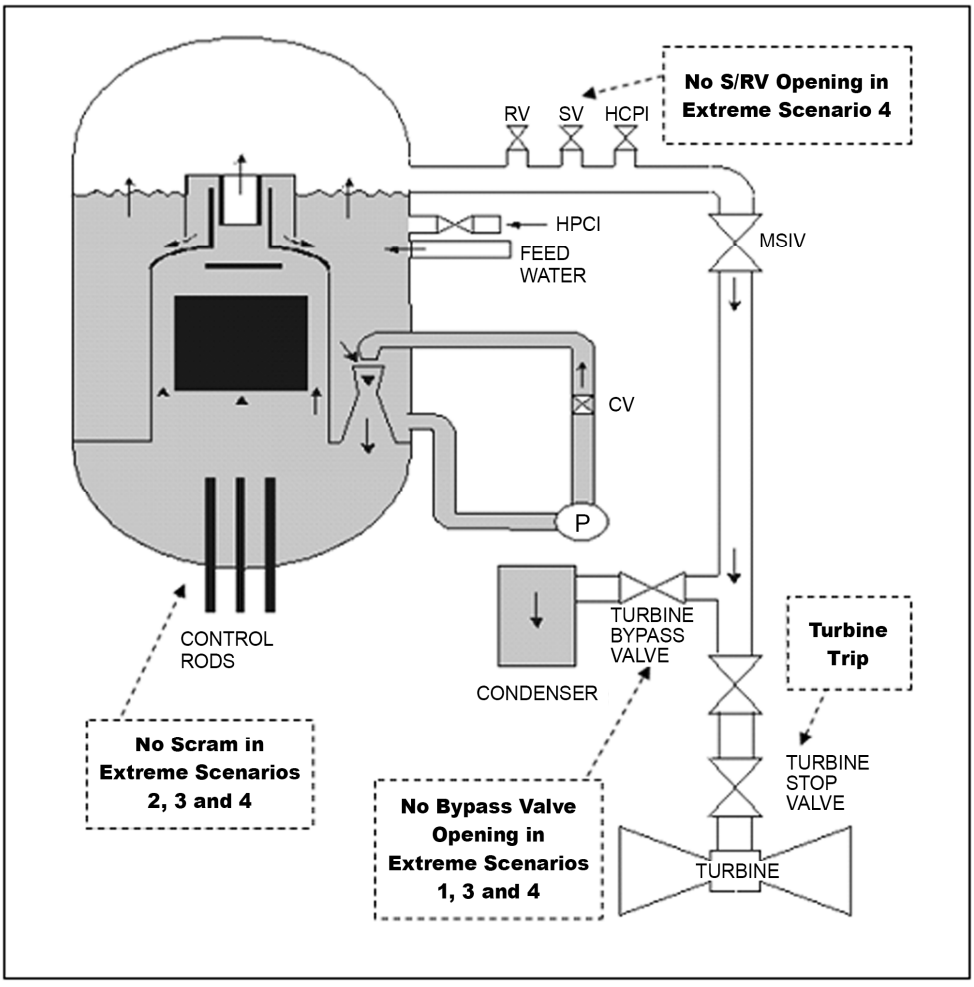

For the convenience of the reader, PB2 neutronics and thermal-hydraulic data as well as initial TT2 conditions for steady-state and transient calculations are given in the following subsections of this chapter.

2.2 Core and neutronics data

The reference design for the BWR is derived from real reactor, plant and operation data for the PB2 BWR/4 NPP and it is based on the information provided in EPRI reports and some additional sources such as the PECo Energy topical report (Olson, 1988). This section specifies the core and neutronic data to be used in the calculations of Exercise 3.

The radial geometry of the reactor core is shown in Figure 2-1. At radial plane, the core is divided into cells 15.24 cm wide, each corresponding to one fuel assembly (FA), plus a radial reflector (shaded area of Figure 2-1) of the same width. There are a total of 888 assemblies, 764 FA and 124 reflector assemblies. Axially, the reactor core is divided into 26 layers (24 core layers plus top and bottom reflectors) with a constant height of 15.24 cm (including reflector nodes). The total active core height is 365.76 cm. The axial nodalisation accounts for material changes in the fuel design and for exposure and history variations. Geometric data for the FA and fuel rod is provided in Table 2-1. Data for different assembly designs is given in Tables 2-2 through 2-7. Fuel assembly lattice drawings, including detailed dimensions, for initial fuel, reload fuel with 100 and 120 mil channels and the lead test assemblies (LTA) are shown in Figures 2-2 through 2-5. The numbers 100 and 120 refer to the wall thickness of the channel (1 mil = 0.001 inches).

The core loading during the test was as follows: 576 fuel assemblies were the original 7×7 type from Cycle 1 (C1), and the remaining 188 were a reload of 8×8 fuel assemblies. One hundred and eighty-five control rods provided reactivity control. To build a given neutronic model, these control rods can be grouped according to their initial insertion position. The control rod grouping used by PSU to perform reference calculations is presented in Figure 2-7.

Two neutron energy groups and six delayed neutron precursor families are modelled. The energy release per fission for the two prompt neutron groups is 0.3213×10^{-10} and 0.3206×10^{-10} W-s/fission, and this energy release is considered to be independent of time and space. It is assumed that 2% of fission power is released as direct gamma heating for the in-channel coolant flow and 1.7% for the bypass flow. Table 2-8 shows global core-wide decay time constants and fractions of delayed neutrons. In addition delayed parameters are provided in the cross-section library for each of the compositions. The prompt neutron lifetime is 0.45085E-04.

It is recommended that ANS-79 be used as a decay heat standard model. Seventy-one (71) decay heat groups are used: 69 groups are used for the three isotopes ^{235}U, ^{239}Pu and ^{238}U with the decay heat constants defined in the 1979 ANS standard; plus, the heavy-element decay heat groups for ^{239}U and ^{239}Np are used with constants given in Table 2-9. It is recommended that the participants also use the assumption of an infinite operation at a power of 3 293 MW_t. For participants who are not capable of using the ANS-79 decay heat standard, a file of the decay heat evolution throughout the transient is provided on CD-ROM and at the benchmark ftp site under the directory "Decay-Heat". These predictions are obtained using the PSU coupled code results. The effective decay heat energy fraction of the total thermal power (the relative contribution in the steady state) is equal to 0.065583.

Nineteen (19) assembly types are contained within the core geometry. There are 435 compositions. The corresponding sets of cross-sections are provided. Each composition is defined by material properties (due to changes in the fuel design) and burn-up. The burn-up dependence is a three-component vector of variables: exposure (GWd/t), spectral history (void fraction) and control rod history. Assembly designs are defined in Tables 2-10 through 2-15. Control rod geometry data is provided in Table 2-16. The definition of assembly types is shown in Table 2-17. The radial distribution of these assembly types within the reactor geometry is shown in Figure 2-8. The axial locations of compositions for each assembly type are shown in Table 2-18.

A complete set of diffusion coefficients, macroscopic cross-sections for scattering, absorption and fission, assembly discontinuity factors (ADF), as a function of the moderator density and fuel temperature is defined for each composition. The group inverse neutron velocities are also provided for each composition. Dependences of the cross-sections on the above variables are specified through a two-dimensional table look-up. Each composition is assigned to a cross-section set containing separate tables for the diffusion coefficients and cross-sections, with each point in the table representing a possible core state. The expected transient ranges are covered by the selection of adequate ranges for the independent variables shown in Table 2-19. Specifically, Exercise 1 was used for selecting the range of thermal-hydraulic variables. A steady-state calculation was run using the TRAC-BF1 code and initial

conditions of the second turbine trip for choosing discrete values of the thermal-hydraulic variables (pressure, void fraction and coolant/moderator temperature). Transient calculations were performed to determine the expected range of change of the above variables.

A modified linear interpolation scheme (which includes extrapolation outside the thermal-hydraulic range) is used to obtain the appropriate total cross-sections from the tabulated ones based on the reactor conditions being modelled. Table 2-20 shows the definition of a cross-section table associated with a composition. Table 2-21 shows the macroscopic cross-section table structure for one cross-section set. All cross-section sets are assembled into a cross-section library. The cross-sections are provided in separate libraries for rodded (nemtabr) and un-rodded compositions (nemtab). The format of each library is as follows:

- The first line of data displays the number of data points used for the independent thermal-hydraulic parameters. The parameters used in this benchmark include fuel temperature and moderator density.
- Each cross-section set is in the order shown in Table 2-21. Each table is in the format described in Table 2-20. More detailed information on this format is presented in Appendix B. First, the values of the independent thermal-hydraulic parameters (fuel temperature and moderator density) used to specify that particular set of cross-sections are listed, followed by the values of the cross-sections[1] and ADF. Since there is one-half symmetry for all of the assembly designs, two ADF per composition per energy group are provided – West (wide gap) and South (narrow gap). Because the fuel assembly designs employed in PB2 core design have one-half symmetry, it is assumed that North is equal to West and East is equal to South (*e.g.* Figure 2-9). Detector parameters[2] are included after the two-group cross-sections followed by the delayed neutron parameters for six groups. Finally, the group inverse neutron velocities complete the data for a given cross-section set.
- The dependence on fuel temperature in the reflector cross-section tables is also modelled. This is because the reflector cross-sections are generated by performing colour-set lattice physics transport calculations, including the next fuel region. In order to simplify the reflector feedback modelling the following assumptions are made for this benchmark: an average fuel temperature value equal to 550 K is used for the radial reflector cross-section modelling in both the initial steady state and transient simulations, and the average coolant density for the radial reflector is equal to the inlet coolant density. For the axial reflector regions the following assumptions are made: for the bottom, the fuel temperature is equal to the inlet coolant temperature (per thermal-hydraulic channel or cell) and the coolant density is equal to the inlet coolant density (again per channel); for the top, the fuel temperature is equal to the outlet coolant temperature (per channel) and the coolant density is equal to the outlet coolant density (per channel).

All cross-section data, along with a file of 3-D node-wise xenon number density distribution for initial steady-state conditions and a program for linear interpolation, are supplied on CD-ROM and at the benchmark ftp site under the directory "XS-Lib" in the format described above.

Lattice physics calculations are performed by homogenising the fuel lattice and the bypass flow associated with it. When obtaining the average coolant density, a correction (bypass flow density correction) that accounts for the bypass channel conditions should be included since this is going to influence the feedback effect on the cross-section calculation through the average coolant density. The following approach should be applied:

$$\rho_{act}^{eff} = \frac{A_{act}\rho_{act} + A_{byp}\left(\rho_{byp} - \rho_{sat}\right)}{A_{act}} \qquad 2.1$$

1. Please note that the provided absorption thermal macroscopic cross-sections already take the equilibrium xenon thermal macroscopic cross-sections at nominal power into account. The thermal macro- and microscopic xenon cross-sections are listed in the cross-section sets. The benchmark team has also provided to participants a file with 3-D node-wise xenon number density distribution corresponding to the power level (61.6 % of nominal power) of initial steady-state conditions. This data can be used to correct the absorption thermal macroscopic cross-sections to be consistent with the power level of the initial steady state. This correction is called the "xenon correction".
2. Detector parameters are described in Volume I, Section 2.6.

where ρ_{act}^{eff} is the effective average coolant density for cross-section calculation, ρ_{byp} is the average moderator coolant density of the bypass channel, ρ_{sat} is the saturated moderator coolant density of the bypass channel, A_{act} is flow cross-sectional area of the active heated channel and A_{byp} is the flow cross-sectional area of the bypass channel.

Bypass conditions should be obtained by adding a bypass channel to represent the core bypass region in the thermal-hydraulic model.

Table 2-1: PB2 fuel assembly data

	Initial load			Reload	Reload	LTA special
Assembly type	1	2	3	4	5	6
No. of assemblies, initial core	168	263	333	0	0	0
No. of assemblies, Cycle 2	0	261	315	68	116	4
Geometry	7 × 7	7 × 7	7 × 7	8 × 8	8 × 8	8 × 8
Assembly pitch, in	6.0	6.0	6.0	6.0	6.0	6.0
Fuel rod pitch	0.738	0.738	0.738	0.640	0.640	0.640
Fuel rods per assembly	49	49	49	63	63	62
Water rods per assembly	0	0	0	1	1	2
Burnable poison positions	0	4	5	5	5	5
No. of spacer grids	7	7	7	7	7	7
Inconel per grid, lb	0.102	0.102	0.102	0.102	0.102	0.102
Zr-4 per grid, lb	0.537	0.537	0.537	0.614	0.614	0.614
Spacer width, in	1.625	1.625	1.625	1.625	1.625	1.625
Assembly average fuel composition:						
Gd_2O_3, g	0	441	547	490	328	313
UO_2, kg	222.44	212.21	212.06	207.78	208.0	207.14
Total fuel, kg	222.44	212.65	212.61	208.27	208.33	207.45

Table 2-2: Assembly design 1

Rod type	Number of rods	Pellet density UO_2 (g/cm³)	Pellet density UO_2+Gd_2O_3 (g/cm³)	Stack density (g/cm³)	Gd_2O_3 (g)	UO_2 (g)	Stack length (cm)
1	31	10.42	–	10.34	0	4 548	365.76
2	17	10.42	–	10.34	0	4 548	365.76
2s	01	10.42	–	10.34	0	4 140	330.2

Pellet outer diameter = 1.23698 cm.

Cladding = Zircaloy-2, 1.43002 cm outer diameter × .08128 cm wall thickness, all rods.

Gas plenum length = 40.64 cm.

Table 2-3: Assembly design 2

Rod type	Number of rods	Pellet density UO_2 (g/cm³)	Pellet density UO_2+Gd_2O_3 (g/cm³)	Stack density (g/cm³)	Gd_2O_3 (g)	UO_2 (g)	Stack length (cm)
1	25	10.42	–	10.32	0	4 352	365.76
1s	1	10.42	–	10.32	0	3 935	330.20
2	12	10.42	–	10.32	0	4 352	365.76
3	6	10.42	–	10.32	0	4 352	365.76
4	1	10.42	–	10.32	0	4 352	365.76
5A	3	–	10.29	10.19	129	4 171	365.76
6B	1	10.42	10.29	10.27	54	4 277	365.76

Pellet outer diameter = 1.21158 cm.

Cladding = Zircaloy-2, 1.43002 cm outer diameter × .09398 cm wall thickness, all rods.

Gas plenum length = 40.132 cm.

Table 2-4: Assembly design 3

Rod type	Number of rods	Pellet density UO_2 (g/cm³)	Pellet density UO_2+Gd_2O_3 (g/cm³)	Stack density (g/cm³)	Gd_2O_3 (g)	UO_2 (g)	Stack length (cm)
1	26	10.42	–	10.32	0	4 352	365.76
2	11	10.42	–	10.32	0	4 352	365.76
3	6	10.42	–	10.32	0	4 352	365.76
4	1	10.42	–	10.32	0	4 352	365.76
5A	2	–	10.29	10.19	129	4 171	365.76
6C	1	–	10.29	10.19	117	3 771	330.20
7E	1	10.42	10.25	10.28	43	4 292	365.76
8D	1	10.42	10.25	10.19	129	4 172	365.76

Pellet outer diameter = 1.21158 cm.

Cladding = Zircaloy-2, 1.43002 cm outer diameter × .09398 cm wall thickness, all rods.

Gas plenum length = 40.132 cm.

Table 2-5: Assembly design 4

Rod type	Number of rods	Pellet density UO_2 (g/cm³)	Pellet density UO_2+Gd_2O_3 (g/cm³)	Stack density (g/cm³)	Gd_2O_3 (g)	UO_2 (g)	Stack length (cm)
1	39	10.42	–	10.32	0	3 309	365.76
2	14	10.42	–	10.32	0	3 309	365.76
3	4	10.42	–	10.32	0	3 309	365.76
4	1	10.42	–	10.32	0	3 309	365.76
5	5	–	10.29	10.19	98	3 172	365.76
WS	1	–	–	–	0	0	–

Pellet outer diameter = 1.05664 cm.

Cladding = Zircaloy-2, 1.25222 cm outer diameter × .08636 cm wall thickness, all rods.

Gas plenum length = 40.64 cm except water rod.

Gd_2O_3 in rod Type 5 runs full 365.76 cm.

Water rod (WS) has holes drilled top and bottom to provide water flow and little or no boiling.

Water rod is also a spacer positioning rod.

Table 2-6: Assembly design 5

Rod type	Number of rods	Pellet density UO_2 (g/cm³)	Pellet density UO_2+Gd_2O_3 (g/cm³)	Stack density (g/cm³)	Gd_2O_3 (g)	UO_2 (g)	Stack length (cm)
1	39	10.42	–	10.32	0	3 309	365.76
2	14	10.42	–	10.32	0	3 309	365.76
3	4	10.42	–	10.32	0	3 309	365.76
4	1	10.42	–	10.32	0	3 309	365.76
5	5	–	10.33	10.23	66	3 216	365.76
WS	1	–	–	–	0	0	–

Pellet outer diameter = 1.05664 cm.

Cladding = Zircaloy-2, 1.25222 cm outer diameter × .08636 cm wall thickness, all rods.

Gas plenum length = 40.64 cm, except water rod.

Gd_2O_3 in rod Type 5 runs full 365.76 cm.

Water rod (WS) has holes drilled top and bottom to provide water flow and little or no boiling.

Water rod is also a spacer positioning rod.

Table 2-7: Assembly design 6

Rod type	Number of rods	Pellet density UO_2 (g/cm³)	Pellet density UO_2+Gd_2O_3 (g/cm³)	Stack density (g/cm³)	Gd_2O_3 (g)	UO_2 (g)	Stack length (cm)
1	38	10.42	–	10.32	0	3 125	355.6
2	14	10.42	–	10.32	0	3 125	355.6
3	4	10.42	–	10.32	0	3 125	355.6
4	1	10.42	–	10.32	0	3 125	355.6
5	5	–	10.33	10.23	63	3 037	355.6
WR,WS	2	–	–	–	0	0	–
ENDS	62	10.42	–	10.32	0	223	25.4

Pellet outer diameter = 1.0414 cm.

Cladding = Zircaloy-2, 1.22682 cm outer diameter × .08128 cm wall thickness, all fuelled rods

= Zircaloy-2, 1.50114 cm outer diameter × .07620 cm wall thickness, water rods.

Gas plenum length = 24.0792 cm.

Gd_2O_3 in rod Type 5 runs full 355.6 cm.

Water rod (WS) has holes drilled top and bottom to provide water flow and little or no boiling.

Water rod is also a spacer positioning rod.

Table 2-8: Decay constant and fractions of delayed neutrons

Group	Decay constant (s^{-1})	Relative fraction of delayed neutrons in %
1	0.012813	0.0167
2	0.031536	0.1134
3	0.124703	0.1022
4	0.328273	0.2152
5	1.405280	0.0837
6	3.844728	0.0214

Total fraction of delayed neutrons: 0.5526%.

Table 2-9: Heavy element decay heat constants

Group no. (isotope)	Decay constant (s^{-1})	Available energy from a single atom (MeV)
70 (^{239}U)	4.91×10^{-4}	0.474
71 (^{239}Np)	3.41×10^{-6}	0.419

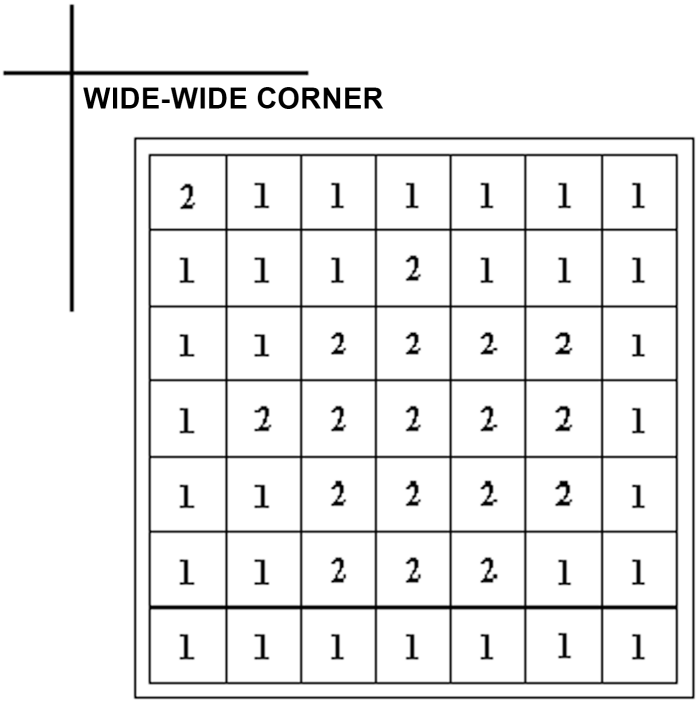

Table 2-10: Assembly design for Type 1 initial fuel

Rod type	^{235}U (wt.%)	Gd_2O_3 (wt.%)	No. of rods
1	1.33	0	31
2	0.71	0	18

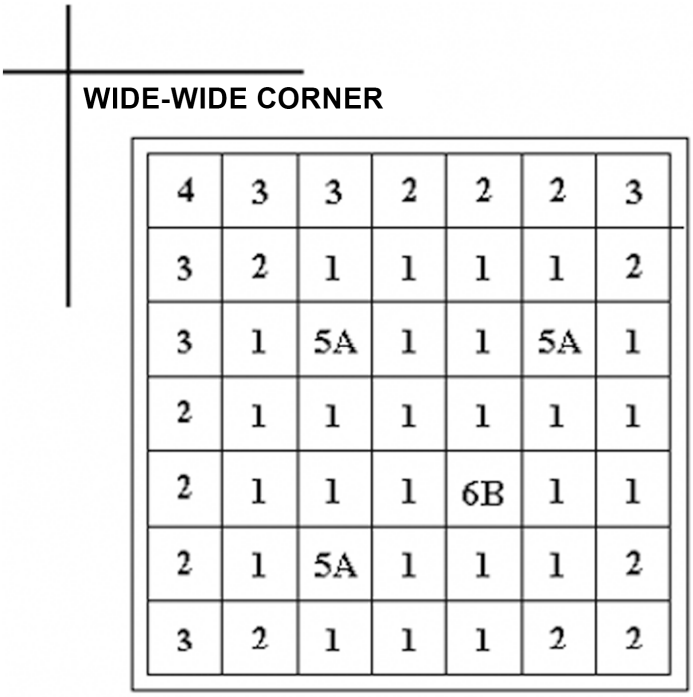

Table 2-11: Assembly design for Type 2 initial fuel

Rod type	^{235}U (wt.%)	Gd_2O_3 (wt.%)	No. of rods
1	2.93	0	26
2	1.94	0	12
3	1.69	0	6
4	1.33	0	1
5A	2.93	3.0	3
6B	2.93	3.0	1

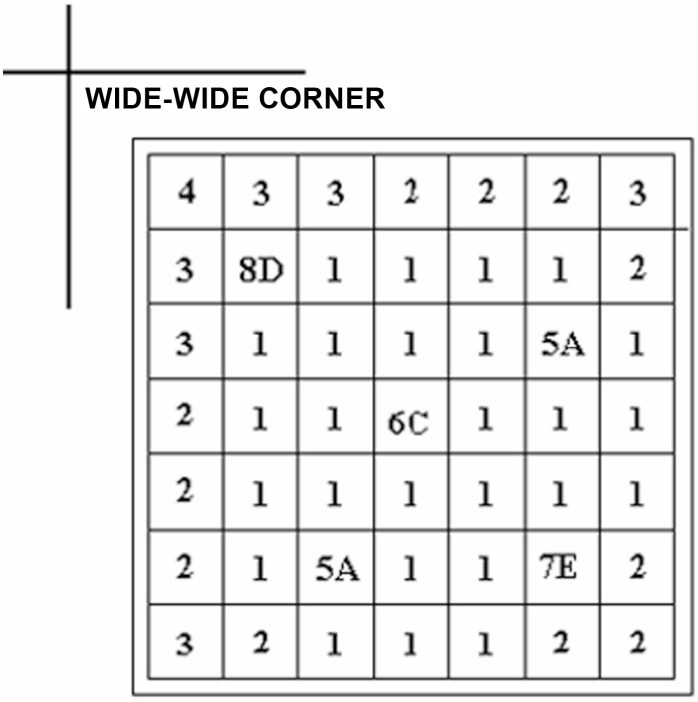

Table 2-12: Assembly design for Type 3 initial fuel

Rod type	^{235}U (wt.%)	Gd_2O_3 (wt.%)	No. of rods
1	2.93	0	26
2	1.94	0	11
3	1.69	0	6
4	1.33	0	1
5A	2.93	3.0	2
6C	2.93	3.0	1
7E	2.93	4.0	1
8D	1.94	4.0	1

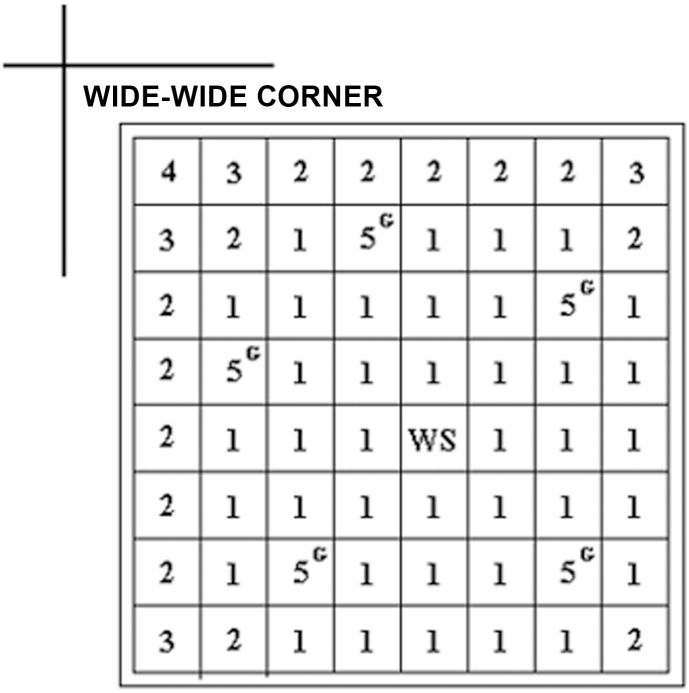

Table 2-13: Assembly design for Type 4, 8 × 8 UO_2 reload

Rod type	^{235}U (wt.%)	Gd_2O_3 (wt.%)	No. of rods
1	3.01	0	39
2	2.22	0	14
3	1.87	0	4
4	1.45	0	1
5	3.01	3.0	5
WS	–	0	1

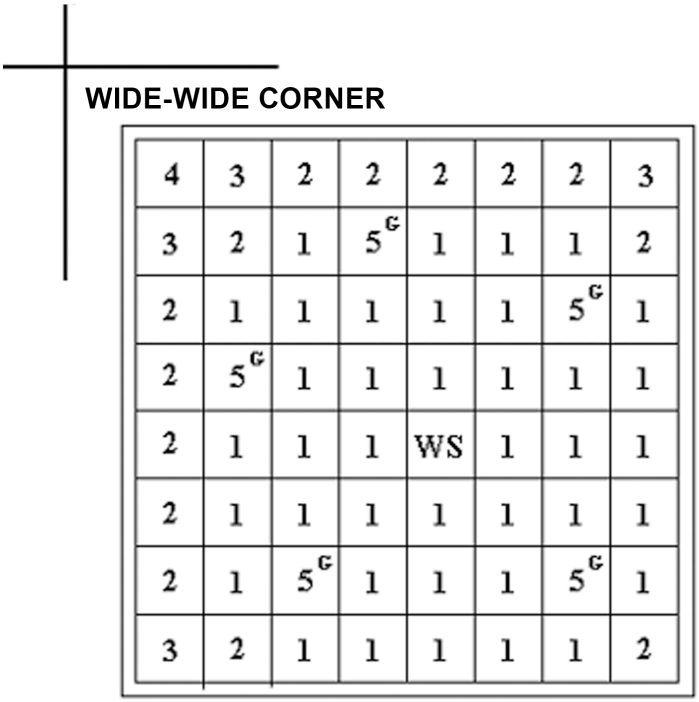

Table 2-14: Assembly design for Type 5, 8 × 8 UO_2 reload

Rod type	^{235}U (wt.%)	Gd_2O_3 (wt.%)	No. of rods
1	3.01	0	39
2	2.22	0	14
3	1.87	0	4
4	1.45	0	1
5	3.01	2.0	5
WS	–	0	1

WS – Spacer positioning water rod.

G – Gadolinium rods.

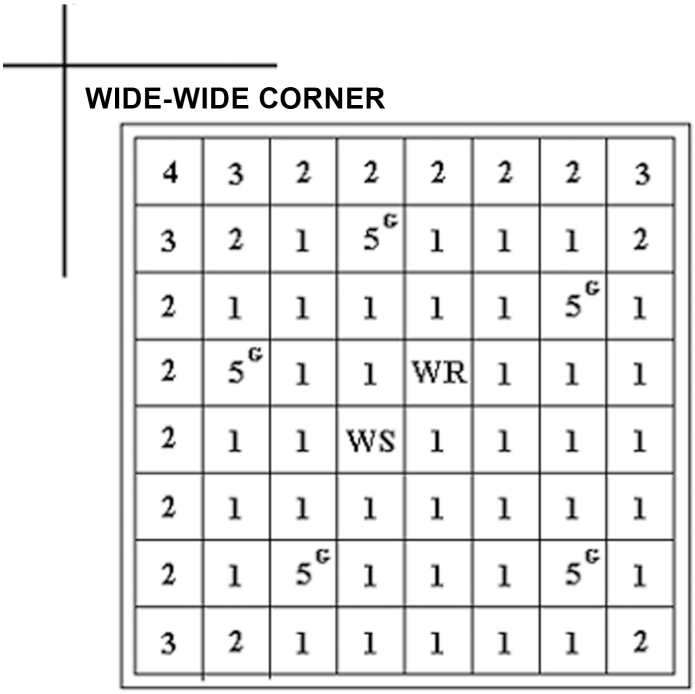

Table 2-15: Assembly design for Type 6, 8 × 8 UO_2 reload, LTA

Rod type	^{235}U (wt.%)	Gd_2O_3 (wt.%)	No. of rods
1	3.01	0	38
2	2.22	0	14
3	1.87	0	4
4	1.45	0	1
5	3.01	2.0	5
WS	–	0	1
WR	–	0	1

WS – Spacer positioning water rod.

WR – Water rod.

G – Gadolinium rods.

Table 2-16: Control rod data (movable control rods)

Shape	Cruciform
Pitch, cm	30.48
Stroke, cm	365.76
Control length, cm	363.22
Control material	B_4C granules in Type-304, stainless steel tubes and sheath
Material density	70% of theoretical
Number of control material tubes per rod	84
Tube dimensions	.47752 cm outer diameter by .0635 cm wall
Control blade half span, cm	12.3825
Control blade full thickness, cm	.79248
Control blade tip radius, cm	.39624
Sheath thickness, cm	.14224
Central structure wing length, cm	1.98501
Blank tubes per wing	None

Table 2-17: Definition of assembly types

Assembly type	Assembly design (see Tables 2-10 through 2-15)
1	5
2	4
3	5
4	6
5	2
6	2
7	2
8	2
9	2
10	2
11	3
12	2
13	3
14	2
15	3
16	2
17	3
18	2
19	Reflector

Table 2-18: Composition numbers in axial layer for each assembly type

	1	2	3	4	5	6	7	8	9	10	11	12	13	14	15	16	17	18	19
1	433	433	433	433	433	433	433	433	433	433	433	433	433	433	433	433	433	433	433
2	1	25	49	73	97	121	145	169	193	217	241	265	289	313	337	361	385	409	435
3	2	26	50	74	98	122	146	170	194	218	242	266	290	314	338	362	386	410	435
4	3	27	51	75	99	123	147	171	195	219	243	267	291	315	339	363	387	411	435
5	4	28	52	76	100	124	148	172	196	220	244	268	292	316	340	364	388	412	435
6	5	29	53	77	101	125	149	173	197	221	245	269	293	317	341	365	389	413	435
7	6	30	54	78	102	126	150	174	198	222	246	270	294	318	342	366	390	414	435
8	7	31	55	79	103	127	151	175	199	223	247	271	295	319	343	367	391	415	435
9	8	32	56	80	104	128	152	176	200	224	248	272	296	320	344	368	392	416	435
10	9	33	57	81	105	129	153	177	201	225	249	273	297	321	345	369	393	417	435
11	10	34	58	82	106	130	154	178	202	226	250	274	298	322	346	370	394	418	435
12	11	35	59	83	107	131	155	179	203	227	251	275	299	323	347	371	395	419	435
13	12	36	60	84	108	132	156	180	204	228	252	276	300	324	348	372	396	420	435
14	13	37	61	85	109	133	157	181	205	229	253	277	301	325	349	373	397	421	435
15	14	38	62	86	110	134	158	182	206	230	254	278	302	326	350	374	398	422	435
16	15	39	63	87	111	135	159	183	207	231	255	279	303	327	351	375	399	423	435
17	16	40	64	88	112	136	160	184	208	232	256	280	304	328	352	376	400	424	435
18	17	41	65	89	113	137	161	185	209	233	257	281	305	329	353	377	401	425	435
19	18	42	66	90	114	138	162	186	210	234	258	282	306	330	354	378	402	426	435
20	19	43	67	91	115	139	163	187	211	235	259	283	307	331	355	379	403	427	435
21	20	44	68	92	116	140	164	188	212	236	260	284	308	332	356	380	404	428	435
22	21	45	69	93	117	141	165	189	213	237	261	285	309	333	357	381	405	429	435
23	22	46	70	94	118	142	166	190	214	238	262	286	310	334	358	382	406	430	435
24	23	47	71	95	119	143	167	191	215	239	263	287	311	335	359	383	407	431	435
25	24	48	72	96	120	144	168	192	216	240	264	288	312	336	360	384	408	432	435
26	434	434	434	434	434	434	434	434	434	434	434	434	434	434	434	434	434	434	434

Table 2-19: Range of variables

T Fuel (°K)	Rho M. (kg/m^3)
400.0	141.595
800.0	141.595
1 200.0	141.595
1 600.0	141.595
2 000.0	141.595
2 400.0	141.595
400.0	226.154
800.0	226.154
1 200.0	226.154
1 600.0	226.154
2 000.0	226.154
2 400.0	226.154
400.0	299.645
800.0	299.645
1 200.0	299.645
1 600.0	299.645
2 000.0	299.645
2 400.0	299.645
400.0	435.045
800.0	435.045
1 200.0	435.045
1 600.0	435.045
2 000.0	435.045
2 400.0	435.045
400.0	599.172
800.0	599.172
1 200.0	599.172
1 600.0	599.172
2 000.0	599.172
2 400.0	599.172
400.0	779.405
800.0	779.405
1 200.0	779.405
1 600.0	779.405
2 000.0	779.405
2 400.0	779.405

Table 2-20: Key to macroscopic cross-section tables

T_{f1}	T_{f2}	T_{f3}	T_{f4}	T_{f5}	T_{f6}
ρ_{m1}	ρ_{m2}	ρ_{m3}	ρ_{m4}	ρ_{m5}	ρ_{m6}
Σ_1	Σ_2	…			
		…	Σ_{34}	Σ_{35}	Σ_{36}

Where:

– T_f is the Doppler (fuel) temperature (°K)

– ρ_m is the moderator density (kg/m^3)

Macroscopic cross-sections are in units of cm^{-1}

Table 2-21: Macroscopic cross-section tables' structure

```
**************************************************************************
        Cross-Section Table Input
*
*       T Fuel          Rho Mod.
        6 6
*
**********  X-Section Set #
  #
**************************************************************************
        Group No. 1
*
**********  Diffusion Coefficient Table
*
**********  Absorption X-Section Table
*
**********  Fission X-Section Table
*
**********  Nu-Fission X-Section Table
*
**********  Scattering From Group 1 to 2 X-Section Table
*
**********  Assembly Disc. Factor Table - W
*
**********  Assembly Disc. Factor Table - S
*
**********  Detector Flux Ratio Table
*
**********  Detector Microscopic Fission X-Section Table
        *
```

```
**********************************************************************
        Group No. 2
*
*************  Diffusion Coefficient Table
*
*************  Absorption X-Section Table
*
*************  Fission X-Section Table
*
*************  Nu-Fission X-Section Table
*
*************  Xe Macroscopic X-Section Table
*
*************  Xe Microscopic X-Section Table
*
*************  Assembly Disc. Factor Table - W
*
*************  Assembly Disc. Factor Table - S
*
*************  Detector Flux Ratio Table
*
*************  Detector Microscopic Fission X-Section Table
*
*************  Detector Flux Ratio Table (not energy group dependent)
*
*************  Detector Microscopic Fission X-Section Table (not energy group dependent)
*
*************  Effective Delayed Neutron Yield in Six Groups
*
*************  Decay Constants for Delayed Neutron Groups
*
*************  Inv. Neutron Velocities
```

Figure 2-2: Reactor core cross-sectional view

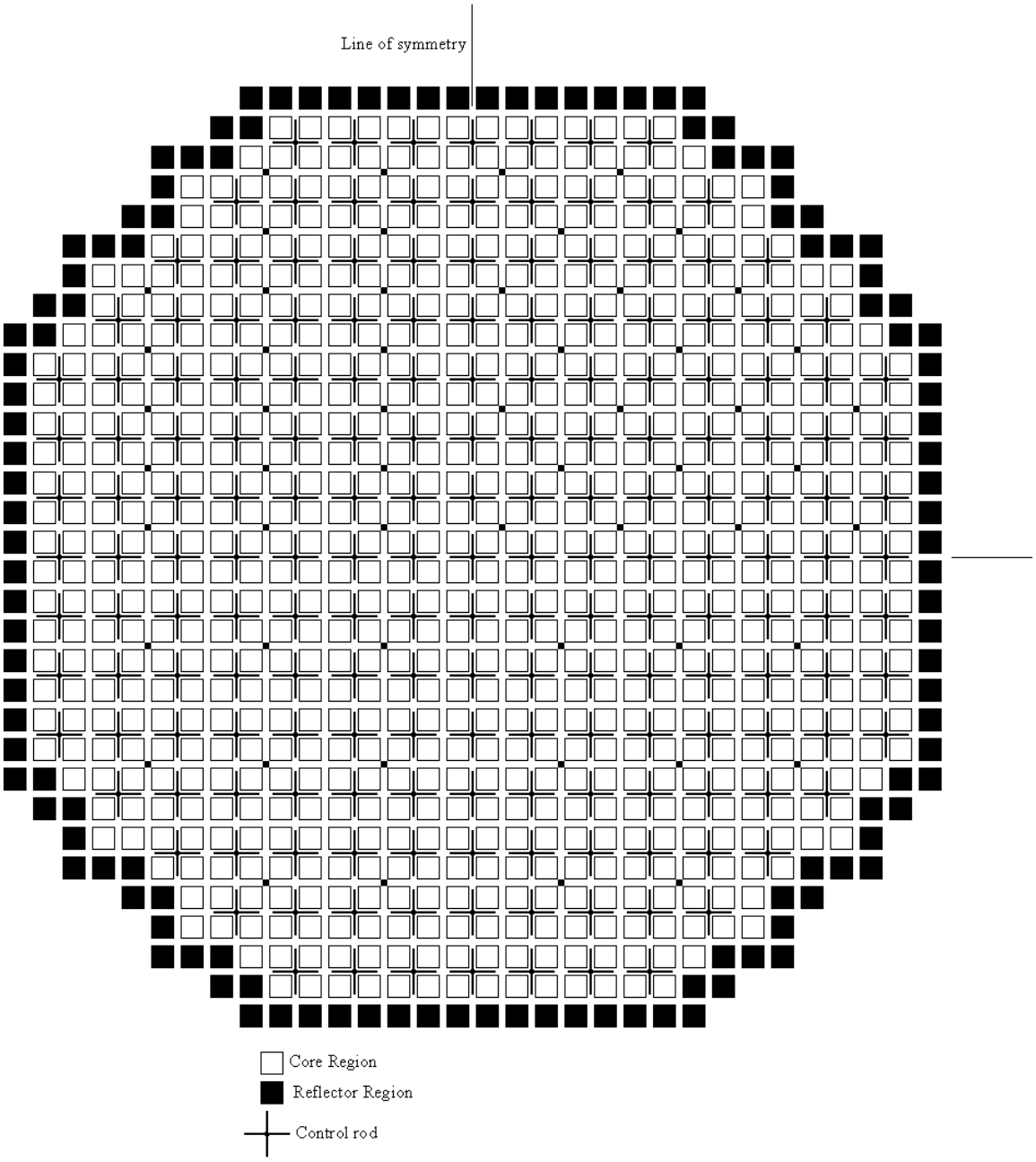

Figure 2-3: PB2 initial fuel assembly lattice

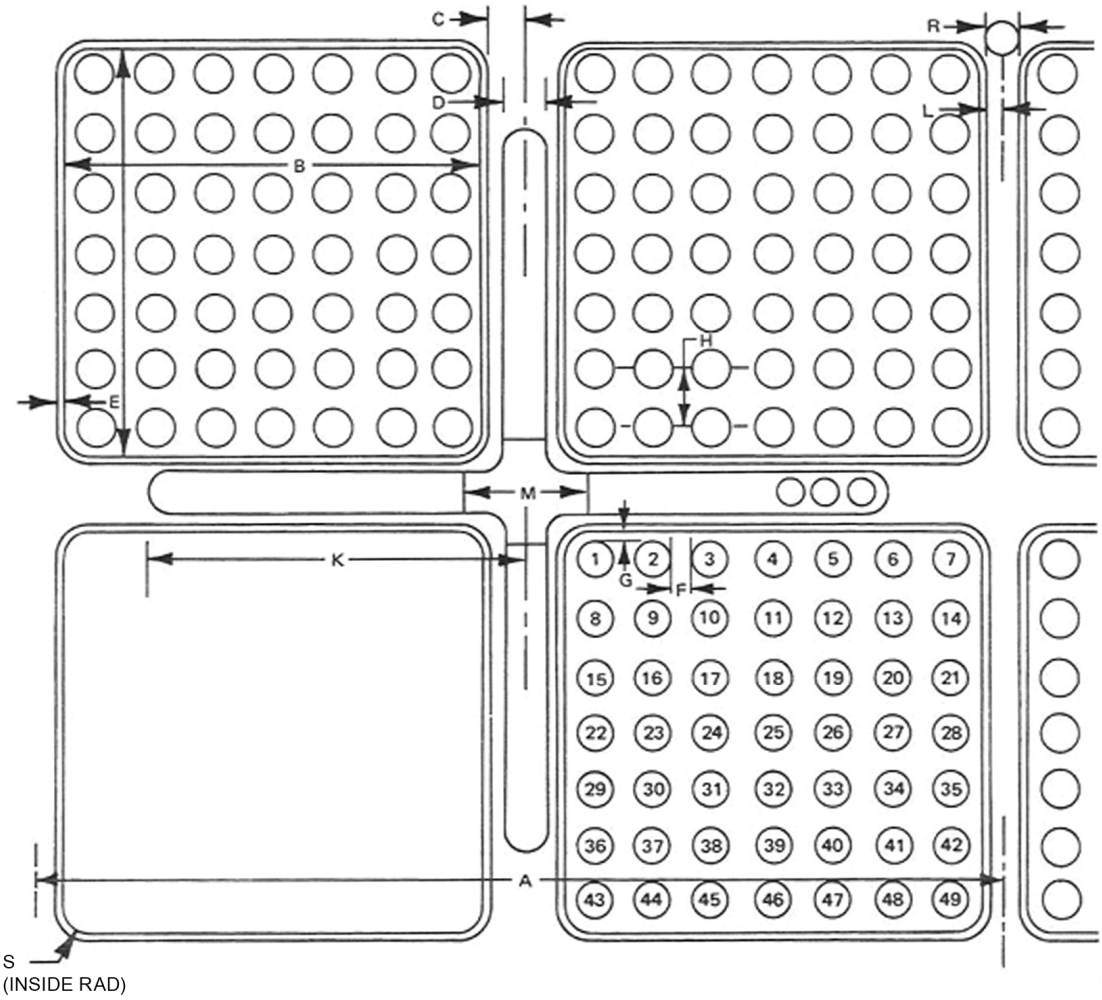

Dim. ID	A	B	C	D	E	F	G	H	I	J
Dim. (in)	12.0	5.278	0.375		0.080	0.175	0.1435	0.738		
Dim. (cm)	30.48	13.40612	.9525		.2032	.4445	.36449	1.87452		
Dim. ID	**K**	**L**	**M**	**N**	**O**	**P**	**Q**	**R**	**S**	
Dim. (in)		0.187							0.38	
Dim. (cm)		.47498							.9652	

Figure 2-4: PB2 reload fuel assembly lattice for 100 mil channels

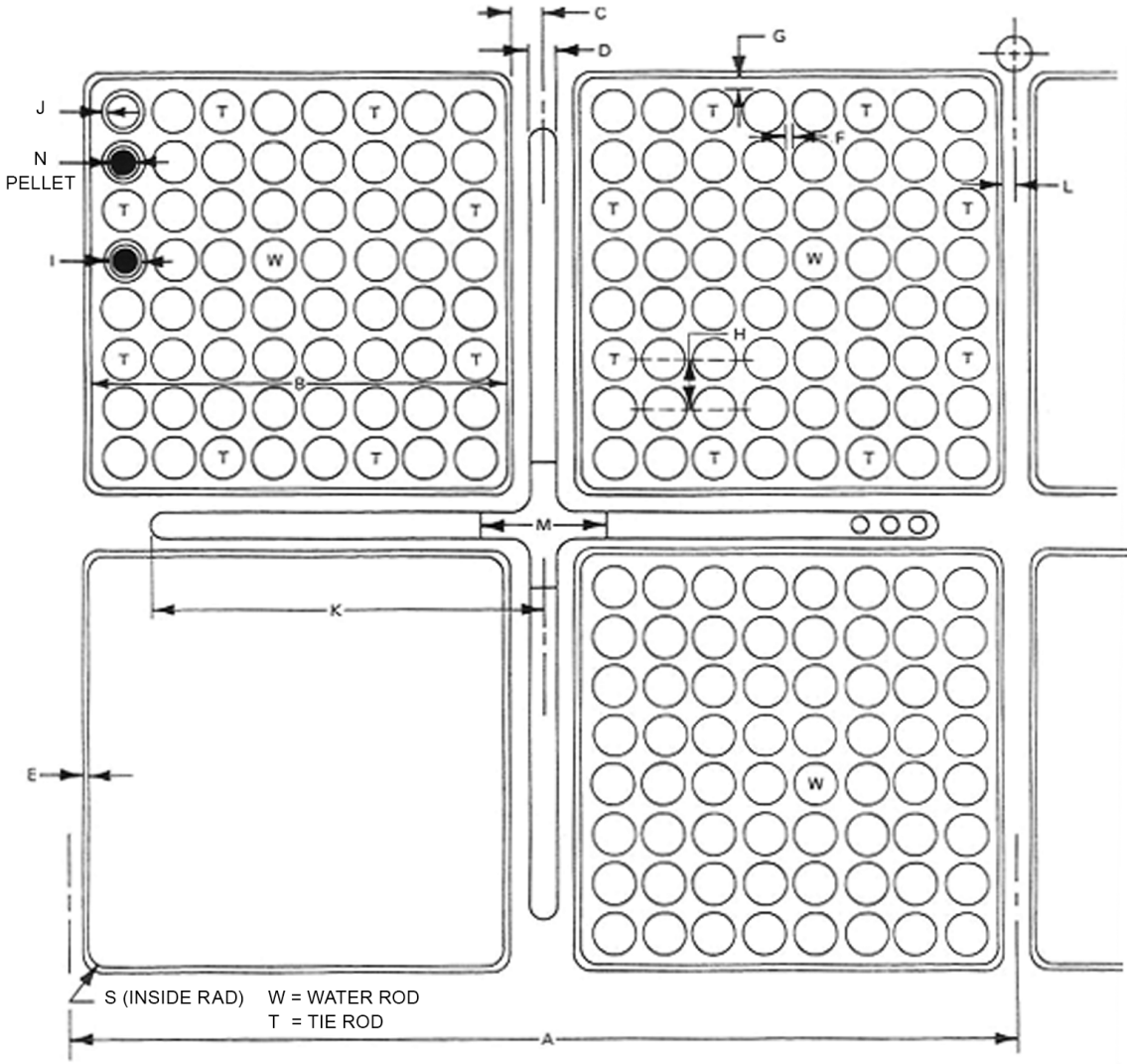

Dim. ID	A	B	C	D	E	F	G	H	I	J
Dim. (in)	12.0	5.278	0.355		0.100	0.147	0.153	0.64		
Dim. (cm)	30.48	13.40612	.9017		.254	.37338	.38862	1.6256		
Dim. ID	**K**	**L**	**M**	**N**	**O**	**P**	**Q**	**R**	**S**	
Dim. (in)		0.167							0.38	
Dim. (cm)		.42418							.9652	

Figure 2-5: PB2 reload fuel assembly lattice for 120 mil channels

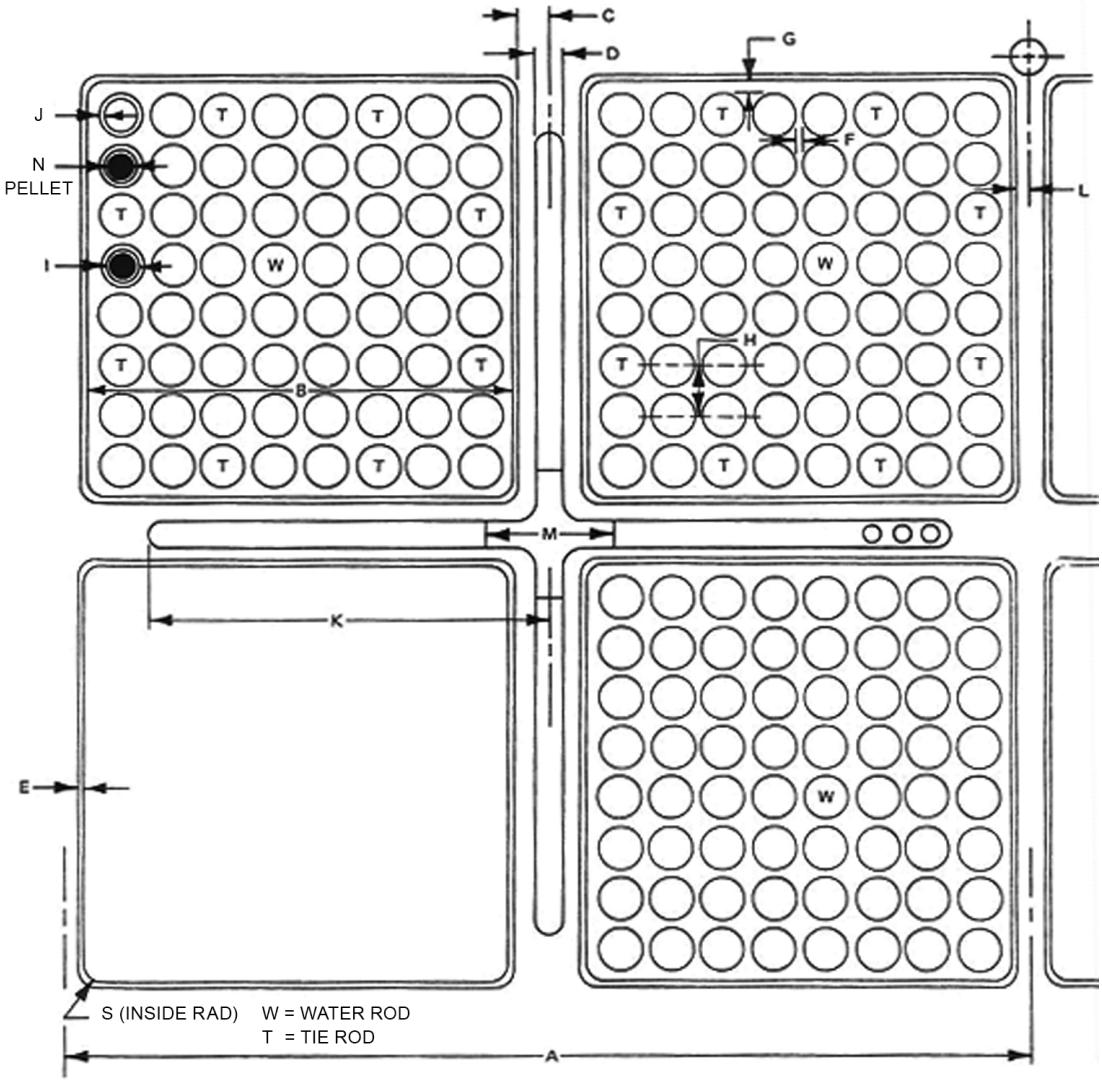

Dim. ID	A	B	C	D	E	F	G	H	I	J
Dim. (in)	12.0	5.278	0.355		0.120	0.147	0.153	0.64		
Dim. (cm)	30.48	13.40612	.8509		.3048	.37338	.38862	1.6256		
Dim. ID	**K**	**L**	**M**	**N**	**O**	**P**	**Q**	**R**	**S**	
Dim. (in)		0.167							0.38	
Dim. (cm)		.42418							.9652	

Figure 2-6: PB2 reload fuel assembly lattice for LTA assemblies

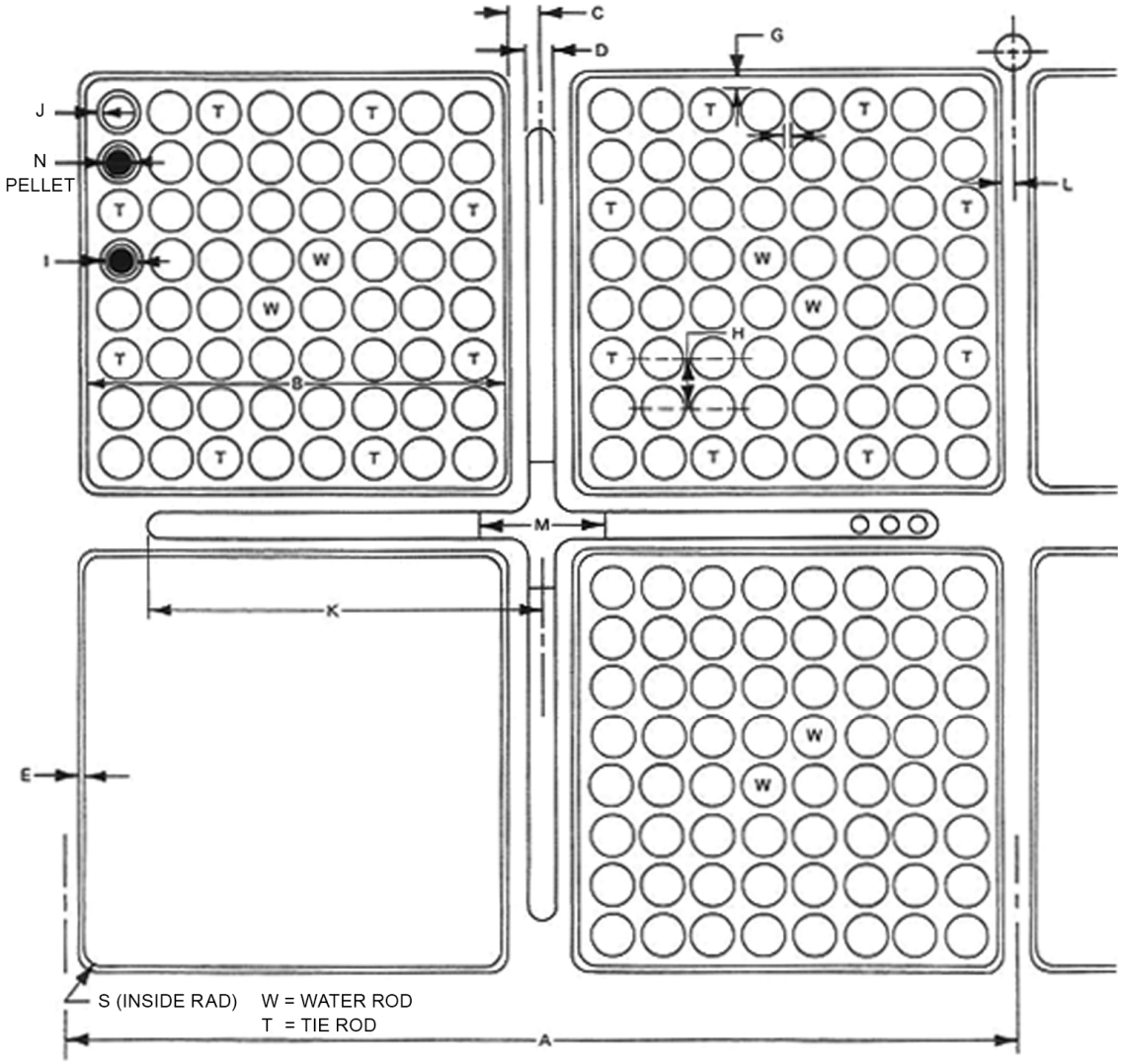

Dim. ID	A	B	C	D	E	F	G	H	I	J
Dim. (in)	12.0	5.278	0.355		0.100	0.157	0.158	0.64		
Dim. (cm)	30.48	13.40612	.9017		.254	.39878	.40132	1.6256		
Dim. ID	**K**	**L**	**M**	**N**	**O**	**P**	**Q**	**R**	**S**	
Dim. (in)		0.167							0.38	
Dim. (cm)		.42418							.9652	

Figure 2-7: PSU control rod grouping

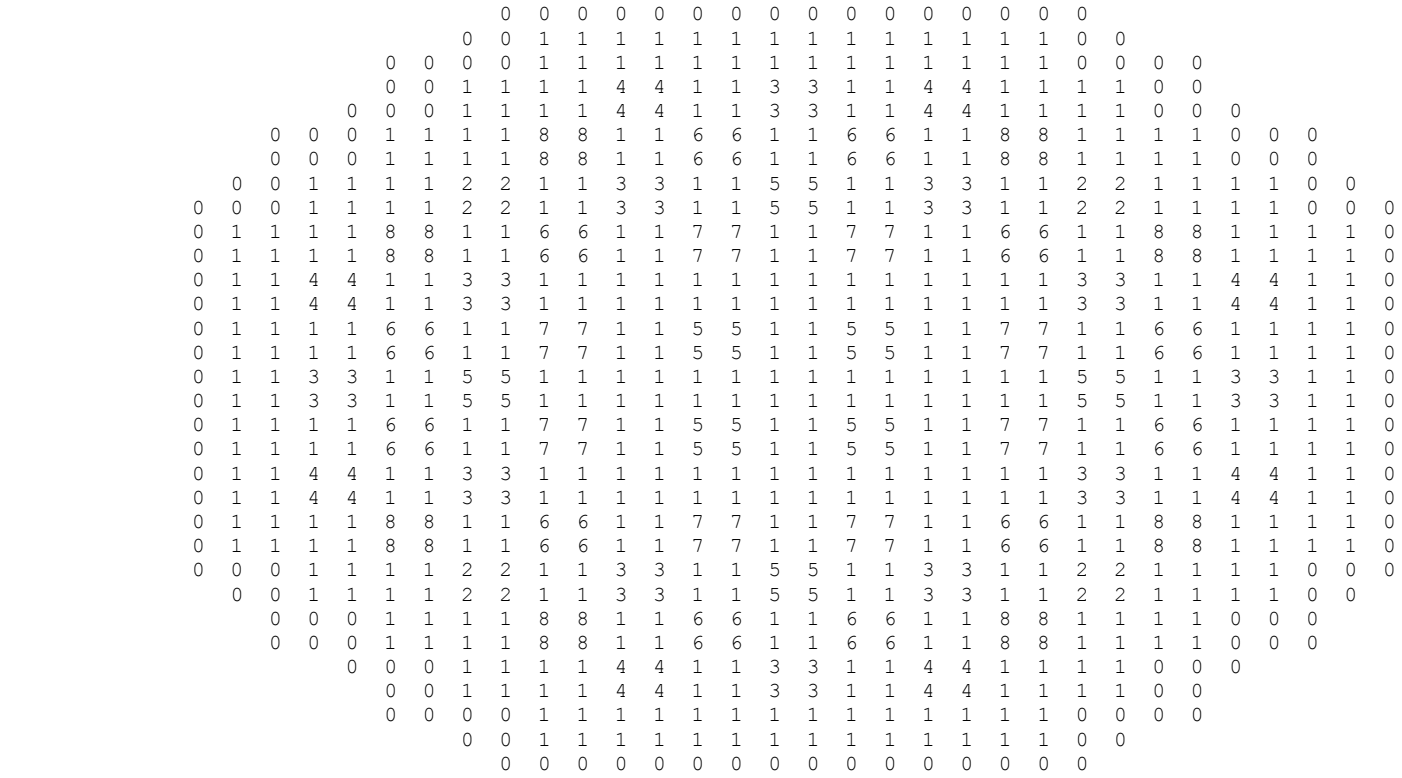

Figure 2-8: Radial distribution of assembly types

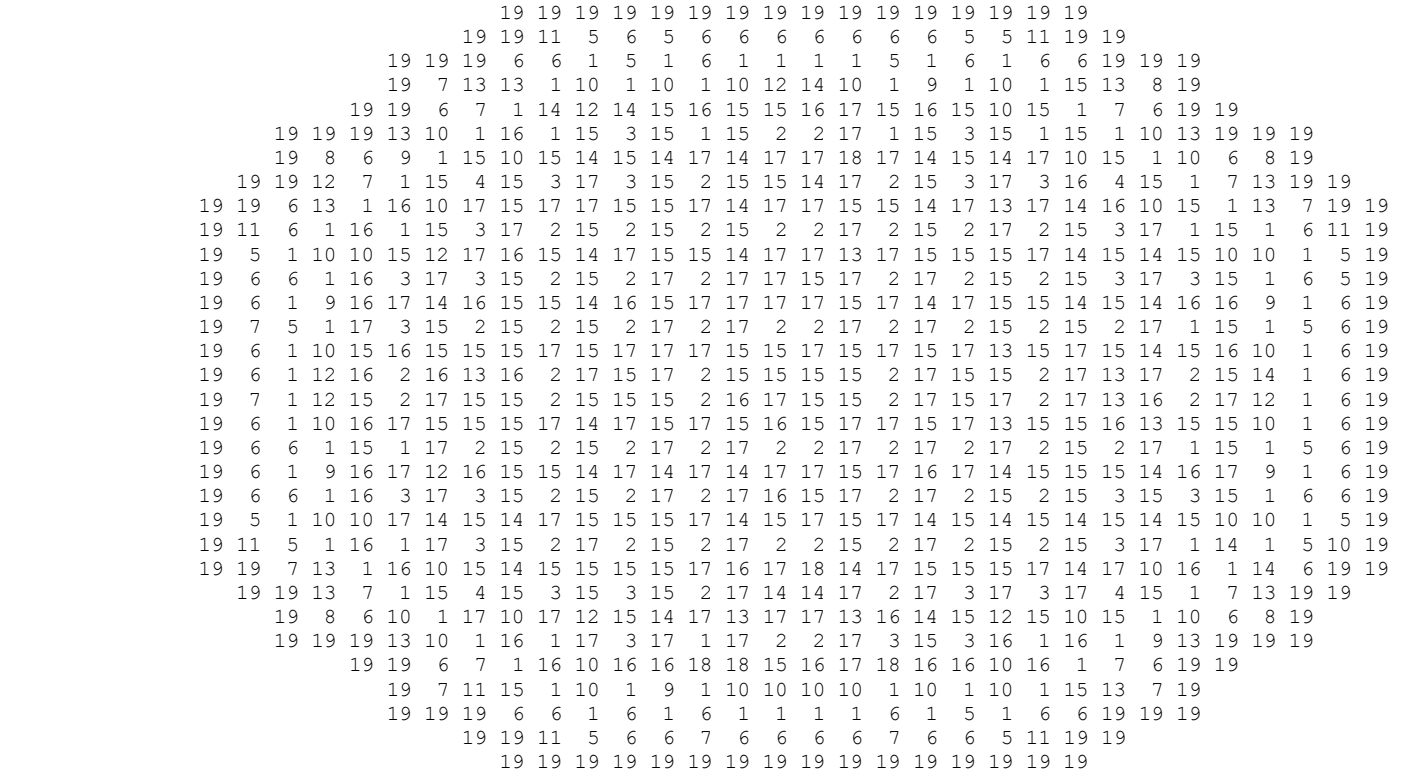

Figure 2-9: Fuel assembly orientation for ADF assignment

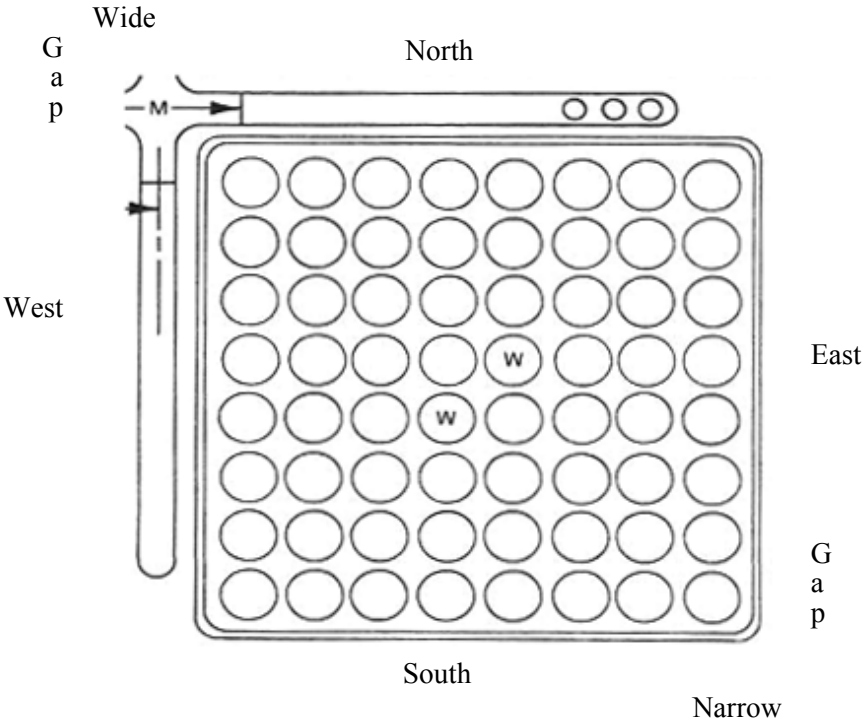

Figure 2-10: Core orificing and TIP system arrangement

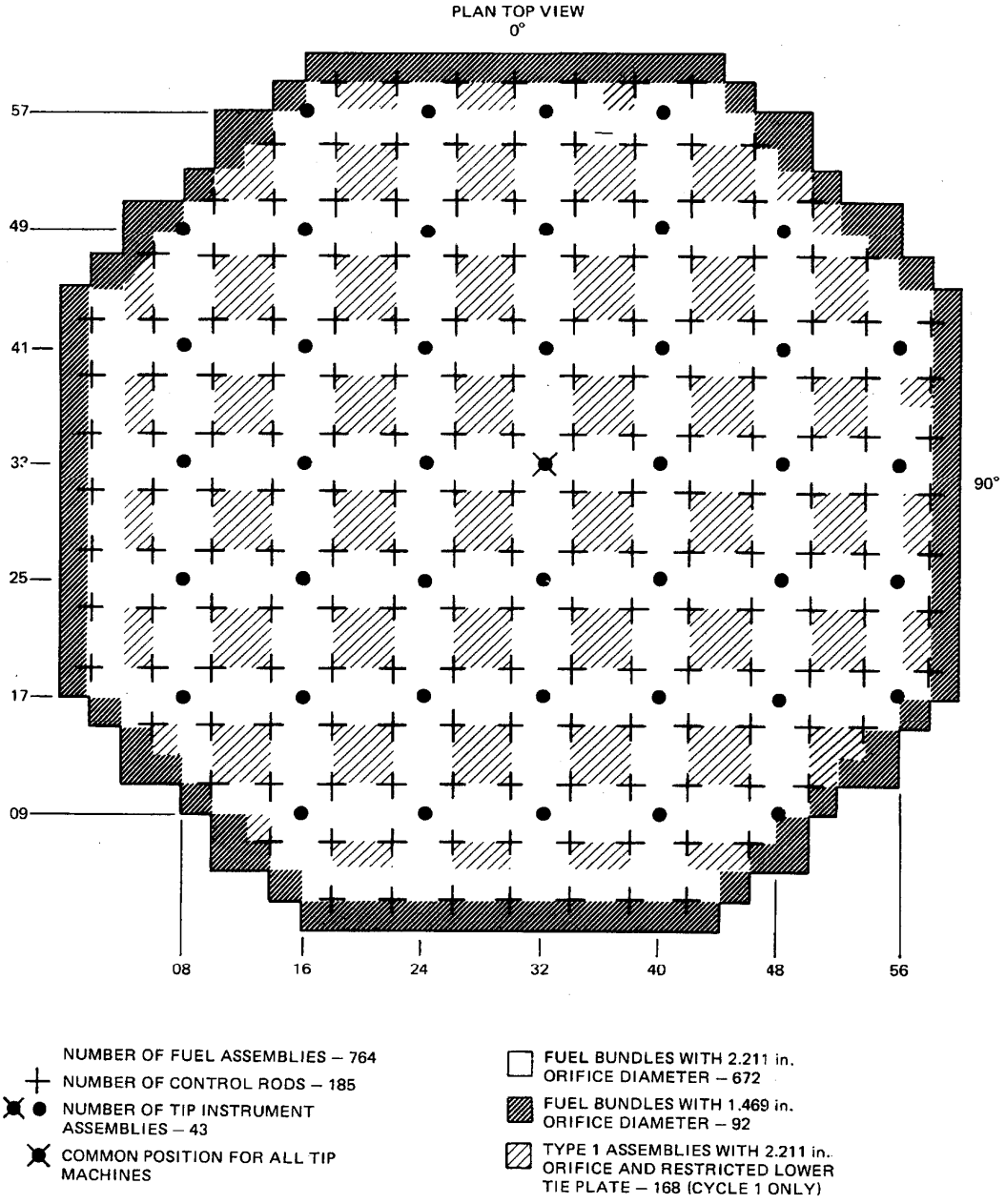

Figure 2-11: Elevation of core components

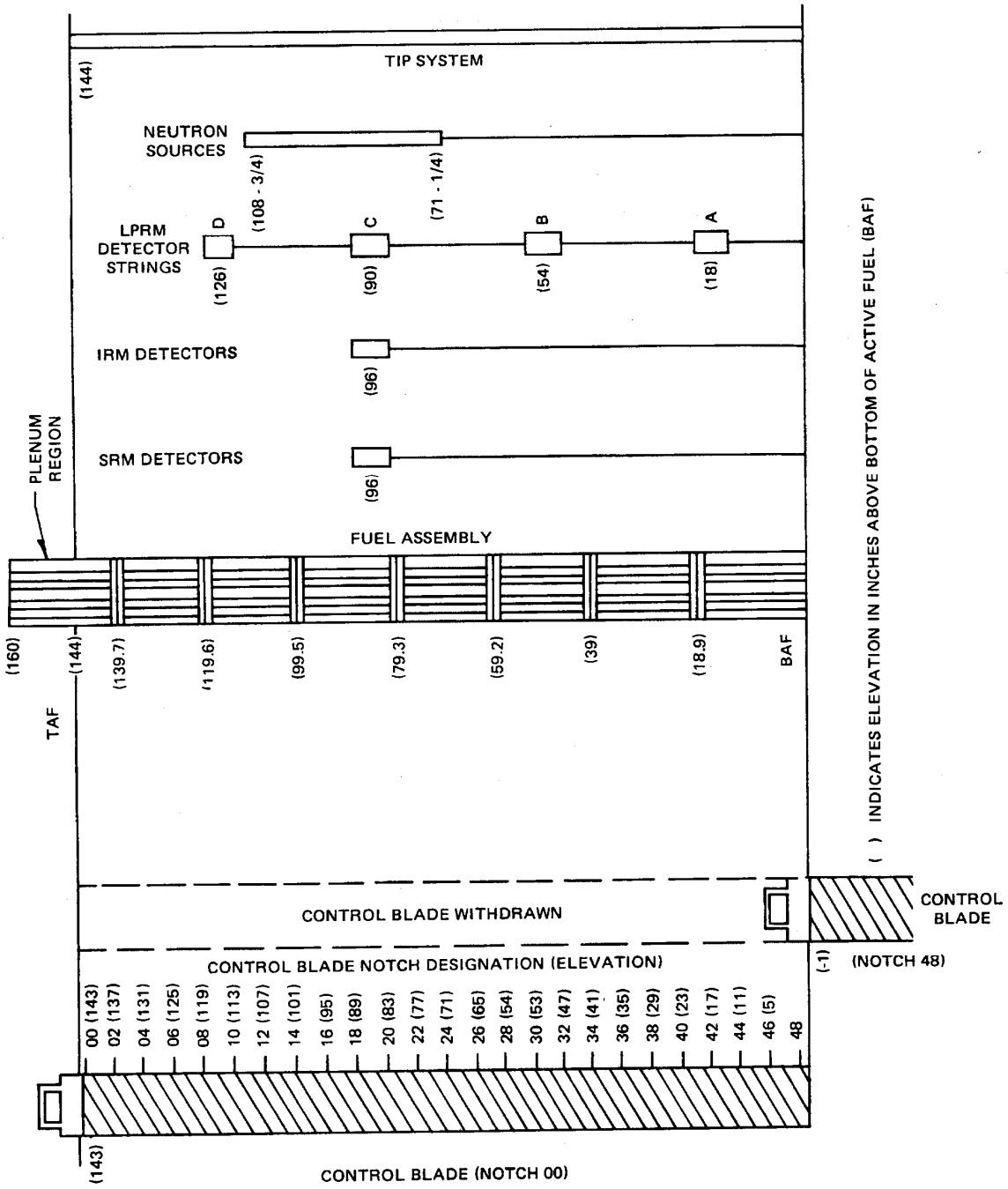

2.3 Thermal-hydraulic data

PB2 is a GE-designed BWR/4 with a rated thermal power of 3 293 MW, a rated core flow of 12 915 kg/s (102.5×10^6 lb/hr), a rated steam flow of 1 685 kg/s (13.37×10^6 lb/hr), and a turbine inlet pressure of 6.65 MPa (965 psia). The nuclear steam supply system (NSSS) has turbine-driven feed pumps and a two-loop M-G driven recirculation system feeding a total of 20 jet pumps. There are a total of four steam lines and each has a flow-limiting nozzle, main steam isolation valves (MSIV), safety relief valves (SRV), and a turbine stop valve (TSV). The steam bypass system consists of nine bypass valves (BPV) mounted on a common header, which is connected to each of the four steam lines.

Figure 2-12 shows PSU thermal-hydraulic radial mapping scheme utilised to represent the PB2 reactor core. The feedback, or coupling, between neutronics and thermal-hydraulics can be characterised by choosing user-supplied mapping schemes (spatial mesh overlays) in the radial and axial core planes. Some of the inlet perturbations (inlet disturbances of both temperature and flow rate) are specified as a fraction of the position across the core inlet. This requires either a 3-D modelling of the vessel, or some type of a multi-channel model. The PSU developed core multi-channel model consisting of 33 channels to represent the 764 fuel assemblies of the PB2 reactor core. The core thermal-hydraulic model was built according to the following criteria. First, the fuel assemblies are ranked according to the inlet orifice characteristics. A second criterion is the fuel assembly type (*e.g.* 7×7 or 8×8). Finally, thermal-hydraulic conditions are also considered (*e.g.* fuel assembly power, mass flow, etc.).

It is recommended that an assembly flow area of 15.535 in^2 (1.0023E^{-02} m^2) for fuel assemblies with 7×7 fuel rod arrays, and 15.5277 in^2 (1.0017E^{-02} m^2) for fuel assemblies with 8×8 fuel rod arrays be used in the core thermal-hydraulic multi-channel models. There are 764 fuel assemblies in the PB2 reactor core. At EOC 2, there are 576 fuel assemblies of 7×7 type, and 188 of the 8×8 type. The radial distribution of assembly types is shown in Figure 2-8 in which the assembly types from 1 to 4 identify a fuel assembly with 8×8 fuel arrays and the assembly types from 5 to 18 identify a fuel assembly with 7×7 fuel rod arrays. The core hydraulic characteristics (*e.g.* core pressure drop) can be found in Carmichael (1978).

Figure 2-12: Reactor core thermal-hydraulic channel radial map

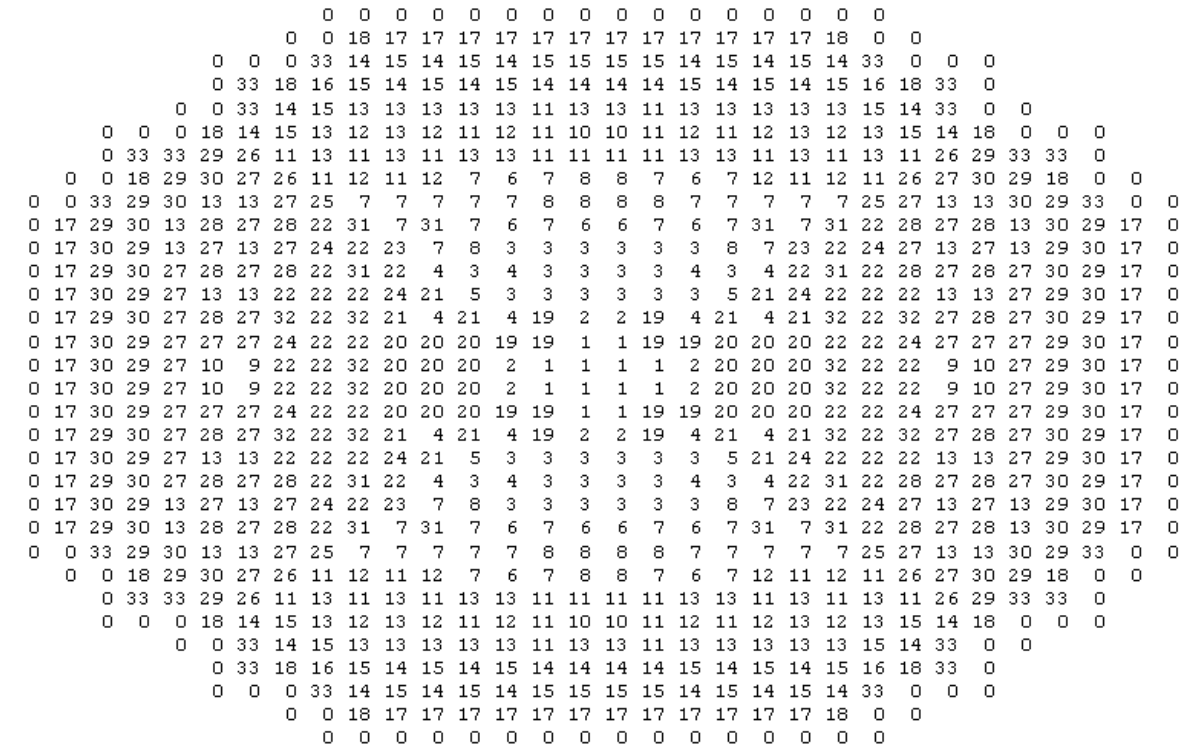

2.4 Initial steady-state conditions

Although HZP results are not asked from the participants for this exercise, hot zero power (HZP) data is provided for the convenience of the participant in the case of clean HZP initialisation is necessary in participant's analysis. The initial conditions for performing PB2 HZP core calculations are chosen as 552.833 K for fuel temperature, 753.9777 kg/m^3 for average coolant density and 32.93 MW for the reactor power (see Table 2-22). The fixed thermal-hydraulic variables should be equally distributed through the whole core. The initial power corresponds to 1% of the PB2 nominal power. Figure 2-13 shows the HZP control rod pattern that should be used for the analysis of this calculation. The initial conditions along with the control rod pattern produce a critical or very near to critical reactor core. A similar control rod grouping approach as shown in Figure 2-13 could be useful to set up the control rod mapping scheme for just two control rod groups.

Table 2-22: PB2 HZP initial conditions

Fuel temperature, K	552.833
Average coolant density, kg/m^3	753.9777
Reactor power, MW	32.93

Figure 2-13: PB2 HZP control rod pattern

(48 – full withdrawn, 0 – full insertion)

	02	06	10	14	18	22	26	30	34	38	42	46	50	54	58
59					0	48	0	48	0	48	0				
55				0	48	0	48	0	48	0	48	0			
51			0	48	0	48	0	48	0	48	0	48	0		
47		0	48	0	48	0	48	0	48	0	48	0	48	0	
43	0	48	0	48	0	48	0	48	0	48	0	48	0	48	0
39	48	0	48	0	48	0	48	0	48	0	48	0	48	0	48
35	0	48	0	48	0	48	0	48	0	48	0	48	0	48	0
31	48	0	48	0	48	0	48	0	48	0	48	0	48	0	48
27	0	48	0	48	0	48	0	48	0	48	0	48	0	48	0
23	48	0	48	0	48	0	48	0	48	0	48	0	48	0	48
19	0	48	0	48	0	48	0	48	0	48	0	48	0	48	0
15		0	48	0	48	0	48	0	48	0	48	0	48	0	
11			0	48	0	48	0	48	0	48	0	48	0		
07				0	48	0	48	0	48	0	48	0			
03					0	48	0	48	0	48	0				

Table 2-23 provides the reactor initial conditions (hot power – HP) for performing steady-state calculations while Figure 2-14 shows the PB2 TT2 initial control rod pattern. TT2 was initiated from steady-state conditions after obtaining P1 edits from the process computer for nuclear and thermal-hydraulic conditions of the core. PB2 was chosen for the turbine trip tests because it is a large BWR/4 with relatively small turbine bypass capacity. During the test, the initial thermal power level was 61.6% of rated (2 030 MW); core flow was 80.9% of rated (10 445 kg/s – 82.9 $\times$ 10^6 lb/hr); and average range power monitor (APRM) scram setting was 95% of nominal power. For the TT2 test, the dynamic measurements were taken with a high-speed digital data acquisition system capable of sampling over 150 signals every 6 milliseconds and the core power distribution measurements were taken from the plant's local in-core flux detectors. Special fast response pressure and differential pressure transducers were installed in parallel with the existing plant instruments in the nuclear steam supply system.

Table 2-23: PB2 TT2 initial conditions from process computer P1 edit

Core thermal power, MWt	2 030
Initial power level, % of rated	61.6
Gross power output, MWe	625.1
Feedwater flow, kg/s	980.26
Reactor pressure, Pa	6 798 470.0
Total core flow, kg/s	10 445.0
Core inlet subcooling, J/kg	48 005.291
Feedwater temperature, K	442.31
Core pressure drop, Pa	113 560.7
Jet-pump driving flow, kg/s	2 871.24
Core average exit quality, fraction	0.097
Core average void fraction, fraction	0.304
Core average power density, kW/l	31.28

Figure 2-14: PB2 HP control rod pattern

(48 – full withdrawn, 0 – full insertion)

	02	06	10	14	18	22	26	30	34	38	42	46	50	54	58
59					48	48	48	48	48	48	48				
55				48	48	34	48	36	48	34	48	48			
51			48	48	0	48	26	48	26	48	0	48	48		
47		48	48	40	48	36	48	32	48	36	48	40	48	48	
43	48	48	0	48	26	48	4	48	4	48	26	48	0	48	48
39	48	34	48	36	48	48	48	48	48	48	48	36	48	34	48
35	48	48	26	48	4	48	32	48	32	48	4	48	26	48	48
31	48	36	48	32	48	48	48	48	48	48	48	32	48	36	48
27	48	48	26	48	4	48	32	48	32	48	4	48	26	48	48
23	48	34	48	36	48	48	48	48	48	48	48	36	48	34	48
19	48	48	0	48	26	48	4	48	4	48	26	48	0	48	48
15		48	48	40	48	36	48	32	48	36	48	40	48	48	
11			48	48	0	48	26	48	26	48	0	48	48		
07				48	48	34	48	36	48	34	48	48			
03					48	48	48	48	48	48	48				

The initial water level above vessel zero (AVZ) is equal to 14.1478 m (557 in). This measured level is the actual level inside the steam dryer shroud. The initial level AVZ is equal to 14.3256 m (564 in) for the narrow range measurement outside steam dryer shroud. AVZ is the lowest interior elevation of the vessel (bottom of lower plenum). Table 2-24 and Figure 2-15 provide the process computer P1 edit for initial core axial relative power distribution.

Table 2-24: PB2 TT2 initial core axial relative power from P1 edit

Axial node number	Axial location (cm)	Relative power
1	7.62	0.308051
2	22.86	0.616103
3	38.10	0.707754
4	53.34	0.773947
5	68.58	0.814681
6	83.82	0.880874
7	99.06	0.972526
8	114.30	1.066723
9	129.54	1.163467
10	144.78	1.260210
11	160.02	1.356953
12	175.26	1.407871
13	190.50	1.412963
14	205.74	1.402779
15	220.98	1.377320
16	236.22	1.328949
17	251.46	1.257664
18	266.70	1.188925
19	281.94	1.122733
20	297.18	1.031081
21	312.42	0.913971
22	327.66	0.763764
23	342.90	0.580460
24	358.14	0.290230

Figure 2-15: PB2 TT2 initial core axial relative power from P1 edit

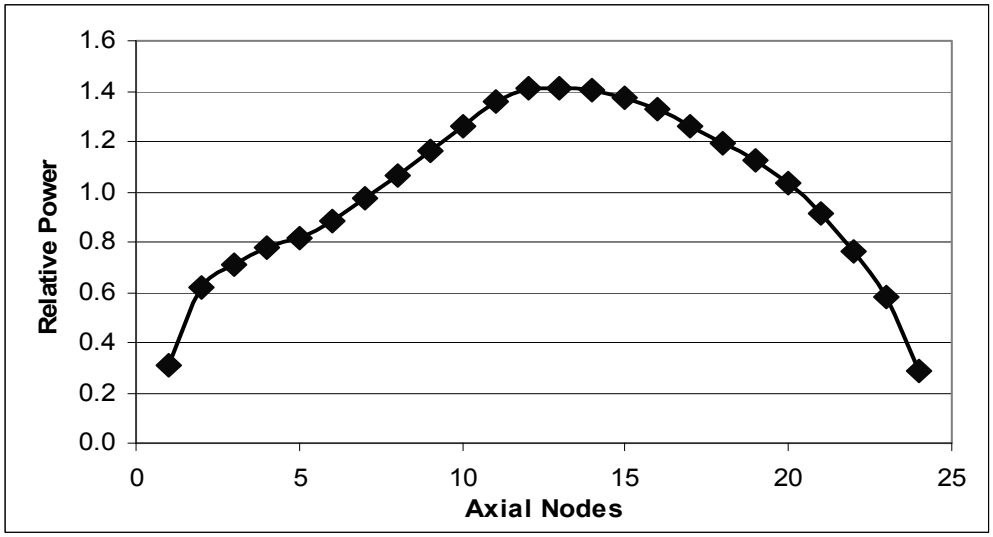

2.5 Transient calculations

During the TT2 test, most of the important phenomena occur in the first five seconds of the transient. Therefore, the test is simulated for five-second time period. This approach simplifies the number of components required for performing the analysis of TT2. Basically, the transient begins with the closure of the TSV. At some point in time, the turbine BPV begins to open. The only boundary conditions imposed in the analysis should be limited to the opening and closure of the above valves. Table 2-25

shows the event timing during the transient. Table 2-26 shows the scram initiation time and the delay time that should be used in Exercise 3 while Table 2-27 shows the average control rod density (CRD) position during reactor scram. An average velocity can be obtained from Table 2-27 for the scram modelling in the 3-D kinetics case. An approximate value obtained from this table is 2.34 ft/s (0.713 m/s) for the first 0.04 seconds and 4.67 ft/s (1.423 m/s) thereafter. Also, it should be noted that during the Exercise 3 best-estimate case, the set points of the SRV are never reached. Table 2-28 summarises the safety relief valve reference design information to be utilised in Extreme Scenarios 1, 2 and 3.

Table 2-25: PB2 TT2 event timing (time in ms)

TSV begins to close	0
TSV closed	96
Begin bypass opening	60
Bypass full-open	846
Turbine pressure initial response	
Steam line A	02
Steam line D	126
Steam line pressure initial response	
Steam line A	348
Steam line D	378
Vessel pressure initial response	432
Core exit pressure initial response	486

Table 2-26: PB2 TT2 scram characteristics

APRM high flux scram set-point, % rated	95 (3128.35 MWt)
Time delay prior to rod motion, msec	120
Time of scram initiation, sec	0.63
Initiates CR insertion, sec	0.75

Table 2-27: CRD position after scram vs. time

Time (sec)	Position (ft)
0.000	0.0000
0.120	0.0000
0.160	0.0935
0.247	0.5000
0.354	1.0000
0.457	1.5000
2.500	10.200
3.080	12.000
5.000	12.000

Table 2-28: Nuclear system safety and relief valves

	Number of valves	Set pressure (psig/Pa)	Capacity at 103% of set pressure (each), (lb/h)/(kg/s)
Relief valves	4	1 105/7.720E06	819 000/103.19
	4	1 115/7.789E06	827 000/104.20
	3	1 125/7.858E06	834 000/105.08
Total*	11 (5)		
Safety valves	2	1 230/8.582E06	939 858/118.40

* The number in parentheses indicates the number of relief valves which serve in the automatic depressurisation capacity.

Chapter 3: Methodologies to quantify the accuracy of the calculations

As mentioned briefly in Chapter 1, participants of Exercise 3 have submitted various results that were available for the statistical analysis. The submitted results can be classified in four types. These are integral parameter values, 1-D distribution, 2-D distributions and time histories. It was decided by the participants in the benchmark that the reference data used in the Exercise 3 comparative analysis is either the available measured data or the so-called averaged data if measured data is not available. The reference averaged data for each requested parameter is based upon the statistical mean (averaged) value of all submitted results.

3.1 Standard techniques for the comparison of results

In Exercise 3, four types of data were analysed and the results of all participants were compared based on this classification. These data types were:

1) integral parameter values;
2) one-dimensional (1-D) axial distributions;
3) two-dimensional (2-D) radial distributions;
4) time history data.

Tables 3-1, 3-2 and 3-3 summarise the submitted data types for Exercise 3 problem conditions and the classifications of these data types.

The statistical methods used in the comparative analysis of Exercise 3 are described in the following subsections.

3.1.1 Integral parameter values

Steady-state k_{eff} values for the initial conditions of TT2 as well as time and value of maximum power results of the participants are analysed as described in this subsection. No statistical comparison is performed for the sequence of events. These values are simply given in the tables of Chapter 4. In the analysis of integral values, there is no need to condition the data by isolating points of interest. Likewise, there are no curves to analyse. Thus, the mean value and standard deviation should be sufficient to facilitate a comparison of the results. Mean value, standard deviation, deviation and figure of merit (FOM) are calculated according to Eqs. (3.1), (3.2), (3.3) and (3.4) respectively:

$$x_{reference} = \frac{\sum_{i}^{N} x_i}{N} \tag{3.1}$$

$$\sigma = \pm\sqrt{\frac{\sum \left(x_i - x_{reference}\right)^2}{N-1}} \tag{3.2}$$

where σ is the standard deviation, x_i is the data submitted by each participant and N is the total number of received results.

The deviation and FOM can be computed as:

$$e_i = x_i - x_{reference} \tag{3.3}$$

$$\Phi_i = \frac{e_i}{\sigma} \tag{3.4}$$

where e_i is the difference between the participant's value and the mean value.

Table 3.1: Exercise 3 parameters for statistical comparisons in steady-state analysis

Case	Submitted data for statistical analysis	Classification
Best estimate	k_{eff}	Integral value
	Core-averaged axial void fraction	1-D distribution
	Normalised axial power	1-D distribution
	Relative power for FA 75	1-D distribution
	Relative power for FA 367	1-D distribution
	Normalised radial power	2-D distribution

Table 3-2: Parameters for statistical comparisons in Exercise 3 transient analysis – best-estimate case

Case	Condition	Submitted data for statistical analysis	Classification
Best estimate	Transient	Sequence of events	Integral values
		Core power	Time history
		Dome pressure	Time history
		Core exit pressure	Time history
		Total core flow rate	Time history
		Total reactivity	Time history
		Doppler reactivity	Time history
		Void reactivity	Time history
		Maximum cladding temperature	Time history
		Radial power peaking factors	Time history
		Power of LPRM-A	Time history
		Power of LPRM-B	Time history
		Power of LPRM-C	Time history
		Power of LPRM-D	Time history
	Snapshot at maximum power	Time of maximum transient power	Integral value
		Value of maximum transient power	Integral value
		Axial power	1-D distribution
		Relative power for fuel assembly 75	1-D distribution
		Relative power for assembly 367	1-D distribution
		Radial power	2-D distribution
	Snapshot at the end of transient	Axial power	1-D distribution
		Relative power for fuel assembly 75	1-D distribution
		Relative power for assembly 367	1-D distribution
		Radial power	2-D distribution

Table 3-3: Parameters for statistical comparisons in Exercise 3 transient analysis – Extreme Scenarios 1, 2, 3 and 4

Case	Condition	Submitted data for statistical analysis	Classification
Extreme scenarios (1-2-3-4)	Transient	Sequence of events	Integral values
		Core power	Time history
		Dome pressure	Time history
		Core exit pressure	Time history
		S/RV pressure*	Time history
		Total reactivity	Time history
		Doppler reactivity	Time history
		Void reactivity	Time history
		Power of LPRM-A	Time history
		Power of LPRM-B	Time history
		Power of LPRM-C	Time history
		Power of LPRM-D	Time history

* S/RV pressure is analysed only for Extreme Scenarios 1, 2 and 3.

3.1.2 One-dimensional (1-D) steady-state axial distributions

Steady-state core average axial void fraction and power distributions are functions of height or number of axial nodes. They can be displayed as an x-y plot. Similar methods of statistical analysis described in the previous section can be applied for each axial cell. Normalised axial power from the steady-state result is compared with the measured data which is also provided in Table 2-15. Other 1-D axial distributions are compared with the average data submitted by the participants. Analyses are performed for each 1-D cell according to Eqs. (3.5), (3.6) and (3.7):

$$\sigma = \pm\sqrt{\frac{\sum \left(x_i - x_{reference}\right)^2}{N-1}} \tag{3.5}$$

where x_i is the each participant's data and N is the total number of received results. FOM is computed as:

$$\Phi_i = \frac{e_i}{\sigma} \tag{3.6}$$

$$e_i = x_i - x_{reference} \tag{3.7}$$

For each participant, a single table is prepared that shows the deviations from mean and FOM at each axial position.

3.1.3 Two-dimensional (2-D) steady-state radial distributions

Exercise 3 also contains the steady-state core radial power distribution. Due to the two-dimensional nature of such data, it is difficult to plot the results as with time history data and 1-D distributions. However, the same statistical methods can be used to generate mean values, standard deviations and participant deviations, and figures of merit.

Mean and standard deviation for each 2-D cell can be computed according to Eqs. (3.1) and (3.2). Such an analysis results in a 2-D map for mean values and standard deviations, rather than a single value for each parameter. Comparisons can thus be made for each cell, rather than only specific cells of interest.

The deviation and FOM can be computed according to Eqs. (3.3) and (3.4) respectively. For each participant, a map will be generated that shows deviations from the mean at each radial position. A second map will report the figures of merit.

3.2 Time histories

Participants were asked to submit various sets of time histories for Exercise 3. Time history data are explicitly described in Tables 3-1 and 3-2. When measured data are not available, the averaged values were used as reference data for the statistical comparison purpose in the comparative analysis of the time histories. The averaged data are calculated according to the equation that follows:

$$x_{reference} = \frac{\sum_{i}^{N} x_i}{N} \tag{3.8}$$

where x_i is the each participant's values for the specified time interval and N is the total number of received results. The comparative analysis of data with time histories requires an advance tool explained in the following subsection.

3.2.1 ACAP analysis

The comparative analysis was performed for code-to-code comparisons using the standard statistical methodology with the Automated Code Assessment Program (ACAP) (Ivanov, 2001). ACAP is a tool developed to provide quantitative comparisons between nuclear reactor systems code results and experimental measurements. This software was developed under a contract between PSU and the NRC for use in the TRACE code consolidation efforts. ACAP's capabilities are described as follows:

- draws upon a mathematical toolkit to compare experimental data and NRS code simulations;
- returns quantitative FOM associated with individual and suite comparisons;
- accommodates the multiple data types encountered in NRS environments;
- incorporates experimental uncertainty in the assessment;
- provides "event windowing" capability;
- accommodates inconsistencies between measured and computed independent variables (*e.g.* different time steps);
- provides a framework for automated, tunable weighting of component measures in the construction of overall FOM accuracy.

ACAP is a PC and UNIX station based application that can be run interactively on PC with Windows 95/98/NT, in batch mode on PC as a WINDOWS console application, or in batch mode on UNIX stations as a command line executable. The D'Auria Fast Fourier Transformation (FFT) and Mean Error (ME) methods were used for the FOM calculations for time histories (Ambrosini, 1990; Kuntz, 1998). Figure 3-1 shows a snapshot of the FOM configuration for ACAP calculations in Exercise 2 of the benchmark. These methods are advanced techniques for analysis of time history data. Eqs. (3.9) through (3.14) represent the theory portion of the D'Auria FFT and ME methods (Ambrosini, 1990).

The Discrete Fourier Transform (DFT) can be calculated as:

$$\hat{\Phi}_m = \frac{1}{N}\sum_{i=1}^{N} \Phi_i e^{-2\pi Imi/N} \tag{3.9}$$

The D'Auria measures are as follows:

- Average Amplitude (AA):

$$AA = \frac{\sum_{m=0}^{M} \left| \hat{P}_m - \hat{O}_m \right|}{\sum_{m=0}^{M} \left| \hat{O}_m \right|} \tag{3.10}$$

- Weighted Frequency (WF):

$$WF = \frac{\sum_{m=0}^{M} \left| \hat{P}_m - \hat{O}_m \right| \bullet f_m}{\sum_{m=0}^{M} \left| \hat{P}_m - \hat{O}_m \right|} \tag{3.11}$$

where N is the number of data values, i is the sample index, Φ_i is the values spaced Δt apart, O_i is the i-th datum in experimental set P_i is the i-th datum in computed set, and f_m is the frequency of mode m.

Figure 3-1: FOM configuration in ACAP

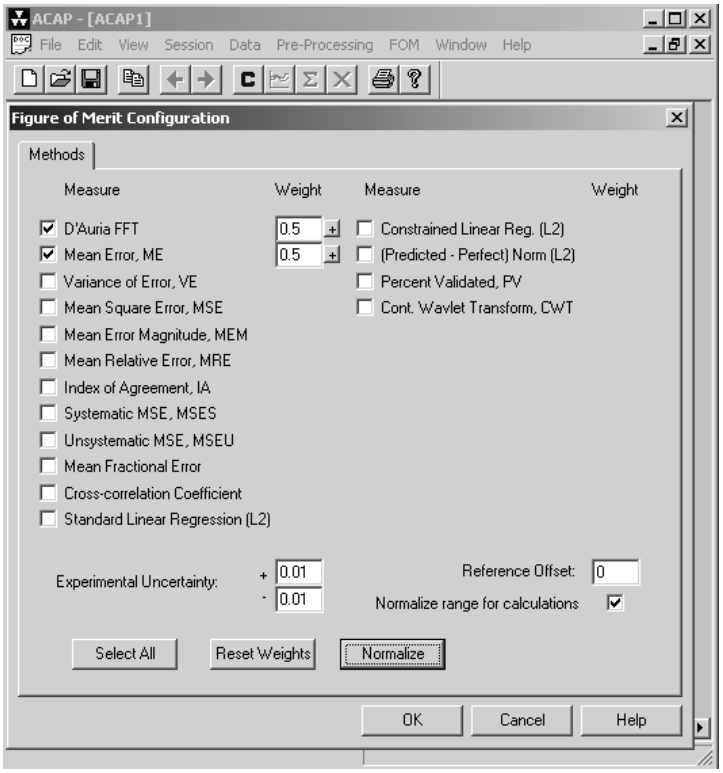

Mean error (ME) can be computed as:

$$ME = \frac{1}{N}\left\{\sum_{i=1}^{N}\left(O_i - P_i\right)\right\} \tag{3.12}$$

The D'Auria and ME FOM equations are outlined below:

$$FOM_{D'AURIA} = \frac{1}{\left(\left[AA^2 + \left(\frac{K}{WF}\right)^2\right]^{1/2} + 1\right)} \tag{3.13}$$

where K is the constant used to weight the relative importance of the weighted frequency (WF) relative to the average amplitude (AA).

$$FOM_{ME} = \frac{1}{\left(|ME| + 1\right)} \tag{3.14}$$

Note that the statistical FOM given by Eqs. (3.3) and (3.6) differs from the FOM calculated using Eqs. (3.13) and (3.14). FOM indicates that the participant results are closer to the reference solution if the former FOM is closer to zero, while the later FOM has to be closer to unity (1) to indicate better agreement.

The following procedure was applied during the ACAP calculation:

Step 1: Data synchronisation was necessary due to the varying time steps of submitted participant data for the time histories. Regarding synchronisation, the cubic spline function was written in Visual Basic for Applications (VBA) and macro module inserted into the Microsoft Excel workbook file (SRS1, 2003). Then, all participants' results were set to a time interval of precisely 6 ms. The inserted module was outlined in Volume I (NEA, 2001).

Step 2: In order to avoid the effects of differing participant initialisation on the comparative analysis, actual values of the time history data were set to zero and they were called "delta changes". The delta changes were calculated by subtraction of initial value (at time zero) from all of other transient values (as shown below where *t* represents time in seconds):

$$\textit{Delta Changes } (t = 0.000) = \textit{Value } (t = 0.000) - \textit{Value } (t = 0.000)$$

$$\textit{Delta Changes } (t = 0.006) = \textit{Value } (t = 0.006) - \textit{Value } (t = 0.000)$$

$$\textit{Delta Changes } (t = 0.012) = \textit{Value } (t = 0.012) - \textit{Value } (t = 0.000)$$

$$\textit{Delta Changes } (t = 0.018) = \textit{Value } (t = 0.018) - \textit{Value } (t = 0.000)$$

$$\textit{Delta Changes } (t = 0.024) = \textit{Value } (t = 0.024) - \textit{Value } (t = 0.000)$$

$$\textit{Delta Changes } (t = 0.030) = \textit{Value } (t = 0.030) - \textit{Value } (t = 0.000)$$

…

and so on.

Step 3: Using ACAP's user-friendly interactive options with the data type explained in the above step, a configuration must be selected and FOM calculation should be performed in accordance with the reference data.

It should also be noted that marker frequencies on the time histories plots were reduced to infrequent intervals in order to visualise participants' data in an elegant way. The following example of an Excel function statement was used for this purpose:

$$=IF(MOD(ROW()-ROW(Sheet3!B\$2),\$E\$1)=0,Sheet3!B4,NA())$$

3.3 Statistical analysis of normalised parameters from transient calculations

In Exercise 3 comparative analysis, some parameters require special attention because under certain circumstances the normalisation will become skewed. These parameters in Exercise 3 are:

- normalised axial power (snapshot) at the time of maximum power;
- relative axial power for fuel assemblies 75 and 367 (snapshot) at the time of maximum power;
- normalised radial power (snapshot) at the time of maximum power;
- normalised axial power (snapshot) at the end of the transient (5 s);
- relative axial power for fuel assemblies 75 and 367 (snapshot) at the end of the transient (5 s);
- normalised radial power (snapshot) at the end of the transient (5 s).

Treating each of these parameters separately, the procedure for generating a comprehensive analysis that preserves the normalisation is discussed in the subsections below.

3.3.1 Two-dimensional (2-D) core-averaged radial power distribution

This parameter is collected for the transient snapshots. The goal of the statistical analysis is to derive an average normalised power for each assembly:

$$\overline{NP}_i = \frac{\overline{p}_i}{\overline{p}_{FA}} \tag{3.15}$$

where, for *N* participants, $\overline{p}_i$, the average power density in radial assembly location i, is:

$$\overline{p}_i = \frac{1}{N}\sum_{j=1}^{N} p_{ij} \tag{3.16}$$

and $\overline{p}_{FA}$, the averaged assembly power density, is:

$$\overline{p}_{FA} = \frac{1}{N}\sum_{j=1}^{N} p_{FA,j} \tag{3.17}$$

Thus:

$$\overline{NP}_i = \frac{\sum_{j=1}^{N} p_{ij}}{\sum_{j=1}^{N} p_{FA,j}} \tag{3.18}$$

In the initial steady-state case the total rated core power is specified as Q = 2 030 MWt so that the average power per fuel assembly is the same for all participants and:

$$\overline{NP}_i = \frac{1}{N}\frac{\sum_{j=1}^{N} p_{ij}}{p_{FA,c}} = \frac{1}{N}\sum_{j=1}^{N}\frac{p_{ij}}{p_{FA,c}} = \frac{1}{N}\sum_{j=1}^{N} NP_{ij} \tag{3.19}$$

where, given that the total number of assemblies, *M*, is 764:

$$p_{FA,c} = \frac{Q}{M} \tag{3.20}$$

Thus, for the transient snapshots, where total power level and power per assembly vary among the participants, the following corrected procedure must be applied:

Step 1: Convert normalised values into absolute values. Absolute values are achieved by multiplying the normalised value in each 2-D cell for each participant by the average power per assembly for the same participant, where the latter value is the total core power for that participant divided by 764 fuel assemblies.

Step 2: Calculate participant-averaged average power per assembly. All participant values for total core power are averaged by the standard averaging technique to get the average core power. This value is divided by the number of fuel assemblies, 764, to get the average power per assembly, averaged over all participants. The same result can be obtained by averaging directly, with Eq. (3.1), all participants' values for average power per assembly.

Step 3: Generate mean solution using absolute values. The map of absolute mean values is generated by the standard averaging procedure.

Step 4: Re-normalise mean solution. Normalisation is attained by dividing each cell of the absolute map by the average power per assembly calculated in Step 2.

Unfortunately, the standard deviation and figure of merit cannot be included in a normalised form, since the meaning of these statistical functions would be lost. Therefore, three maps must be provided instead of the usual two. Mean values and standard deviations are provided using absolute powers, and are accompanied by maps of the normalised mean values. Participant deviations and figures of merit are calculated relative to the absolute mean solution.

3.3.2 One-dimensional (1-D) core-averaged axial power distribution

This parameter is also collected for transient snapshots, and the final specifications require that all participants divide the core into 24 equal axial nodes. Where this is the case, the statistical analysis will be similar to that for the radial power distribution. The normalised mean axial power for a given axial node is given by:

$$\overline{NP}_{z,i} = \frac{\overline{p}_{z,i}}{\overline{p}_z} \tag{3.21}$$

where $\overline{p}_{z,i}$, the average power density at axial layer i, is given by:

$$\overline{p}_{z,i} = \frac{1}{N}\sum_{j=1}^{N} p_{z,ij} \tag{3.22}$$

where $\overline{p}_z$, the core-averaged axial power density, is:

$$\overline{p}_z = \frac{1}{N}\sum_{j=1}^{N} p_{z,j} = \frac{1}{N}\sum_{j=1}^{N} \frac{p_{FA,j}}{24} \tag{3.23}$$

Thus:

$$\overline{NP}_{z,i} = \frac{\sum_{j=1}^{N} p_{z,ij}}{\sum_{j=1}^{N} \frac{p_{FA,j}}{24}} \tag{3.24}$$

For the steady-state cases, where the total core power level, Q, and average power per assembly are constant for all participants:

$$\overline{NP}_{z,i} = \frac{1}{N}\frac{1}{24}\sum_{j=1}^{N} \frac{p_{z,ij}}{p_{FA,j}} = \frac{1}{N}\sum_{j=1}^{N} NP_{z,ij} \tag{3.25}$$

As a result, the standard techniques for 1-D distribution can be applied for the steady-state cases; however, for the transient snapshots, where the average power per assembly will vary among the participants, the following procedure must be utilised:

Step 1: Convert normalised values into absolute values. Absolute values are achieved by multiplying the normalised value in each axial node for each participant by the average power per node in the average assembly for the same participant, where the latter value is the total core power for that participant divided by 764 fuel assemblies and 24 axial nodes.

Step 2: Calculate participant-averaged average power per assembly. All participant values for total core power are averaged by the standard averaging technique to get the average core power. This value is divided by the number of fuel assemblies, 764, to get the average power per assembly, which is finally divided by 24 to get the average power per axial node, averaged over all participants. The same result can be obtained by averaging directly all participants' values for average power per axial node using Eq. (3.1).

Step 3: *Generate mean solution using absolute values*. The table of absolute mean values is generated by the standard averaging procedure.

Step 4: *Re-normalise mean solution*. Normalisation is attained by dividing each cell of the absolute map by the average power per node calculated in Step 2.

Once again, the standard deviation and figure of merit cannot be included in a normalised form and two axial tables will be provided. Absolute mean values and standard deviations are provided along with re-normalised mean values in one table. Participant deviations and figures of merit, calculated relative to the absolute values, are presented in a second table. It should be noted that this procedure can be applied only where the participants have used 24 equal axial layers. Results from participants who do not adhere to this specification must first have their data converted to 24 equal nodes via a cell-volume weighting procedure.

3.3.3 One-dimensional (1-D) relative power distributions for FA 75 and 367

For maximum power before scram and at the end of transient snapshot cases, one-dimensional relative power distributions are collected for the fuel assemblies 75 and 367. It is treated in a similar manner as for the core-averaged axial power. Again, the specifications request that the fuel assembly be divided into 24 equal nodes. For the transient snapshots, the power in the assemblies 75 and 367 varies among the participants and the average normalised power per node is given by:

$$\overline{NP}_{z,i} = \frac{\sum_{j=1}^{N} p_{z,ij}}{\sum_{j=1}^{N} \frac{p_{FA,j}}{24}} \tag{3.26}$$

where the total power in fuel assemblies 75 and 367 can be extracted from each participant's 2-D core-averaged radial power distribution. The following method must be applied in every transient case:

Step 1: Convert normalised values into absolute values. The absolute values are found by multiplying the normalised value in each axial node for each participant by the average power per 3-D node in the core for the same participant, where the latter value is the total core power divided by 764 assemblies and 24 axial nodes.

Step 2: Calculate participant-averaged average power per assembly. All participant values for total core power are averaged by the standard averaging technique to get the average core power. This value is divided by the number of cells in the core – 764 assemblies times 24 axial layers – to get the average power per 3-D node, averaged over all participants.

Step 3: Generate mean solution using absolute values. The map of absolute mean values is generated by the standard averaging procedure.

Step 4: Re-normalise mean solution. Normalisation is attained by dividing each cell of the absolute map by the average power per node calculated in Step 2.

As with the previous two parameters, the results are reported in the form of mean values and standard deviations of the absolute values along with a re-normalised mean solution. Participant deviations and figures of merit are again calculated relative to the absolute mean solution

3.4 Multiple code dependencies

It has been noted that some sets of results that have been submitted for this exercise are not fully independent of each other. That is, certain participants have submitted multiple sets from codes that differ from each other to varying degrees. In some cases, the differences are significant, and involve quite different kinetics models. In other cases, the differences are subtler. In the case of codes with only subtle differences, it may not be appropriate to treat the results as fully separate, and therefore subject to independent treatment in the averaging techniques described above.

To account for this circumstance, a two-step averaging process has been developed whereby sets of results that are determined to be "dependent" on each other are first averaged together, and the subsequent mean participant values are then included in the final averaging process. However, after examining the descriptions of each code that has been used in developing the submitted results, it was determined that such a two-step averaging process is not necessary in the present case, and it has not been applied.

Chapter 4: Results and discussion

The results presented in this chapter demonstrate the importance of the coupled neutronic/ thermal-hydraulics core modelling as well as coupled core/plant system simulation for analysis of pressure transients for BWR, which are dynamically complex events. The tables and figures presented in this chapter provide comparisons of the participants' results with the reference solutions. In the case when measured plant data (designated "measured") for TT2 is not available as a reference solution, the results are compared with an average of the results of the benchmark participants (designated "average"). In addition, discussions of observed agreement or disagreement of the participants' results with reference solutions are also provided in this chapter. The objective of the systematic approach applied to the comparative analyses given in this chapter is to help participants in assessing the capability of their codes for the simulation of complex transients with coupled core-system interactions.

It should be reiterated that Exercise 3 comprises the best-estimate coupled 3-D core/ thermal-hydraulic system modelling. This exercise combines elements of the first two exercises of this benchmark and is an analysis of the transient in its entirety. The participants in Exercise 3 are required to provide steady-state and transient results for a best-estimate case and four different extreme scenarios. For the transient analysis of the best-estimate case, in addition to time histories, the participants are also asked to submit results for two snapshots of the transient: one is at the time of maximum power, and the other is at the end of the transient. The outline of comparative analyses presented in this chapter is as follows:

- Steady-state results.
- Transient results:
  - Best-estimate case;
  - Extreme Scenario 1;
  - Extreme Scenario 2;
  - Extreme Scenario 3;
  - Extreme Scenario 4.

The comparisons shown in this chapter are made for the parameters that have an important effect on the steady-state and the transient analysis. Statistical data analysis is performed for each submitted parameter based on the methodology described in Chapter 3. The tables show values of the standard deviation and the figure of merit for each participant's result for a given parameter. The figures included in this chapter show the scatter of data about the reference solution.

The complete set of reference results with associated standard deviations is given in Appendix C while the complete set of the deviations of submitted results for all parameters from the reference solutions for each participant is given in Appendix D. This appendix is divided into four parts: D.1 for integral parameters, D.2 for one-dimensional (1-D) axial distributions, D.3 for two-dimensional (2-D) radial distributions and D.4 for system and core-averaged time histories. It should be noted that Appendices C and D are only available in electronic format on a CD-ROM that is available upon request.

4.1 Steady-state results

Participants are asked to submit the following parameters for steady-state analysis:

- k_{eff};
- core-averaged axial void fraction distribution;
- core-averaged normalised axial power distribution;
- relative power distributions for fuel assemblies 75 (rodded bundle) and 367 (unrodded bundle) – with numbering of the 2-D core fuel region map performed from top to bottom and from left to right;
- radial power distribution – two-dimensional assembly normalised power distribution.

Table 4-1 presents the number of channels utilised in the thermal-hydraulics core models of the participants and the type of power model used in their calculations. This information should be taken into account during the discussion of the participants' deviations from the reference solutions. The term "total" in the table refers to the total power, which includes power from decay heat and fission power together. Participants results presented in the figures are divided into two groups (Group 1 and Group 2) in order to visualise them clearly.

Hot power (HP) steady state refers to the initial conditions of turbine trip test at the EOC 2. The results of this section should be considered together with Table 4-2. Core bypass flow density correction, xenon correction and BWR-type ADF and ADF rotation models are important for the HP results while the decay heat modelling is important for the transient. In particular, the utilisation of ADF is important for k_{eff} values and radial power distribution predictions, and the core bypass flow density correction affects the axial power distributions.

Figure 4-1 presents a graphical comparison of participants' k_{eff} predictions with the mean value as a reference value while Table 4-3 provides k_{eff} values with the mean and standard deviation. The maximum deviated result can be found to be less then 2σ, which also shows a good agreement of all of the participants' results with the reference (mean) solution.

The most challenging part of the BWR steady-state analysis is the prediction of the void fraction distribution. Participants' core-averaged axial void fraction distribution results are given in two figures, Figure 4-2 and Figure 4-3 while the mean and standard deviation are given in Figure 4-4. In principal the core-averaged void fraction distribution results are in good agreement; however, PSI-A and PSI-B deviate noticeably at the lower part of the core. From Figure 4-4 it can be seen that the standard deviation increases in the lower (bottom) part of the core, which indicates differences in the void modelling in terms of sub-cooled boiling and vapour slip. Subsequently these deviations are propagated in the axial power profile predictions due to the void feedback mechanism – see Figures 4-5, 4-6 and Figure 4-7. The axial power profile predictions are also affected by utilisation (or not) of core bypass flow density correction.

The comparisons of participants' relative axial power profile solutions for fuel assemblies 75 and 367 are given in Figures 4-8 through 4-13, and they show more pronounced deviations as compared to the core average axial power profile results. This is especially valid for the rodded bundle 75. The reason for such increased deviations are that at HP conditions the number of T-H channels and spatial mesh overlays with neutronics core model effect the local power predictions. The mean and standard deviation of radial power distribution at HP are given in Figures 4-14 and Figure 4-15. In addition to utilisation or not of ADF the coupling spatial mesh overlays also affect the radial power distribution predictions at HP. The utilisation or not of the xenon correction also contributes to observed deviations. The mean values and standard deviations of the submitted results can be found in Appendix C and the deviations of each participant's prediction from the mean solution can be found in Appendix D.

Table 4-1: Number of channels used and power submitted by the participants – best-estimate case

Participant	Number of channels	Power submitted
CEA-33	33	Fission
CEA-764	764	Fission
FANP	33	Fission
FZD	764	Total
GRS	33	Fission
NFI	33	Total
NUPEC	33	Fission
PSI	34	Fission
PSU/PURDUE/NRC	33	Total
TEPSYS	33	Total
UPISA	33	Total
UPV-1 (MODKIN)	33	Total
UPV-2 (NOKIN)	33	Total
WESTINGHOUSE	764	Total

Table 4-2: Models used at initial HP steady state

Participant	Xenon	ADF	Bypass	Decay
CEA-33	No	No	Yes	No
CEA-764	No	No	Yes	No
FANP	Yes	Yes	Yes	Yes
FZD	Yes	Yes	Yes	Yes
GRS	Yes	No	Yes	Yes
NFI	Yes	No	Yes	No
NUPEC	Yes	Yes	No	Yes
PSI	Yes	Yes	Yes	No
PSU/PURDUE/NRC	Yes	Yes	Yes	Yes
TEPSYS	Yes	Yes	Yes	Yes
UPISA	No	Yes	Yes	Yes
UPV-1 (MODKIN)	Yes	Yes	Yes	Yes
UPV-2 (NOKIN)	Yes	Yes	Yes	Yes
WESTINGHOUSE	No	Yes	Yes	Yes

Figure 4-1: Steady-state k_{eff}

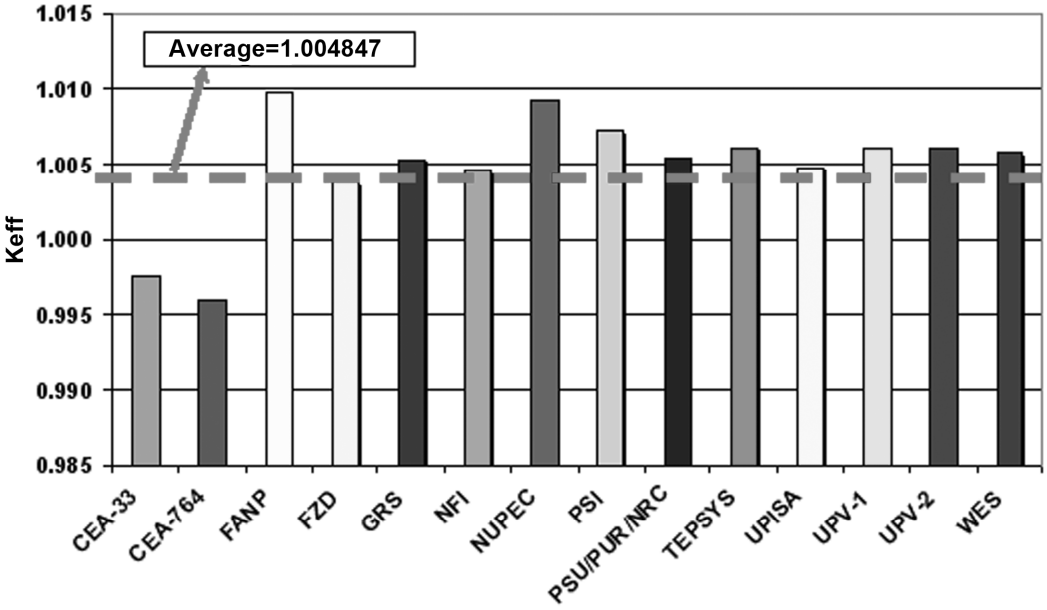

Table 4-3: Steady-state k_{eff}

Participant	k_{eff}	Deviation (e_i)
CEA-33	0.997665	-0.007182
CEA-764	0.995907	-0.008940
FANP	1.009760	0.004913
FZD	1.003710	-0.001137
GRS	1.005330	0.000483
NFI	1.004620	-0.000227
NUPEC	1.009200	0.004353
PSI	1.007259	0.002412
PSU/PUR/NRC	1.005452	0.000605
TEPSYS	1.006113	0.001266
UPISA	1.004856	0.000009
UPV-1	1.006087	0.001240
UPV-2	1.006085	0.001239
WES	1.005810	0.000963
AVERAGE =	**1.004847**	
Standard deviation (σ) =	**0.003802**	

Figure 4-2: Steady-state core average axial void fraction distribution (Group 1)

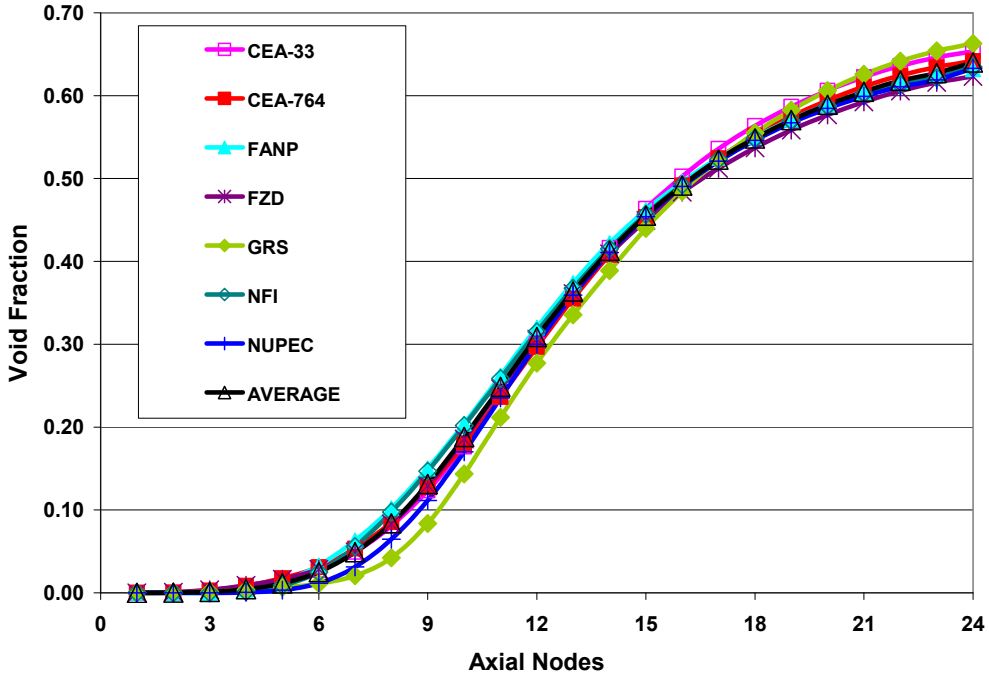

Figure 4-3: Steady-state core average axial void fraction distribution (Group 2)

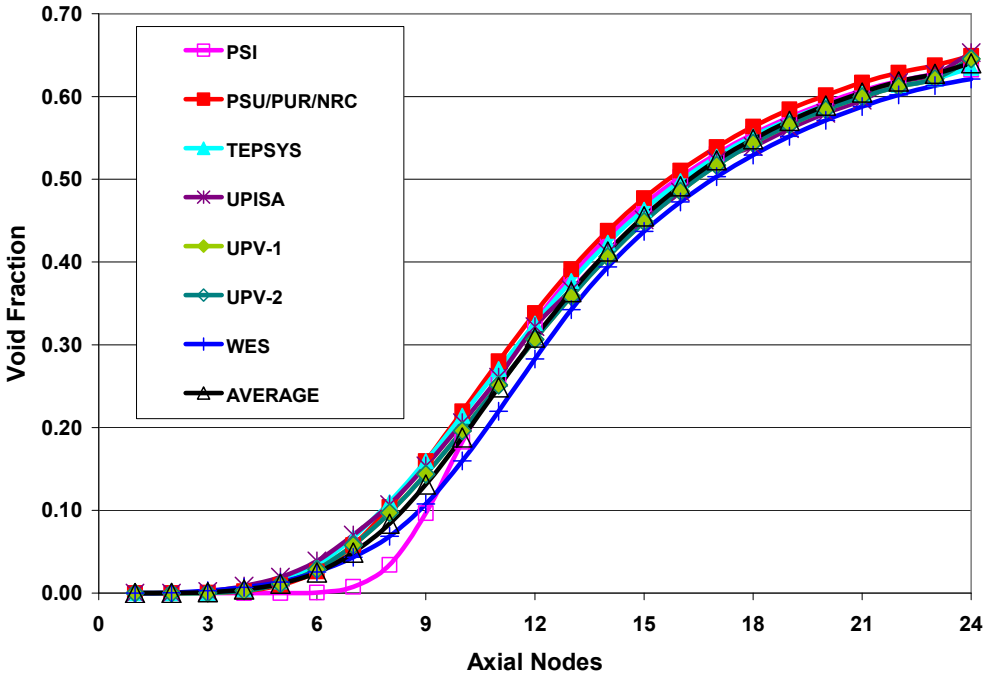

Figure 4-4: Steady-state core average axial void fraction (mean and standard deviation)

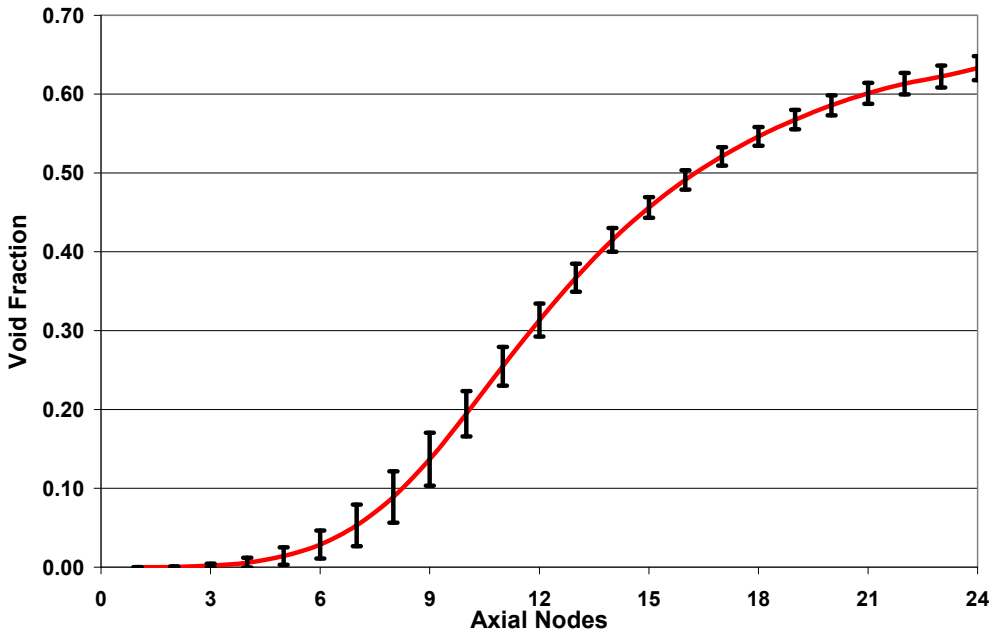

Figure 4-5: Steady-state core average normalised axial power distribution (Group 1)

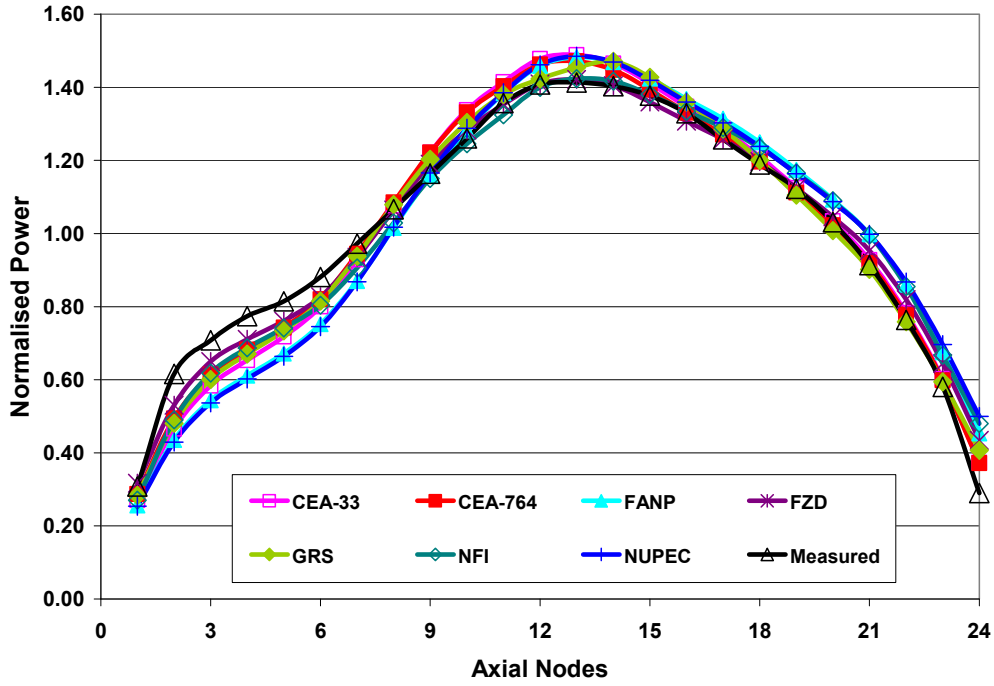

Figure 4-6: Steady-state core average normalised axial power distribution (Group 2)

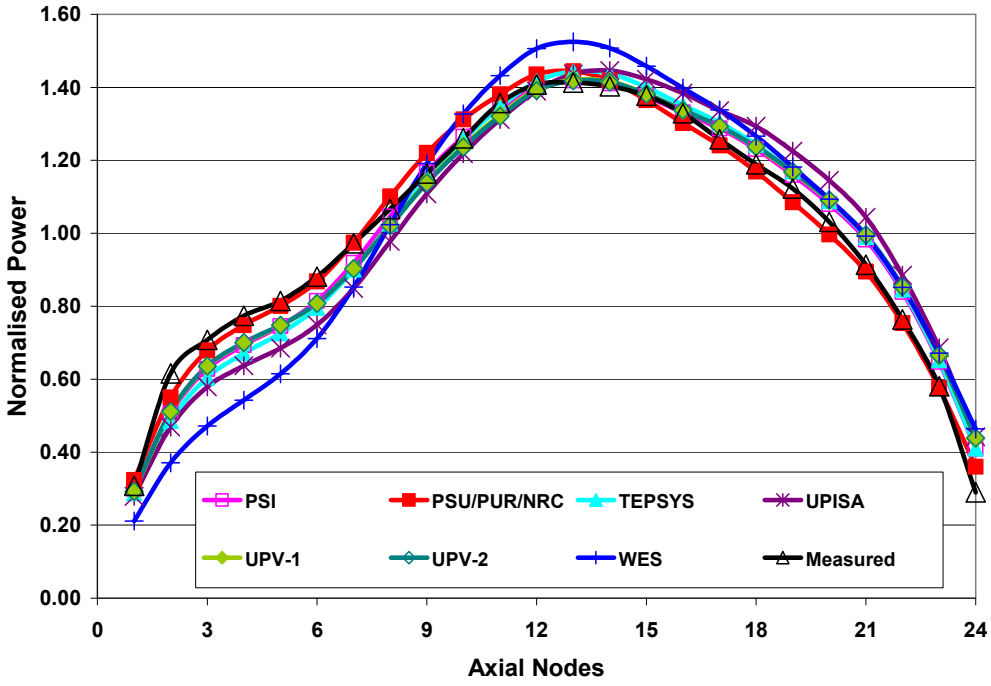

Figure 4-7: Steady-state core average normalised axial power distribution (measured vs. mean and standard deviations)

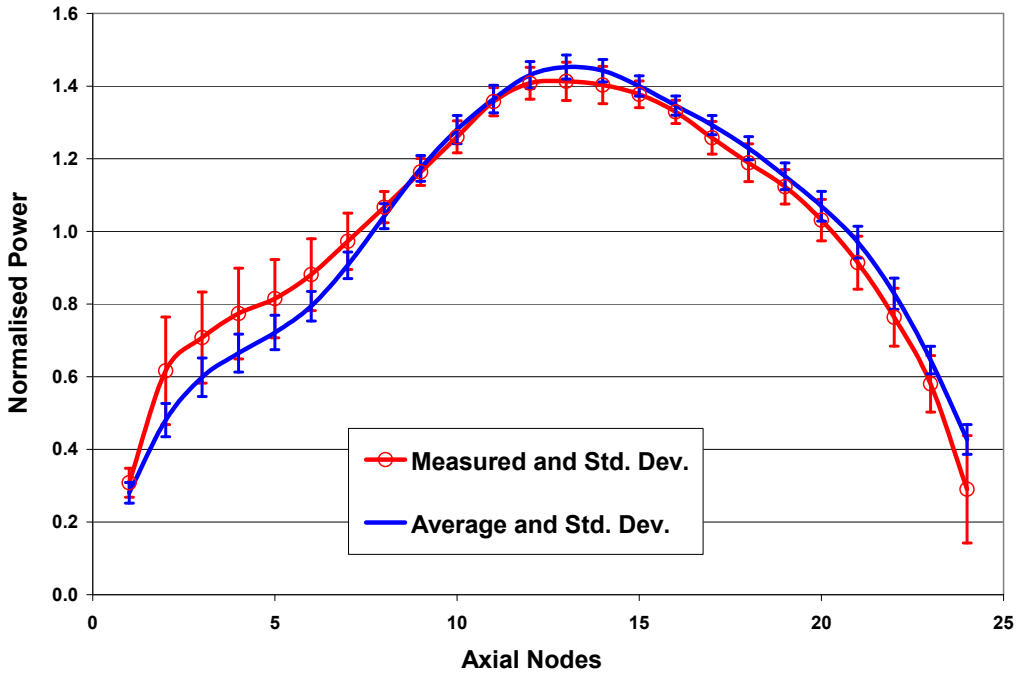

Figure 4-8: Steady-state axial power distribution for FA 75 (Group 1)

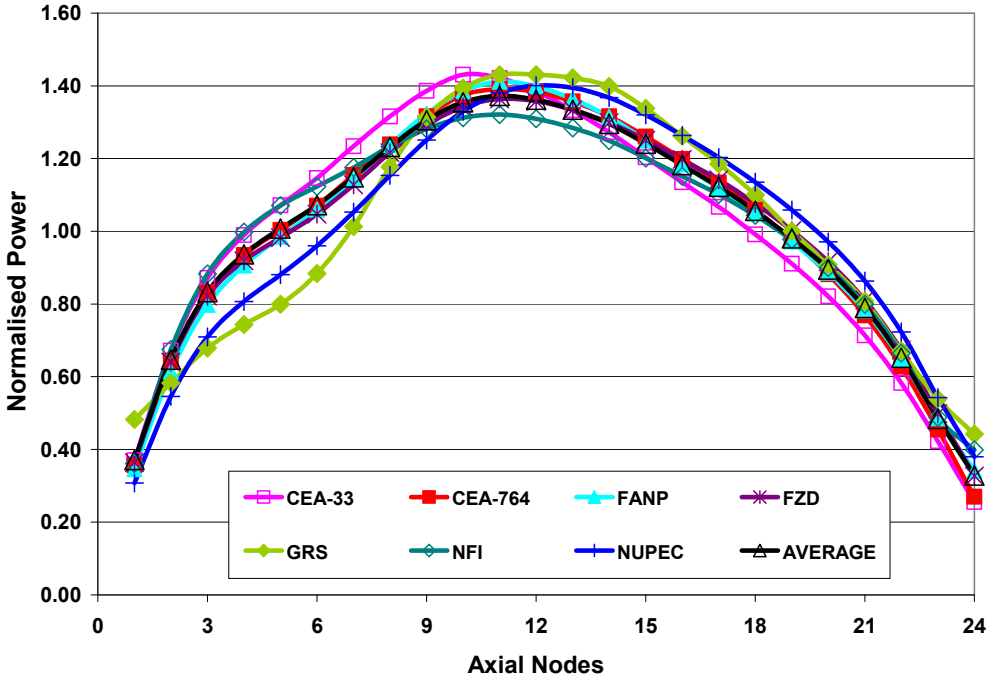

Figure 4-9: Steady-state axial power distribution for FA 75 (Group 2)

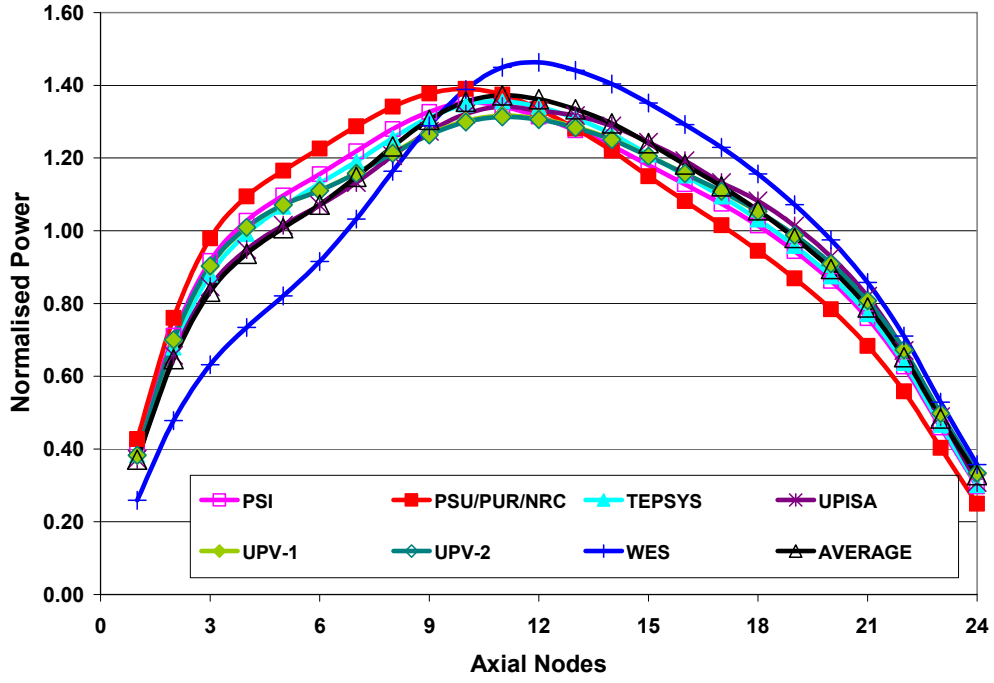

Figure 4-10: Steady-state axial power distribution for FA 75 (mean and standard deviation)

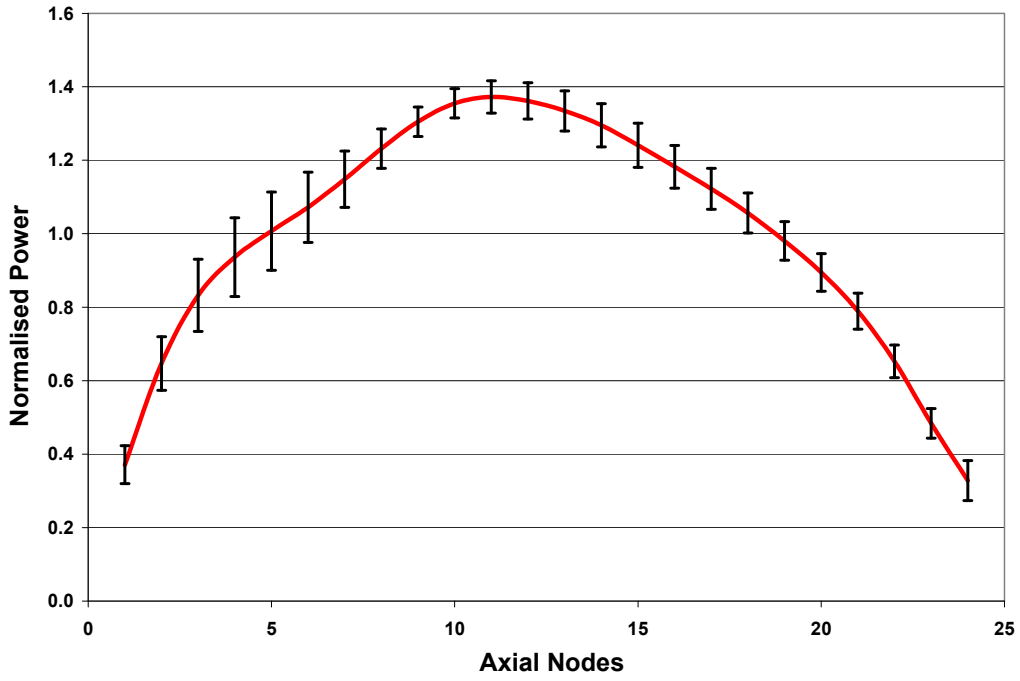

Figure 4-11: Steady-state axial power distribution for FA 367 (Group 1)

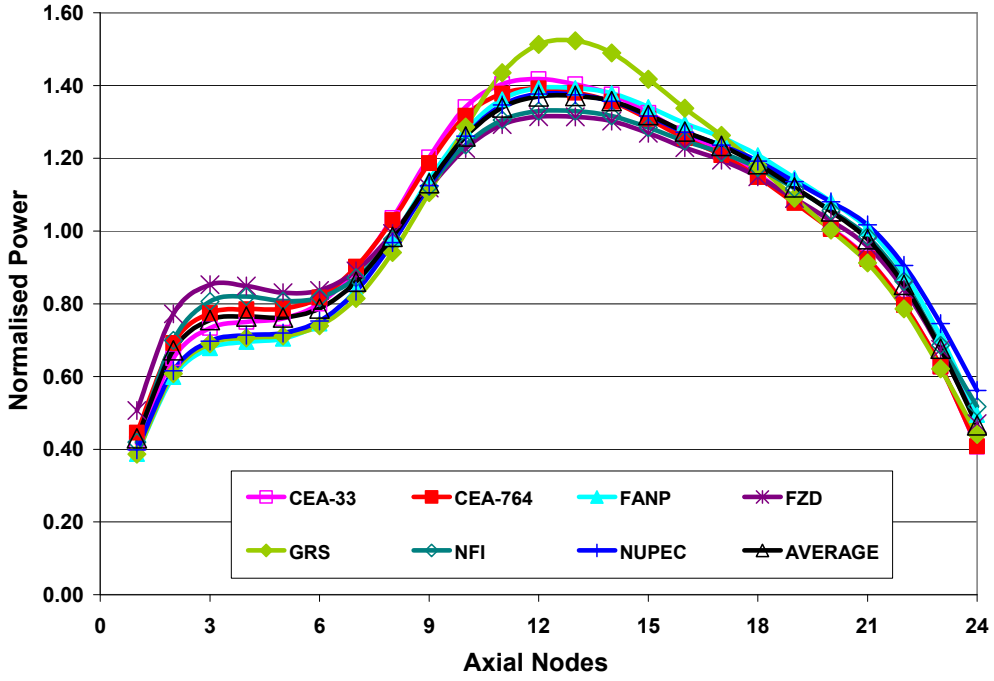

Figure 4-12: Steady-state axial power distribution for FA 367 (Group 2)

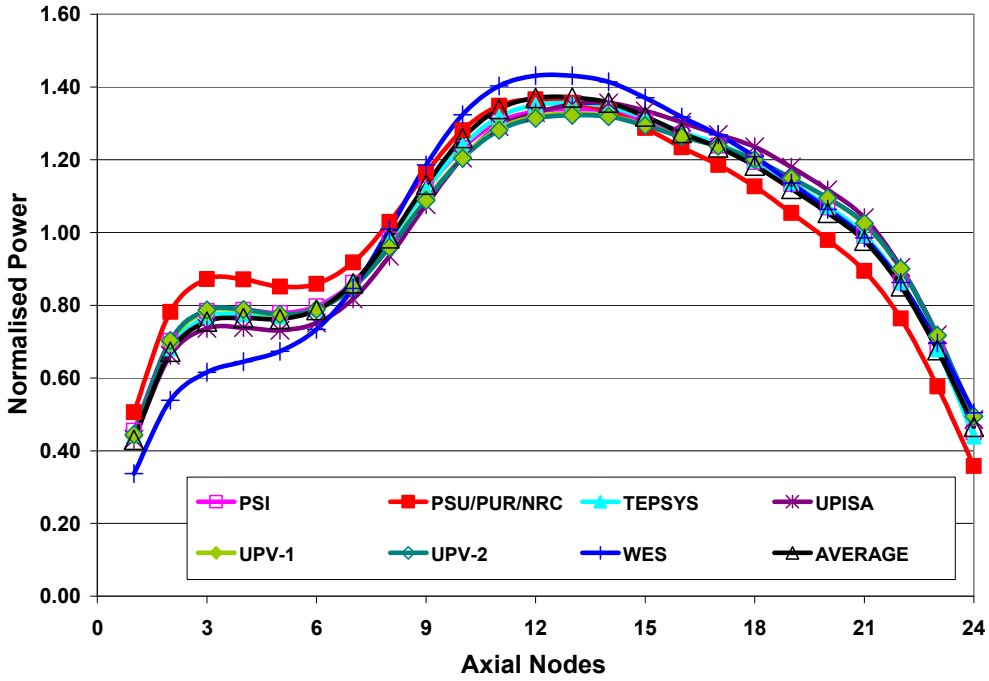

Figure 4-13: Steady-state axial power distribution for FA 367 (mean and standard deviation)

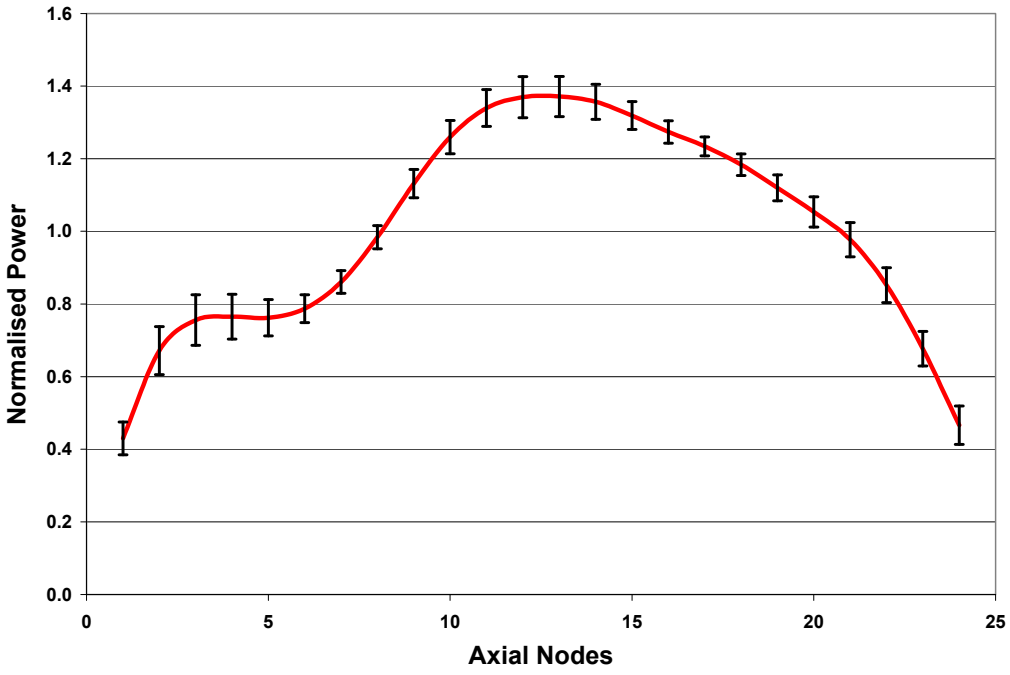

Figure 4-14: Steady-state radial power distribution (average of participants)

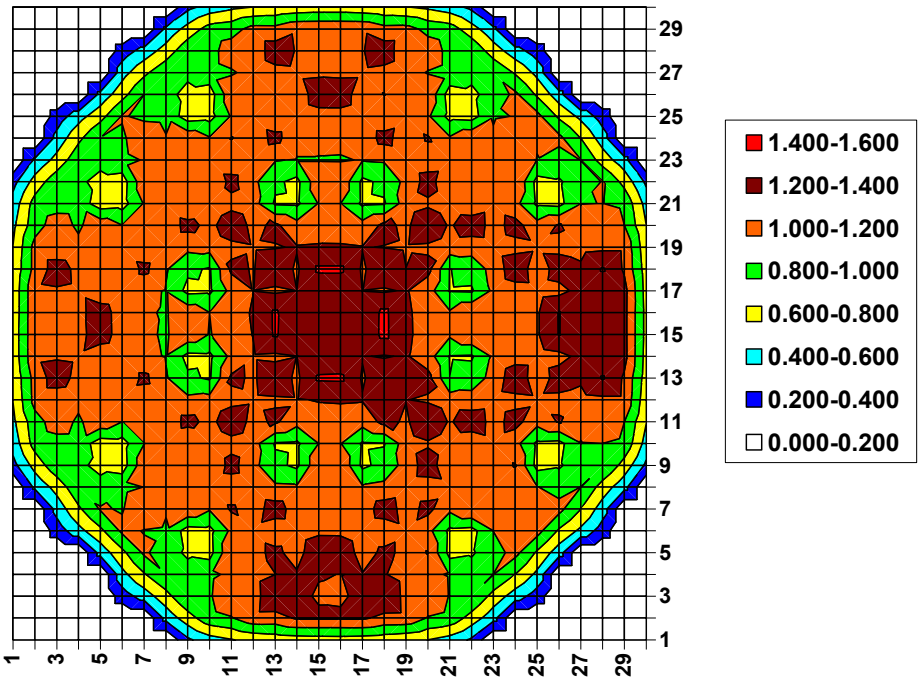

Figure 4-15: Standard deviation of steady-state radial power distribution

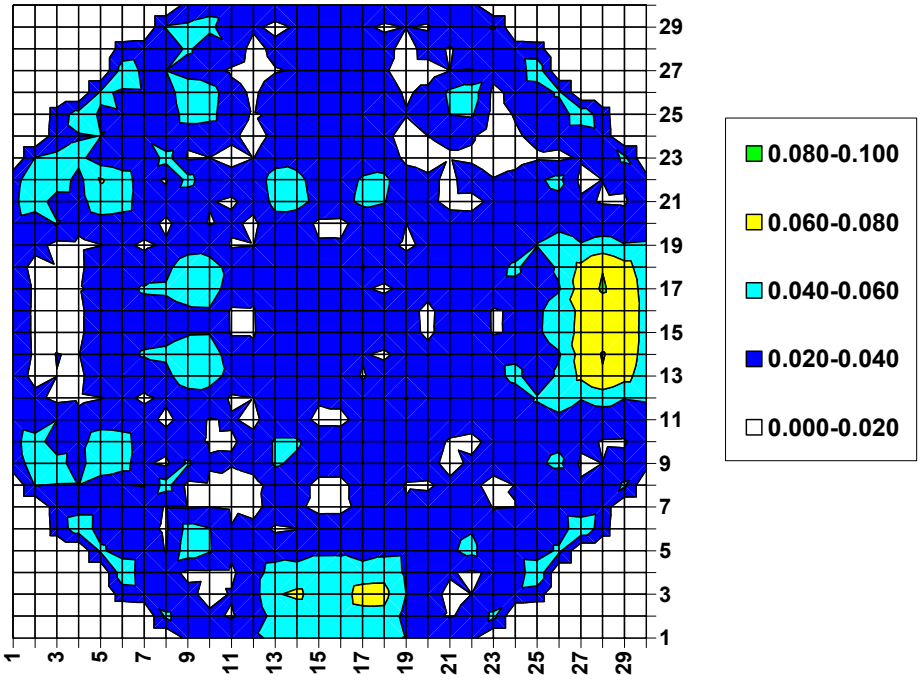

4.2 Transient results of best-estimate case

Exercise 3 best-estimate transient scenario results are presented in this subsection in three groups (parts): core-averaged time histories, snapshot at the time of maximum power, and snapshot at the end of the 5 s transient. Participants are asked to submit the following parameters for each relevant part:

- Time histories:
  - core power;
  - dome pressure;
  - core exit pressure;
  - total core flow rate;
  - total reactivity;
  - Doppler reactivity;
  - void reactivity;
  - maximum cladding temperature;
  - radial power peaking factors;
  - power of LPRM-A;
  - power of LPRM-B;
  - power of LPRM-C;
  - power of LPRM-D.
- Snapshot at the time of maximum transient power:
  - time of maximum transient power;
  - value of maximum transient power;
  - axial power distribution;
  - relative power distribution for FA 75;
  - Relative power distribution for FA 367;
  - radial power distribution.
- Snapshot at the end of the transient:
  - axial power distribution;
  - relative power distribution for FA 75;
  - relative power distribution for FA 367;
  - radial power distribution.

Table 4-1, which presents the number of channels utilised in the thermal-hydraulics core models of the participants and the type of power model used in their calculations of the best-estimate case, should be referred to once again. The information in the table should be taken into account during the discussion of the participants' deviations from the reference solutions. The term "total" in the table refers to the total power, which includes power from decay heat and fission power combined. Participants' results presented in the figures are divided into two groups (Group 1 and Group 2) in order to visualise them clearly.

Participants' sequences of events in the best-estimate scenario are given in Table 4-4.

Table 4-4: Sequence of events in best-estimate case

Participant	Event* (msec)				
	TSVC	BVBO	BVFO	DPIR	CEPIR
CEA-33	0.096	0.060	0.846	0.390	0.384
CEA-764	0.096	0.060	0.846	0.390	0.384
FANP	0.096	0.060	0.846	0.396	0.390
FZD	0.096	0.060	0.846	0.378	0.390
GRS	0.096	0.060	0.846	0.372	0.378
NFI	0.096	0.060	0.846	0.402	0.408
NUPEC	0.096	0.060	0.846	0.438	0.456
PSI	0.096	0.060	0.852	0.438	0.444
PSU/PURDUE/NRC	0.096	0.060	0.846	0.408	0.372
TEPSYS	0.096	0.060	0.852	0.366	0.366
UPISA	0.096	0.060	0.846	0.348	0.324
UPV-1 (MODKIN)	0.000	0.060	0.950	0.390	0.402
UPV-2 (NOKIN)	0.000	0.060	0.950	0.390	0.402
WESTINGHOUSE	0.090	0.066	0.846	0.402	0.450

* Description of the events: TSVC – turbine stop valve closed, BVBO – bypass valve begins opening, BVFO – bypass valve full open, DPIR – vessel dome pressure initial response (0.78% increased over initial value), CEPIR – core exit pressure initial response (0.27% increased over initial value).

4.2.1 Time histories (best-estimate case)

Transient analyses of the best-estimate scenario involve coupled 3-D core/thermal-hydraulic system modelling. It combines elements of the first two exercises of this benchmark and is an analysis of the transient in its entirety. The purpose of the Exercise 3 best-estimate case is to provide a comprehensive assessment of the participating coupled codes in analysing complex transient pressurisation events in which the coupling between core space-dependent neutronics phenomena and system dynamics plays an important role. The simulated transient and the comparison of submitted results, presented in this section, not only provide an opportunity to understand the core reactivity feedback phenomena during a turbine trip transient but also allow for a comprehensive testing of the coupled core/plant system models concerning the pressure wave propagation through steam line, vessel, core and separators.

The plots and tables given in this section provide a comparison of the participants' results for the parameters that have the greatest effect on the Exercise 3 analysis. For this reason core (averaged and local) and system time histories were requested from the participants to be submitted. These histories are: core averaged (core power, total reactivity, Doppler reactivity and void reactivity), core local (maximum cladding temperature, radial power peaking factors, and powers of LPRM A, B, C and D), and system (dome pressure, core exit pressure and total core flow rate). In order to minimise the impact of the deviations in code predictions at the initial steady-state conditions (which were analysed in the previous section) and focus on the deviations in transient calculations the comparisons on the predictions of time evolutions of the above parameters are performed not on the absolute values of the parameters but on the delta changes of the parameters as compared to the values at the initial steady state.

Please note that the participants have already performed sensitivity studies on temporal coupling schemes and time step sizes for obtaining converged solutions (NSE, 2004). The results in this section should be considered together with Table 4-5 since all of the models given in the table are important for the transient calculations.

The reference time histories (measured or average, *i.e.* mean) are provided in this section as well as in Appendix C. The figures of merit are presented in the tables of this section. Additionally, the participant deviations and figures of merit are presented in Appendix D, and are listed in the same order as the reference solutions. Appendices C and D are available on CD-ROM upon request.

In each case the figures (Figures 4-16 through 4-51) graphically illustrate the agreement or disagreement of participants' predictions. Statistical evaluation is employed to generate a mean solution for parameters for which measured data is not available. The reference solutions (measured or average) are also shown in the plots.

Table 4-5: Models used in transient – best-estimate case

Participant	Xenon	ADF	Bypass	Decay
CEA-33	No	No	Yes	Yes
CEA-764	No	No	Yes	Yes
FANP	Yes	Yes	Yes	Yes
FZD	Yes	Yes	Yes	Yes
GRS	Yes	No	Yes	Yes
NFI	Yes	No	Yes	Yes
NUPEC	Yes	Yes	No	Yes
PSI	Yes	Yes	Yes	No
PSU/PURDUE/NRC	Yes	Yes	Yes	Yes
TEPSYS	Yes	Yes	Yes	Yes
UPISA	No	Yes	Yes	Yes
UPV-1 (MODKIN)	Yes	Yes	Yes	Yes
UPV-2 (NOKIN)	Yes	Yes	Yes	Yes
WESTINGHOUSE	No	Yes	Yes	Yes

Core power time evolutions are presented in two groups (fission or total) depending on the submitted core power type. Comparisons of the predictions of fission power evolution and the total power evolution calculated by each code throughout the transient (up to 5 seconds) are shown in Figures 4-16, 4-18 and 4-20 while Figures 4-17, 4-19 and 4-21 zoom on the first one second of the transient where the power peak occurs. Table 4-6 provides figure of merit (FOM) for two different methods, D'Auria FFT and Mean Error.

When analysing the power history results it should be taken into account that in the TT2 test, the thermal-hydraulic feedback alone limited the power peak and initiated the power reduction. The void feedback plays the mayor role while the Doppler feedback plays a subordinate role. The reactor scram then inserted additional negative reactivity and completed the power reduction and eventual core shutdown. The scram initiation time and the speed of the rod insertion were specified. The scram initiation time was specified since one of the objectives of the benchmark is to test coupled codes' capabilities to predict or not that the thermal-hydraulic feedback alone limits the power peak and initiates the power reduction. The power response to the pressure wave caused by the turbine trip in terms of timing and magnitude of power peak during the transient as predicted by different codes is a function of the total reactivity time evolution. In Figure 4-17 (the fission power group), the predicted power peak values of three participants, CEA-33, CEA/DEAN-764 and NUPEC are higher than the measured value. In the total power group (Figure 4-19), all of the codes' predictions (except NFI) form a cluster around the mean solution. The averaged fission power time history distributions over the six participants' results (using different coupled code systems) are compared in Figures 4-19 and 4-20 with measured data in order to outline common modelling tendencies. In general, the power history results are in a good agreement.

System parameter (dome pressure, core exit pressure, and total core flow rate) time evolutions are presented in two groups (Group 1 and Group 2) in order to visualise them clearly. Comparisons of the predictions of these parameters calculated by each code throughout the transient (up to 5 seconds) are shown in Figures 4-22 and 4-23 and in Figures 4-25 through 4-28, while Figure 4-24 illustrates the comparison of participants' mean (average) solution to measured data. Tables 4-7 through 4-9 provide figure of merit (FOM) for two different methods, D'Auria FFT and Mean Error. It is important to note that for dome pressure time history there is available measured data while for core exit pressure and total core flow rate the average (mean) of participants' predictions is used as reference solution.

The accurate prediction of void feedback during the turbine trip transient depends on the modelling of the pressure wave propagation into the vessel. The prediction of dome pressure time history is the indication of how successful this modelling is. As can be seen from Figures 4-22 through 4-24 the participants' results compared very satisfactorily with measured data for the dome pressure time history. This result increased the trustworthiness of the coupled code capabilities.

Figures 4-29 through 4-36 show comparisons of the predictions of the total, Doppler and void reactivity throughout the transient. The total reactivity has three components – the negative tripped rod reactivity, moderator density (void) reactivity and Doppler feedback reactivity. The total reactivity behaviour before the scram is dominated by the void reactivity feedback mechanism. The fuel heat

transfer parameters such as the UO_2 conductivity and gap conductivity and direct heating (2% to in-channel flow and 1.7% to bypass flow) were specified. The sources of modelling uncertainties in the void feedback model for initial conditions were identified in terms of sub-cooled boiling and vapour slip and these sources will also affect the transient behaviour of void feedback reactivity. Different density correlations and standards for water/steam property tables incorporated into the codes also play an important role in the void reactivity predictions by such codes (see Figures 4-35 and 4-36 and Table 4-12). In addition, and as mentioned above, the accurate prediction of void feedback during the turbine trip transient depends on the modelling of the pressure wave propagation into the vessel. In this sense the deviations in prediction of dome pressure time history are propagated to the void feedback reactivity time history. The Doppler feedback plays a subordinate role. The discrepancies in the Doppler reactivity time history predictions (see Figures 4-33 and 4-34 and Table 4-11) are due to the discrepancies in the results for core-averaged Doppler temperature time evolution. The latter are due to the different relations used for calculating the Doppler fuel temperature, and the radial and axial nodalisation of the heat structure used (fuel rod). Discrepancies at the end of the transient are due to different predictions of the tripped control rod reactivity by the participants' codes.

Core local parameter (safety-related) time evolutions such as maximum cladding temperature, radial power peaking factor, and LPRM A, B, C and D power time histories are presented through three types of comparisons. Since the benchmark-measured data for the best-estimate (test) scenario also contain the local power range monitor (LPRM) measurements, the benchmark team provided the participants with the description of an appropriate algorithm to model LPRM response and the necessary associated data as microscopic detector cross-sections, flux factors, etc.

Comparisons of the predictions of local parameter time evolutions calculated by each code throughout the transient (up to 5 seconds) are shown in Figures 4-37, 4-39, 4-40, 4-43, 4-46 and 4-49. Figures 4-38, 4-41, 4-44, 4-47 and 4-50 zoom on the first few seconds of the transient. Figures 4-42, 4-45, 4-48 and 4-51 illustrate the comparison of participants' mean (average) solutions to measured data. Tables 4-14 through 4-18 provide figure of merit (FOM) for two different methods, D'Auria FFT and Mean Error while Table 4-13 gives the values of maximum cladding temperatures as predicted by the participants at the initial steady state (since this is not given in the previous section). It is important to note that for the four LPRM power time histories there is available measured data while for the maximum cladding temperature and radial peaking factor the average (mean) of participants' predictions is used as reference solution.

Figure 4-16: Best-estimate case – transient power (fission)

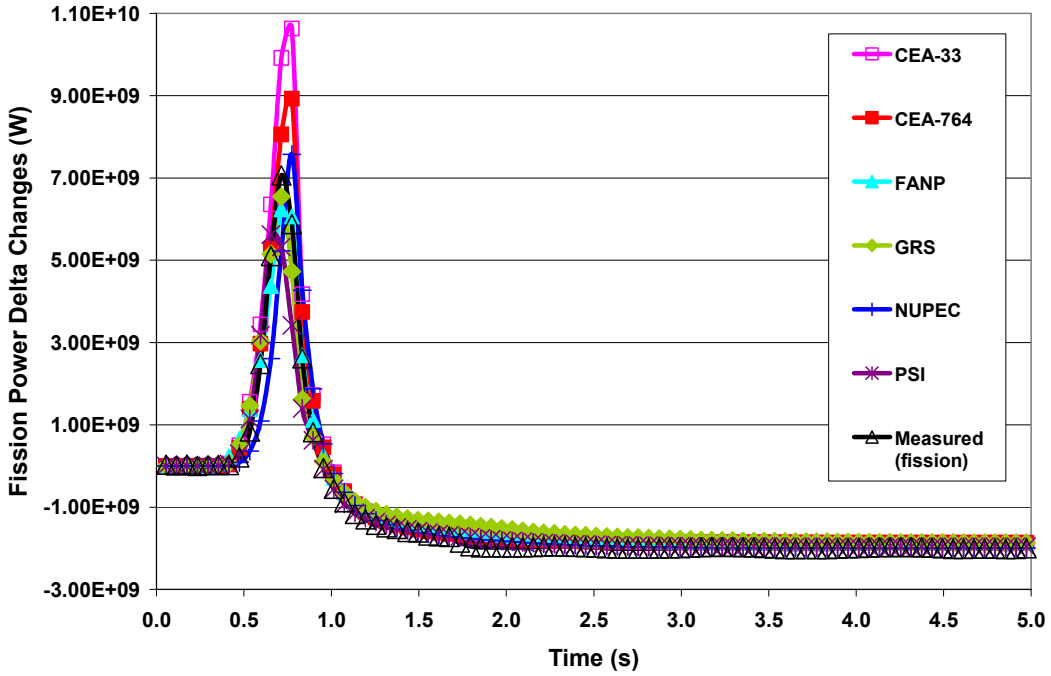

Figure 4-17: Best estimate case – transient power (fission – zoom)

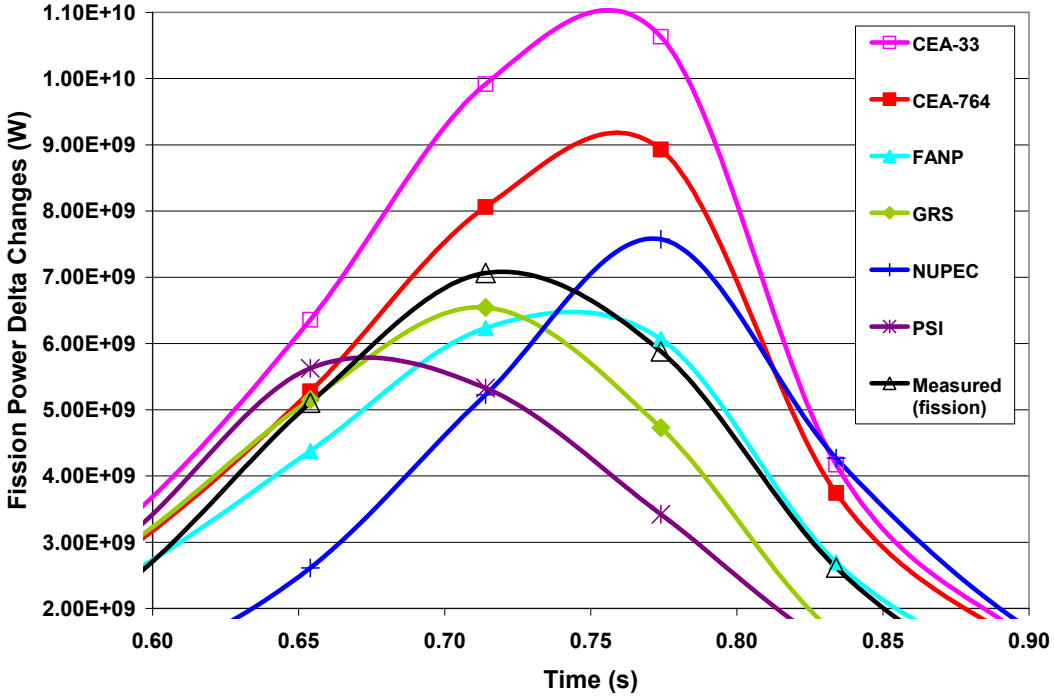

Figure 4-18: Best-estimate case – transient power (total)

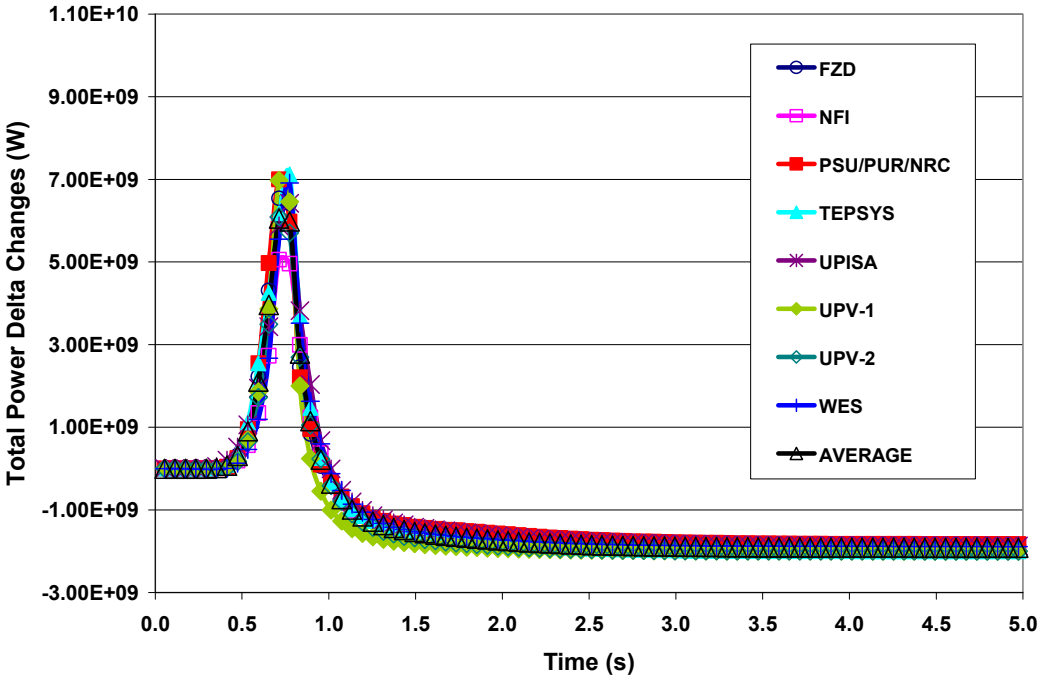

Figure 4-19: Best-estimate case – transient power (total – zoom)

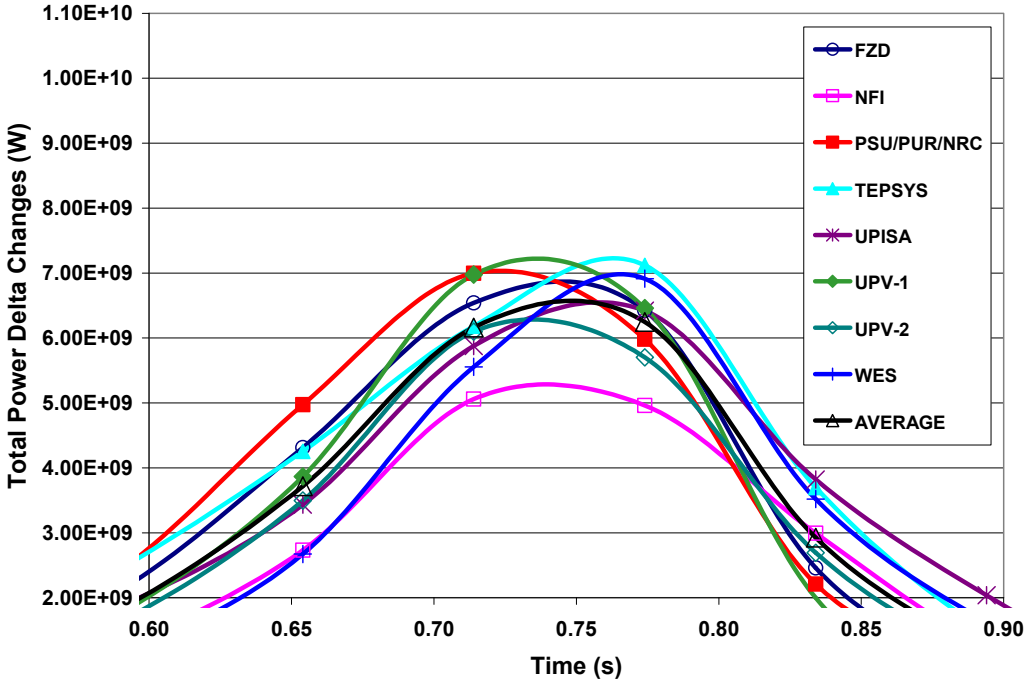

Figure 4-20: Best-estimate case – transient fission power comparison (average vs. measured)

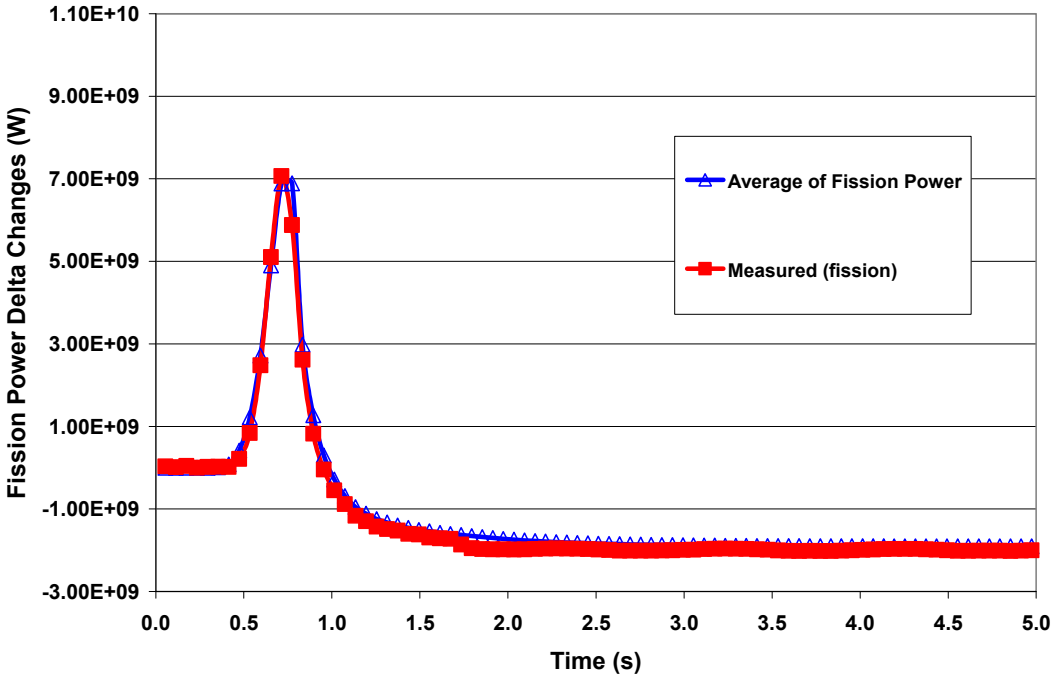

Figure 4-21: Best-estimate case – transient fission power comparison (average vs. measured – zoom)

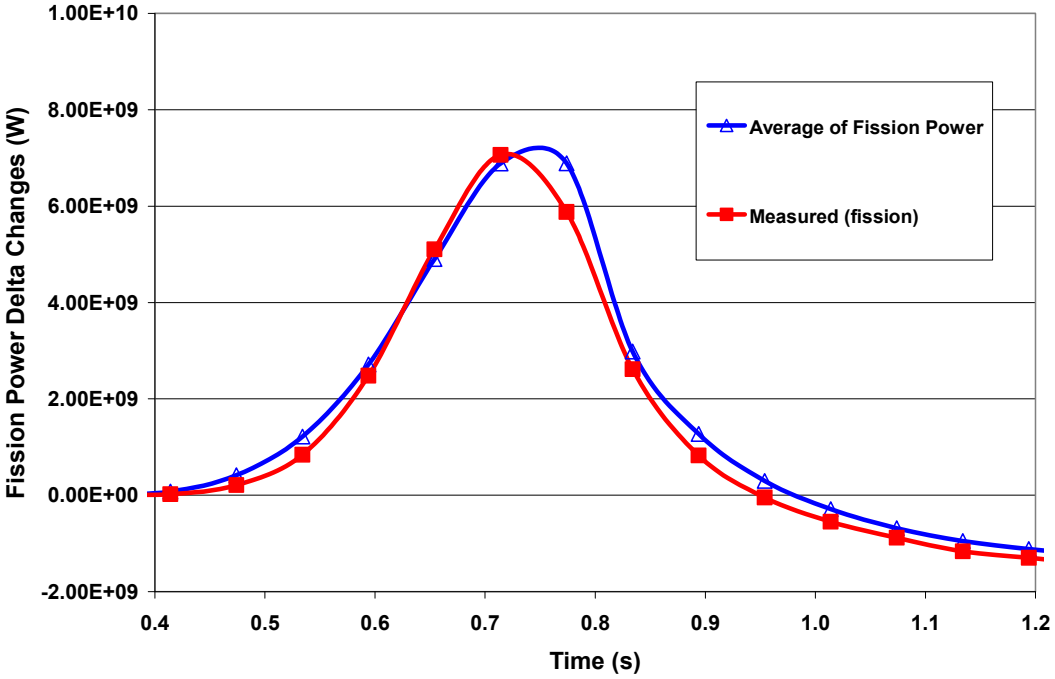

Table 4-6: Best-estimate case – transient power, figure of merit

Fission power submitted			Total power submitted		
Participant	**D'Auria FFT**	**Mean error, ME**	**Participant**	**D'Auria FFT**	**Mean error, ME**
CEA-33	0.6677	0.9699	FZD	0.8509	0.9937
CEA-764	0.7460	0.9775	NFI	0.7996	0.9953
FANP	0.8331	0.9842	PSU/PUR/NRC	0.7971	0.9880
GRS	0.8014	0.9811	TEPSYS	0.8261	0.9992
NUPEC	0.7271	0.9980	UPISA	0.8249	0.9885
PSI	0.7678	0.9996	UPV-1	0.7830	0.9841
			UPV-2	0.8656	0.9890
			WES	0.8008	0.9976

Figure 4-22: Best-estimate case – transient dome pressure (Group 1)

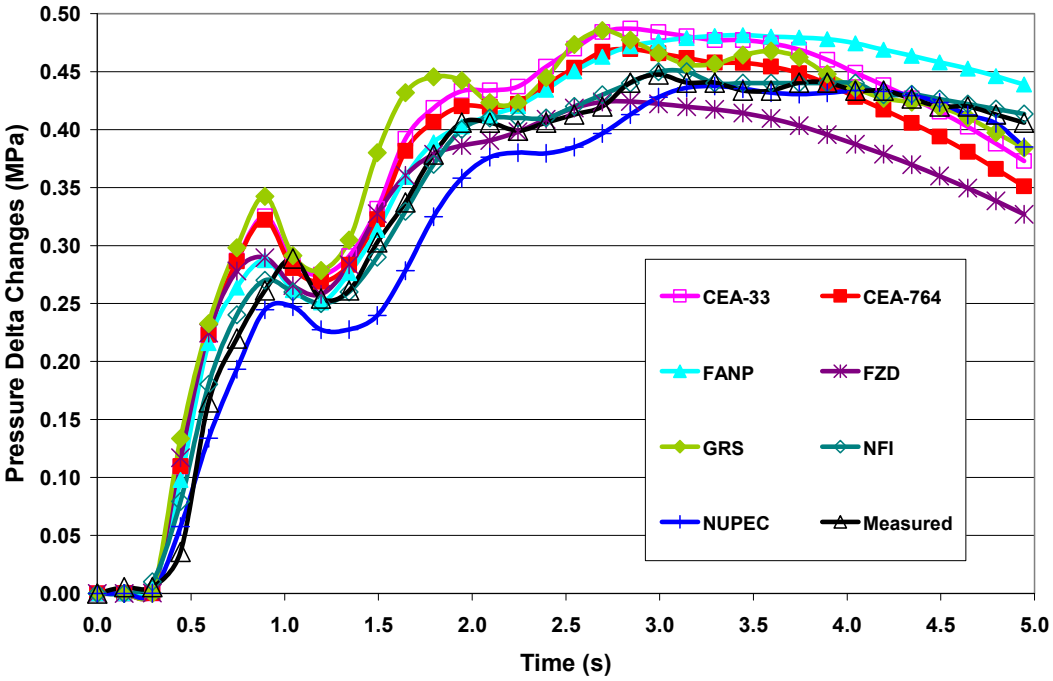

Figure 4-23: Best-estimate case – transient dome pressure (Group 2)

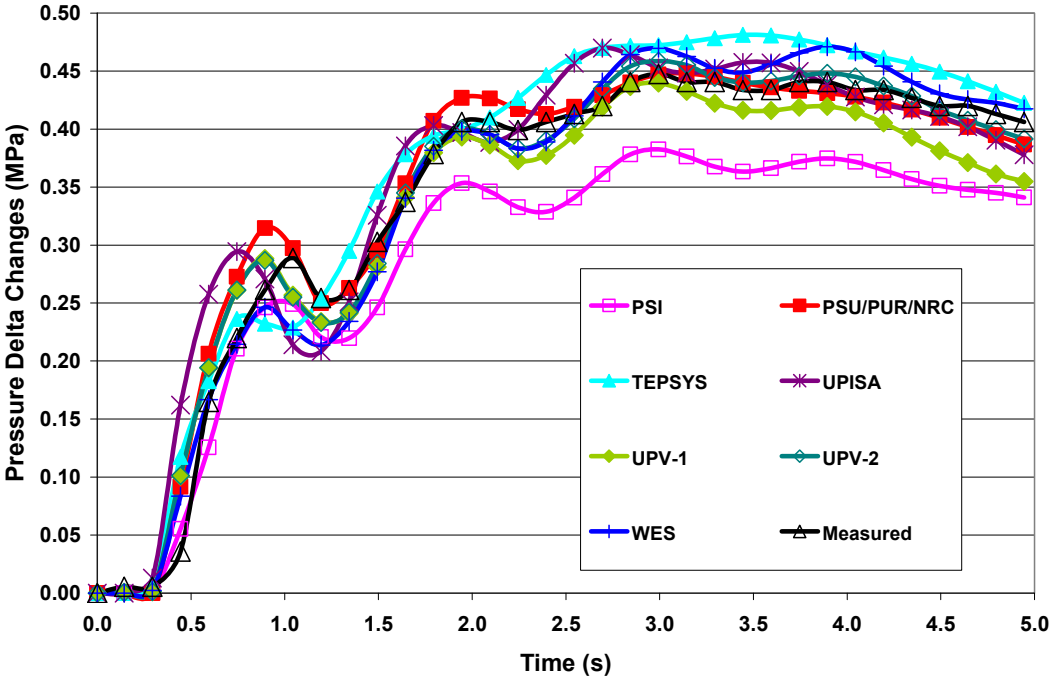

Figure 4-24: Best-estimate case – transient dome pressure (average vs. measured)

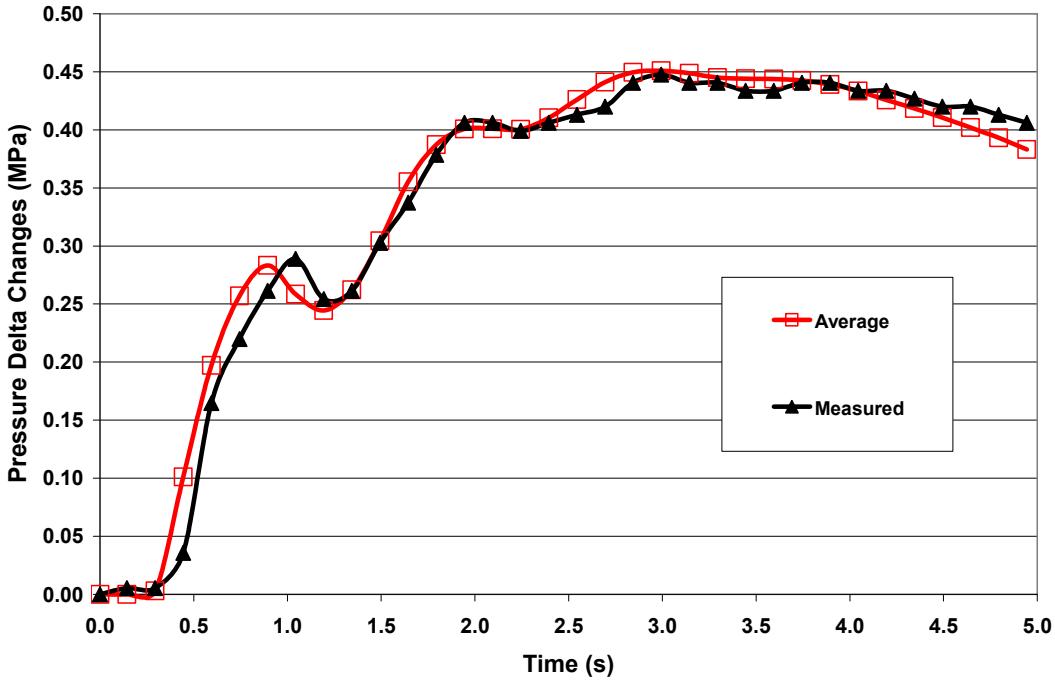

Table 4-7: Best-estimate case – transient dome pressure, figure of merit

Participant	D'Auria FFT	Mean error, ME
CEA-33	0.8215	0.9420
CEA-764	0.8309	0.9685
FANP	0.8481	0.9434
FZD	0.8257	0.9739
GRS	0.8105	0.9391
NFI	0.8949	0.9923
NUPEC	0.8668	0.9611
PSI	0.8192	0.8985
PSU/PUR/NRC	0.8696	0.9840
TEPSYS	0.8368	0.9496
UPISA	0.8241	0.9761
UPV-1	0.8514	0.9738
UPV-2	0.8754	0.9936
WES	0.8716	0.9920

Figure 4-25: Best-estimate case – transient core exit pressure (Group 1)

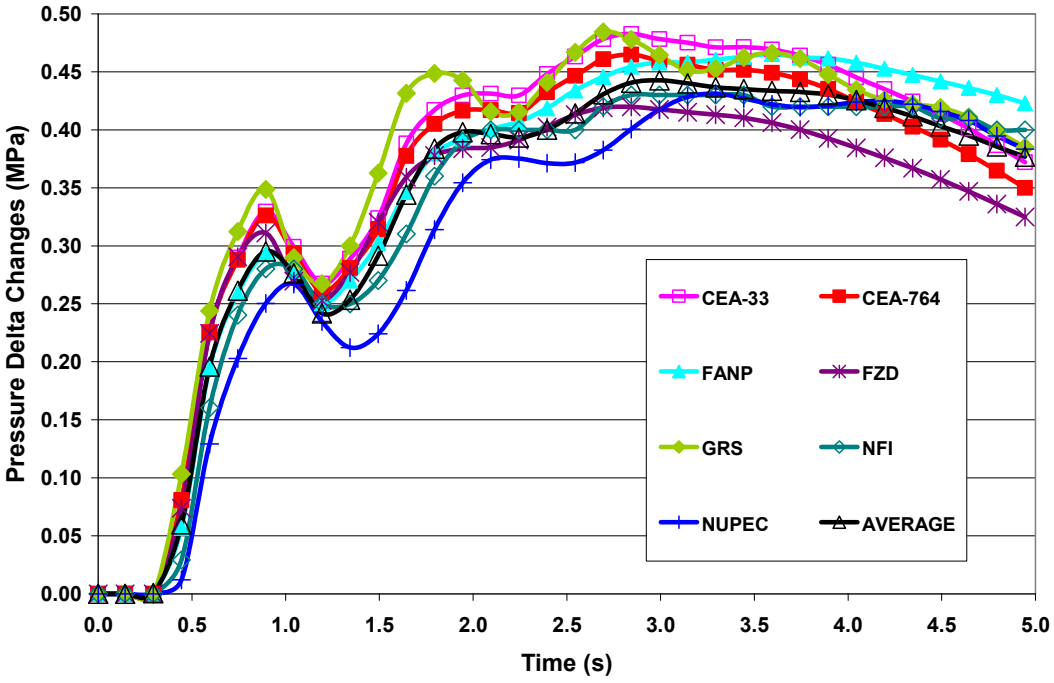

Figure 4-26: Best-estimate case – transient core exit pressure (Group 2)

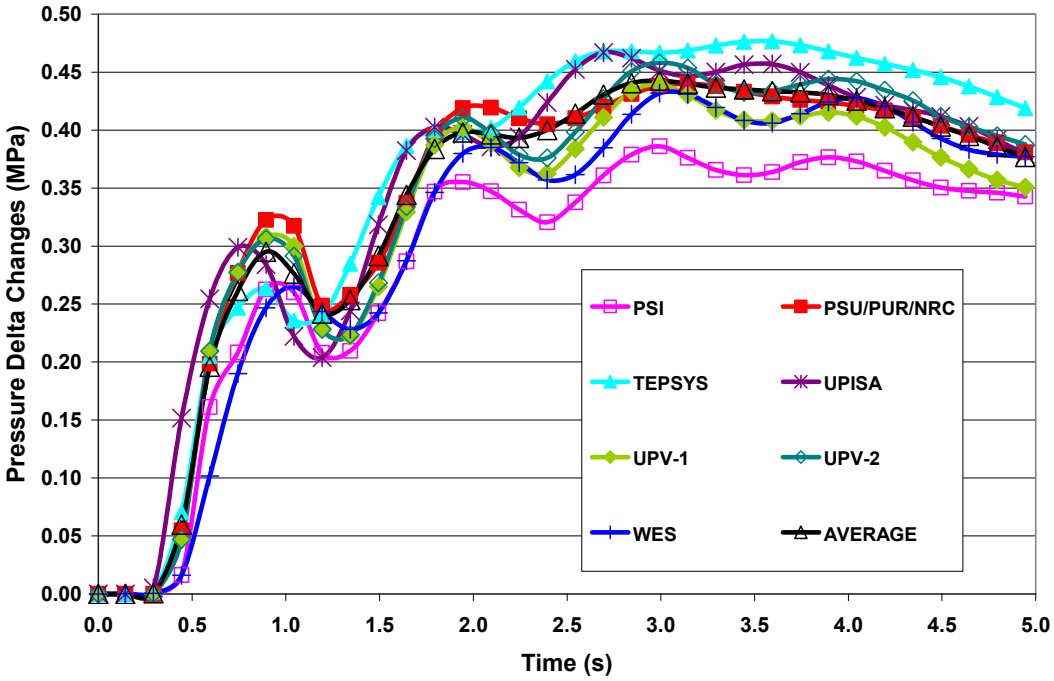

Table 4-8: Best-estimate case – transient core exit pressure, figure of merit

Participant	D'Auria FFT	Mean error, ME
CEA-33	0.8611	0.9432
CEA-764	0.8812	0.9714
FANP	0.8805	0.9639
FZD	0.8718	0.9722
GRS	0.8362	0.9362
NFI	0.9003	0.9849
NUPEC	0.8312	0.9505
PSI	0.8232	0.9010
PSU/PUR/NRC	0.8710	0.9922
TEPSYS	0.8358	0.9493
UPISA	0.8178	0.9731
UPV-1	0.8574	0.9716
UPV-2	0.8818	0.9952
WES	0.8376	0.9486

Figure 4-27: Best-estimate case – transient total core flow rate (Group 1)

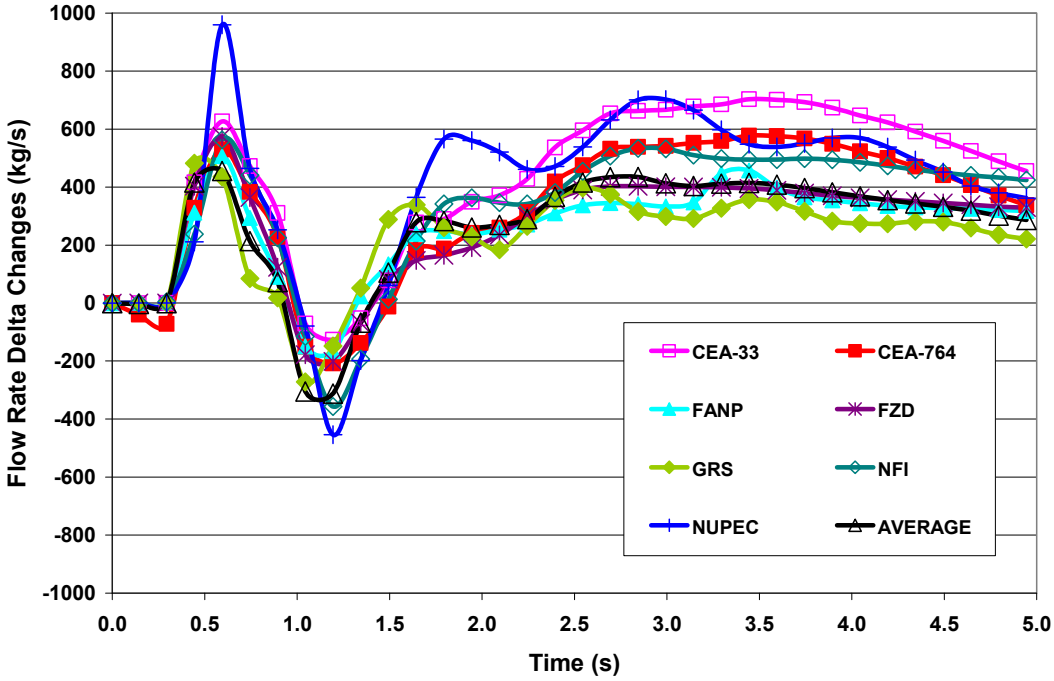

Figure 4-28: Best-estimate case – transient total core flow rate (Group 2)

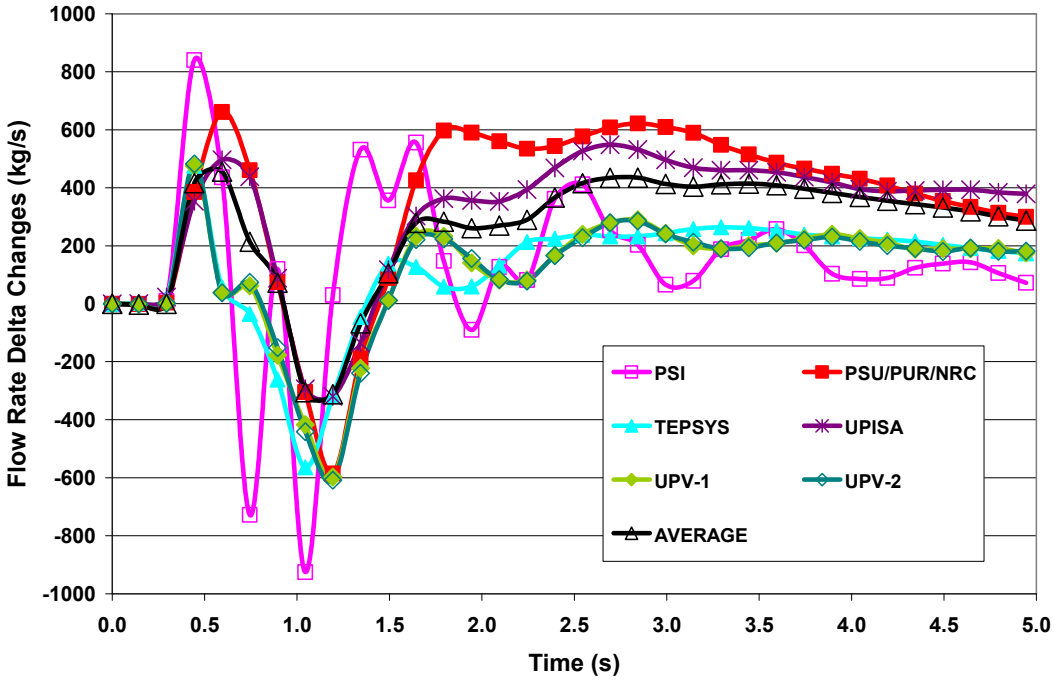

Table 4-9: Best-estimate case – transient total core flow rate, figure of merit

Participant	D'Auria FFT	Mean error, ME
CEA-33	0.6322	0.8576
CEA-764	0.6991	0.9407
FANP	0.7607	0.9965
FZD	0.7687	0.9991
GRS	0.7238	0.9688
NFI	0.6906	0.9392
NUPEC	0.5960	0.8808
PSI	0.4347	0.8922
PSU/PUR/NRC	0.6437	0.9173
TEPSYS	0.6350	0.8874
UPISA	0.7218	0.9510
UPV-1	0.6345	0.8748
UPV-2	0.6280	0.8730

Figure 4-29: Best-estimate case – total reactivity (Group 1)

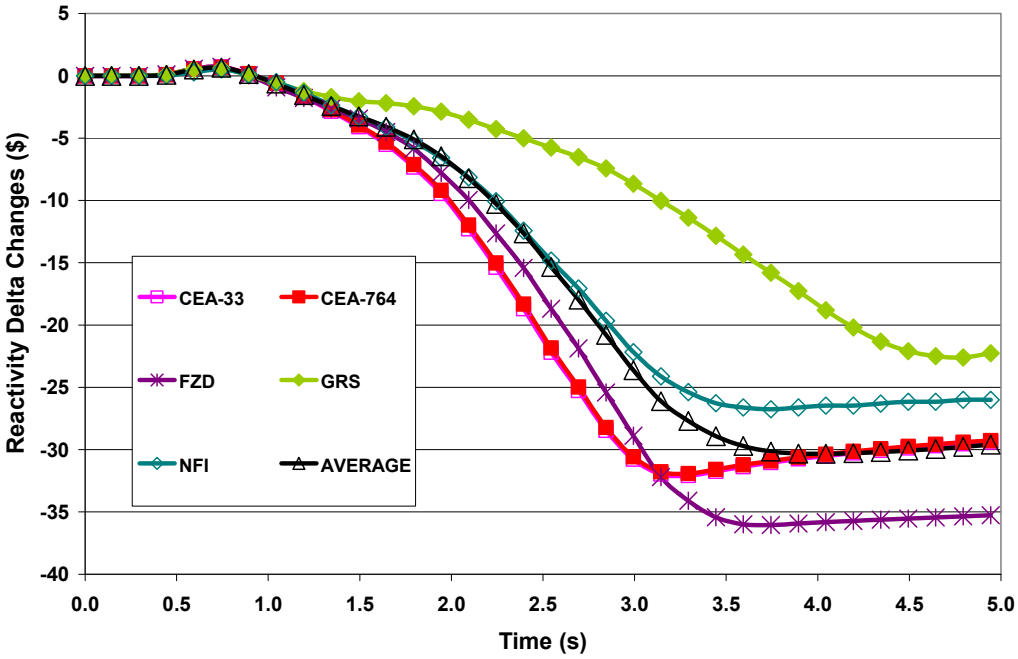

Figure 4-30: Best-estimate case – total reactivity (Group 1 – zoom)

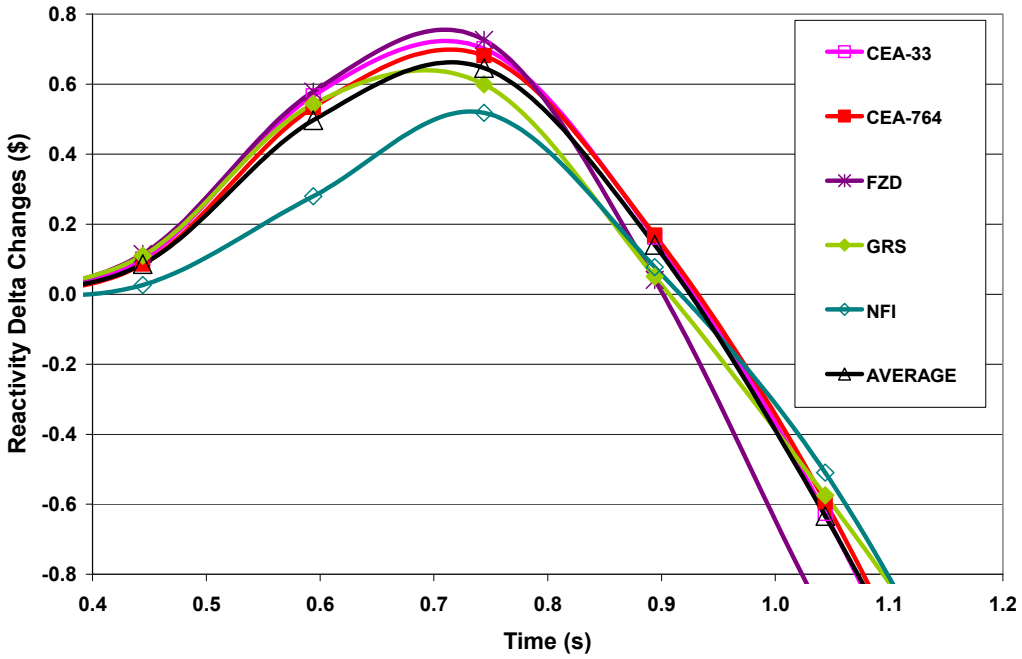

Figure 4-31: Best-estimate case – total reactivity (Group 2)

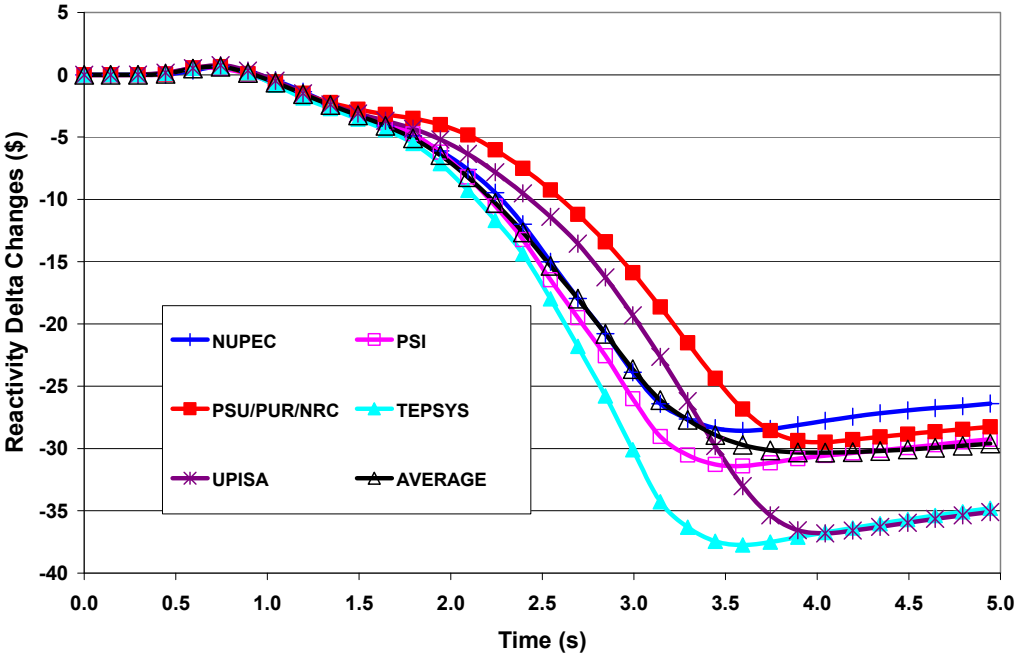

Figure 4-32: Best-estimate case – total reactivity (Group 2 – zoom)

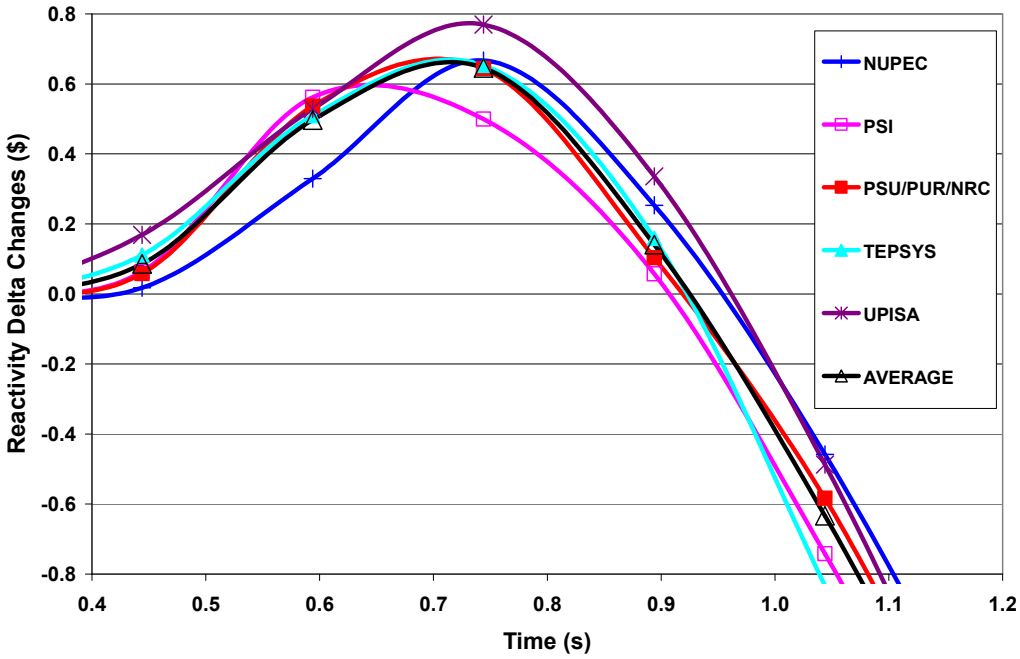

Table 4-10: Best-estimate case – total reactivity, figure of merit

Participant	D'Auria FFT	Mean error, ME
CEA-33	0.8103	0.9388
CEA-764	0.8135	0.9430
FZD	0.8034	0.9102
GRS	0.6765	0.8186
NFI	0.8553	0.9560
NUPEC	0.8726	0.9725
PSI	0.8883	0.9835
PSU/PUR/NRC	0.7996	0.9299
TEPSYS	0.7807	0.9028
UPISA	0.8084	0.9779

Figure 4-33: Best-estimate case – Doppler reactivity

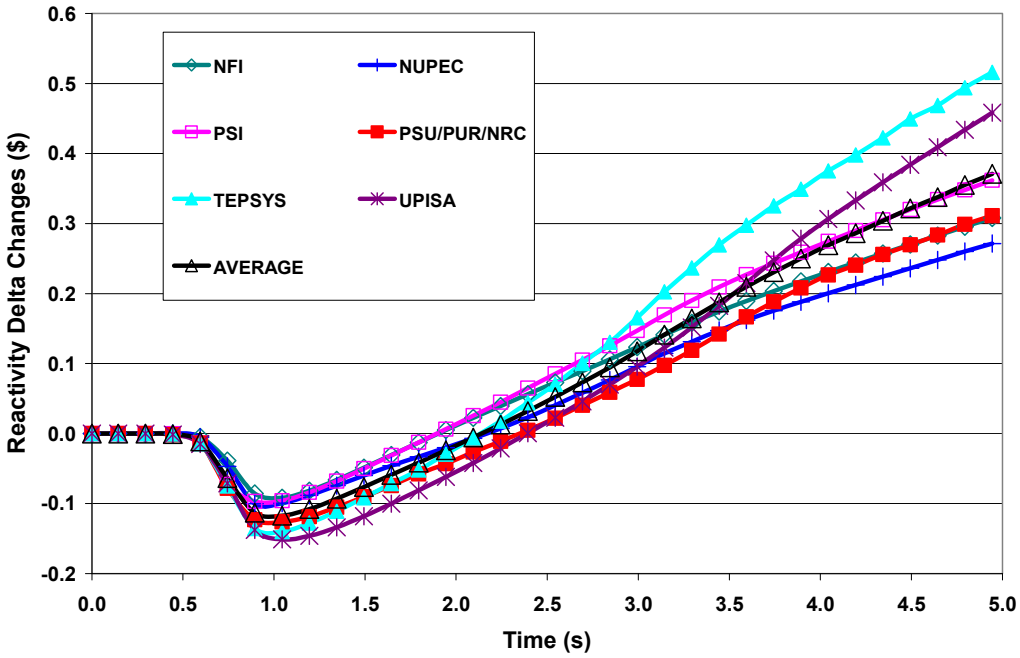

Figure 4-34: Best-estimate case – Doppler reactivity (zoom)

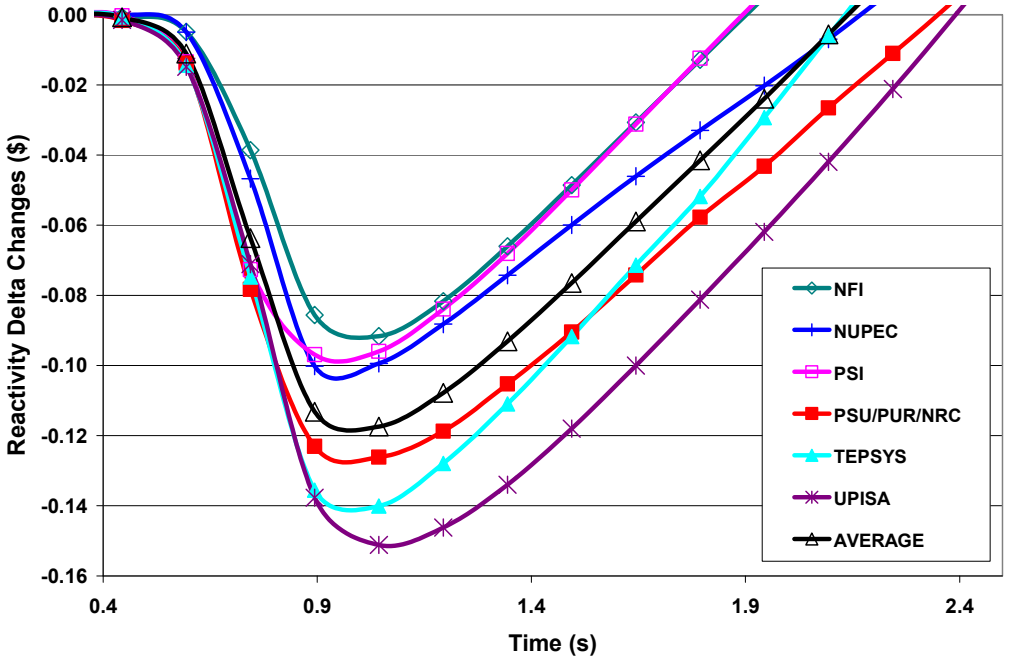

Table 4-11: Best-estimate case – Doppler reactivity, figure of merit

Participant	D'Auria FFT	Mean error, ME
NFI	0.8352	0.9963
NUPEC	0.7783	0.9543
PSI	0.8570	0.9697
PSU/PUR/NRC	0.8289	0.9458
TEPSYS	0.7117	0.9239
UPISA	0.7928	0.9954

Figure 4-35: Best-estimate case – void reactivity

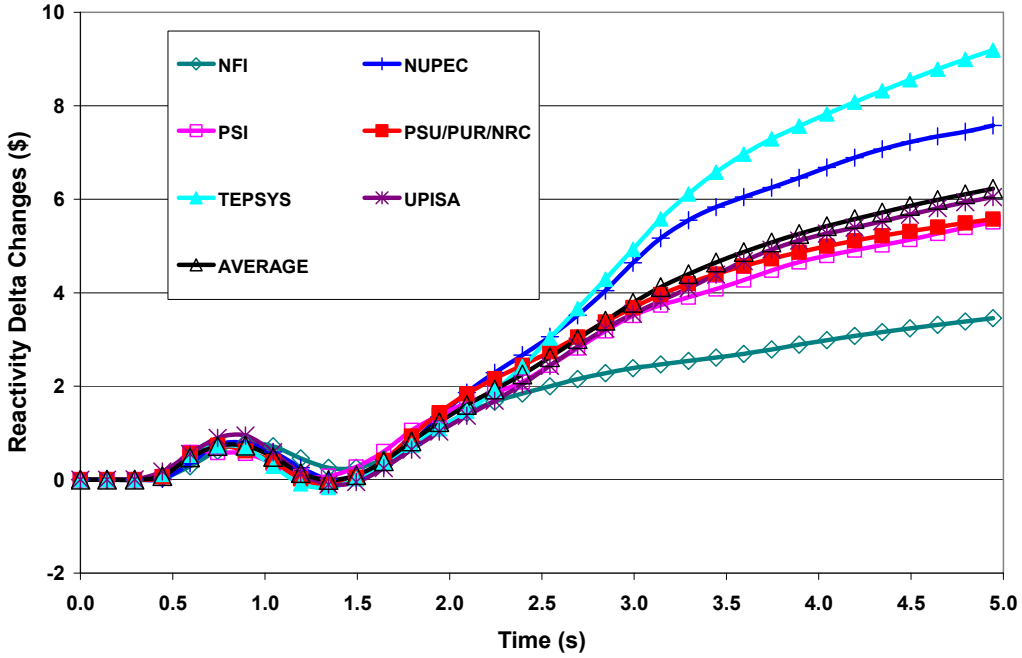

Figure 4-36: Best-estimate case – void reactivity (zoom)

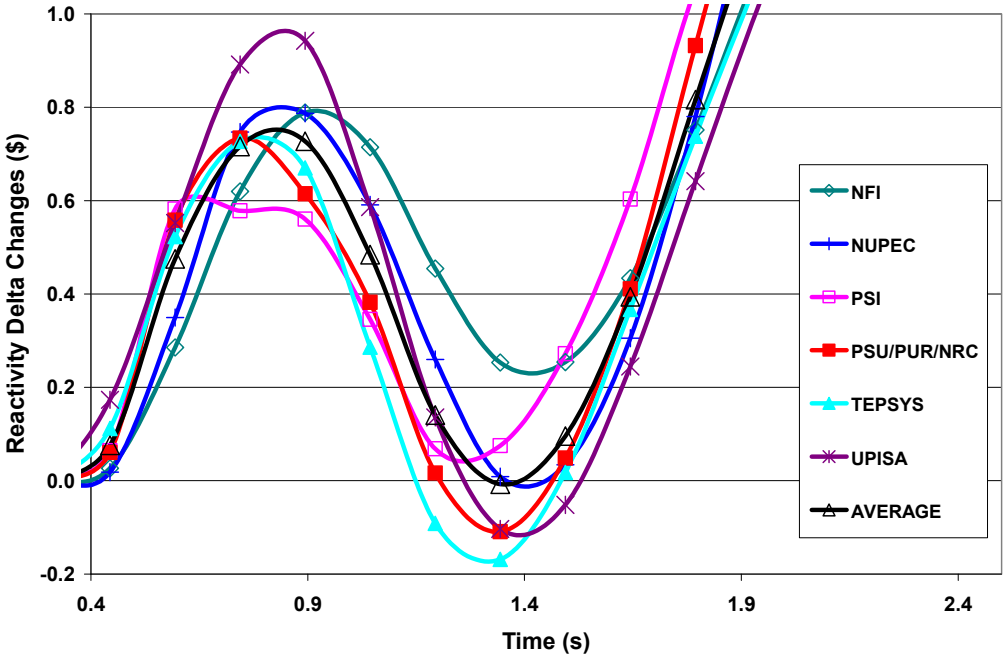

Table 4-12: Best-estimate case – void reactivity, figure of merit

Participant	D'Auria FFT	Mean error, ME
NFI	0.6849	0.8582
NUPEC	0.7962	0.9142
PSI	0.8541	0.9604
PSU/PUR/NRC	0.8738	0.9780
TEPSYS	0.6751	0.8659
UPISA	0.8807	0.9807

Figure 4-37: Best-estimate case – maximum cladding temperature

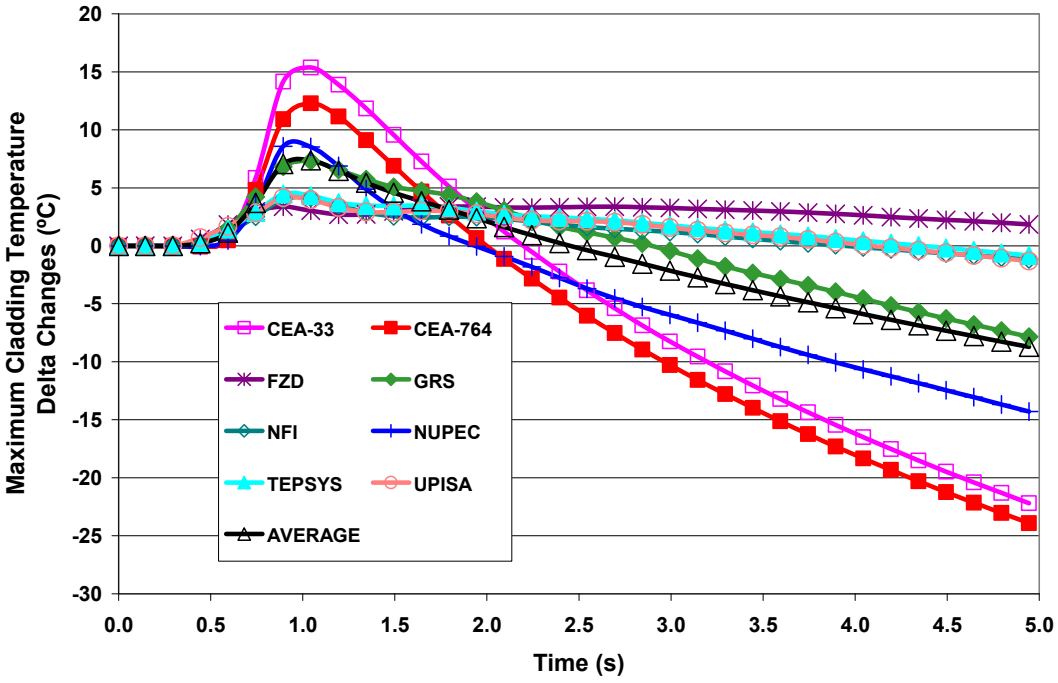

Figure 4-38: Best-estimate case – maximum cladding temperature (zoom)

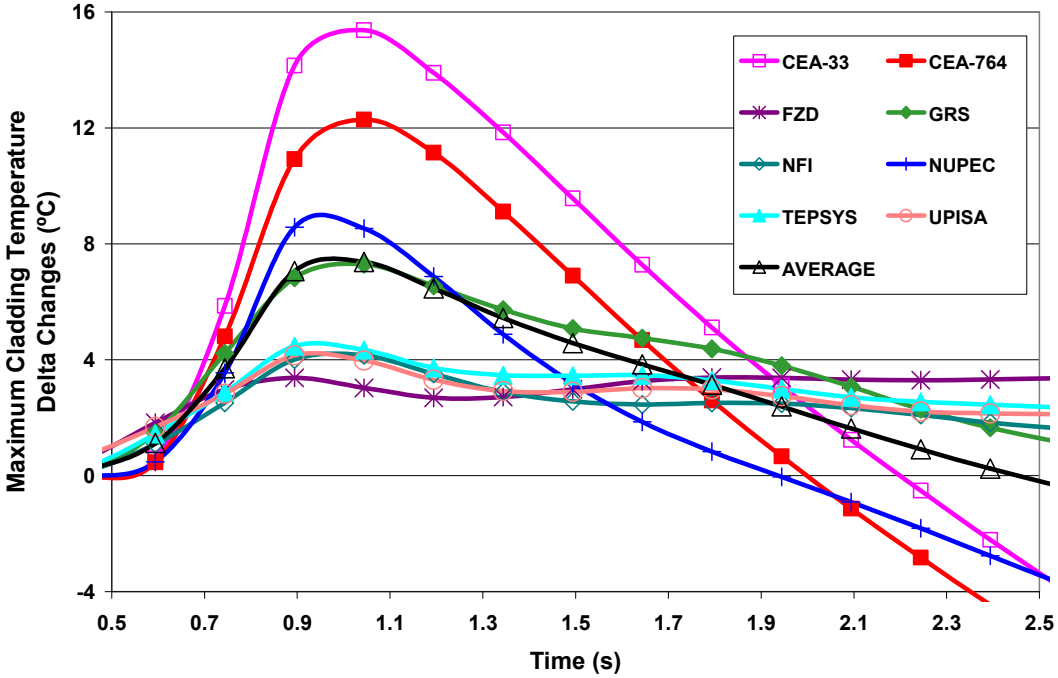

Table 4-13: Best-estimate case – maximum cladding initial (time = 0 s) temperature

Participant	Initial cladding temperature at time = 0 s (°C)
CEA-33	375.15
CEA-764	376.36
FZD	293.93
GRS	324.86
NFI	299.46
NUPEC	336.23
TEPSYS	299.28
UPISA	299.21

Table 4-14: Best-estimate case – maximum cladding temperature, figure of merit

Participant	D'Auria FFT	Mean error, ME
CEA-33	0.3914	0.8249
CEA-764	0.3710	0.7539
FZD	0.4560	0.8223
GRS	0.7888	0.9444
NFI	0.5435	0.8861
NUPEC	0.5929	0.8580
TEPSYS	0.5309	0.8633
UPISA	0.5423	0.8754

Figure 4-39: Best-estimate case – radial power peaking factors

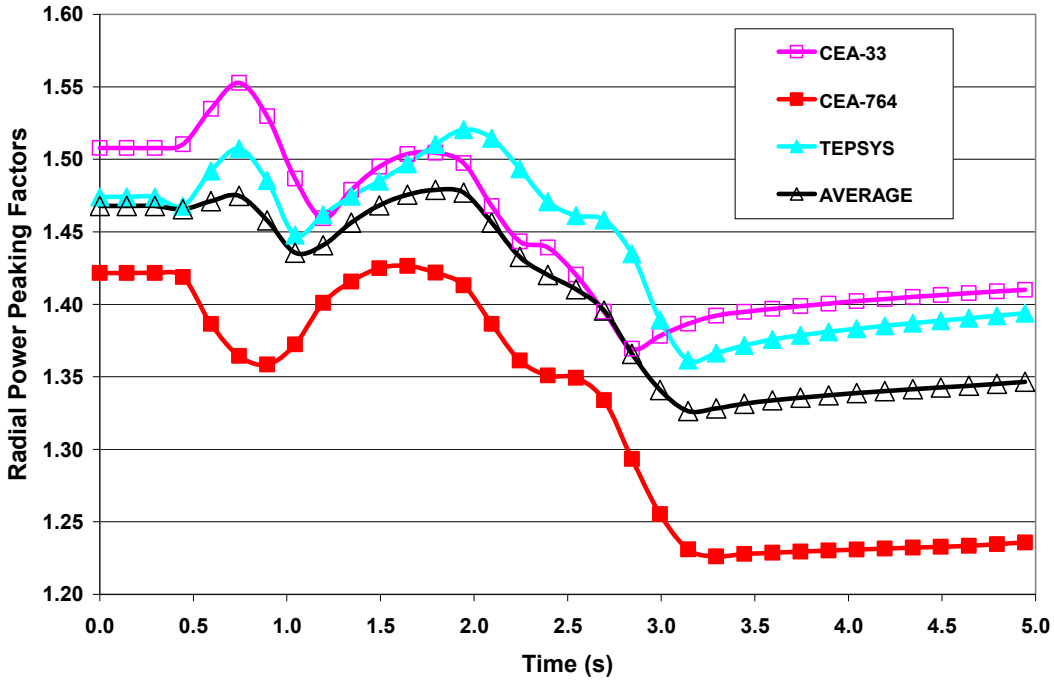

Figure 4-40: Best-estimate case – LPRM-A

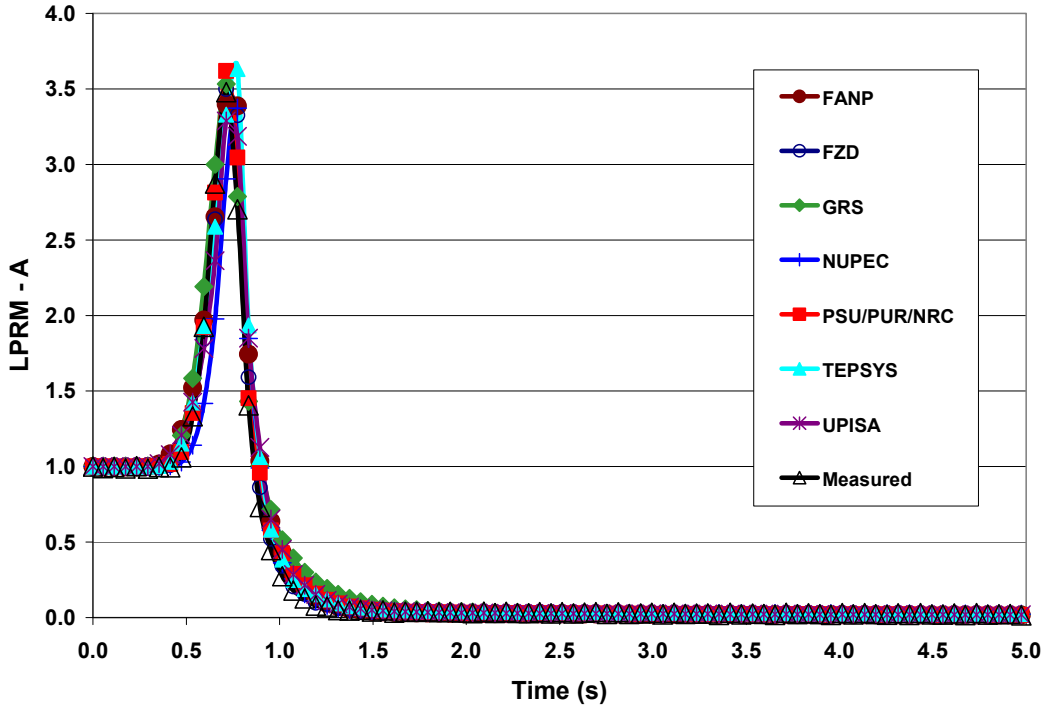

Figure 4-41: Best-estimate case – LPRM-A (zoom)

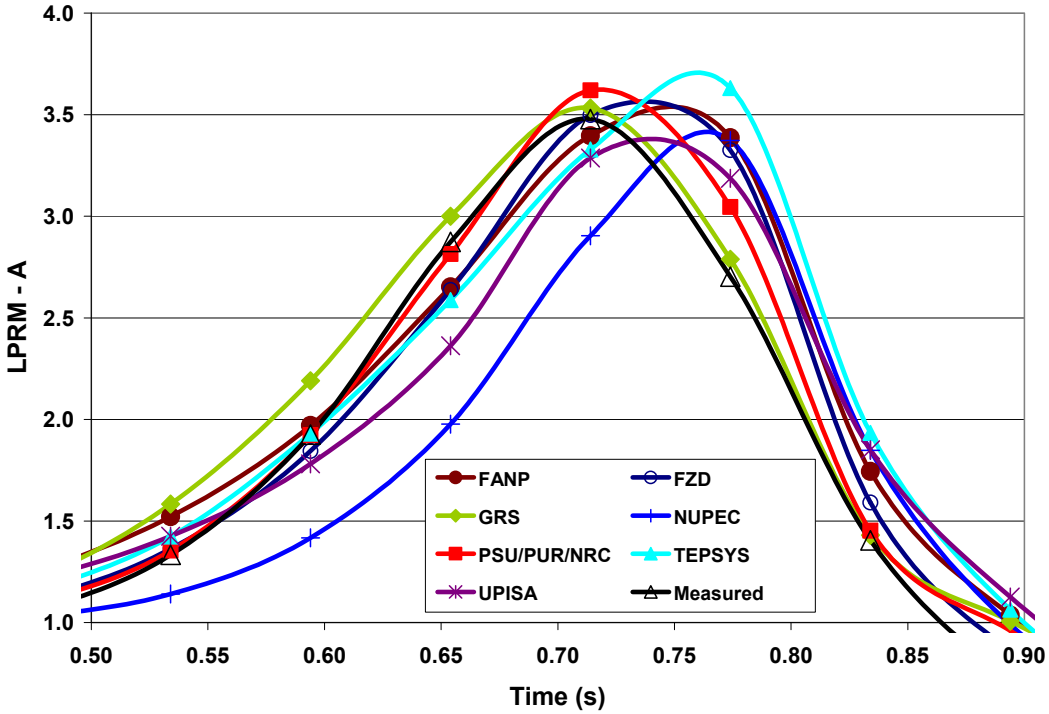

Figure 4-42: Best-estimate case – LPRM-A (average vs. measured)

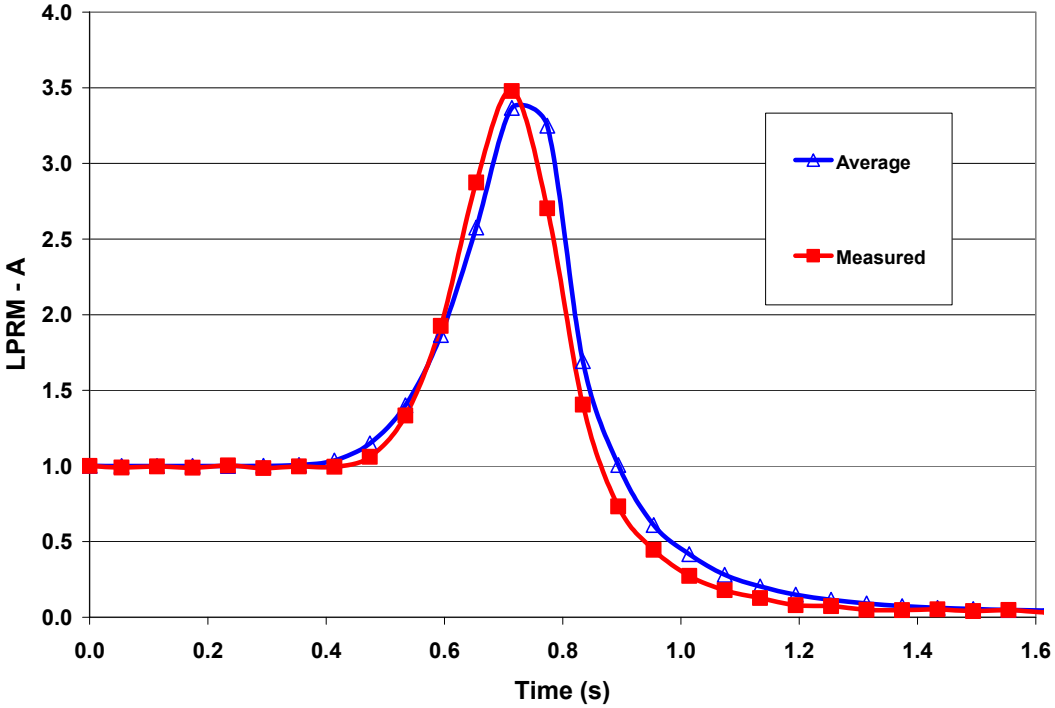

Table 4-15: Best-estimate case – normalised LPRM-A power, figure of merit

Participant	D'Auria FFT	Mean error, ME
FANP	0.7965	0.9939
FZD	0.8189	0.9966
GRS	0.8400	0.9903
NUPEC	0.7401	0.9990
PSU/PUR/NRC	0.8424	0.9954
TEPSYS	0.7524	0.9916
UPISA	0.7832	0.9949

Figure 4-43: Best-estimate case – LPRM-B

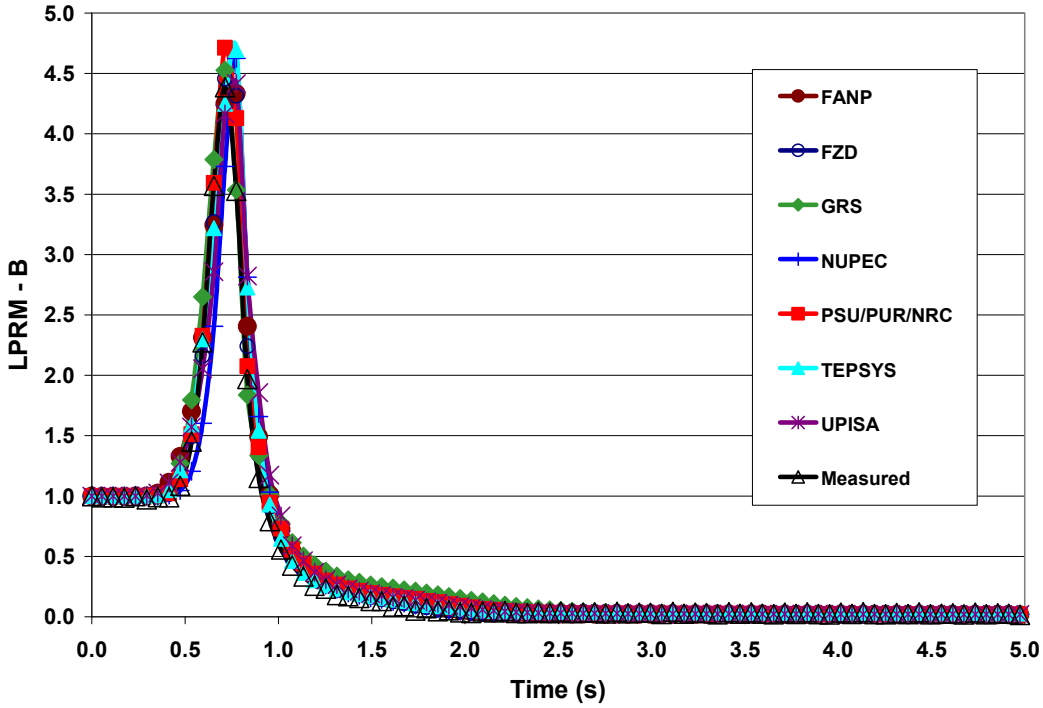

Figure 4-44: Best estimate case – LPRM-B (zoom)

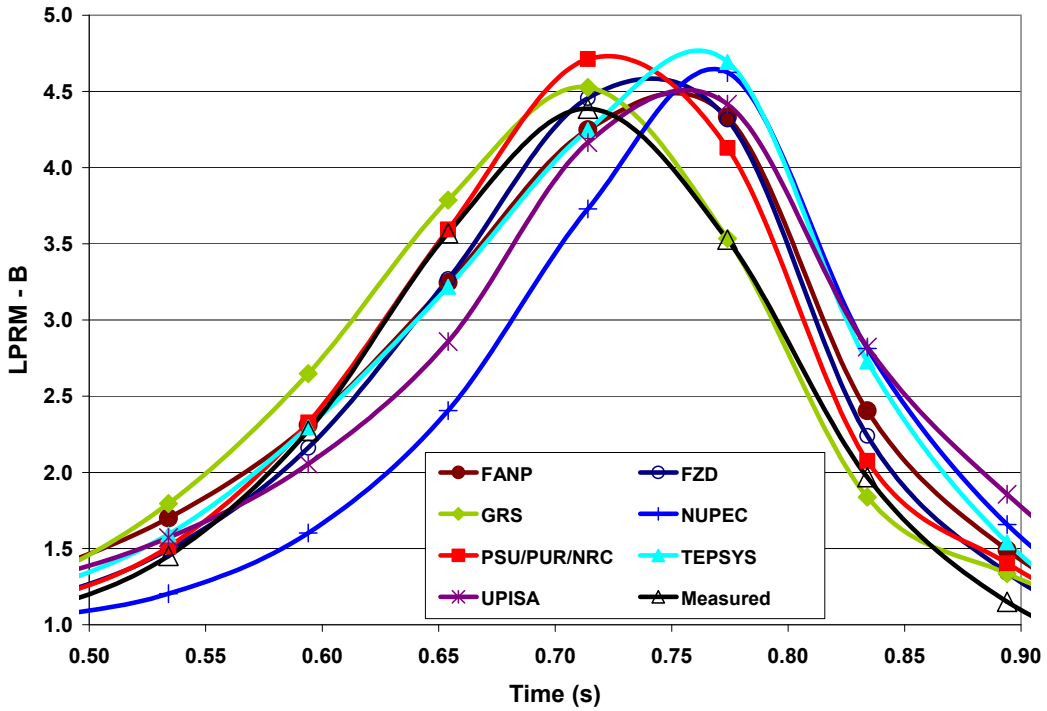

Figure 4-45: Best-estimate case – LPRM-B (average vs. measured)

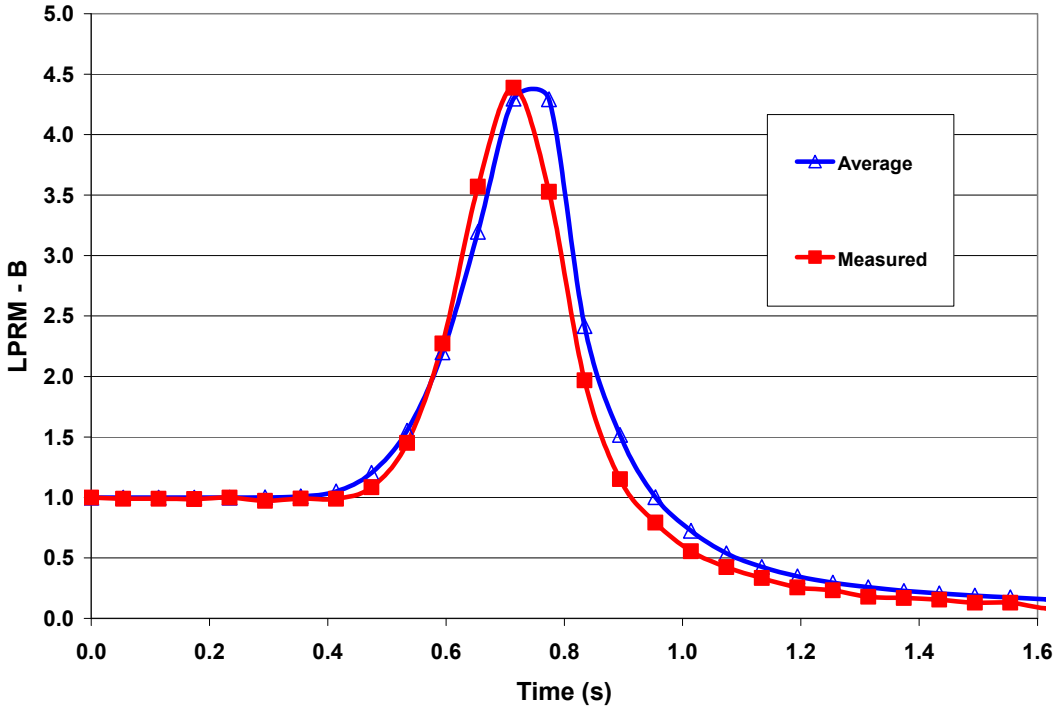

Table 4-16: Best-estimate case – normalised LPRM-B power, figure of merit

Participant	D'Auria FFT	Mean error, ME
FANP	0.7926	0.9931
FZD	0.8101	0.9957
GRS	0.8300	0.9879
NUPEC	0.7101	0.9986
PSU/PUR/NRC	0.8211	0.9920
TEPSYS	0.7426	0.9911
UPISA	0.7376	0.9905

Figure 4-46: Best-estimate case – LPRM-C

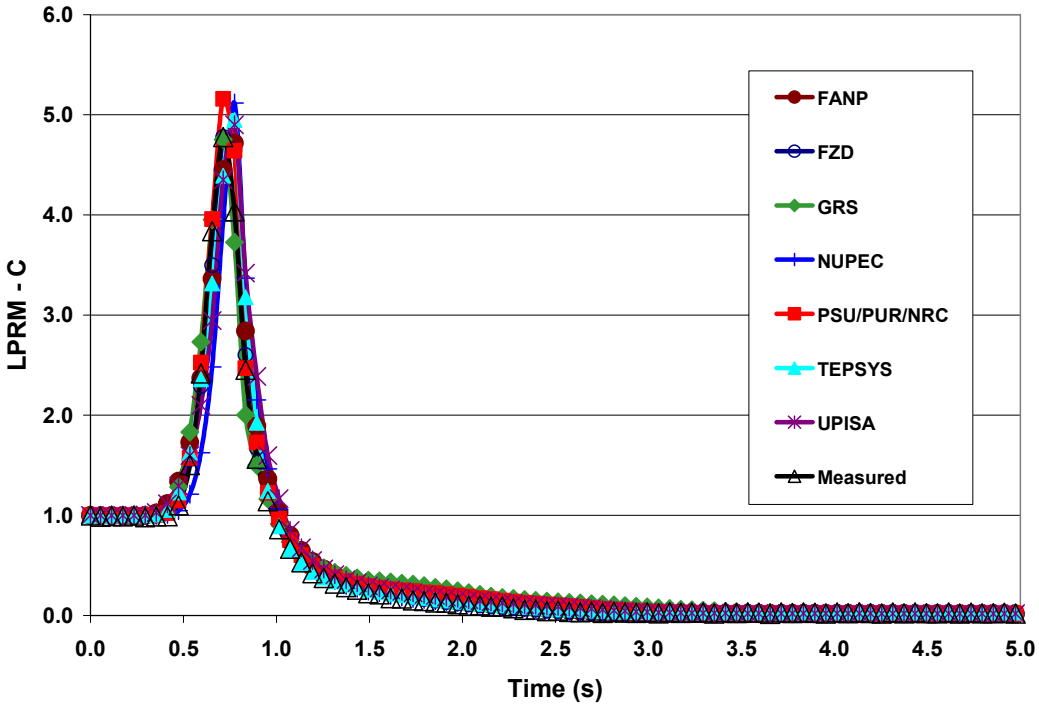

Figure 4-47: Best-estimate case – LPRM-C (zoom)

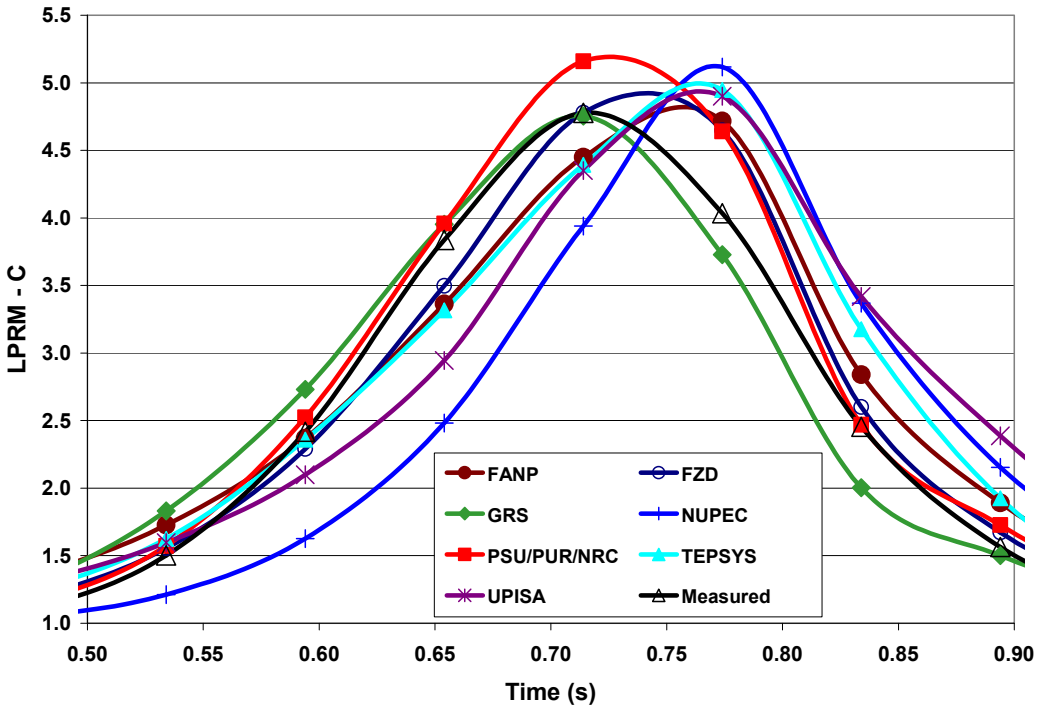

Figure 4-48: Best-estimate case – LPRM-C (average vs. measured)

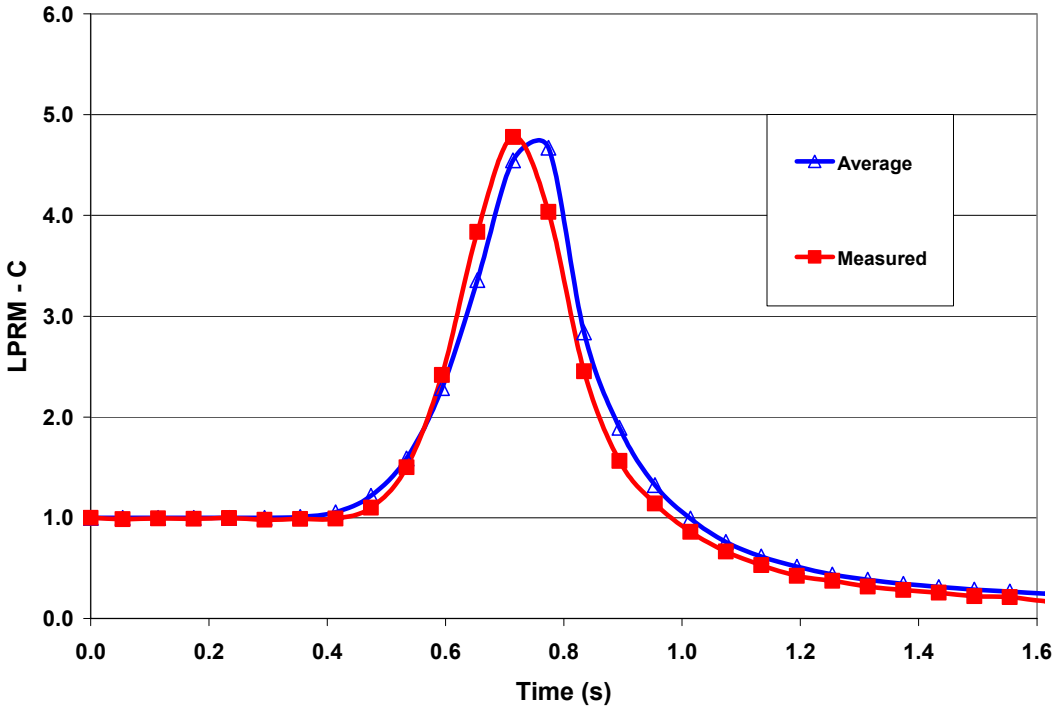

Table 4-17: Best-estimate case – normalised LPRM-C power, figure of merit

Participant	D'Auria FFT	Mean error, ME
FANP	0.7962	0.9938
FZD	0.8355	0.9969
GRS	0.8136	0.9901
NUPEC	0.7007	0.9984
PSU/PUR/NRC	0.8254	0.9908
TEPSYS	0.7630	0.9941
UPISA	0.7256	0.9897

Figure 4-49: Best-estimate case – LPRM-D

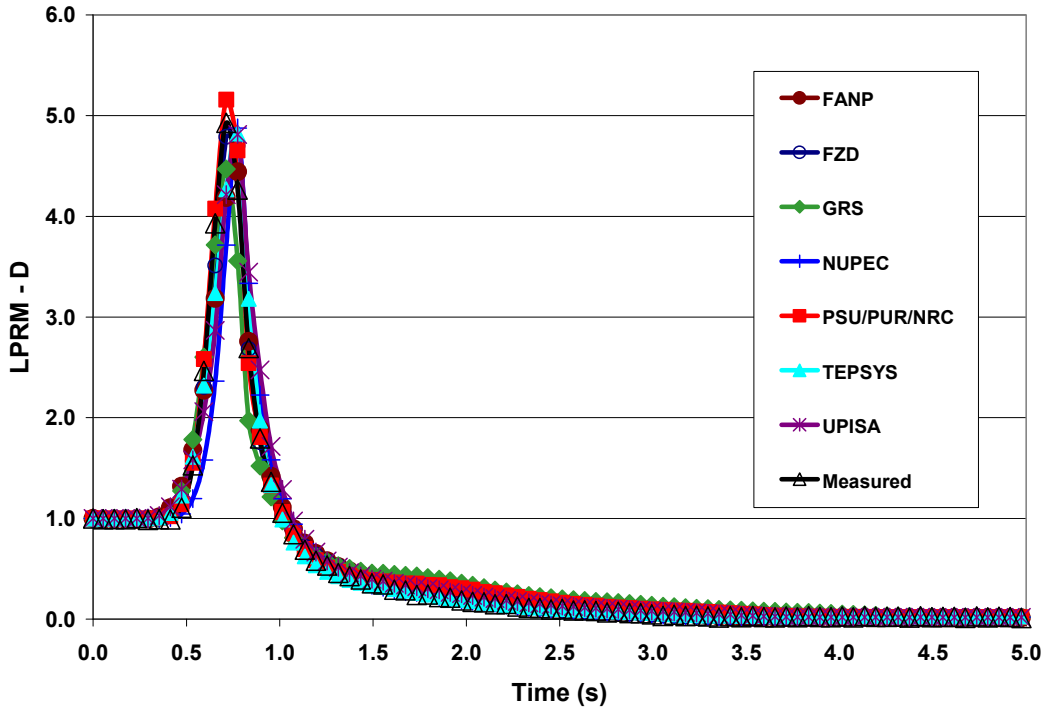

Figure 4-50: Best-estimate case – LPRM-D (zoom)

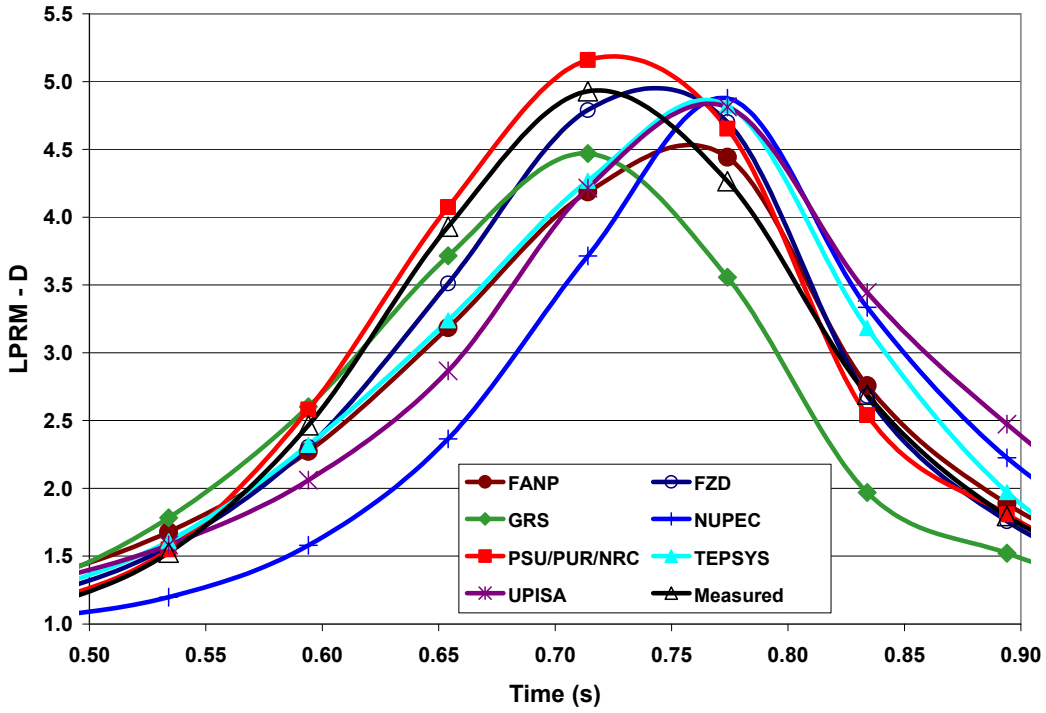

Figure 4-51: Best-estimate case – LPRM-D (average vs. measured)

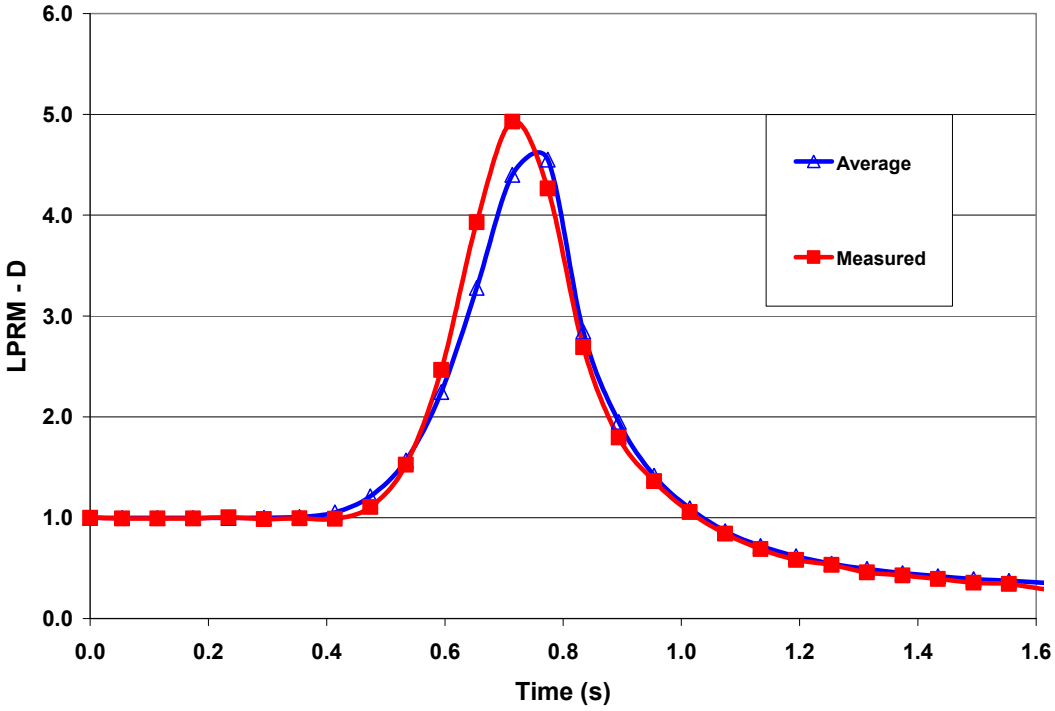

Table 4-18: Best-estimate case – normalised LPRM-D power, figure of merit

Participant	D'Auria FFT	Mean error, ME
FANP	0.8052	0.9995
FZD	0.8584	0.9993
GRS	0.7879	0.9935
NUPEC	0.7056	0.9956
PSU/PUR/NRC	0.8498	0.9923
TEPSYS	0.7932	0.9999
UPISA	0.7459	0.9935

4.2.2 Snapshot at the time of maximum power (best-estimate case)

Participants' results for the snapshot at the time of maximum power before scram were analysed in order to investigate coupled neutronics/thermal-hydraulics modelling and the participants' code prediction capabilities at the conditions where the maximum power is reached and scram is still not activated.

The results in this section are presented in two groups – one for the participants that used fission power and the other for the participants that used total power. Figures 4-52 and 4-53 present graphical comparisons of participants' predictions of the time of maximum power before scram with the mean value as reference, while Table 4-19 provides the values with the mean and standard deviation. In general results are in good agreement. With the exceptions of the PSI result for fission power group and the TEPSYS result for total power group all deviations are within 2σ. The following observations can be made from Table 4-20, which provides the values of maximum power before scram with the mean and standard deviation. For the fission power group all deviations (except CEA-33) are within $\pm\sigma$ while for the total power group all deviations (except NFI and UPV-1) are also within $\pm\sigma$. Small deviations are observed from the mean solution for the core average relative axial power distribution results given in Figures 4-54 and 4-55 while the mean and standard deviations are presented in Figures 4-56 and 4-57. In comparison to the HP results (see Figures 4-5 and 4-6), the discrepancies are in average of the same magnitude but in the snapshot case they are more evenly distributed over the whole core height, while in the HP case the maximum deviations are observed in the bottom part of the core. Good agreements are observed in the predictions of relative axial profiles for the selected rodded and unrodded fuel assemblies as shown in Figures 4-57 through 4-65. One observation from the presented comparisons for axial power distributions is that the results in the total power group agree better than the results fission power group. The major reason for this fact can be deducted in inspecting Table 4-4. It can be seen that all of the participants using total power utilise the bypass model (bypass density correction) while in the fission power group some participants do utilise and some do not. For the total power group results of axial distributions the differences in the decay heat models still do not impact the comparisons since at this snapshot the fission power is the dominating contributor to the total power and the radial fission power distribution in the snapshot is similar to the radial power distribution at the initial HP conditions. The mean solutions for the radial power distribution and the standard deviations for the two groups of results (one based on fission power and the other on total) are given in Figures 4-66 through 4-69. If compared to the initial HP conditions the snapshot comparisons of radial power distribution exhibits similar deviations since what really changed in the snapshot is the total power level and axial distribution but not the radial one since the scram is still not activated.

The complete list of the mean solutions and standard deviations can be found in Appendix C and the deviations of each participant's solution from the mean value can be found in Appendix D. Both appendices are provided upon request on CD-ROM.

Figure 4-52: Best-estimate case – time of maximum power

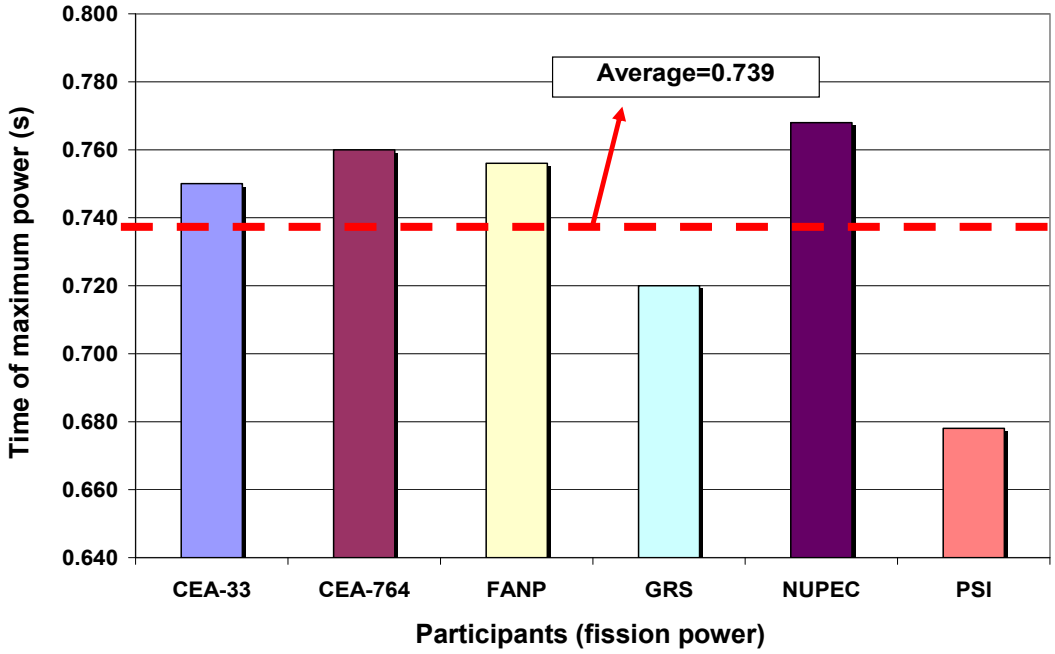

Figure 4-53: Best-estimate case – time of maximum power

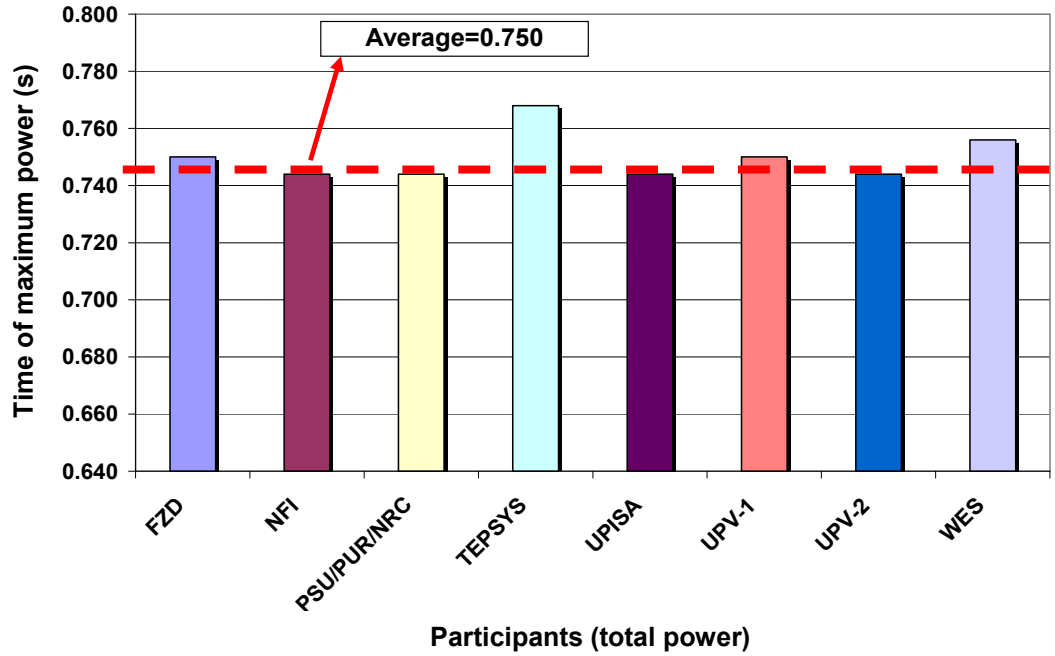

Table 4-19: Best-estimate case – time of maximum transient power and deviation

Fission power submitted			Total power submitted		
Participant	**Time of max power (s)**	**Deviation (e_i)**	**Participant**	**Time of max power (s)**	**Deviation (e_i)**
CEA-33	0.750	0.011	FZD	0.750	0.000
CEA-764	0.760	0.021	NFI	0.744	-0.006
FANP	0.756	0.017	PSU/PUR/NRC	0.744	-0.006
GRS	0.720	-0.019	TEPSYS	0.768	0.018
NUPEC	0.768	0.029	UPISA	0.744	-0.006
PSI	0.678	-0.061	UPV-1	0.750	0.000
			UPV-2	0.744	-0.006
			WES	0.756	0.006

Average (fission) =	0.739	**Average (total) =**	0.750
Standard deviation (σ) =	0.034	**Standard deviation (σ) =**	0.008

Table 4-20: Best-estimate case – maximum transient power and deviation

Fission power submitted			Total power submitted		
Participant	**Time of max power (s)**	**Deviation (e_i)**	**Participant**	**Time of max power (s)**	**Deviation (e_i)**
CEA-33	1.35E+10	3.17E+09	FZD	8.99E+09	-9.71E+07
CEA-764	1.15E+10	1.17E+09	NFI	7.52E+09	-1.58E+09
FANP	8.80E+09	-1.48E+09	PSU/PUR/NRC	9.36E+09	2.62E+08
GRS	8.45E+09	-1.83E+09	TEPSYS	9.18E+09	7.89E+07
NUPEC	9.65E+09	-6.32E+08	UPISA	9.22E+09	1.19E+08
PSI	9.88E+09	-3.97E+08	UPV-1	1.01E+10	1.03E+09
			UPV-2	8.93E+09	-1.66E+08
			WES	9.45E+09	3.52E+08

Average (fission) =	1.03E+10	**Average (total) =**	9.10E+09
Standard deviation (σ) =	1.87E+09	**Standard deviation (σ) =**	7.37E+08

Figure 4-54: Core axial power profile at maximum power (participants submitted fission power)

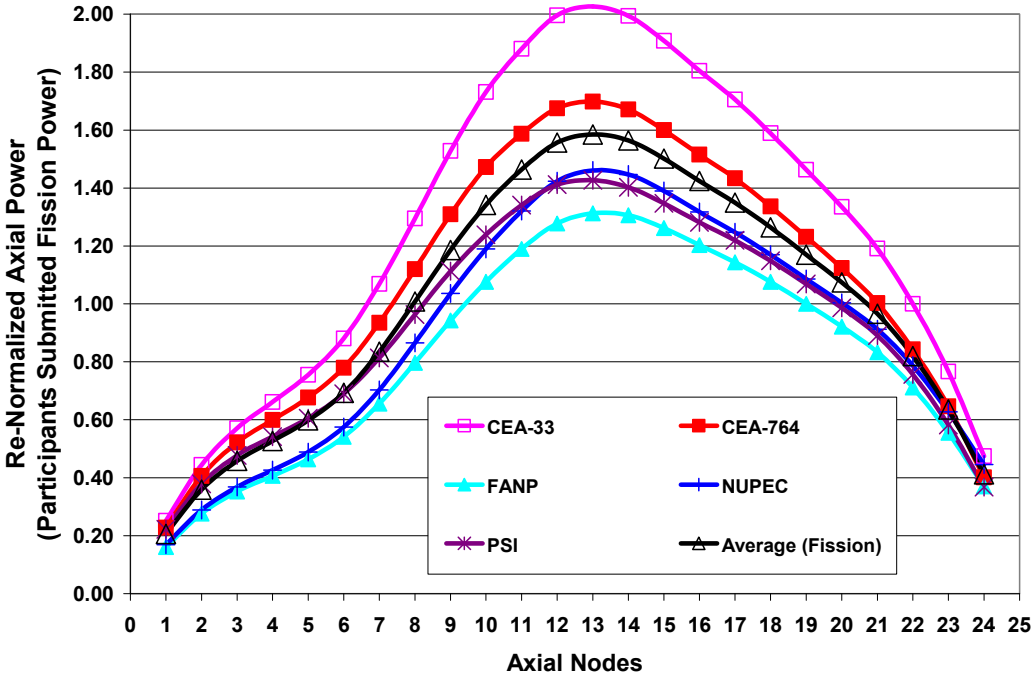

Figure 4-55: Core axial power profile at maximum power (participants submitted total power)

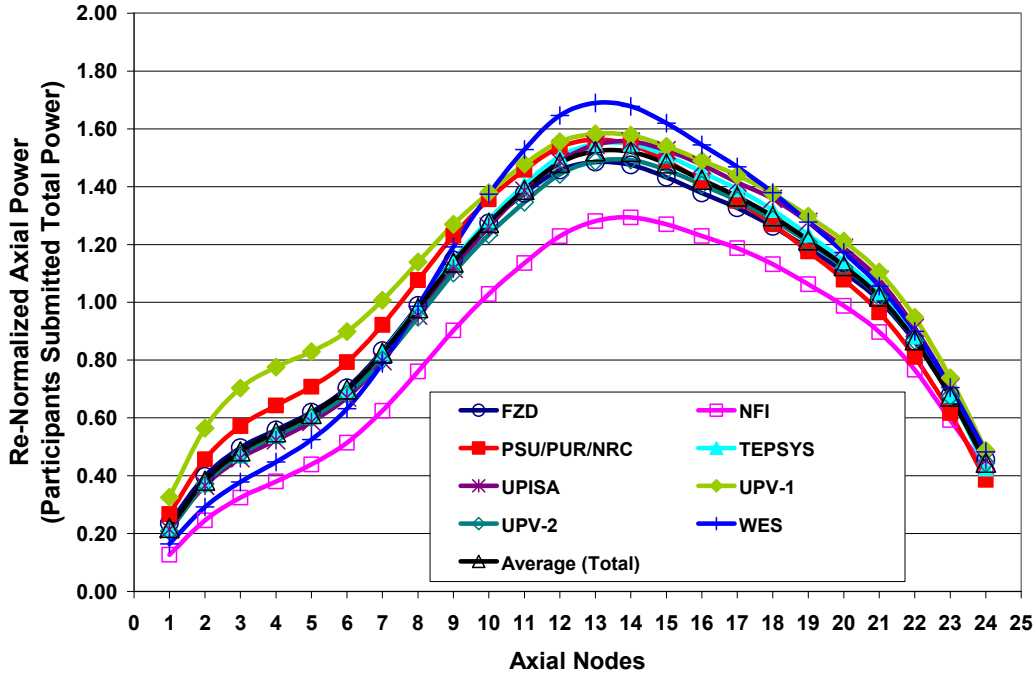

Figure 4-56: Core axial power profile at maximum power (participants submitted fission power) – mean and deviation

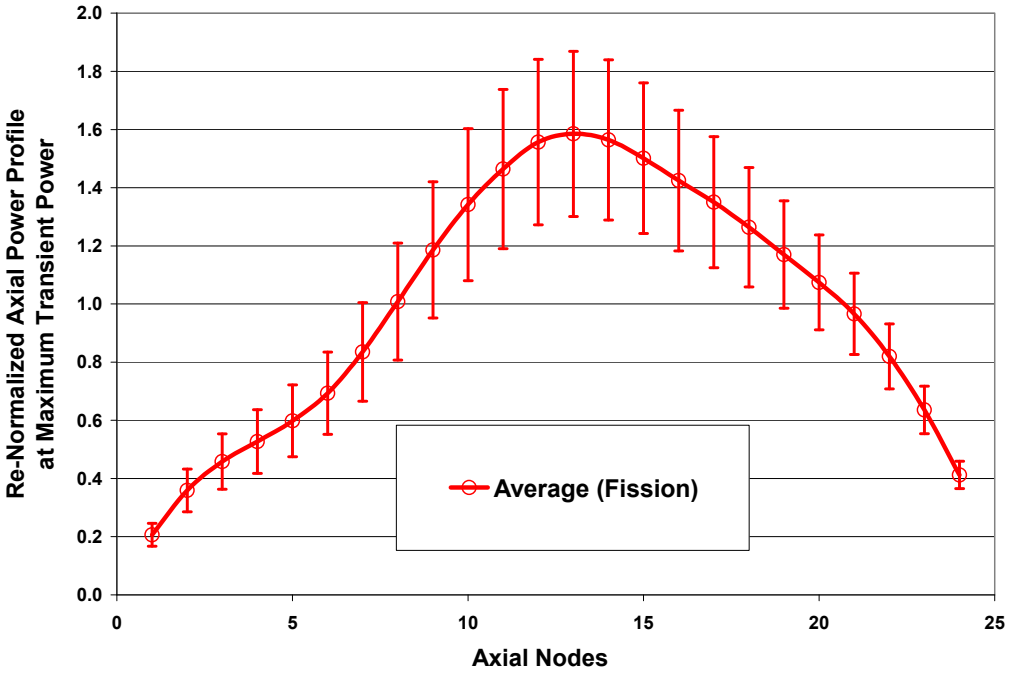

Figure 4-57: Core axial power profile at maximum power (participants submitted total power) – mean and deviation

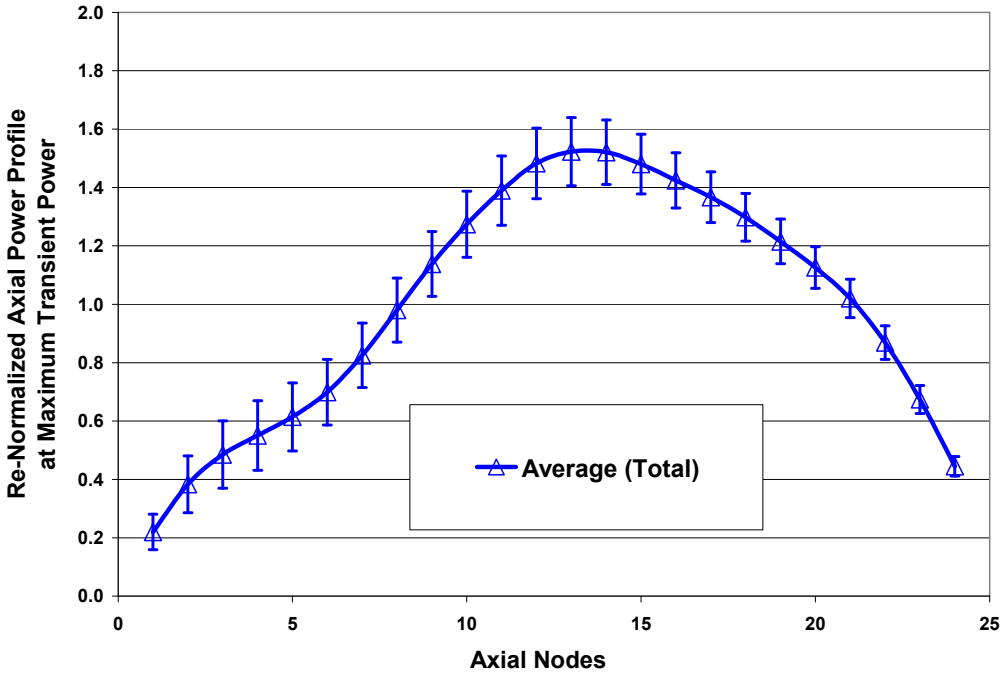

Figure 4-58: Relative power of FA 75 at maximum power (participants submitted fission power)

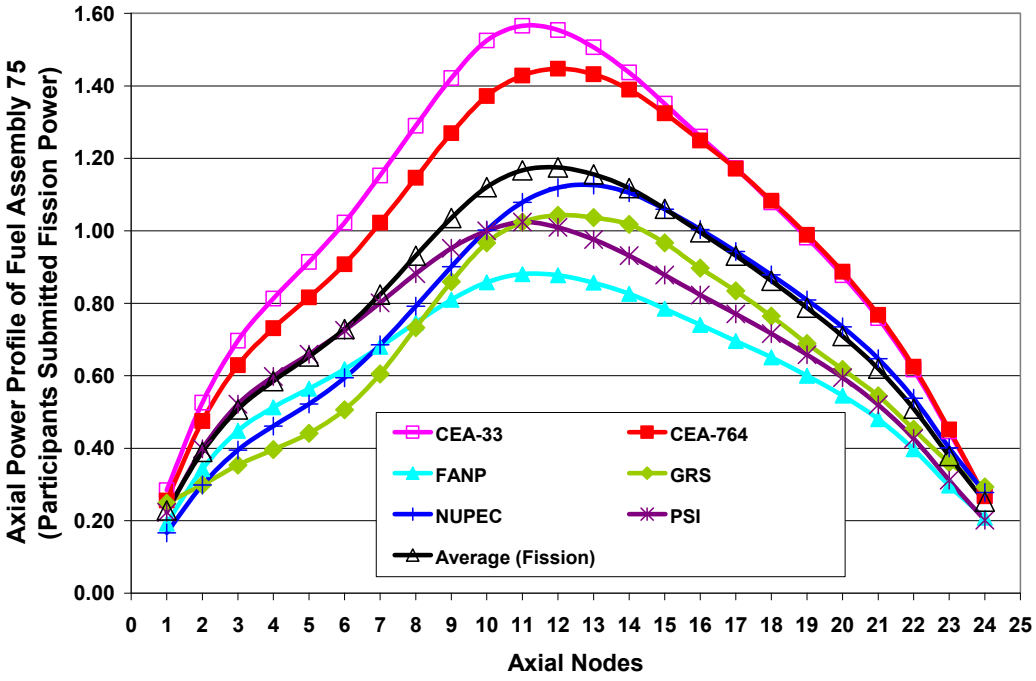

Figure 4-59: Relative power of FA 75 at maximum power (participants submitted total power)

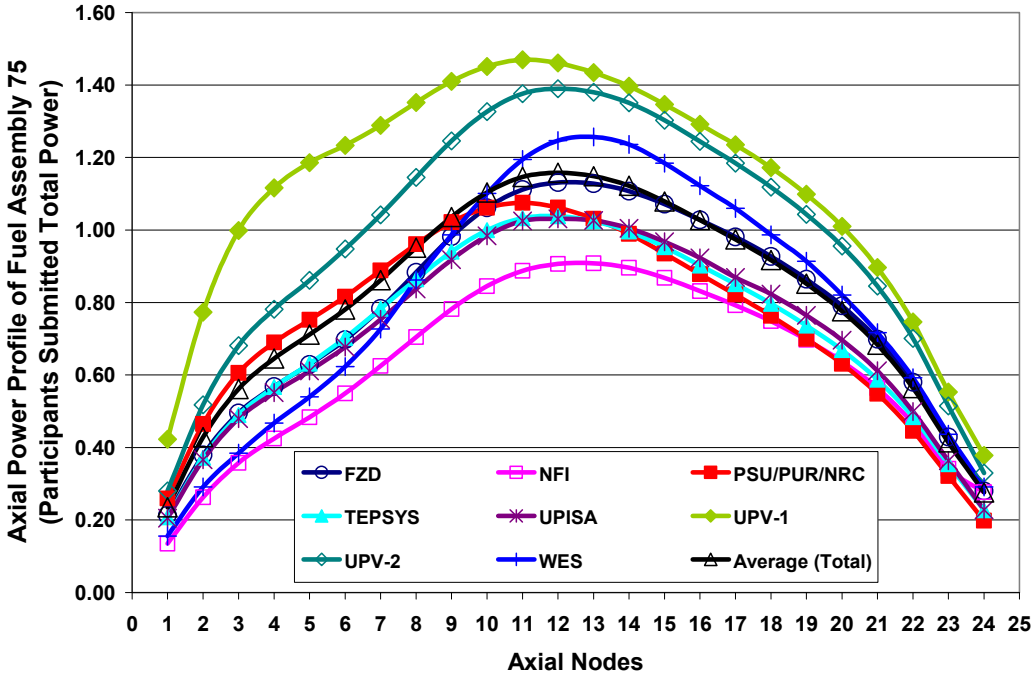

Figure 4-60: Relative power of FA 75 at maximum power (participants submitted fission power) – mean and deviation

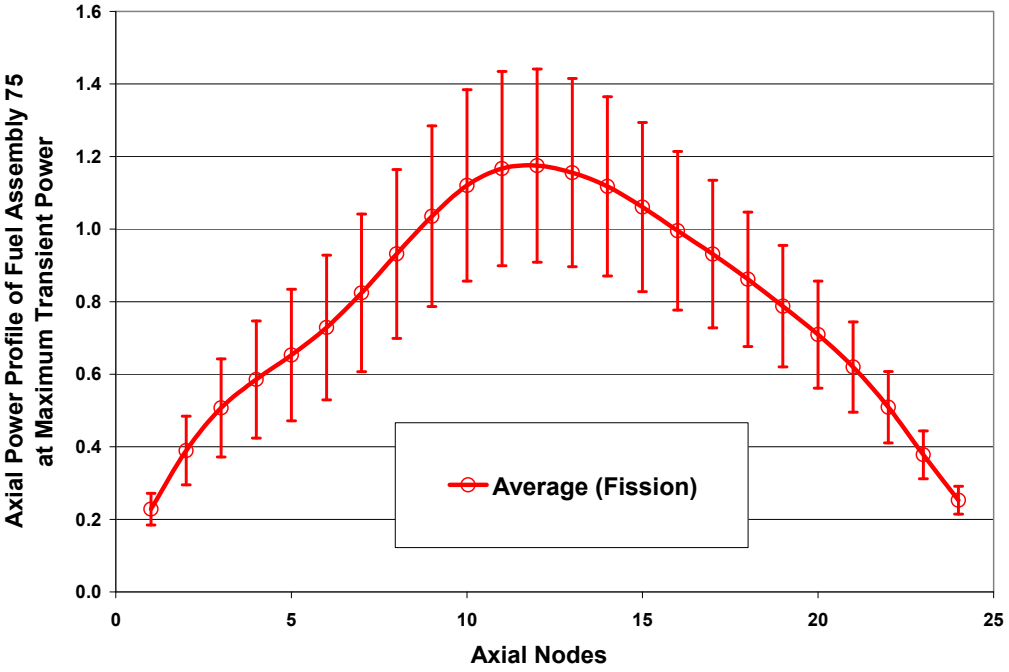

Figure 4-61: Relative power of FA 75 at maximum power (participants submitted total power) – mean and deviation

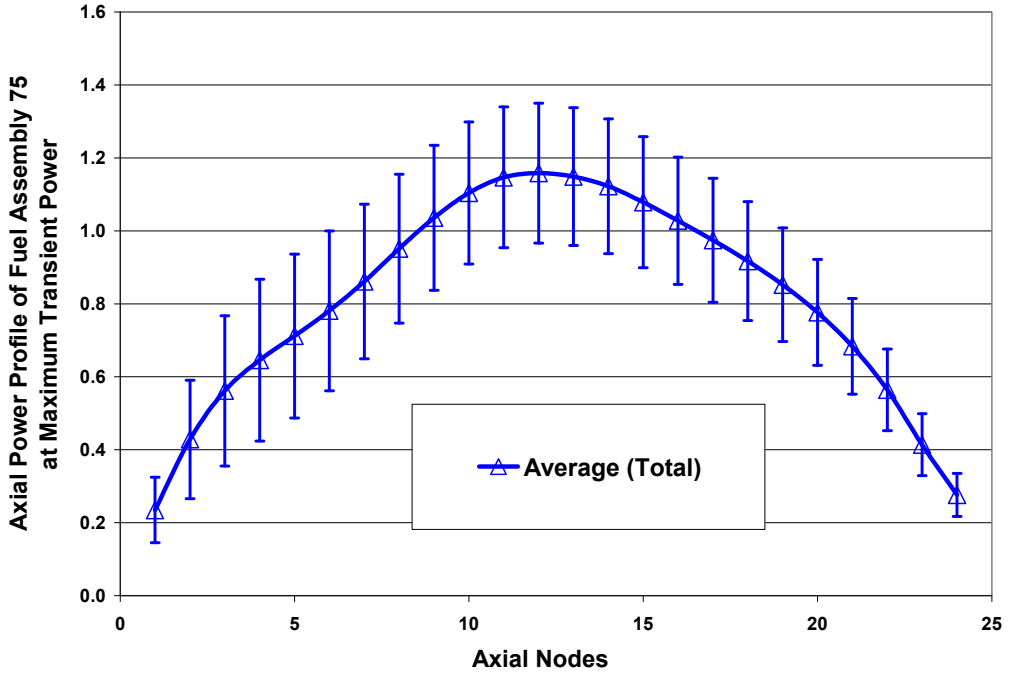

Figure 4-62: Relative power of FA 367 at maximum power (participants submitted fission power)

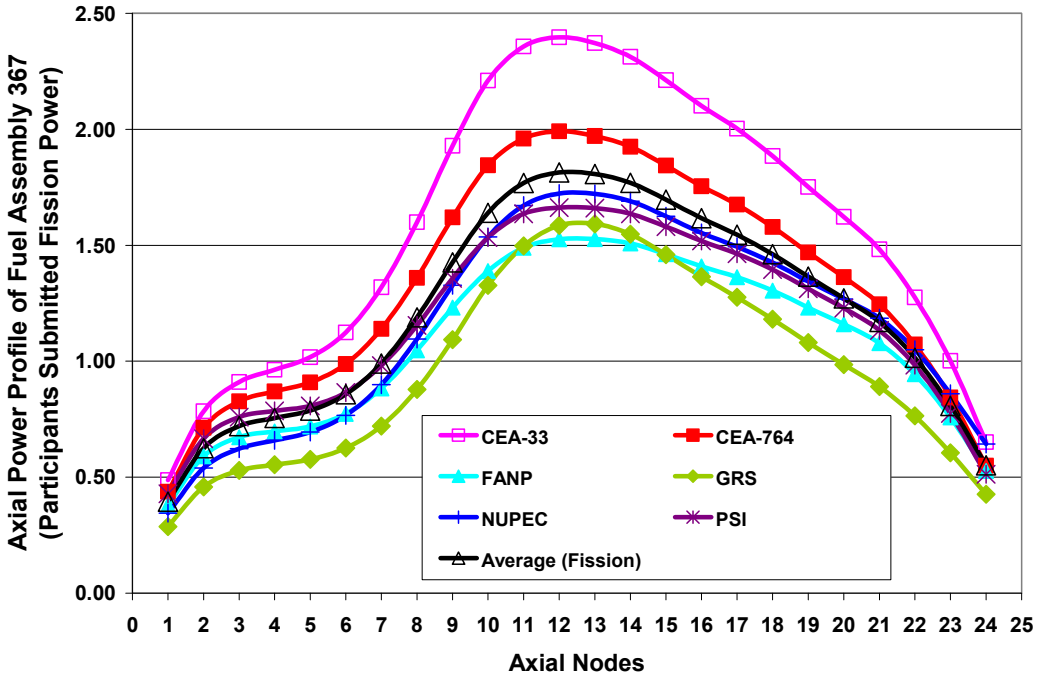

Figure 4-63: Relative power of FA 367 at maximum power (participants submitted total power)

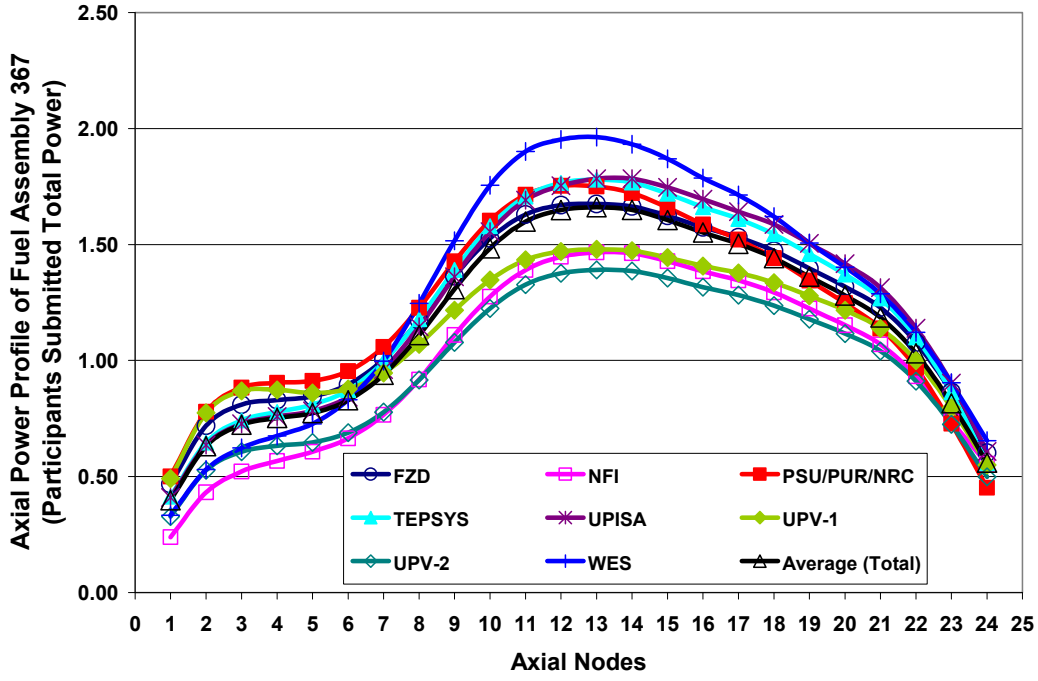

Figure 4-64: Relative power of FA 367 at maximum power (participants submitted fission power) – mean and deviation

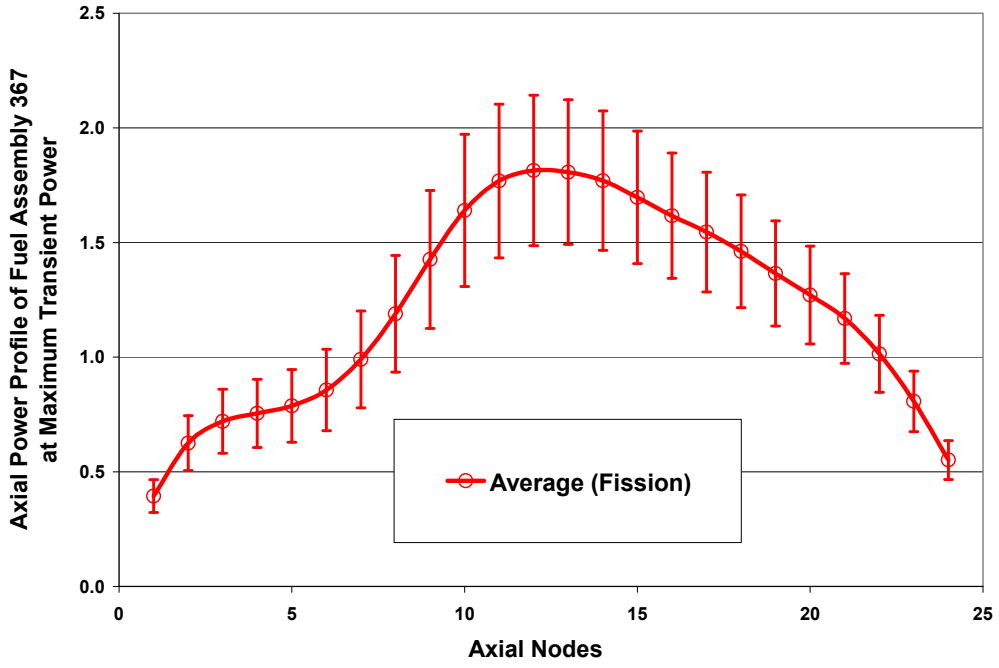

Figure 4-65: Relative power of FA 367 at maximum power (participants submitted total power) – mean and deviation

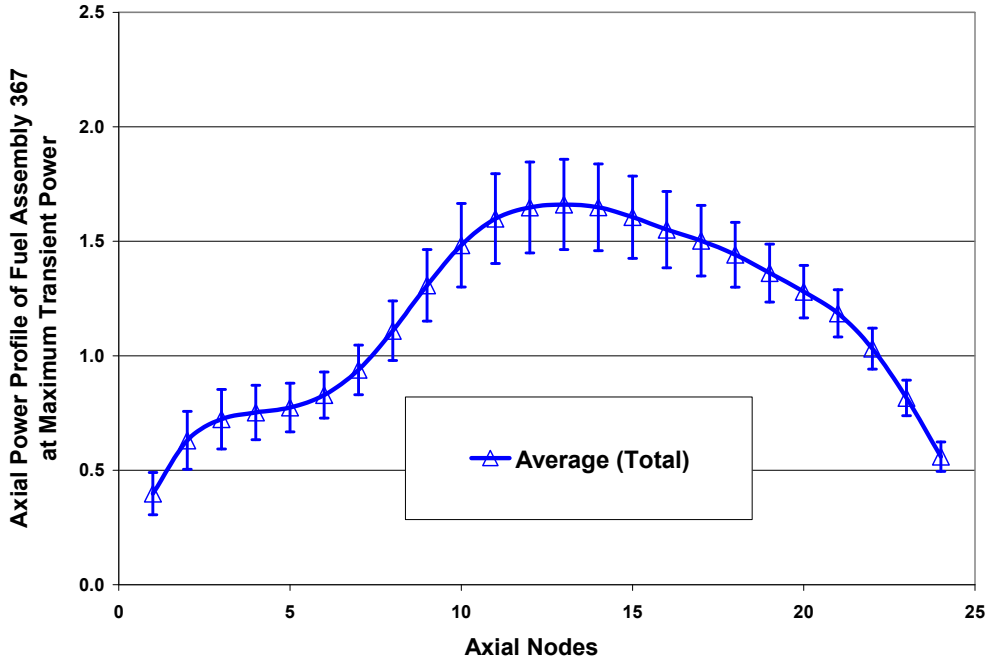

Figure 4-66: Mean radial power distribution at maximum power (participants submitted fission power)

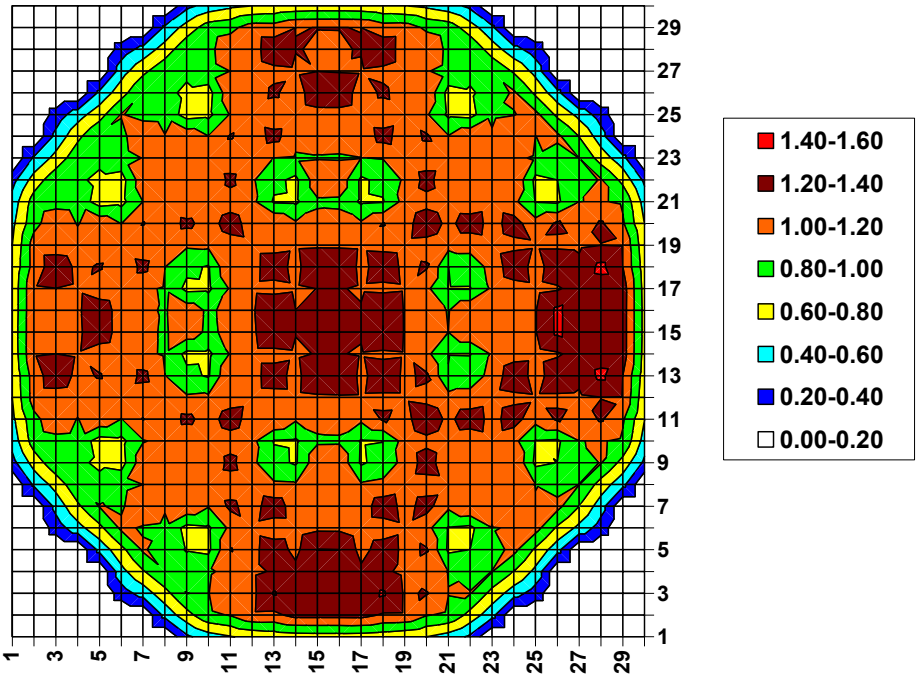

Figure 4-67: Mean radial power distribution at maximum power (participants submitted total power)

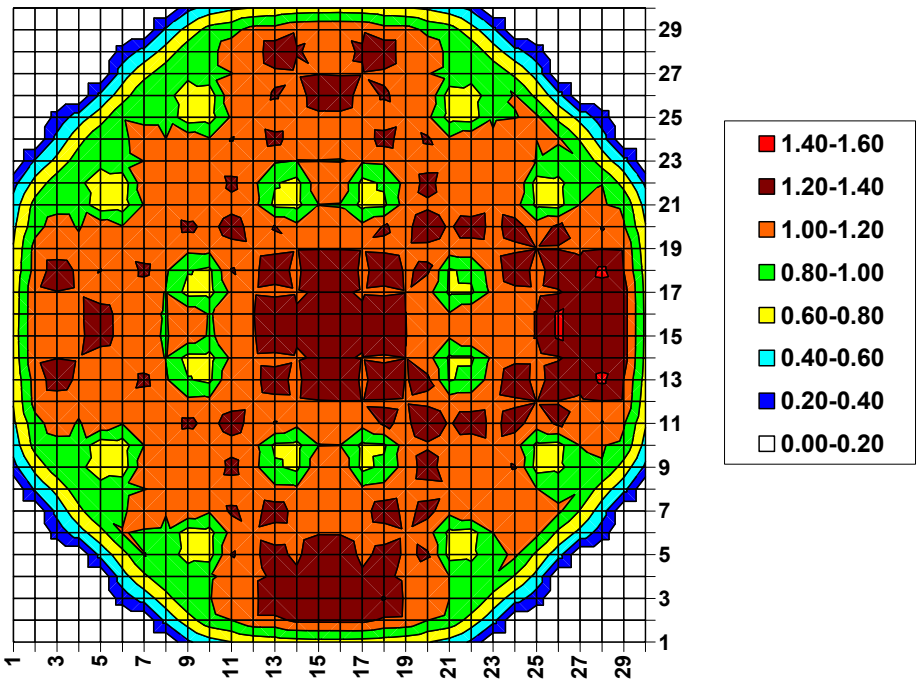

Figure 4-68: Standard deviation of radial power distribution at maximum power (participants submitted fission power)

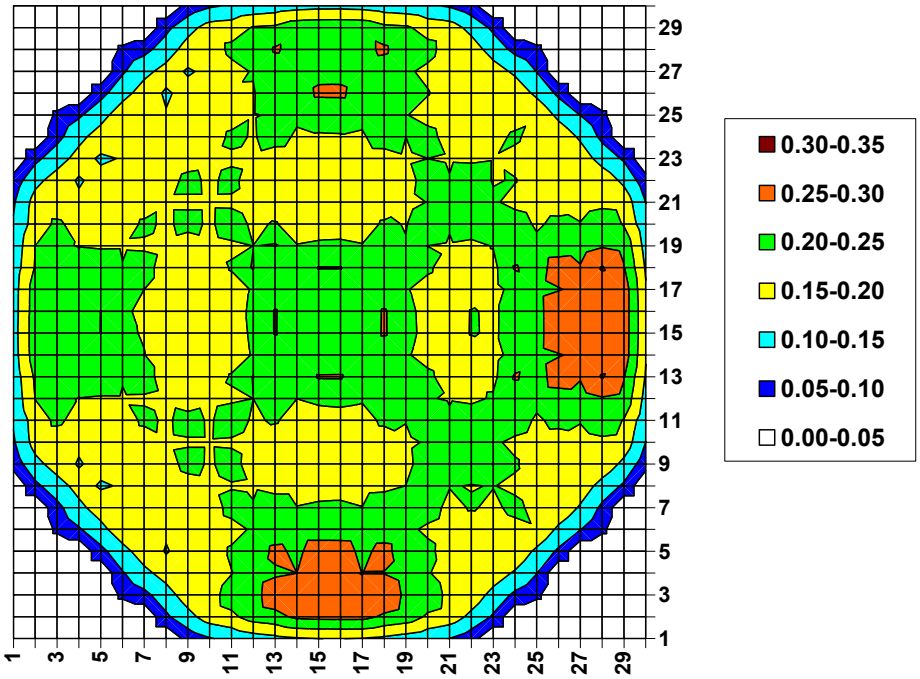

Figure 4-69: Standard deviation of radial power distribution at maximum power (participants submitted total power)

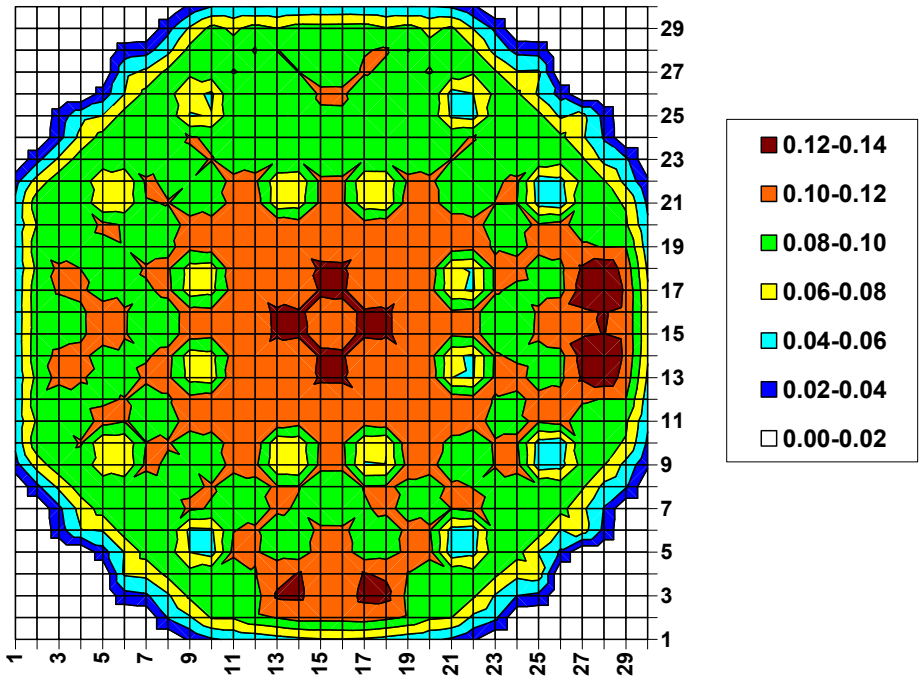

4.2.3 Snapshot at the end of the transient (best-estimate case)

The conditions of the snapshot at 5 s into the transient (the end of the simulated transient) are different from the conditions of the snapshot at the time of maximum power before scram. The bypass model still will play a role since the bypass density correction in the cross-section feedback modelling is to account for the deviations of bypass density from the saturated value used in the cross-section homogenisation (please note that the cross-sections are generated by homogenising the bypass region at saturated conditions associated with the lattice at actual conditions). The consistent utilisation of the ADF and xenon models is also relevant to the agreement (or disagreement) of participants' predictions for this snapshot. Since the control rods were tripped during the scram some of the differences are coming from the neutronics methods and control rod models. The decay modelling in total power group results for axial power distributions is very important because for this snapshot the decay heat is the dominating contributor to the total power and the method used for the spatial distribution of the decay heat is quite important – according to the fission power distribution at the initial HP conditions or according to the fission power distribution at this snapshot.

Table 4-21 provides the values of the power at the end of transient (5 s) with the mean and standard deviation for both groups of results (with fission power and with total power). In general results are in good agreement. Except for the NUPEC results for fission power group and the TEPSYS and UPV results for total power group, all deviations are within $\pm\sigma$.

The core average relative axial power distribution results are compared and analysed in Figures 4-70 through 4-73. From these comparisons it can be clearly seen that the participants' results based on fission power agree much better and form a cluster (with the exception of the NUPEC result) with much less spread (standard deviation around the mean solution) as compared to the results based on total power. The explanation of this observation is that the total power results include and are dominated by decay heat power modelling. A similar tendency is present in the relative power distribution results for selected unrodded and rodded fuel assemblies as shown in Figures 4-74 through 4-81. The mean radial power distributions and standard deviation distributions for the two groups are given in Figures 4-82 through 4-85. In summary, if compared to the comparisons of power distribution results for the snapshot at the time of maximum power before scram case, the discrepancies in the participants' results are higher for the snapshot at the end of the transient.

The complete list of the mean solutions and standard deviations can be found in Appendix C and the deviations of each participant's solutions from the mean value can be found in Appendix D. Both appendices are provided upon request on CD-ROM.

Table 4-21: Best-estimate case – power at the end of the transient (5 s) and deviation

Fission power submitted			Total power submitted		
Participant	**Power at 5 s (W)**	**Deviation (e_i)**	**Participant**	**Power at 5 s (W)**	**Deviation (e_i)**
CEA-33	2.81E+07	-1.34E+06	FZD	1.33E+08	3.29E+07
CEA-764	2.78E+07	-1.76E+06	NFI	1.37E+08	3.69E+07
FANP	2.87E+07	-7.26E+05	PSU/PUR/NRC	1.57E+08	5.61E+07
GRS	3.04E+07	9.40E+05	TEPSYS	2.86E+07	-7.19E+07
NUPEC	3.23E+07	2.91E+06	UPISA	1.57E+08	5.63E+07
PSI	2.94E+07	-2.06E+04	UPV-1	2.86E+07	-7.19E+07
			UPV-2	2.95E+07	-7.10E+07
			WES	1.33E+08	3.24E+07

Figure 4-70: Core axial power profile at the end of the transient (participants submitted fission power)

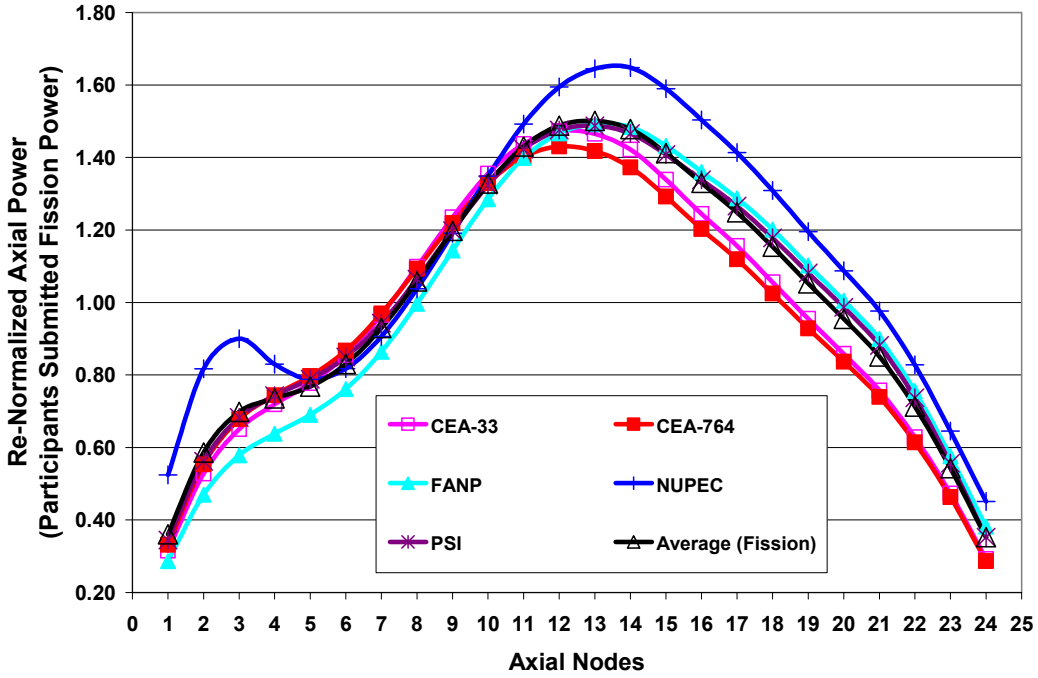

Figure 4-71: Core axial power profile at the end of the transient (participants submitted total power)

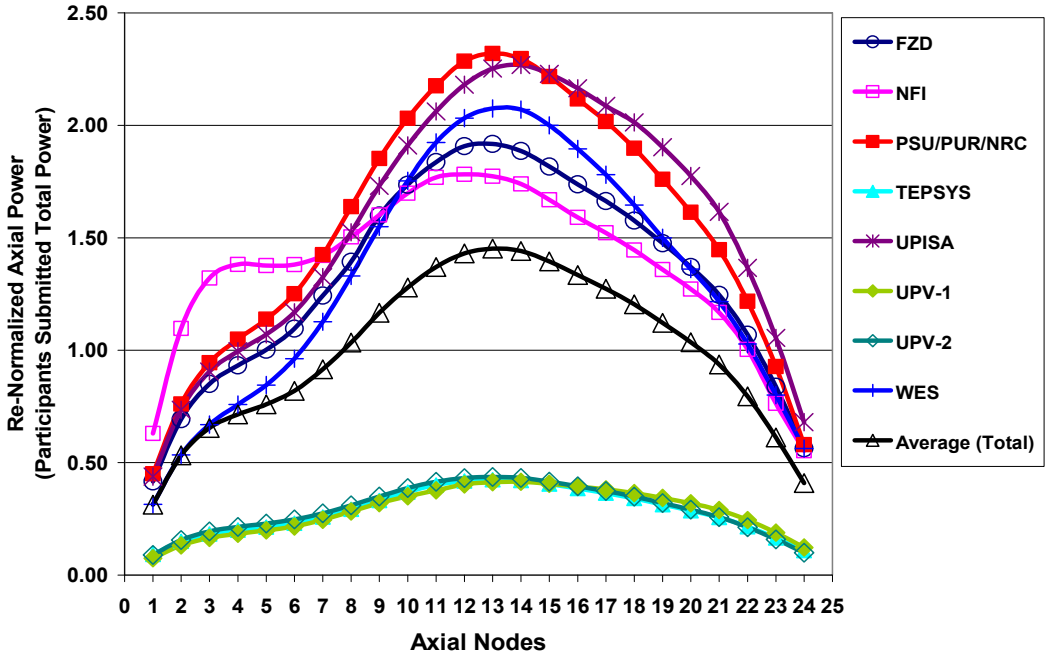

Figure 4-72: Core axial power profile at the end of the transient (participants submitted fission power) – mean and deviation

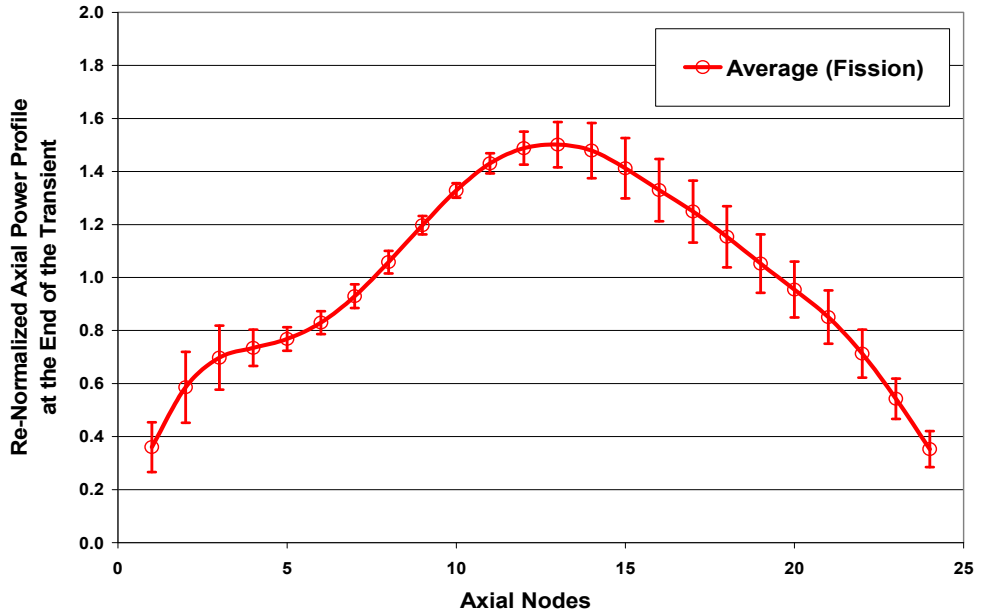

Figure 4-73: Core axial power profile at the end of the transient (participants submitted total power) – mean and deviation

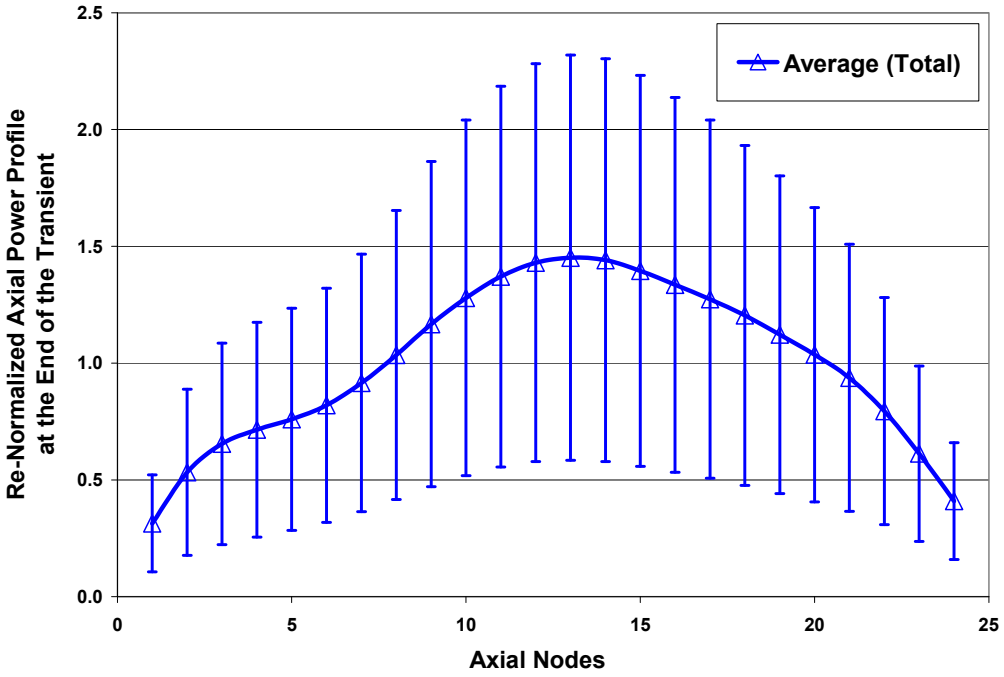

Figure 4-74: Relative power of FA 75 at the end of the transient (participants submitted fission power)

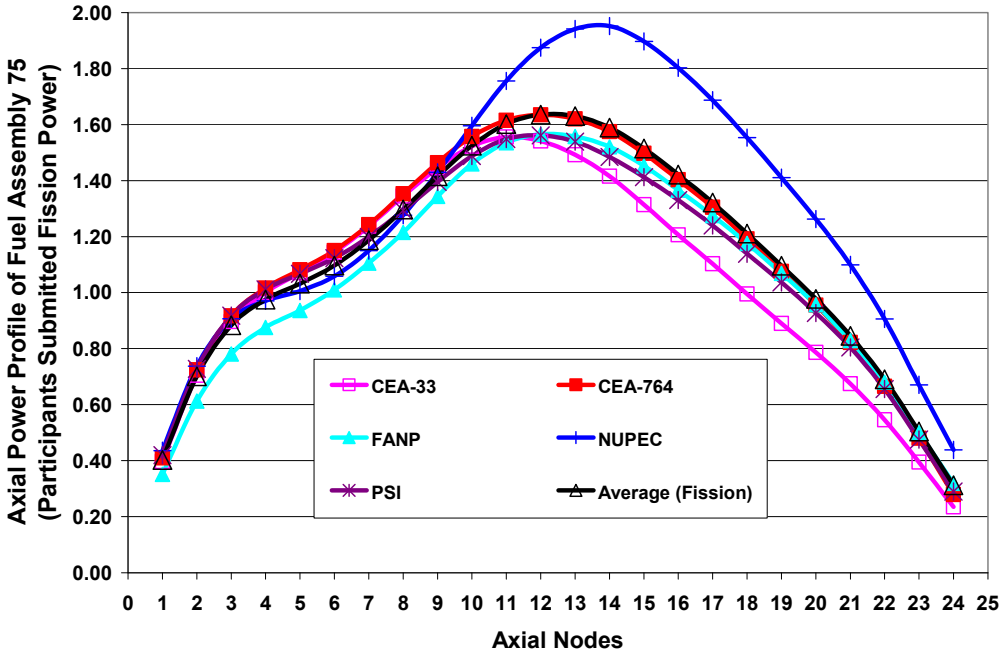

Figure 4-75: Relative power of FA 75 at the end of the transient (participants submitted total power)

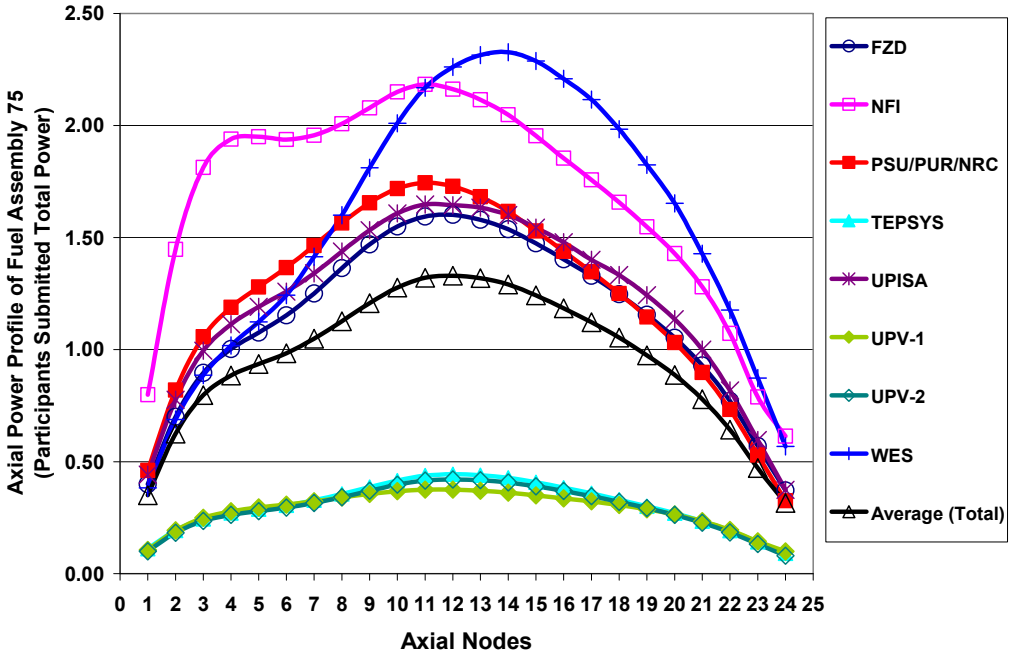

Figure 4-76: Relative power of FA 75 at the end of the transient (participants submitted fission power) – mean and deviation

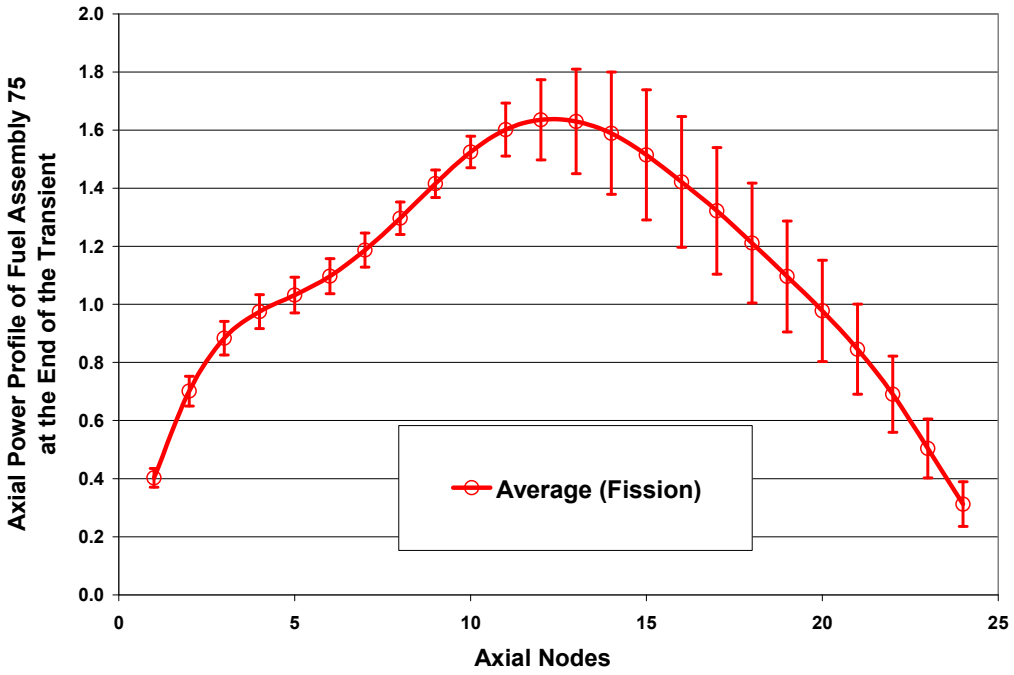

Figure 4-77: Relative power of FA 75 at the end of the transient (participants submitted total power) – mean and deviation

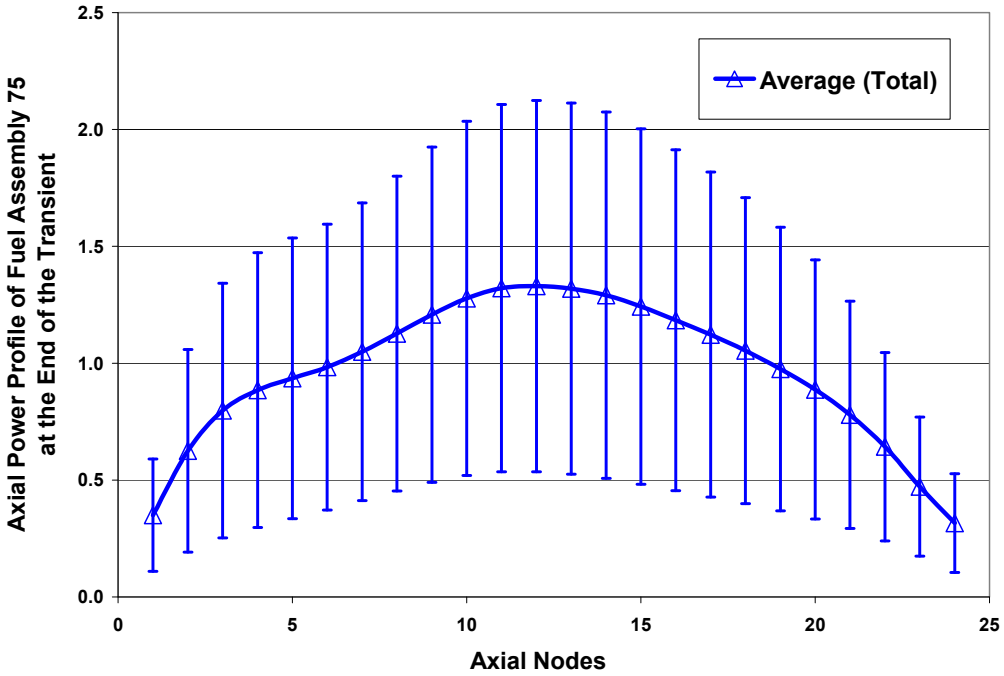

Figure 4-78: Relative power of FA 367 at the end of the transient (participants submitted fission power)

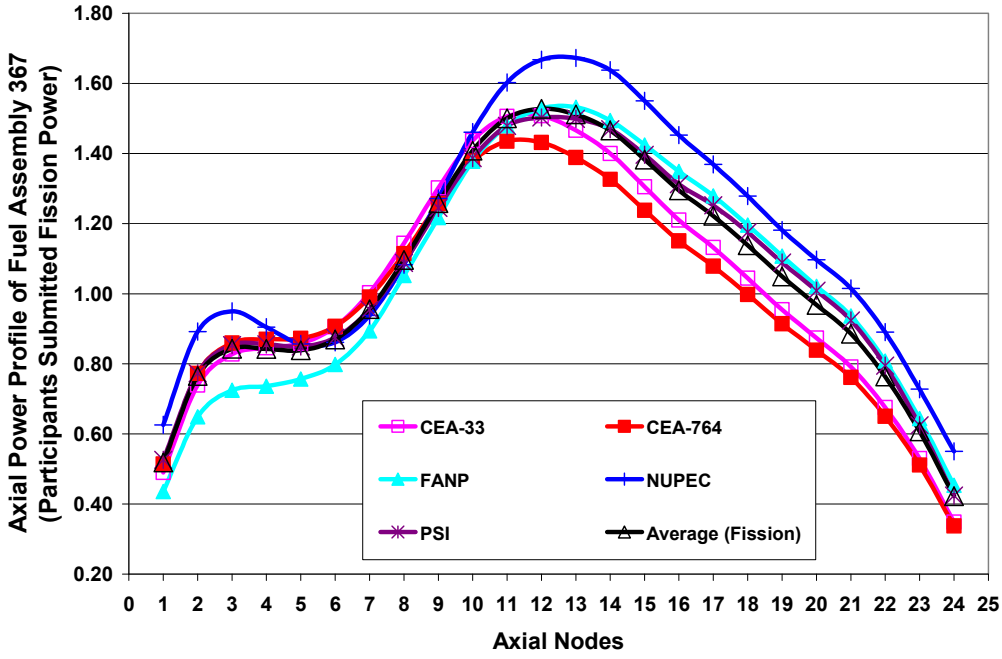

Figure 4-79: Relative power of FA 367 at the end of the transient (participants submitted total power)

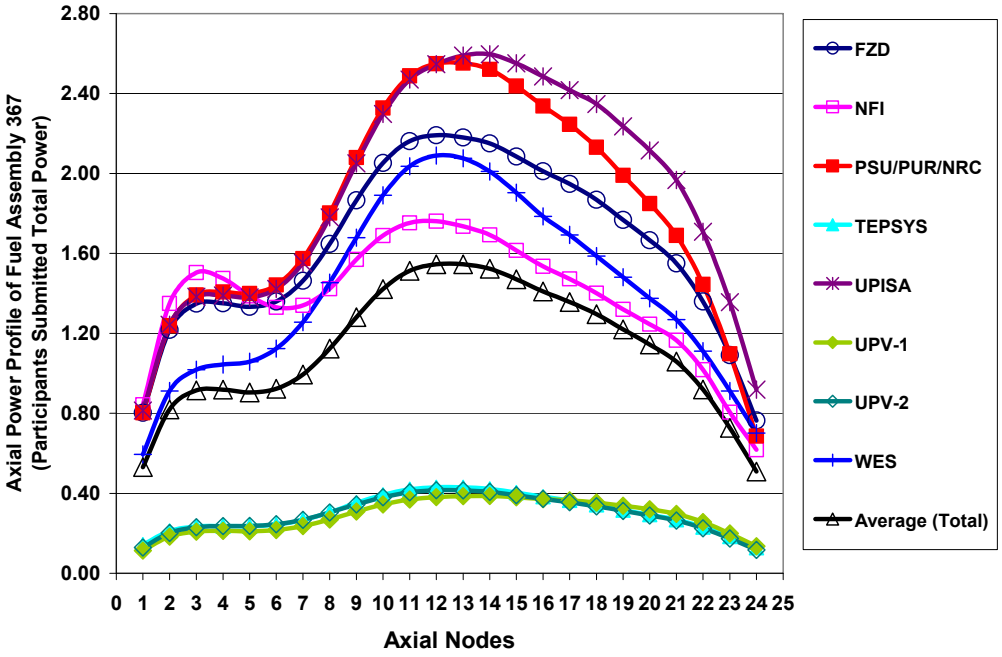

Figure 4-80: Relative power of FA 367 at the end of the transient (participants submitted fission power) – mean and deviation

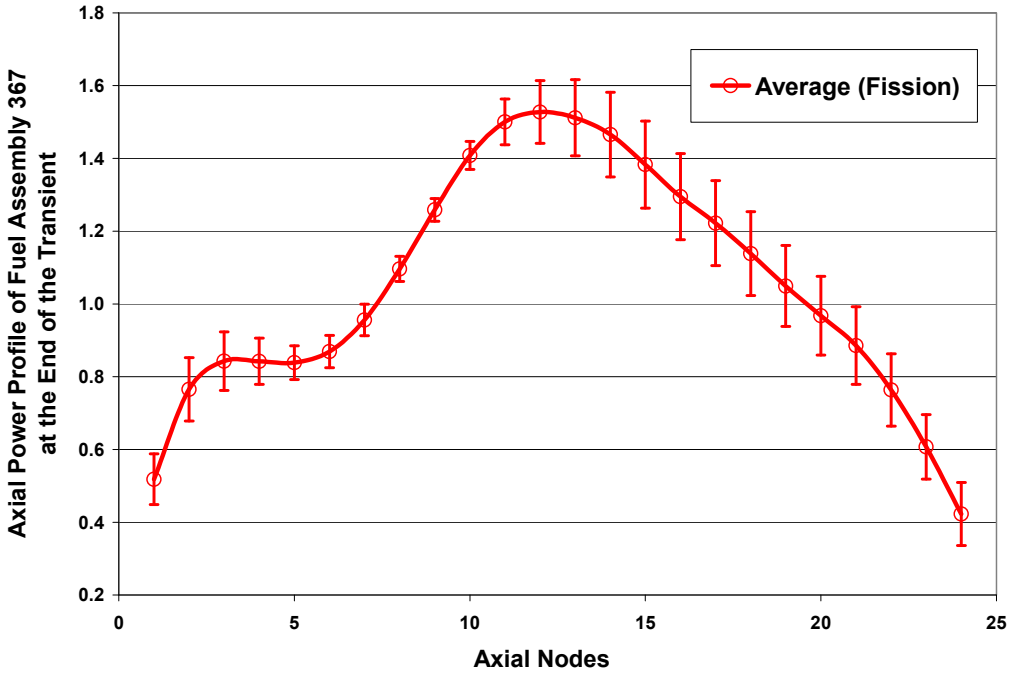

Figure 4-81: Relative power of FA 367 at the end of the transient (participants submitted total power) – mean and deviation

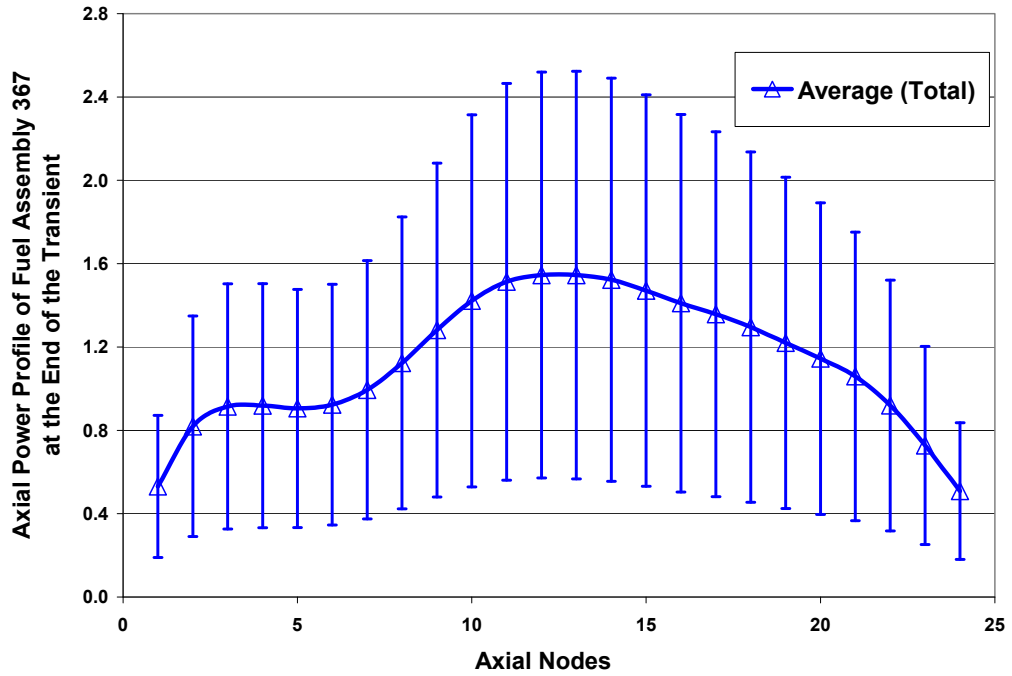

Figure 4-82: Mean radial power distribution at the end of the transient (participants submitted fission power)

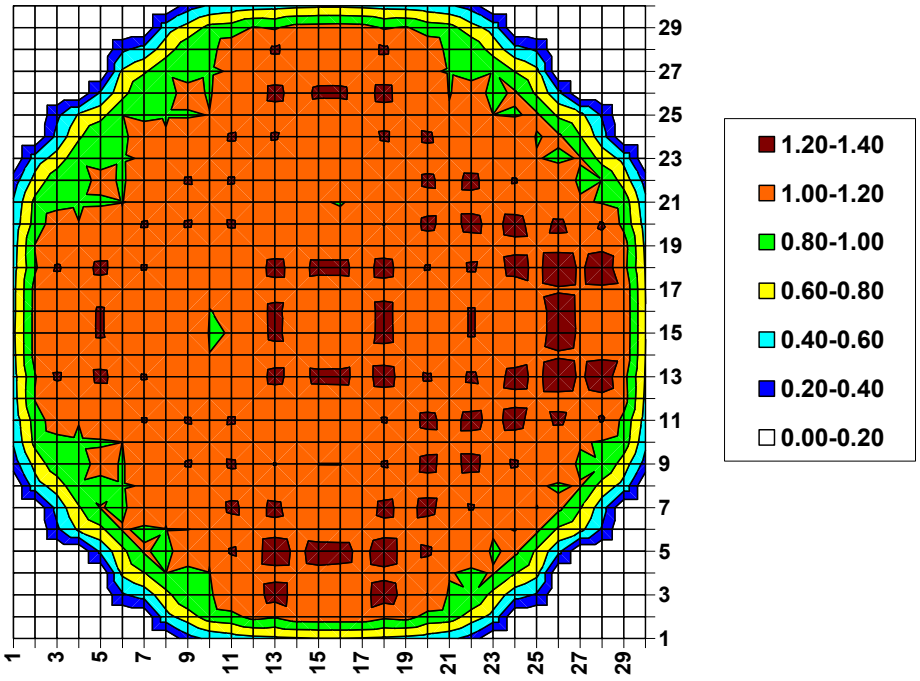

Figure 4-83: Mean radial power distribution at the end of the transient (participants submitted total power)

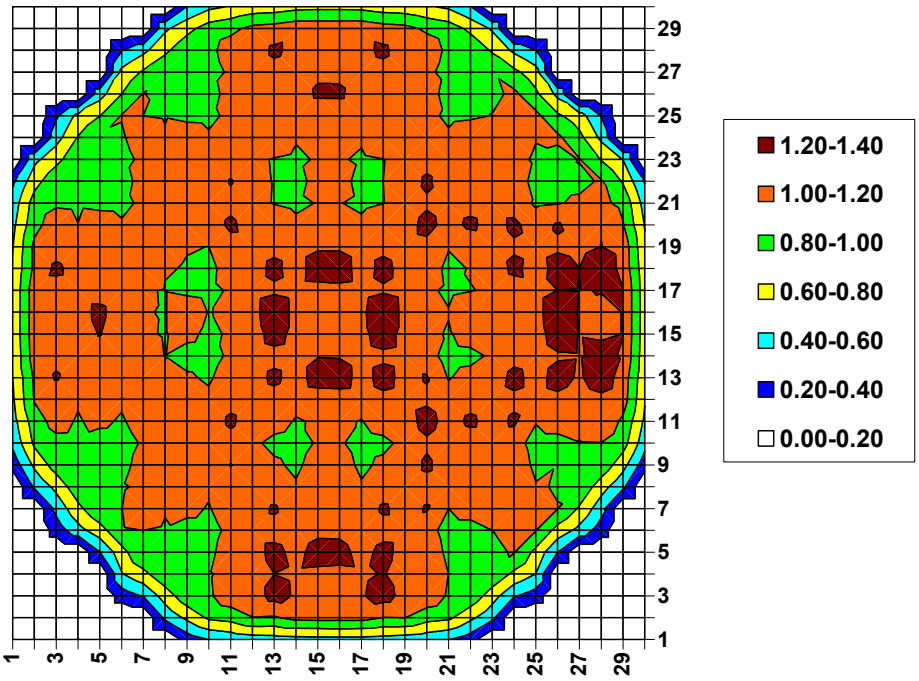

Figure 4-84: Standard deviation of radial power distribution at the end of the transient (participants submitted fission power)

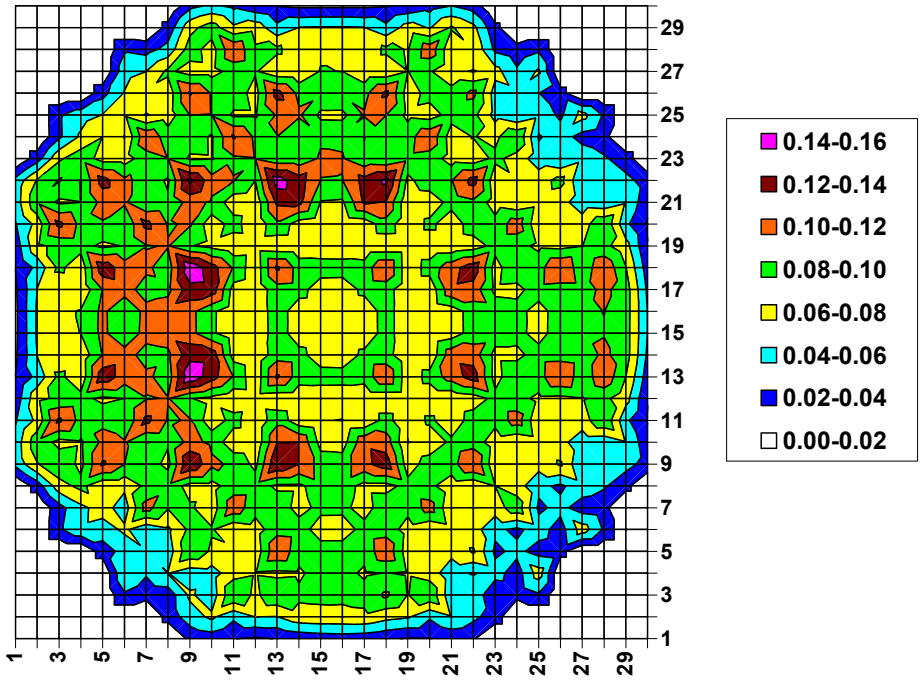

Figure 4-85: Standard deviation of radial power distribution at the end of the transient (participants submitted total power)

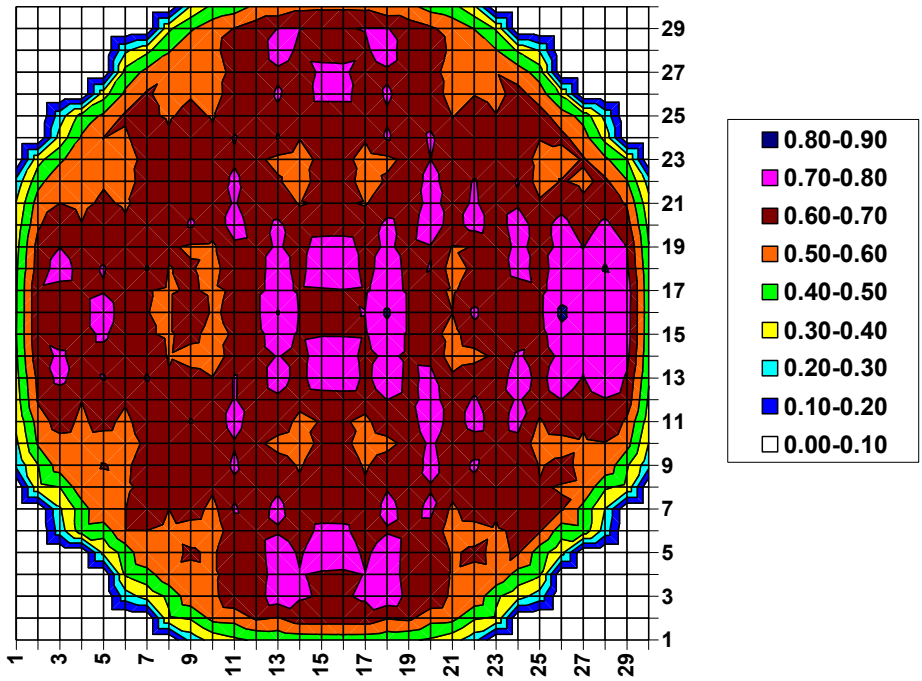

4.3 Transient results of Extreme Scenario 1

Turbine trip (TT) with steam bypass relief system failure is simulated in Exercise 3 Extreme Scenario 1. The analysis of the extreme scenarios provides a further understanding of modelling limitations of coupled codes and the interplays between different feedback mechanisms as well as testing the coupled code capabilities at extreme situations. The following simulation results of participants for this scenario are presented in this subsection:

- core power;
- dome pressure;
- core exit pressure;
- S/RV pressure;
- total reactivity;
- Doppler reactivity;
- void reactivity;
- power of LPRM-A;
- power of LPRM-B;
- power of LPRM-C;
- power of LPRM-D.

Table 4-22 presents the number of channels utilised in the thermal-hydraulics core models of the participants and the type of power model used in their calculations of Extreme Scenario 1. This information should be taken into account during the discussion of the participants' deviations from the reference solutions. The term "total" in the table refers to the total power, which includes power from decay heat and fission power together. Participants results presented in the figures are divided into two groups (Group 1 and Group 2) in order to visualise them clearly. The results in this section should be considered together with Table 4-23 since all of the models given in the table are important for the transient calculations.

Table 4-22: Number of channels used and power submitted by the participants – Extreme Scenario 1

Participant	Number of channels	Power submitted
CEA	33	Fission
FANP	33	Fission
FZD	764	Total
GRS	33	Fission
NFI	33	Total
NUPEC	33	Fission
PSI	34	Fission
PSU/PURDUE/NRC	33	Total
TEPSYS	33	Total
UPISA	33	Total
UPV (NOKIN)	33	Total
WESTINGHOUSE	764	Total

Table 4-23: Models used in Extreme Scenario 1

Participant	Xenon	ADF	Bypass	Decay
CEA	No	No	Yes	Yes
FANP	Yes	Yes	Yes	Yes
FZD	Yes	Yes	Yes	Yes
GRS	Yes	No	Yes	Yes
NFI	Yes	No	Yes	Yes
NUPEC	Yes	Yes	No	Yes
PSI	Yes	Yes	Yes	No
PSU/PURDUE/NRC	Yes	Yes	Yes	Yes
TEPSYS	Yes	Yes	Yes	Yes
UPISA	No	Yes	Yes	Yes
UPV	Yes	Yes	Yes	Yes
WESTINGHOUSE	No	Yes	Yes	Yes

The plots and tables in this section provide a comparison of the participants' results for the parameters that have the greatest effect on the Exercise 3 Extreme Scenario 1 analysis. For this reason core (averaged and local) and system time histories were requested from the participants to be submitted. These histories are: core average (core power, total reactivity, Doppler reactivity and void reactivity), core local (powers of LPRM A, B, C and D), and system (dome pressure, core exit pressure and S/RV pressure). Similar to the Exercise 3 best-estimate scenario, in order to minimise the impact of the deviations in code predictions at the initial steady-state conditions (which already have been analysed in Section 4.1) and to focus on the deviations in transient calculations, the comparisons of the predictions of time evolutions of the above parameters are performed not on the absolute values of the parameters but on the delta changes of the parameters as compared to the values at the initial steady state.

The reference time histories (average, *i.e.* mean) are provided in this section as well as in Appendix C. The figures of merit are presented in the tables of this section. Additionally, the participant deviations and figures of merit are presented in Appendix D, and are listed in the same order as the reference solutions. Appendices C and D are provided upon request on CD-ROM.

In each case the figures (Figures 4-86 through 4-111) graphically illustrate the agreement or disagreement of participants' predictions. Statistical evaluation is employed to generate a mean solution for parameters. The reference solutions are also shown in the plots.

Participants' sequences of events in Extreme Scenario 1 are given in Table 4-24.

Core power time evolutions are presented in two groups (fission or total) depending on the submitted core power type. Comparisons of the predictions of fission power evolution and the total power evolution calculated by each code throughout the transient (up to 10 seconds – it has been decided by participants at the benchmark workshops that the time histories for the extreme scenarios would be simulated and subsequently compared for 10 seconds into transient) are shown in Figures 4-86 and 4-88 while Figures 4-87 and 4-89 zoom on the first seconds of the transient. Table 4-25 provides figure of merit (FOM) for two different methods, D'Auria FFT and Mean Error.

When analysing the power history results it has to be taken into account that in Extreme Scenario 1 the same phenomena takes place as in the actual TT2 test (best-estimate scenario), with the difference that a turbine trip with failure of the steam bypass relief system leads to much larger pressure wave propagated through the system, which results in much stronger power response. This power response in terms of timing and magnitude of power peak during the transient as predicted by different codes is a function of the total reactivity time evolution. In Figure 4-87 (the fission power group), the predicted power peak values of two participants (GRS and FANP) are higher than the mean value. In total power group (Figure 4-89), all of the codes' predictions (except PSU/PUR/NRC) form a cluster around the mean solution. In general, the power history results are in a good agreement.

System parameter (dome pressure, core exit pressure and S/RV pressure) time evolutions are presented in two groups (Group 1 and Group 2) in order to visualise them clearly. Comparisons of the predictions of these parameters calculated by each code throughout the transient (up to 10 seconds) are shown in Figures 4-90 through 4-95 while Tables 4-26 through 4-28 provide figure of merit (FOM)

for two different methods, D'Auria FFT and Mean Error. It is important to note that on the S/RV pressure time history plots the three safety relief set points are provided to show which valves open and when for different participants' simulations.

Figures 4-96 through 4-103 show comparisons of the predictions of the total, Doppler and void reactivity throughout the transient (up to 10 seconds) and zoom of the beginning of transient. Larger deviations from mean solutions are observed after the scram for some participants, the total reactivity (TEPSYS, FZD, GRS), moderator density (void) reactivity (TEPSYS and NFI) and Doppler feedback reactivity (UPISA and TEPSYS) time histories. Discrepancies at the end of the transient are due to different predictions of the tripped control rod reactivity by the participants' codes.

Core local parameter time evolutions such as LPRM A, B, C and D power time histories are presented through three types of comparisons. Comparisons of the predictions of local parameter time evolutions calculated by each code throughout the transient (up to 10 seconds) are shown in Figures 4-104, 4-106, 4-108 and 4-110. Figures 4-105, 4-107, 4-109 and 4-111 zoom on the beginning of the transient. Tables 4-32 through 4-35 provide figure of merit (FOM) for two different methods, D'Auria FFT and Mean Error. It is important to note that for the four LPRM power time histories the average (mean) of participants' predictions is used as a reference solution.

Table 4-24: Sequence of events in Extreme Scenario 1

Participant	Event* (msec)				
	TSVC	DPIR	CEPIR	S/RVO	S/RVC
CEA	0.096	0.390	0.384	None	None
FANP	0.096	0.396	0.390	None	None
FZD	0.096	0.382	0.402	3.000	6.100
GRS	0.096	0.372	0.378	2.790	6.942
NFI	0.096	0.408	0.402	5.219	8.800
NUPEC	0.096	0.438	0.456	None	None
PSI	0.096	0.438	0.444	3.402	6.306
PSU/PUR/NRC	0.096	0.402	0.402	2.780	8.890
TEPSYS	0.096	0.366	0.360	2.946	None
UPISA	0.096	0.348	0.324	None	None
UPV	0.000	0.384	0.390	2.800	None
WES	0.900	0.402	0.450	None	None

* Description of the events: TSVC – turbine stop valve closed, DPIR – vessel dome pressure initial response (0.78% increased over initial value), CEPIR – core exit pressure initial response (0.27% increased over initial value), S/RVO – first safety/relief valve begins opening (refer to valve with lowest opening set-point), S/RVC – last safety/relief valve fully closed (refer to valve with lowest closing set-point).

Figure 4-86: Extreme Scenario 1 – transient power (fission)

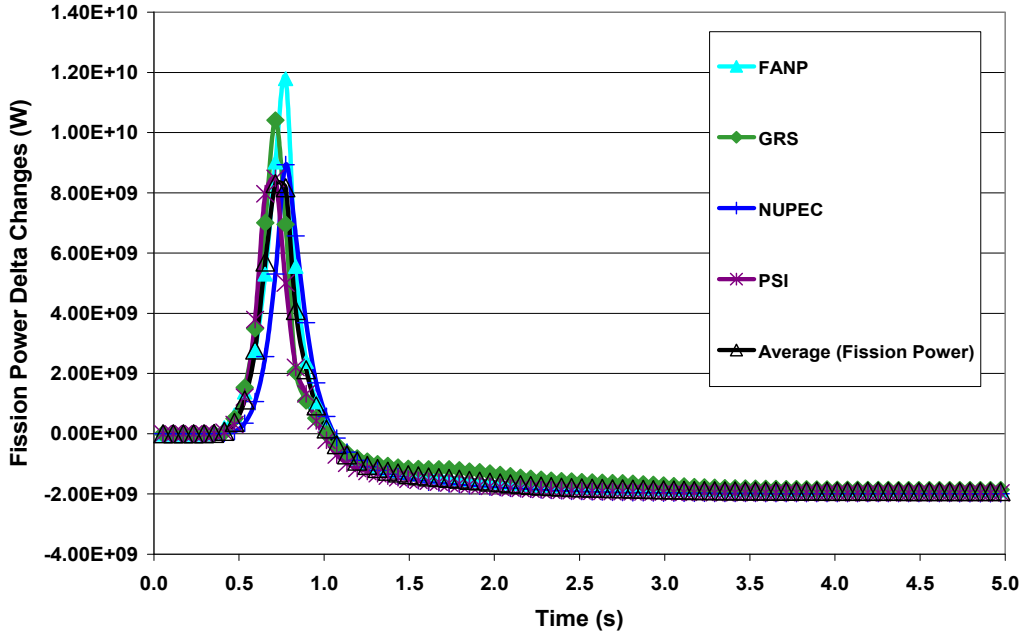

Figure 4-87: Extreme Scenario 1 – transient power (fission – zoom)

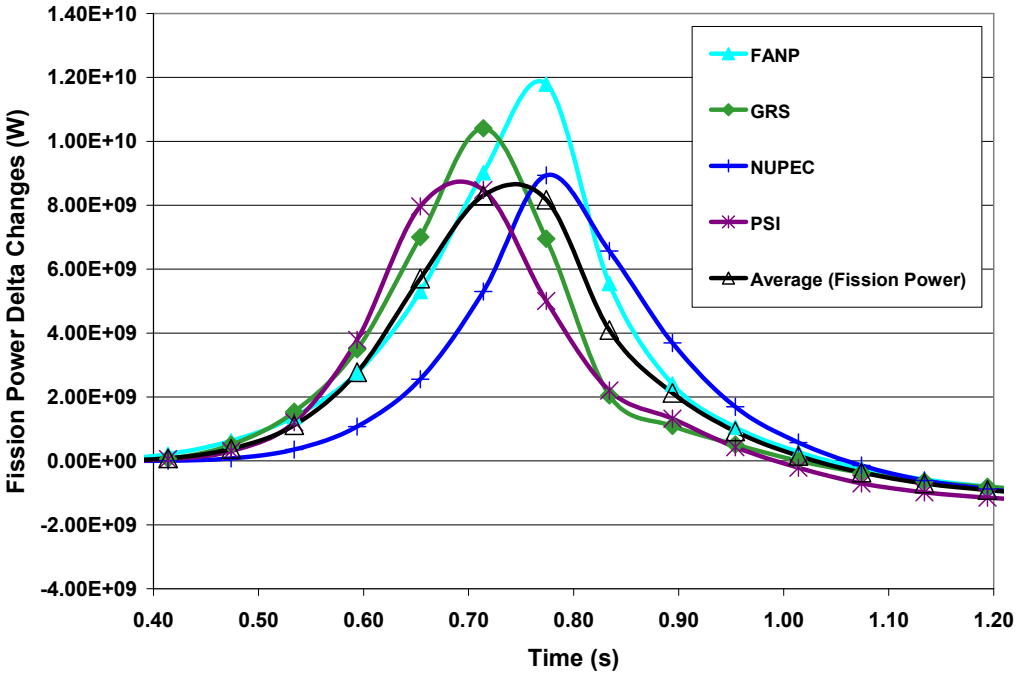

Figure 4-88: Extreme Scenario 1 – transient power (total)

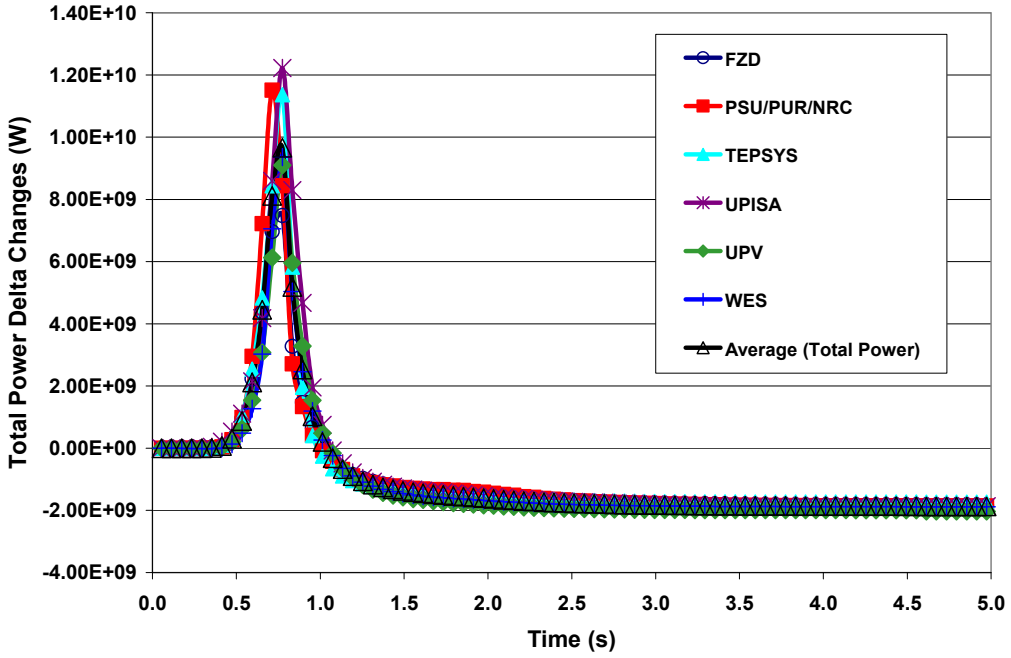

Figure 4-89: Extreme Scenario 1 – transient power (total – zoom)

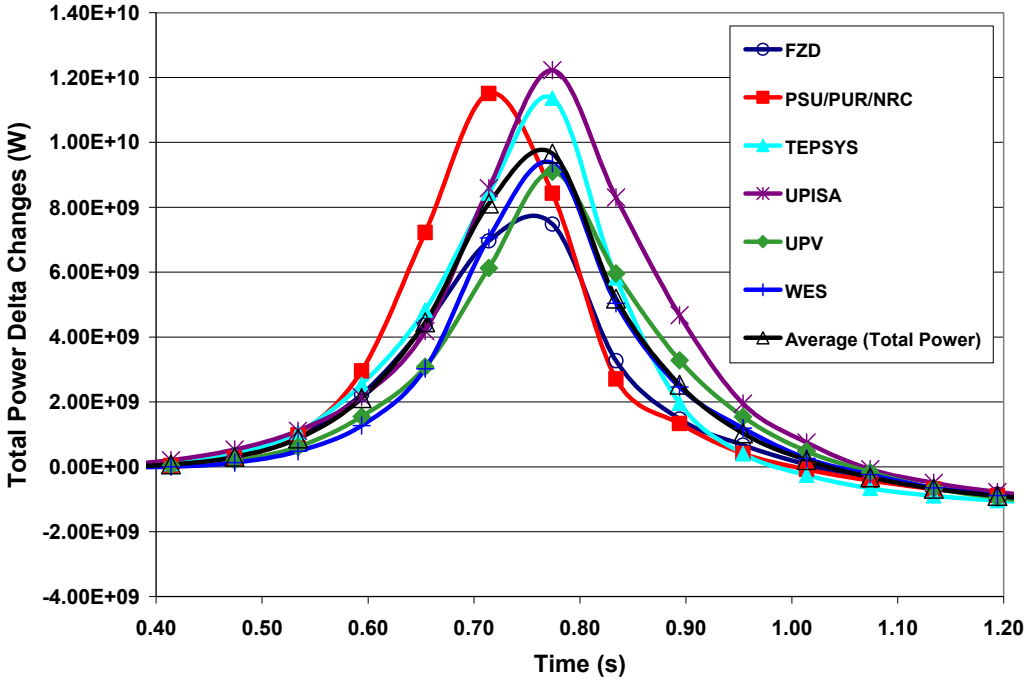

Table 4-25: Extreme Scenario 1 – transient power, figure of merit

Fission power submitted			Total Power Submitted		
Participant	**D'Auria FFT**	**Mean error, ME**	**Participant**	**D'Auria FFT**	**Mean error, ME**
FANP	0.7300	0.9895	FZD	0.7940	0.9963
GRS	0.7226	0.9898	PSU/PUR/NRC	0.7223	0.9917
NUPEC	0.6798	0.9899	TEPSYS	0.7236	0.9887
PSI	0.7080	0.9894	UPISA	0.6532	0.9828
			UPV	0.7157	0.9886
			WES	0.7370	0.9957

Figure 4-90: Extreme Scenario 1 – transient dome pressure (Group 1)

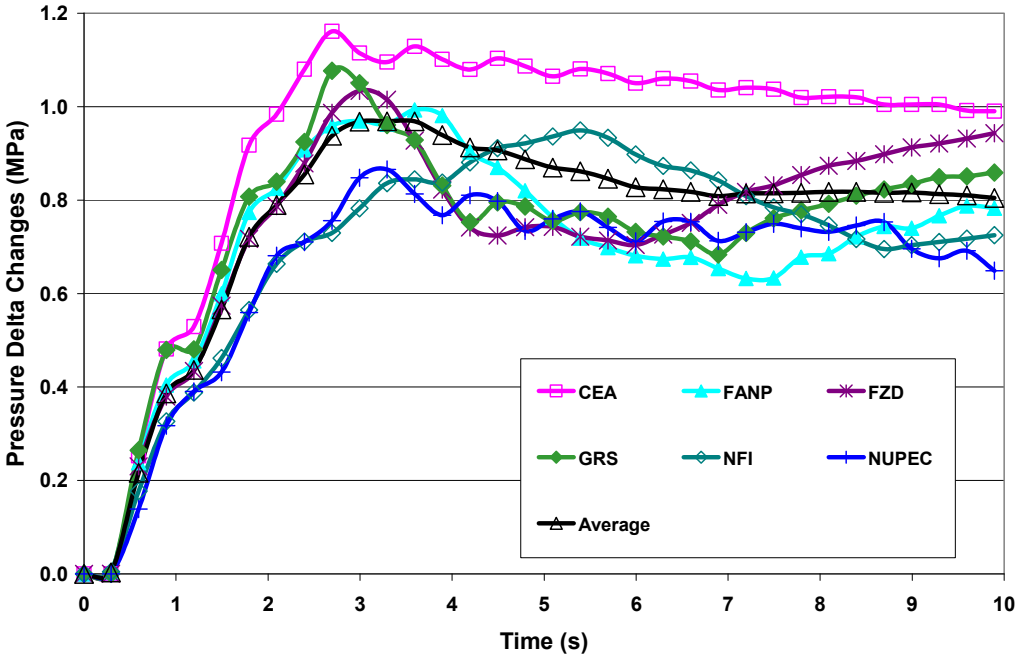

Figure 4-91: Extreme Scenario 1 – transient dome pressure (Group 2)

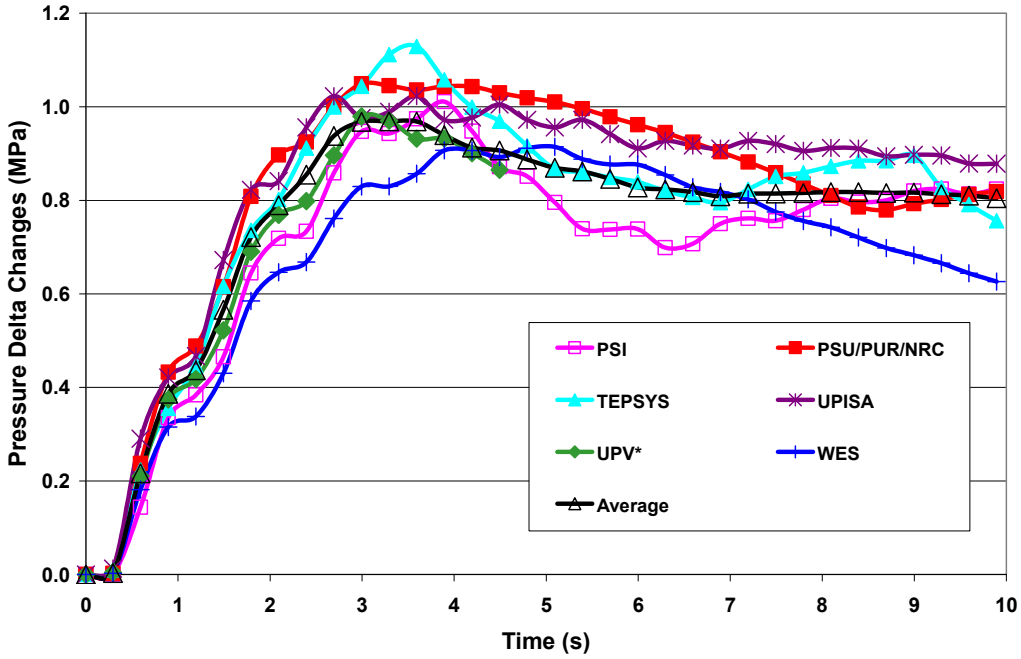

* UPV data is not accounted for in the average calculation due to the missing history after 4.5 s of the transient.

Table 4-26: Extreme Scenario 1 – transient dome pressure, figure of merit

Participant	D'Auria FFT	Mean error, ME
CEA	0.7319	0.8459
FANP	0.7793	0.9491
FZD	0.7643	0.9858
GRS	0.7757	0.9813
NFI	0.7830	0.9499
NUPEC	0.7745	0.9039
PSI	0.7838	0.9574
PSU/PUR/NRC	0.7381	0.9422
TEPSYS	0.7953	0.9646
UPISA	0.7889	0.9275
WES	0.7796	0.9368

Figure 4-92: Extreme Scenario 1 – transient core exit pressure (Group 1)

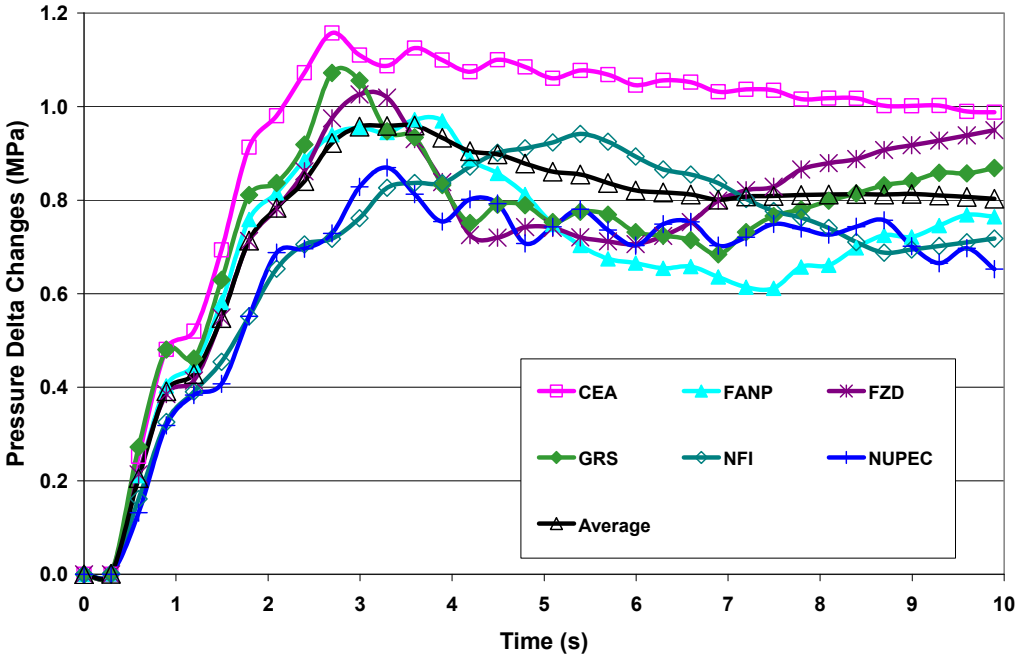

Figure 4-93: Extreme Scenario 1 – transient core exit pressure (Group 2)

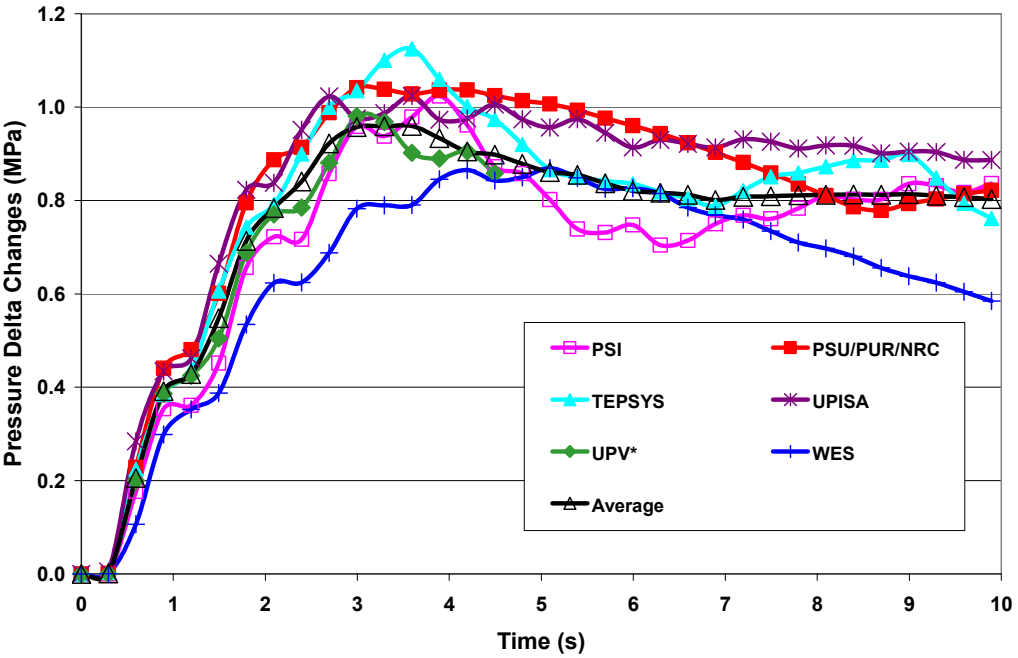

* UPV data is not accounted for in the average calculation due to the missing history after 4.5 s of the transient

Table 4-27: Extreme Scenario 1 – transient core exit pressure, figure of merit

Participant	D'Auria FFT	Mean error, ME
CEA	0.7281	0.8420
FANP	0.7740	0.9397
FZD	0.7620	0.9909
GRS	0.7750	0.9899
NFI	0.7799	0.9482
NUPEC	0.7711	0.9040
PSI	0.7815	0.9661
PSU/PUR/NRC	0.7348	0.9388
TEPSYS	0.7904	0.9585
UPISA	0.7801	0.9188
WES	0.7620	0.9050

Figure 4-94: Extreme Scenario 1 – transient S/RV pressure (Group 1)

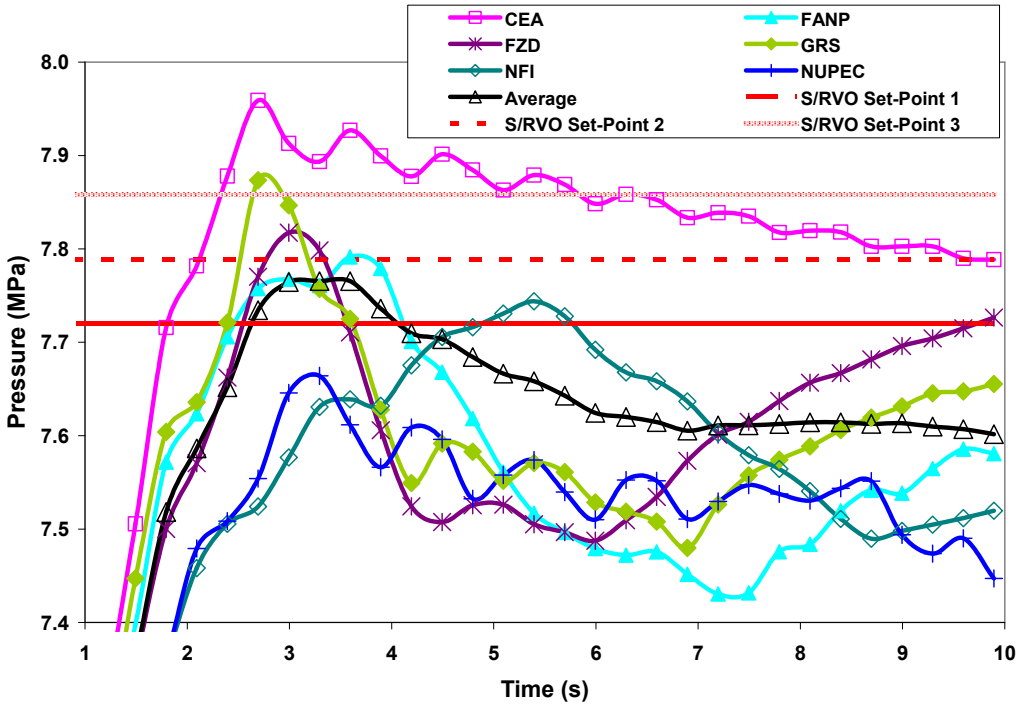

Figure 4-95: Extreme Scenario 1 – transient S/RV pressure (Group 2)

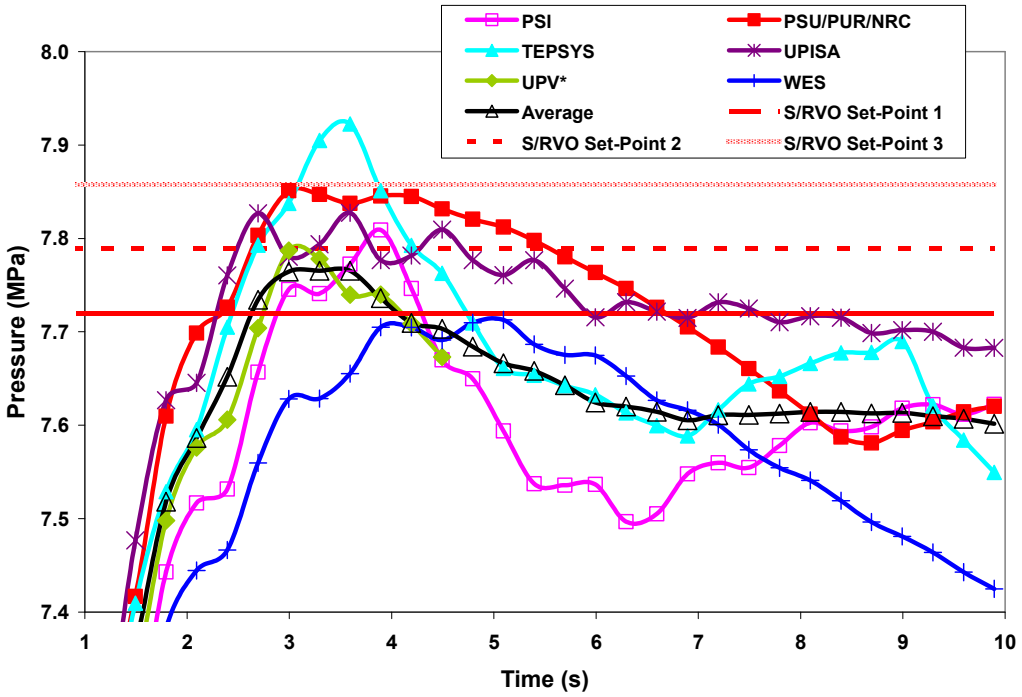

* UPV data is not accounted for in the average calculation due to the missing history after 4.5 s of the transient.

Table 4-28: Extreme Scenario 1 – transient S/RV pressure, figure of merit

Participant	D'Auria FFT	Mean error, ME
CEA	0.7373	0.8446
FANP	0.7834	0.9505
FZD	0.7713	0.9725
GRS	0.7843	0.9815
NFI	0.7893	0.9478
NUPEC	0.7804	0.9053
PSI	0.7909	0.9589
PSU/PUR/NRC	0.7419	0.9375
TEPSYS	0.7998	0.9678
UPISA	0.7895	0.9205
WES	0.7713	0.9385

Figure 4-96: Extreme Scenario 1 – total reactivity (Group 1)

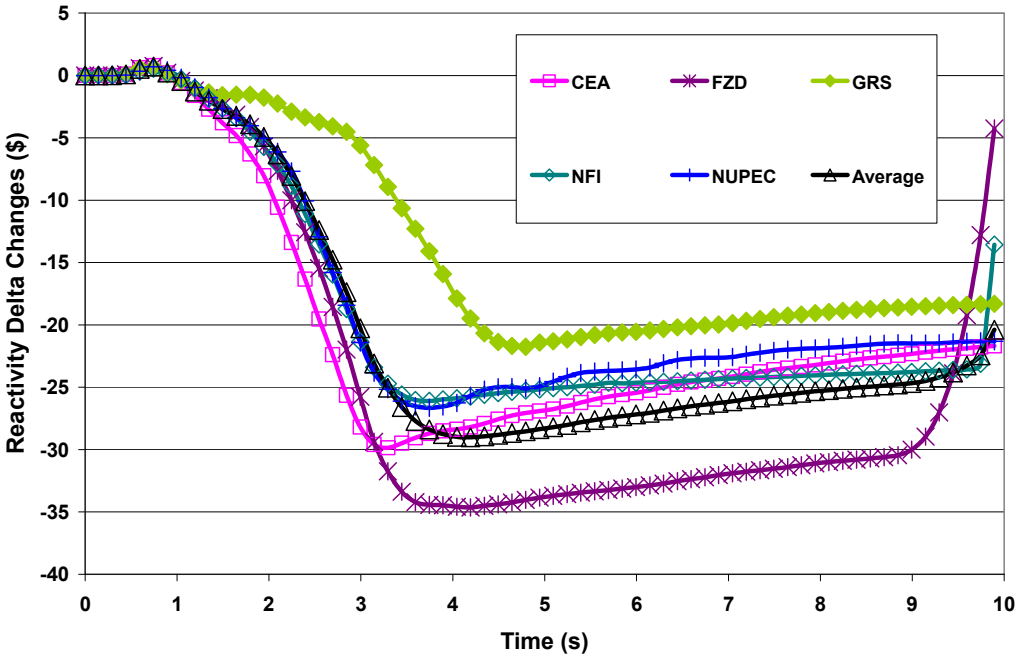

Figure 4-97: Extreme Scenario 1 – total reactivity (Group 1 – zoom)

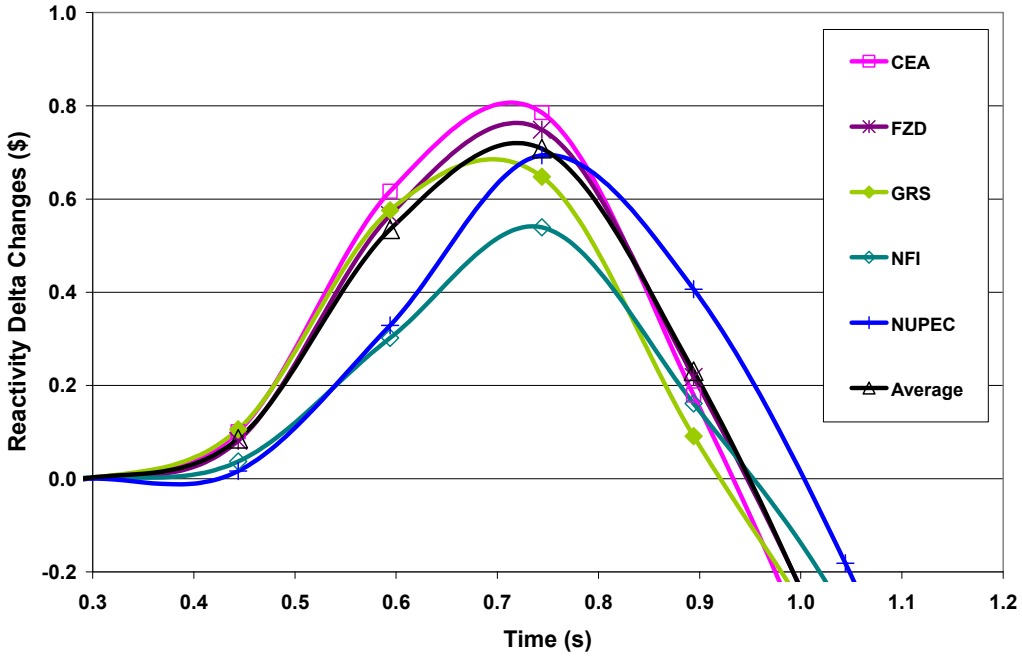

Figure 4-98: Extreme Scenario 1 – total reactivity (Group 2)

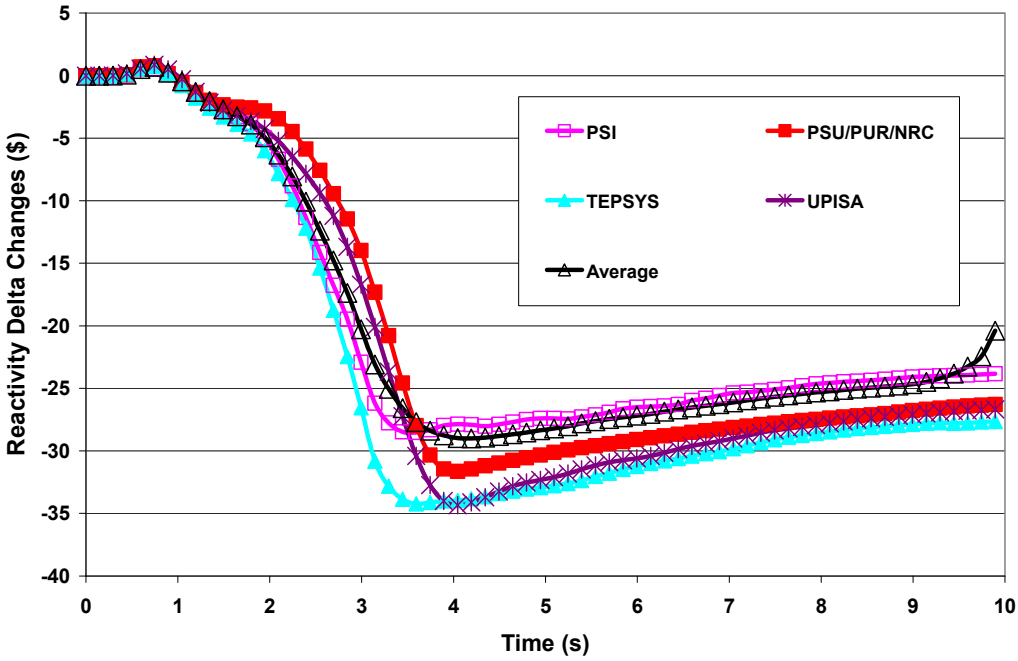

Figure 4-99: Extreme Scenario 1 – total reactivity (Group 2 – zoom)

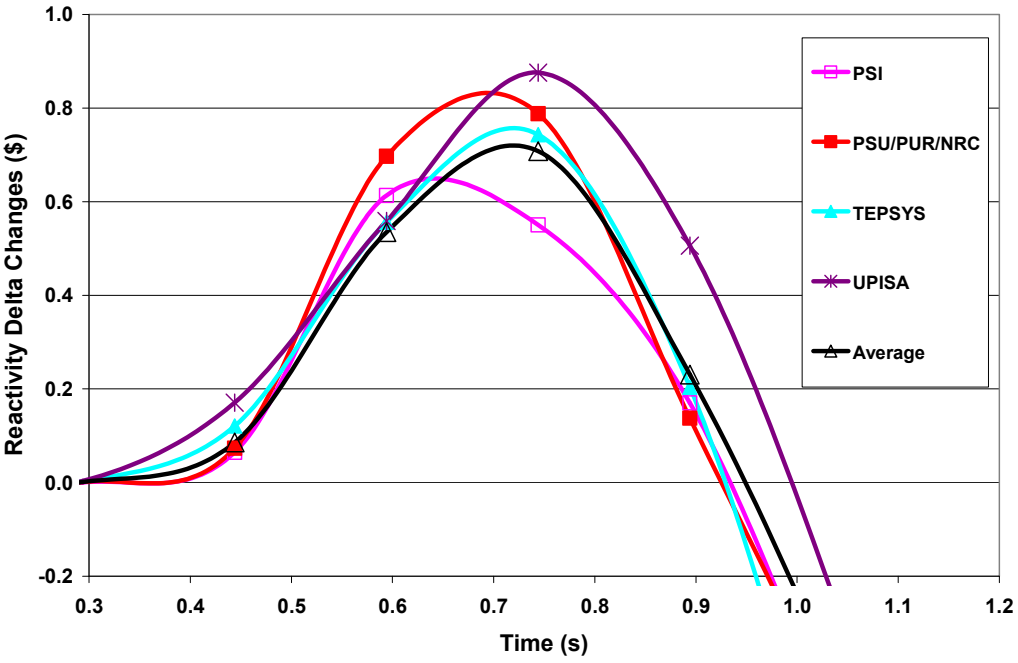

Table 4-29: Extreme Scenario 1 – total reactivity, figure of merit

Participant	D'Auria FFT	Mean error, ME
CEA	0.8540	0.9981
FZD	0.6242	0.8969
GRS	0.7091	0.8246
NFI	0.8248	0.9612
NUPEC	0.8371	0.9370
PSI	0.8760	0.9993
PSU/PUR/NRC	0.7444	0.9769
TEPSYS	0.7967	0.8956
UPISA	0.8059	0.9411

Figure 4-100: Extreme Scenario 1 – Doppler reactivity

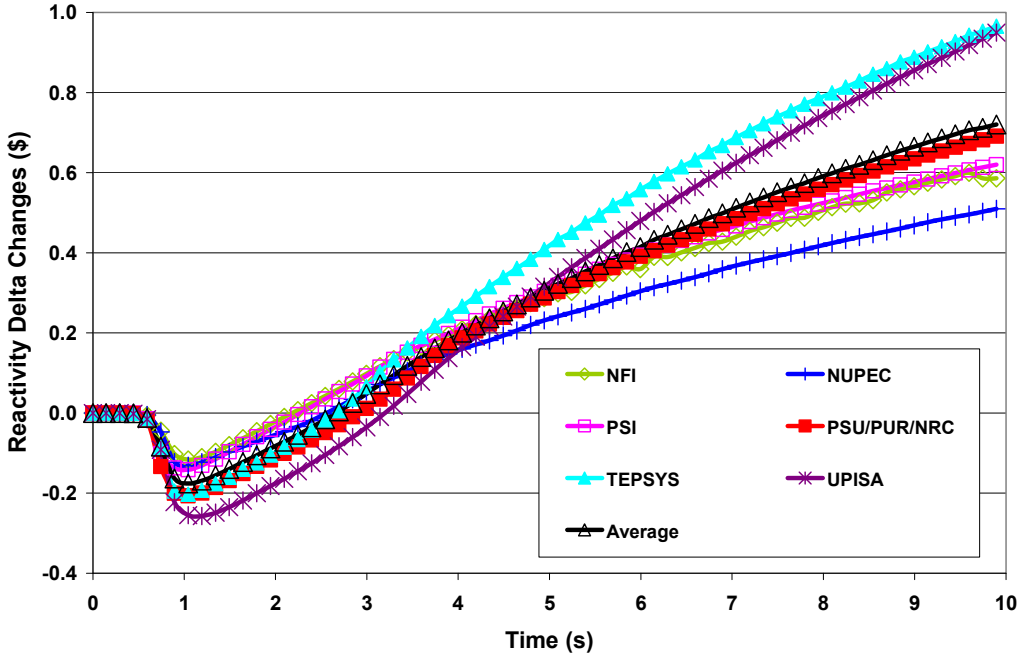

Figure 4-101: Extreme Scenario 1 – Doppler reactivity (zoom)

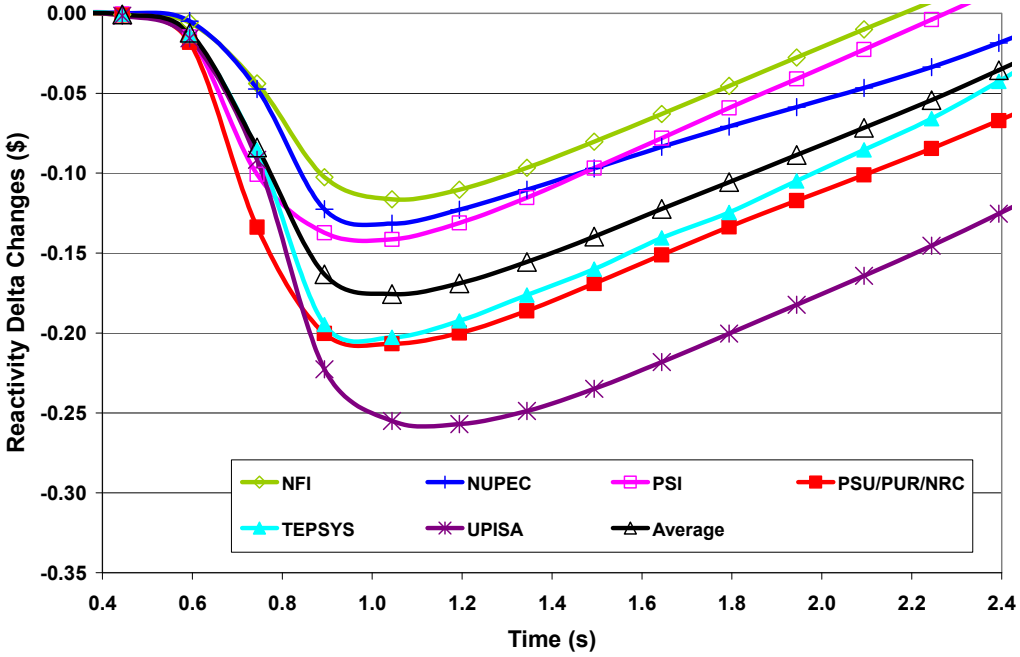

Table 4-30: Extreme Scenario 1 – Doppler reactivity, figure of merit

Participant	D'Auria FFT	Mean error, ME
NFI	0.8233	0.9771
NUPEC	0.7560	0.9205
PSI	0.8525	0.9849
PSU/PUR/NRC	0.7449	0.9722
TEPSYS	0.7174	0.8985
UPISA	0.7316	0.9609

Figure 4-102: Extreme Scenario 1 – void reactivity

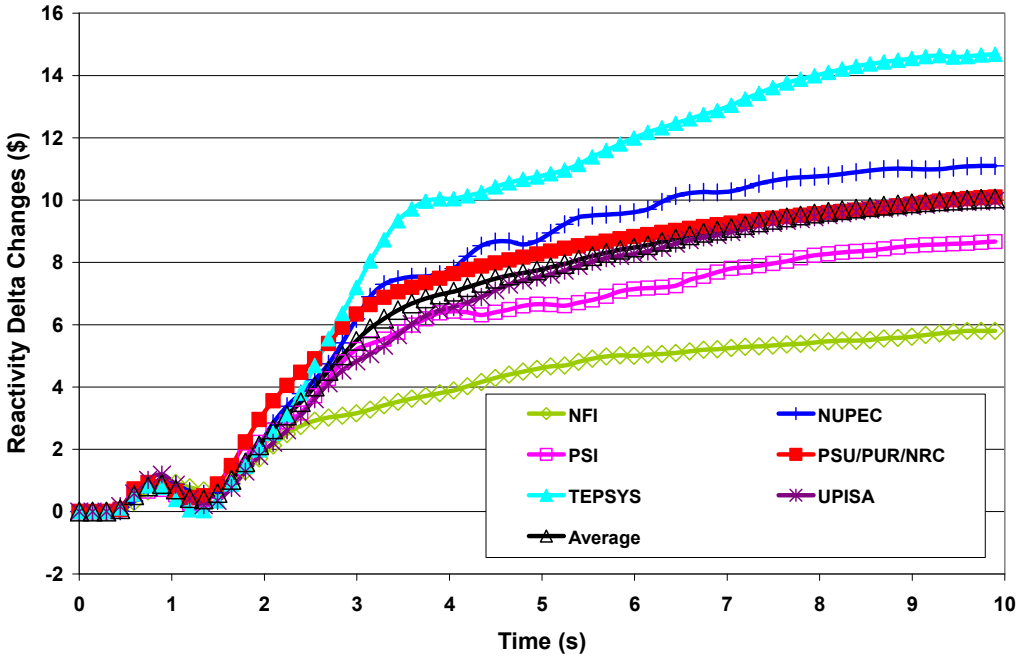

Figure 4-103: Extreme Scenario 1 – void reactivity (zoom)

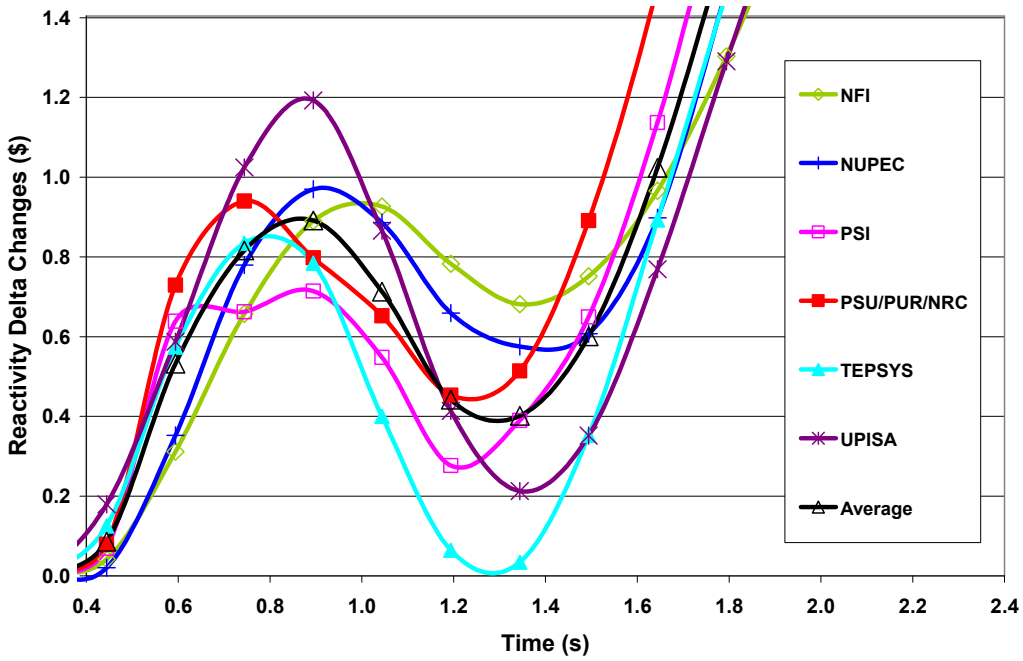

Table 4-31: Extreme Scenario 1 – void reactivity, figure of merit

Participant	D'Auria FFT	Mean error, ME
NFI	0.6884	0.7904
NUPEC	0.8484	0.9252
PSI	0.8450	0.9205
PSU/PUR/NRC	0.7604	0.9703
TEPSYS	0.6748	0.7922
UPISA	0.7316	0.9609

Figure 4-104: Extreme Scenario 1 – LPRM-A

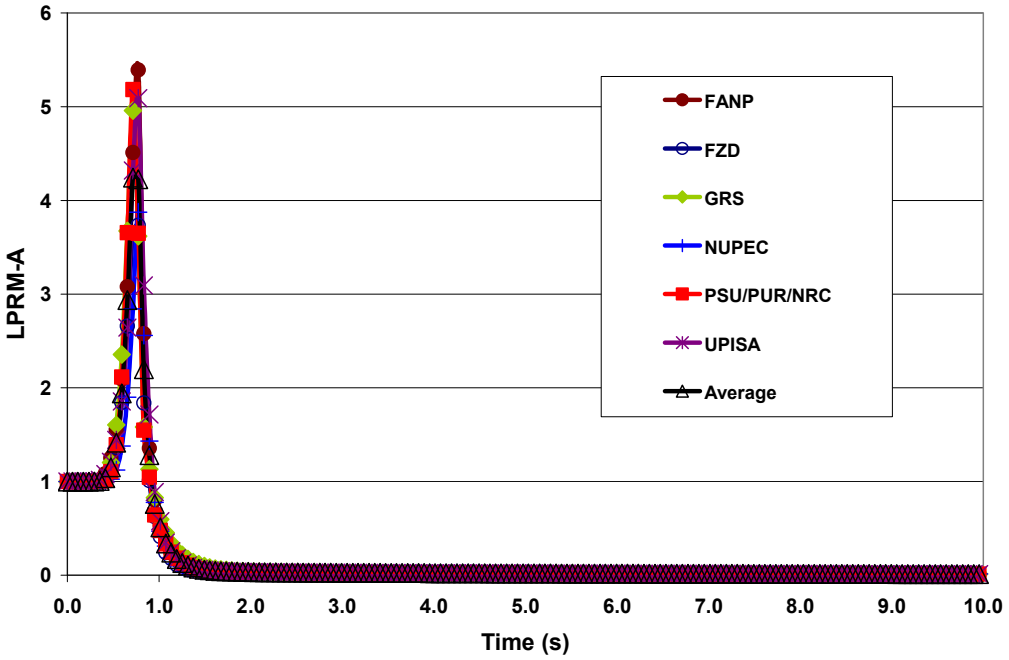

Figure 4-105: Extreme Scenario 1 – LPRM-A (zoom)

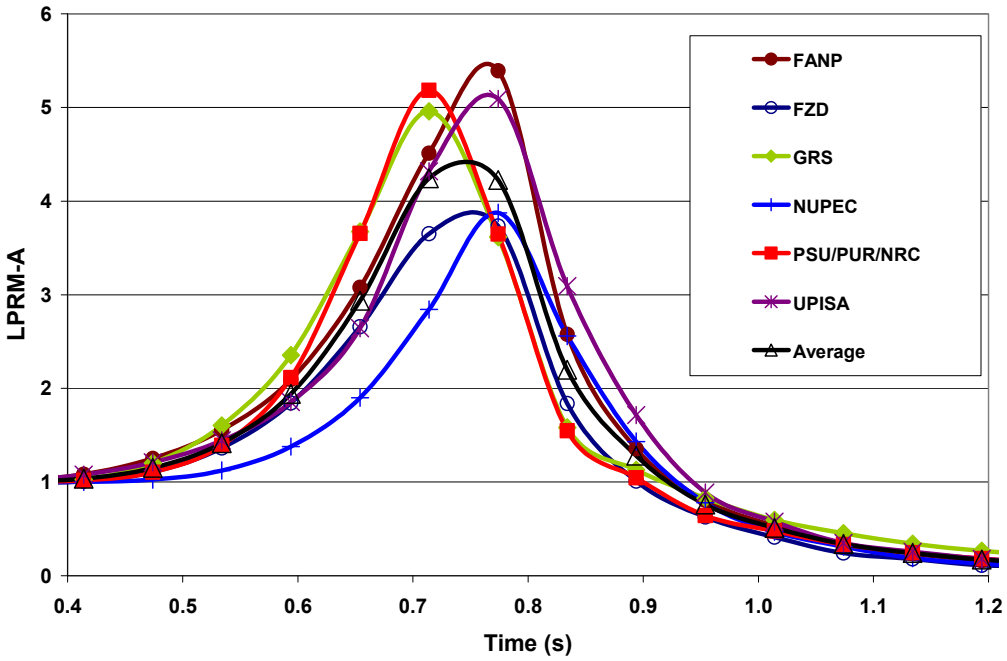

Table 4-32: Extreme Scenario 1 – normalised LPRM-A power, figure of merit

Participant	D'Auria FFT	Mean error, ME
FANP	0.7789	0.9976
FZD	0.7971	0.9965
GRS	0.7557	0.9978
NUPEC	0.7123	0.9960
PSU/PUR/NRC	0.7569	0.9999
UPISA	0.7592	0.9972

Figure 4-106: Extreme Scenario 1 – LPRM-B

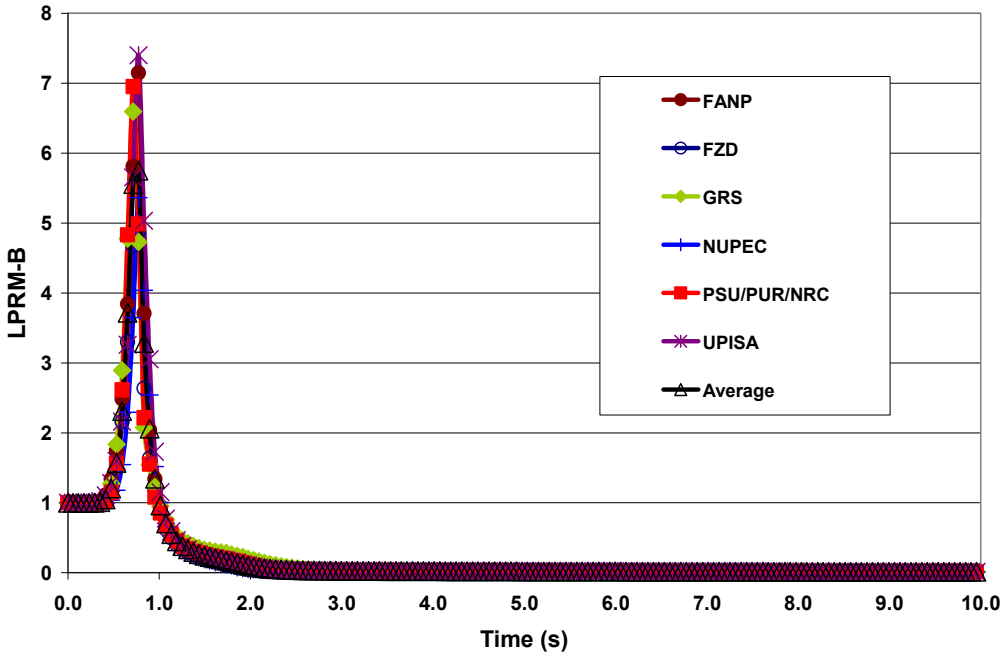

Figure 4-107: Extreme Scenario 1 – LPRM-B (zoom)

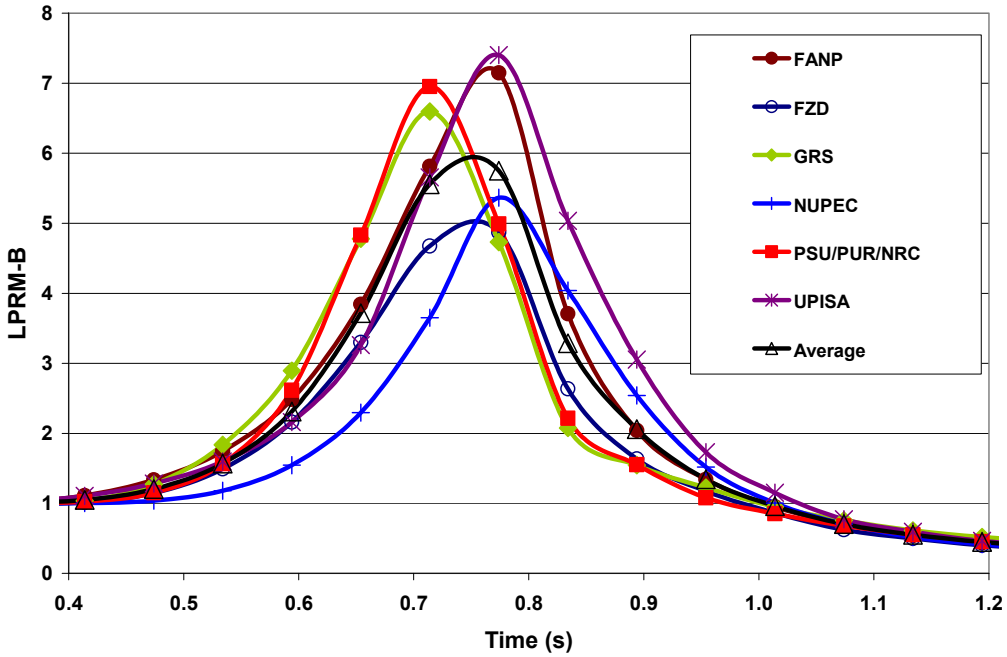

Table 4-33: Extreme Scenario 1 – normalised LPRM-B power, figure of merit

Participant	D'Auria FFT	Mean error, ME
FANP	0.7802	0.9983
FZD	0.7672	0.9954
GRS	0.7202	0.9978
NUPEC	0.6951	0.9957
PSU/PUR/NRC	0.7281	0.9997
UPISA	0.6999	0.9953

Figure 4-108: Extreme Scenario 1 – LPRM-C

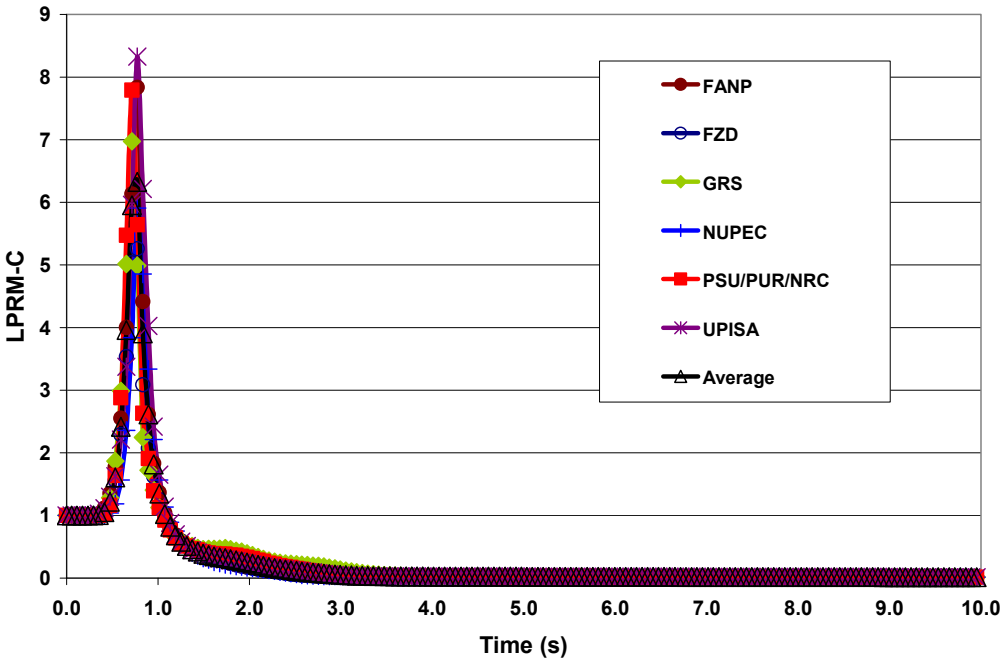

Figure 4-109: Extreme Scenario 1 – LPRM-C (zoom)

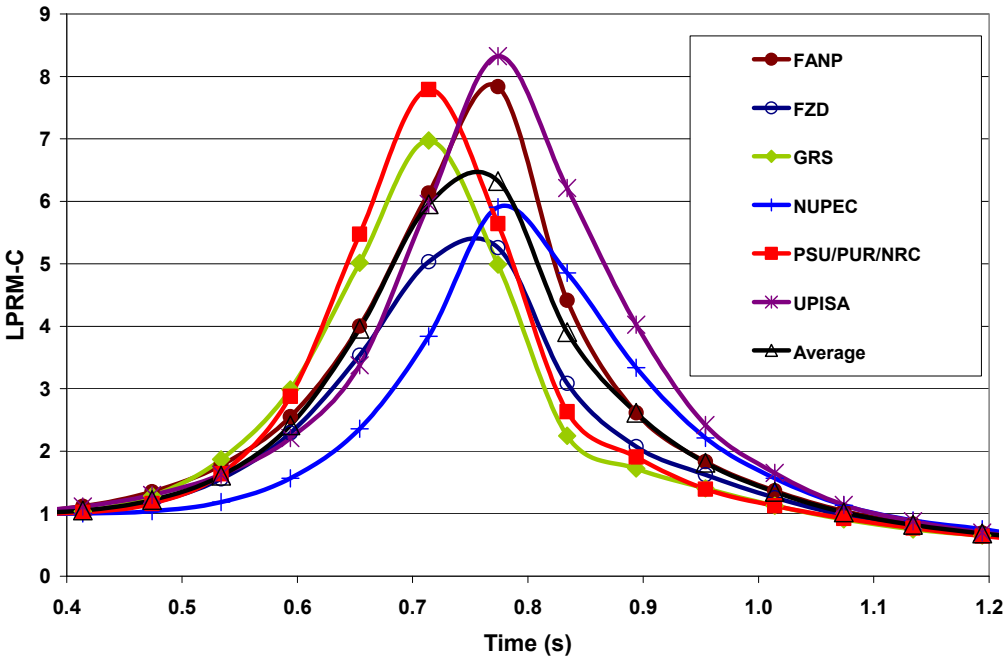

Table 4-34: Extreme Scenario 1 – normalised LPRM-C power, figure of merit

Participant	D'Auria FFT	Mean error, ME
FANP	0.7800	0.9989
FZD	0.7582	0.9947
GRS	0.6965	0.9983
NUPEC	0.6860	0.9958
PSU/PUR/NRC	0.7004	0.9986
UPISA	0.6731	0.9947

Figure 4-110: Extreme Scenario 1 – LPRM-D

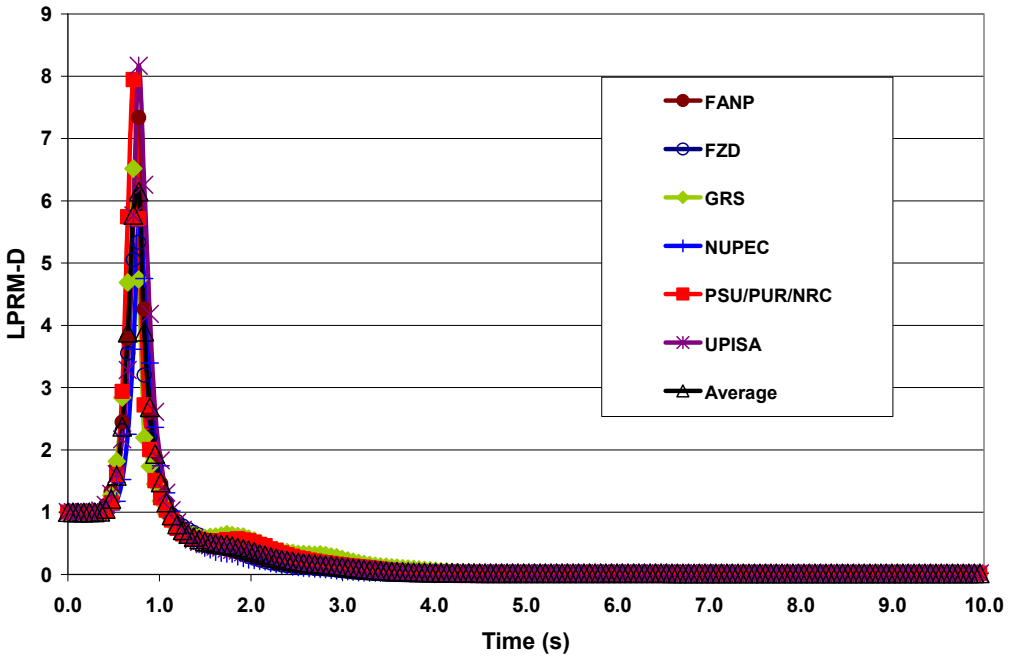

Figure 4-111: Extreme Scenario 1 – LPRM-D (zoom)

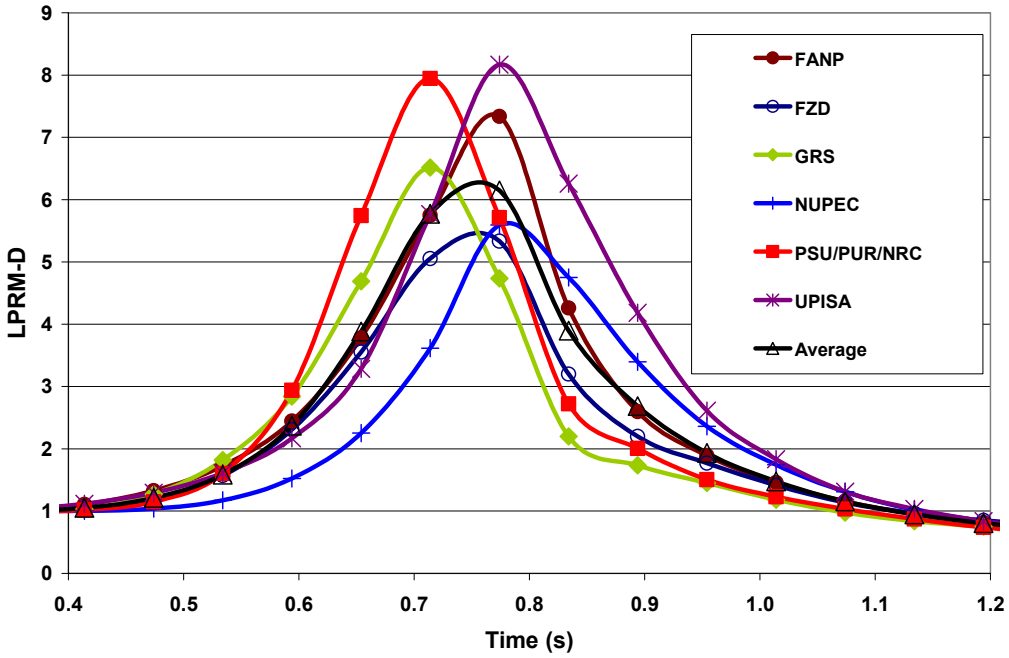

Table 4-35: Extreme Scenario 1 – normalised LPRM-D power, figure of merit

Participant	D'Auria FFT	Mean error, ME
FANP	0.8026	0.9996
FZD	0.7861	0.9951
GRS	0.6919	0.9976
NUPEC	0.6799	0.9942
PSU/PUR/NRC	0.6767	0.9965
UPISA	0.6640	0.9948

4.4 Transient results of Extreme Scenario 2

Turbine rip (TT) without reactor scram event is simulated in Exercise 3 Extreme Scenario 2. The following simulation results of the participants are presented in this subsection:

- core power;
- dome pressure;
- core exit pressure;
- S/RV pressure;
- total reactivity;
- Doppler reactivity;
- void reactivity;
- power of LPRM-A;
- power of LPRM-B;
- power of LPRM-C;
- power of LPRM-D;

In Exercise 3 the calculations of Extreme Scenarios 2, 3 and 4 (all without scram) indicated that the core power shows in-phase oscillations. While in Scenarios 2 and 3 the dynamics of physical interactions between power and feedback mechanisms is interrupted by opening of the bypass valve and/or SRV in Scenario 4 the power oscillatory behaviour continues until the end of the calculation. The modelling of SRV was identified as an important issue causing differences in the solutions in Extreme Scenarios 2 and 3.

The BWR TT benchmark allowed to study the impact of different thermal-hydraulic and neutronics models on code predictions and to identify the key parameters for modelling a TT transient. The Extreme Scenario 2 of Exercise 3 is without scram and thus allows studying the differences in modelling the feedback effects, especially in the later part of the transient where the power oscillations are interplay between void and Doppler feedback mechanisms. This in turn allowed the evaluation of these key parameters, through the performance of sensitivity studies. Please note that the participants performed sensitivity studies on temporal coupling schemes and time step sizes in advance so as to obtain converged solutions. The results in this section should be considered together with Tables 4-36 and 4-37 since all of the models given in the table are important for the transient calculations.

Table 4-36: Number of channels used and power submitted by the participants – Extreme Scenario 2

Participant	Number of channels	Power submitted
CEA	33	Fission
FANP	33	Fission
FZD	764	Total
GRS	33	Fission
NFI	33	Total
NUPEC	33	Fission
PSI	34	Fission
PSU/PURDUE/NRC	33	Total
TEPSYS	33	Total
UPISA	33	Total
UPV (NOKIN)	33	Total
WESTINGHOUSE	764	Total

Table 4-37: Models used in Extreme Scenario 2

Participant	XENON	ADF	BYPASS	DECAY
CEA	No	No	Yes	Yes
FANP	Yes	Yes	Yes	Yes
FZD	Yes	Yes	Yes	Yes
GRS	Yes	No	Yes	Yes
NFI	Yes	No	Yes	Yes
NUPEC	Yes	Yes	No	Yes
PSI	Yes	Yes	Yes	No
PSU/PURDUE/NRC	Yes	Yes	Yes	Yes
TEPSYS	Yes	Yes	Yes	Yes
UPISA	No	Yes	Yes	Yes
UPV	Yes	Yes	Yes	Yes
WESTINGHOUSE	No	Yes	Yes	Yes

The plots and tables in this section provide a comparison of the participants' results for the parameters that have the greatest effect on the Exercise 3 Extreme Scenario 2 analysis. For this reason participants were requested to submit core (averaged and local) and system time histories. These histories are: core-averaged (core power, total reactivity, Doppler reactivity and void reactivity), core local (powers of LPRM A, B, C and D) and system (dome pressure, core exit pressure and S/RV pressure). Similar to the Exercise 3 best-estimate scenario, in order to minimise the impact of the deviations in code predictions at the initial steady-state conditions (which already have been analysed in Section 4.1) and to focus on the deviations in transient calculations, the comparisons of the predictions of time evolutions of the above parameters are performed not on the absolute values of the parameters but on the delta changes of the parameters as compared to the values at the initial steady state.

The mean time histories are used as a reference and are provided in this section as well as in Appendix C. The figures of merit are presented in the tables of this section. Additionally, the participant deviations and figures of merit are presented in Appendix D, and are listed in the same order as the reference solutions. Appendices C and D are provided upon request on CD-ROM.

In each case the figures (Figures 4-112 through 4-137) graphically illustrate the agreement or disagreement of participants' predictions. Statistical evaluation is employed to generate a mean solution, which is also shown in the plots.

Participants' sequences of events in Extreme Scenario 2 are given in Table 4-38.

Core power time evolutions are presented in two groups (fission or total) depending on the submitted core power type. Comparisons of the predictions of fission power evolution and the total power evolution calculated by each code throughout the transient (up to 10 seconds) are shown in Figures 4-112 and 4-114 while Figures 4-113 and 4-115 zoom on the first few seconds of the transient where the power peak occurs. Table 4-39 provides figure of merit (FOM) for two different methods, D'Auria FFT and Mean Error.

When analysing the power history results it has to be taken into account that in Extreme Scenario 2 the same phenomena takes place as in the actual TT2 test (best-estimate scenario), with the difference that a turbine trip without scram leads to continuing power oscillations throughout the transient with subsequent smaller power peaks (after the first peak which is similar to the best-estimate scenario). This power response in terms of timing and magnitude of power peaks during the transient as predicted by different codes is a function of the total reactivity time evolution. In Figure 4-112 (the fission power group), the NUPEC result differs more than the other participants' results from the mean solution. In the total power group (Figure 4-114), all of the codes' predictions (except PSU/PUR/NRC) form a cluster around the mean solution. In general, the power history results are in a good agreement. Since for the Exercise 3 best-estimate case (which is the real test scenario) the void feedback limited alone the power peak at the beginning of transient and initiated the power reduction as well as the scram initiation time is specified that it is expected that each participant would predict a higher power peak for Extreme Scenario 1 (with steam bypass relief system failure) rather than for Extreme Scenario 2 (without reactor scram). This tendency is observed for most of the participants except for NUPEC (fission power group) and FZD, UPV and Westinghouse (total power group) where the power

peak at the beginning of transient is almost the same in both extreme scenarios while the timing of the peak is shifted towards a little bit later into the transient for Extreme Scenario 2. A possible reason for such power time history behaviour is the fact that for these participants the scram first limits the power rise at the beginning of transient for the best-estimate case and Extreme Scenario 1. The effect of the void feedback mechanism comes a little bit later which can be seen from the power history results for these participants for Extreme Scenario 2.

System parameter (dome pressure, core exit pressure and S/RV pressure) time evolutions are presented in two groups (Group 1 and Group 2) in order to visualise them clearly. Comparisons of the predictions of these parameters calculated by each code throughout the transient (up to 10 seconds) are shown in Figures 4-116 through 4-121 while Tables 4-40 through 4-42 provide figure of merit (FOM) for two different methods, D'Auria FFT and Mean Error. It is important to note that for the S/RV pressure time history plots the three safety relief set points are provided to show which valves open and when for different participants' simulations.

Figures 4-122 through 4-129 show comparisons of the predictions of the total, Doppler and void reactivity throughout the transient (up to 10 seconds) and zoom of the beginning of transient. Larger deviations from mean solutions are observed after the first power peak for some participants for the total reactivity (FZD, GRS, PSU/PUR/NRC and UPISA), moderator density (void) reactivity (UPISA and PSU/PUR/NRC) and Doppler feedback reactivity (UPISA and NUPEC) time histories.

Core local parameter time evolutions such as LPRM A, B, C and D power time histories are presented through three types of comparisons. Comparisons of the predictions of local parameter time evolutions calculated by each code throughout the transient (up to 10 seconds) are shown in Figures 4-130, 4-132, 4-134 and 4-136. Figures 4-131, 4-133, 4-135 and 4-137 zoom on the first few seconds of the transient. Tables 4-46 through 4-48 provide figure of merit (FOM) for two different methods, D'Auria FFT and Mean Error. It is important to note that for the four LPRM power time histories the average (mean) of participants' predictions is used as a reference solution.

Table 4-38: Sequence of events in Extreme Scenario 2

Participant	Event* (msec)						
	TSVC	BVBO	BVFO	DPIR	CEPIR	S/RVO	S/RVC
CEA	0.096	0.060	0.846	0.390	0.384	4.828	None
FANP	0.096	0.060	0.846	0.396	0.390	4.290	None
FZD	0.096	0.060	0.846	0.382	0.388	5.250	None
GRS	0.096	0.060	0.846	0.372	0.378	4.356	None
NFI	0.096	0.060	0.846	0.414	0.414	4.814	None
NUPEC	0.096	0.060	0.846	0.438	0.456	4.806	None
PSI	0.096	0.060	0.852	0.438	0.444	4.896	None
PSU/PUR/NRC	0.096	0.060	0.846	0.408	0.402	4.470	None
TEPSYS	0.096	0.060	0.846	0.366	0.366	4.579	None
UPISA	0.096	0.060	0.846	0.348	0.324	4.150	None
UPV	0.096	0.060	0.950	0.402	0.414	4.300	None
WES	0.087	0.066	0.846	0.396	0.444	4.908	None

* Description of the events: TSVC – turbine stop valve closed, BVBO – bypass valve begins opening, BVFO – bypass valve full open, DPIR – vessel dome pressure initial response (0.78% increased over initial value), CEPIR – core exit pressure initial response (0.27% increased over initial value), S/RVO – first safety/relief valve begins opening (refer to valve with lowest opening set-point), S/RVC – last safety/relief valve fully closed (refer to valve with lowest closing set-point).

Figure 4-112: Extreme Scenario 2 – transient power (fission)

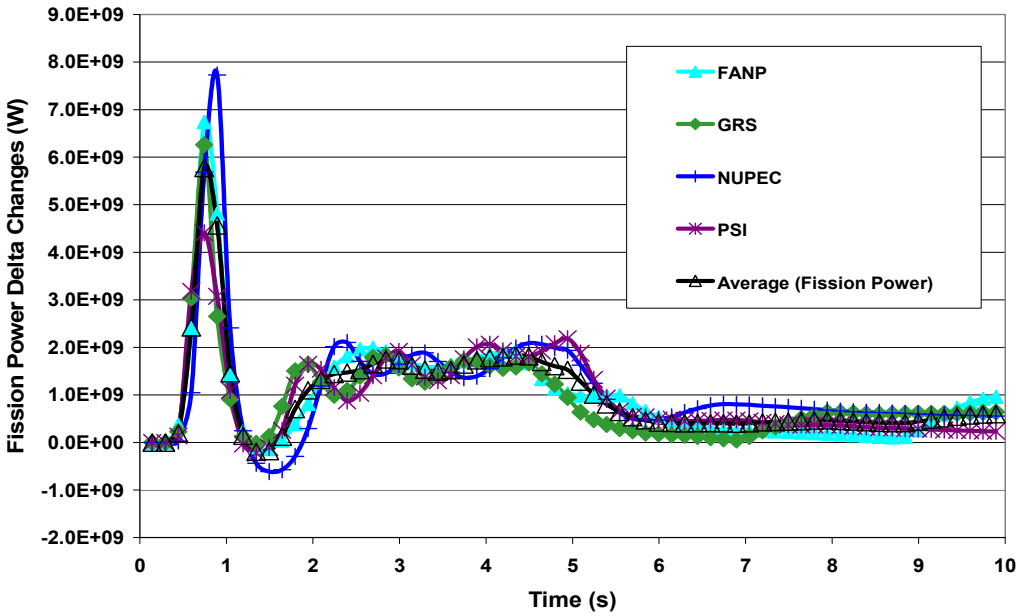

Figure 4-113: Extreme Scenario 2 – transient power (fission – zoom)

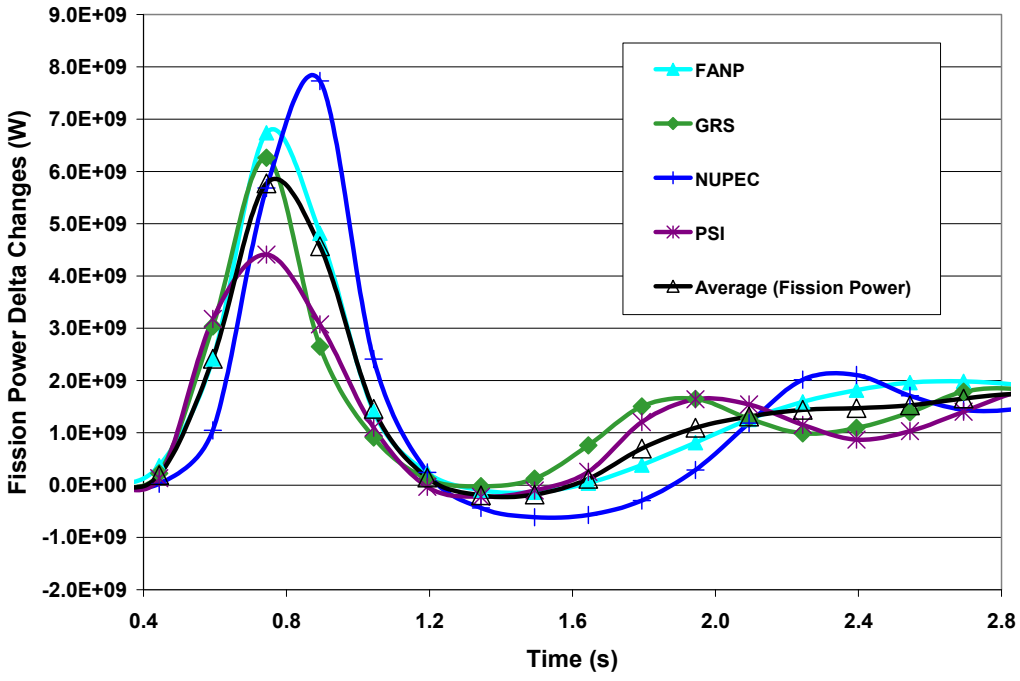

Figure 4-114: Extreme Scenario 2 – transient power (total)

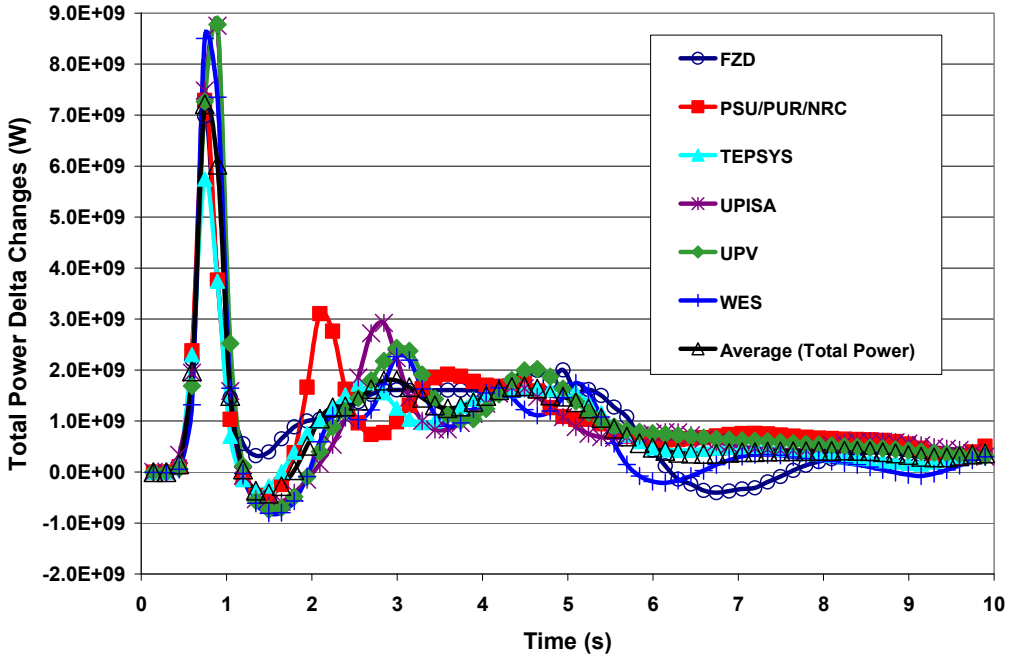

Figure 4-115: Extreme Scenario 2 – transient power (total – zoom)

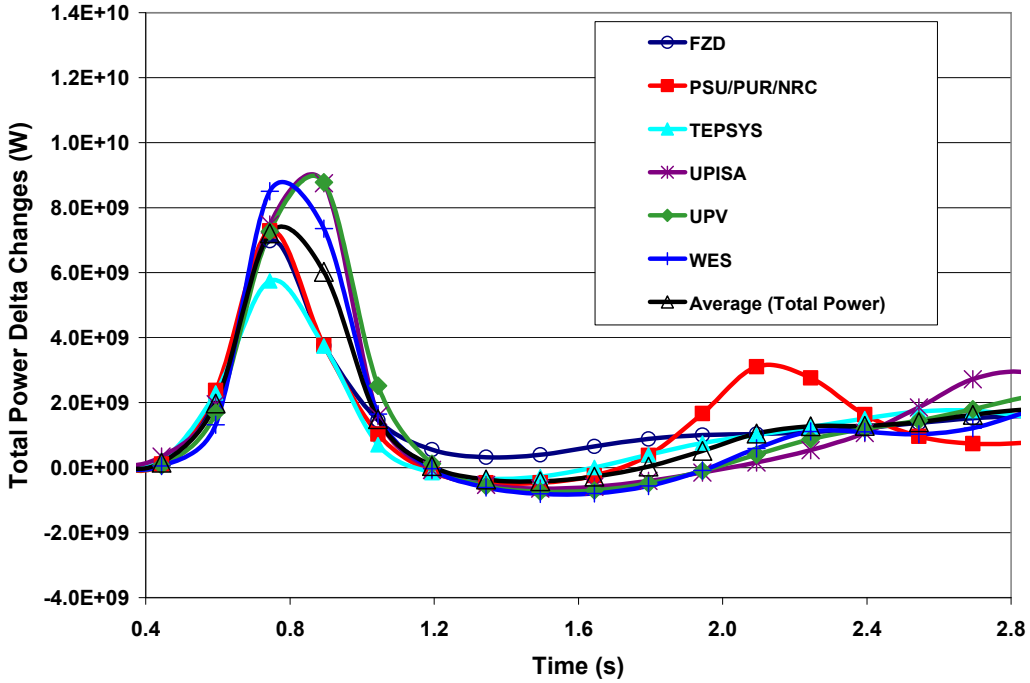

Table 4-39: Extreme Scenario 2 – transient power, figure of merit

Fission power submitted			Total power submitted		
Participant	**D'Auria FFT**	**Mean error, ME**	**Participant**	**D'Auria FFT**	**Mean error, ME**
FANP	0.7616	0.9994	FZD	0.6563	0.9978
GRS	0.6760	0.9866	PSU/PUR/NRC	0.6585	0.9886
NUPEC	0.6169	0.9811	TEPSYS	0.6980	0.9920
PSI	0.6780	0.9950	UPISA	0.6768	0.9957
			UPV	0.6953	0.9874
			WES	0.6656	0.9819

Figure 4-116: Extreme Scenario 2 – transient dome pressure (Group 1)

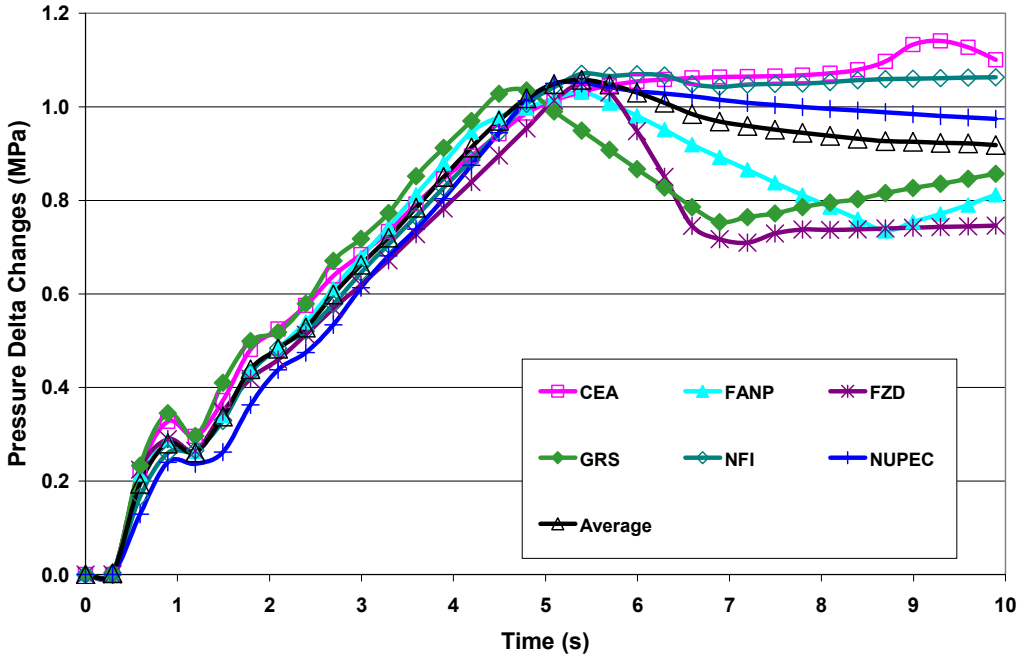

Figure 4-117: Extreme Scenario 2 – transient dome pressure (Group 2)

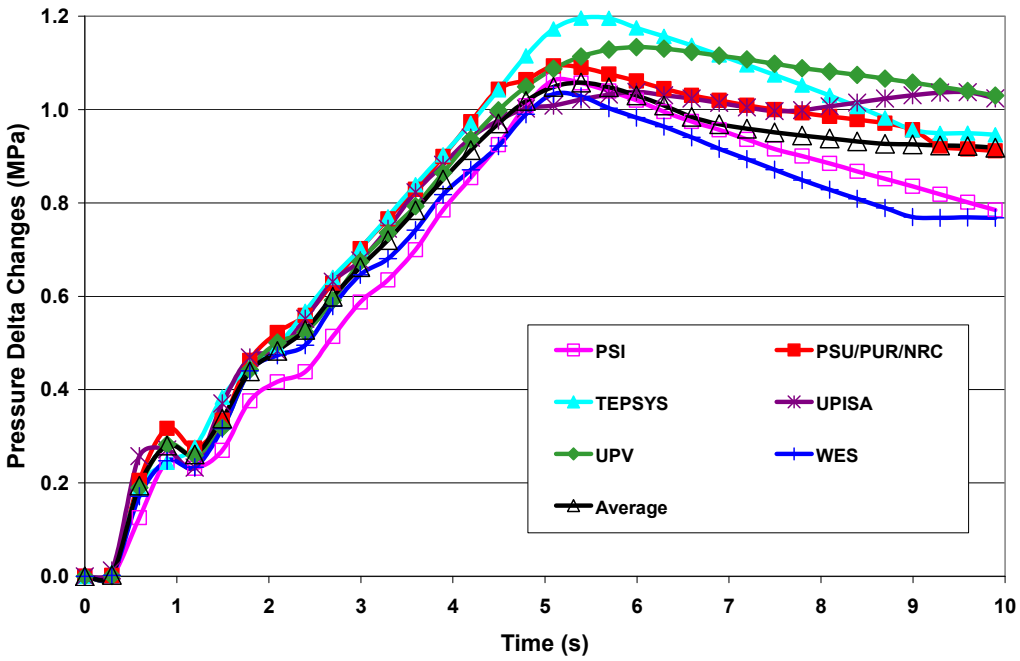

Table 4-40: Extreme Scenario 2 – transient dome pressure, figure of merit

Participant	D'Auria FFT	Mean error, ME
CEA	0.7740	0.9454
FANP	0.8022	0.9575
FZD	0.7715	0.9171
GRS	0.7892	0.9592
NFI	0.7923	0.9660
NUPEC	0.8191	0.9989
PSI	0.8665	0.9547
PSU/PUR/NRC	0.8856	0.9694
TEPSYS	0.8442	0.9394
UPISA	0.8621	0.9690
UPV	0.8501	0.9434
WES	0.8547	0.9491

Figure 4-118: Extreme Scenario 2 – transient core exit pressure (Group 1)

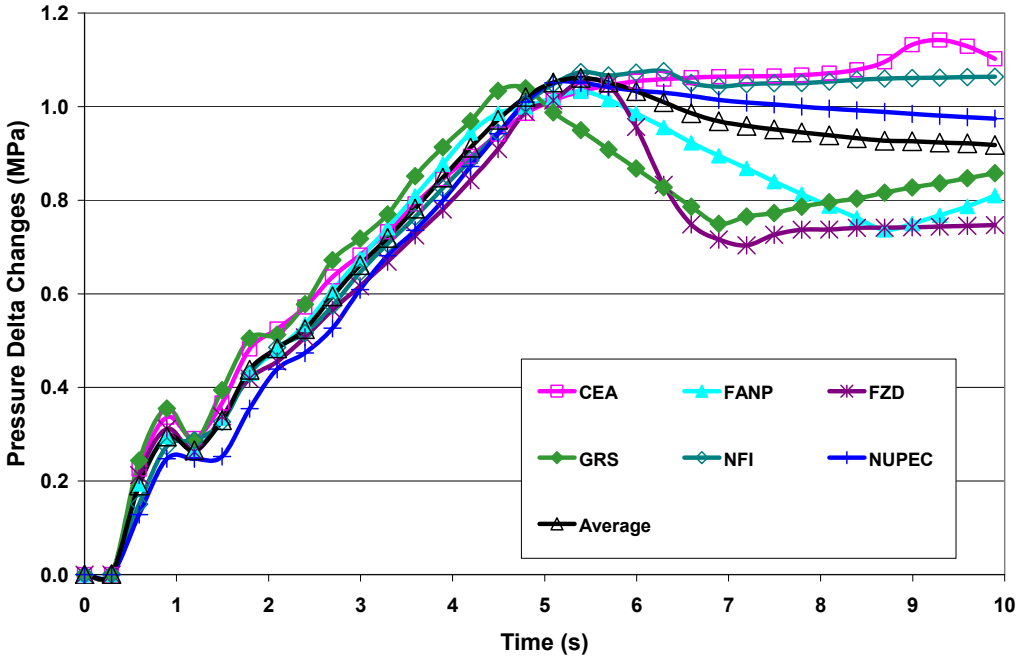

Figure 4-119: Extreme Scenario 2 – transient core exit pressure (Group 2)

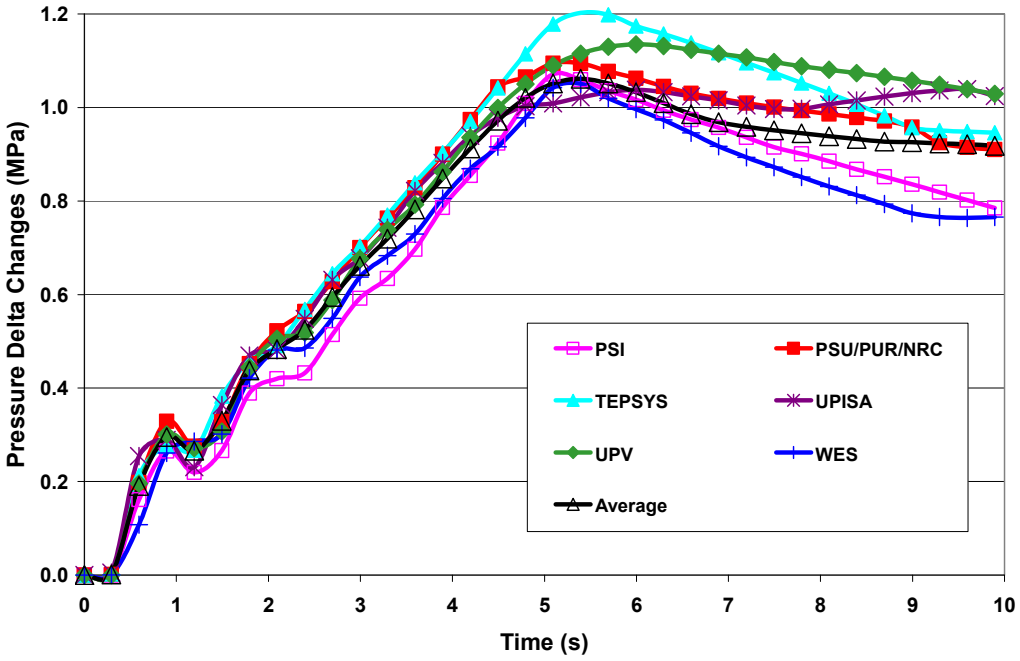

Table 4-41: Extreme Scenario 2 – transient core exit pressure, figure of merit

Participant	D'Auria FFT	Mean error, ME
CEA	0.7731	0.9457
FANP	0.8012	0.9572
FZD	0.7674	0.9169
GRS	0.7866	0.9595
NFI	0.7906	0.9654
NUPEC	0.8164	0.9980
PSI	0.8673	0.9551
PSU/PUR/NRC	0.8849	0.9692
TEPSYS	0.8436	0.9387
UPISA	0.8554	0.9689
UPV	0.8473	0.9429
WES	0.8497	0.9482

Figure 4-120: Extreme Scenario 2 – transient S/RV pressure (Group 1)

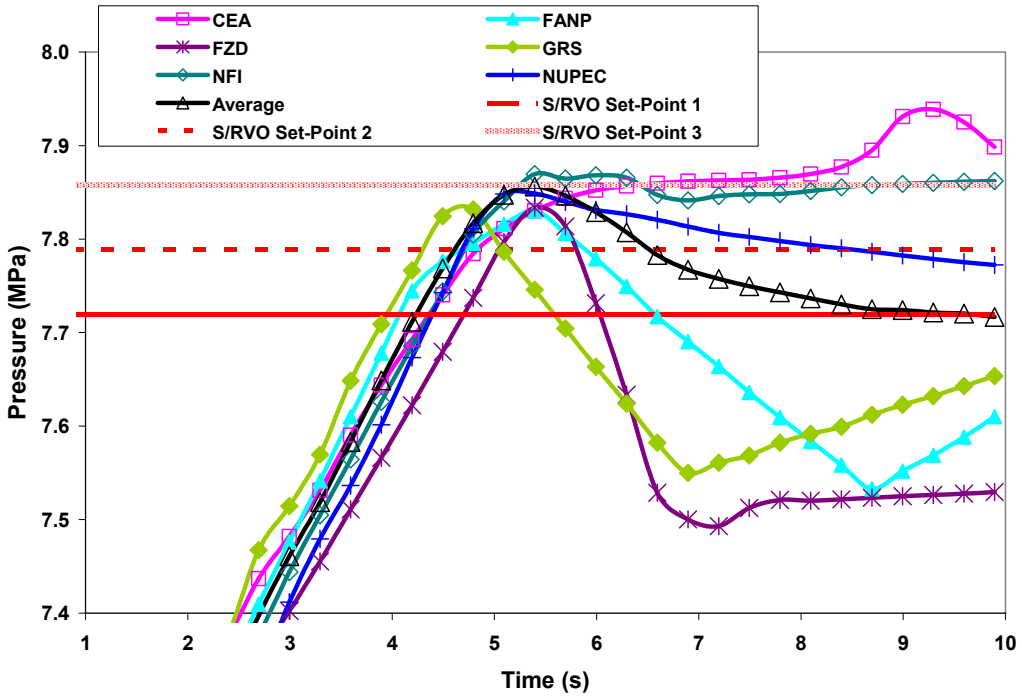

Figure 4-121: Extreme Scenario 2 – transient S/RV pressure (Group 2)

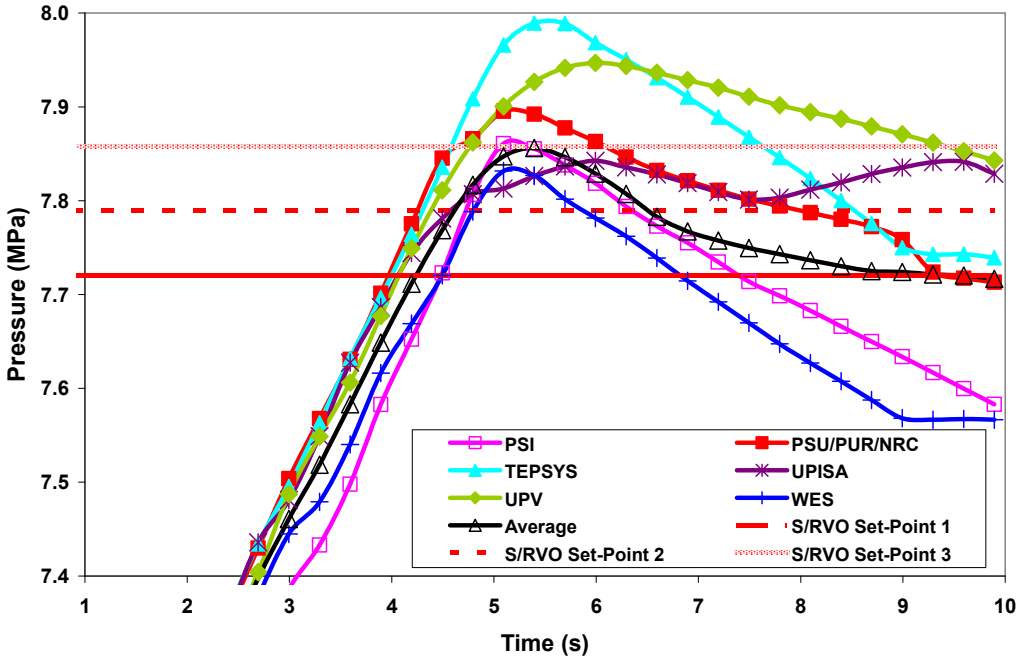

Table 4-42: Extreme Scenario 2 – transient S/RV pressure, figure of merit

Participant	D'Auria FFT	Mean error, ME
CEA	0.7895	0.9501
FANP	0.8182	0.9623
FZD	0.7869	0.9217
GRS	0.8050	0.9640
NFI	0.8081	0.9708
NUPEC	0.8355	0.9989
PSI	0.8838	0.9595
PSU/PUR/NRC	0.9033	0.9742
TEPSYS	0.8611	0.9441
UPISA	0.8793	0.9738
UPV	0.8671	0.9481
WES	0.8718	0.9538

Figure 4-122: Extreme Scenario 2 – total reactivity (Group 1)

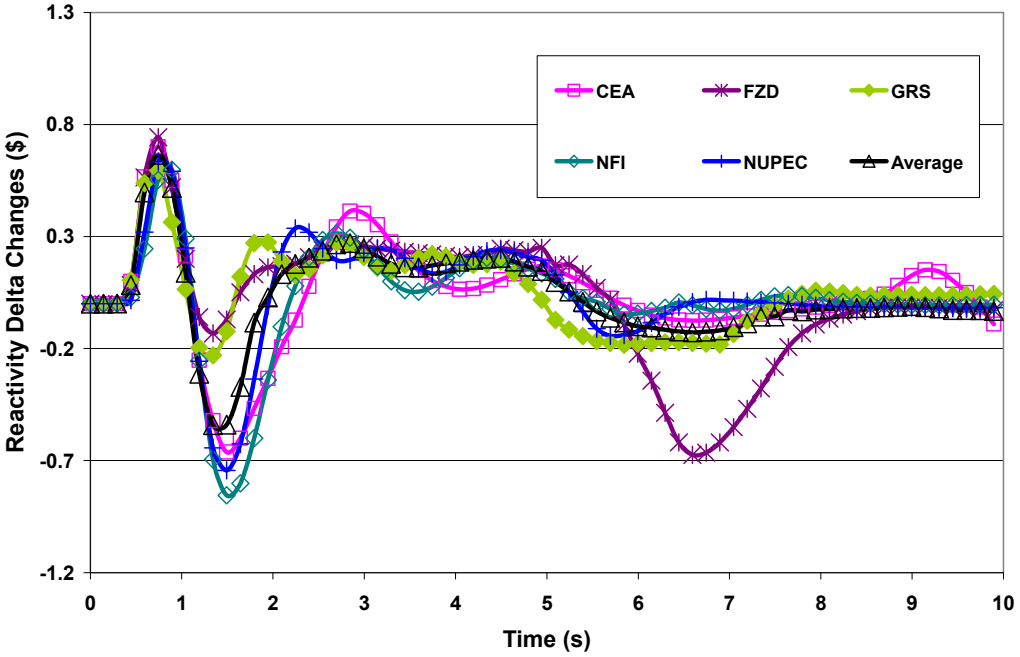

Figure 4-123: Extreme Scenario 2 – total reactivity (Group 1 – zoom)

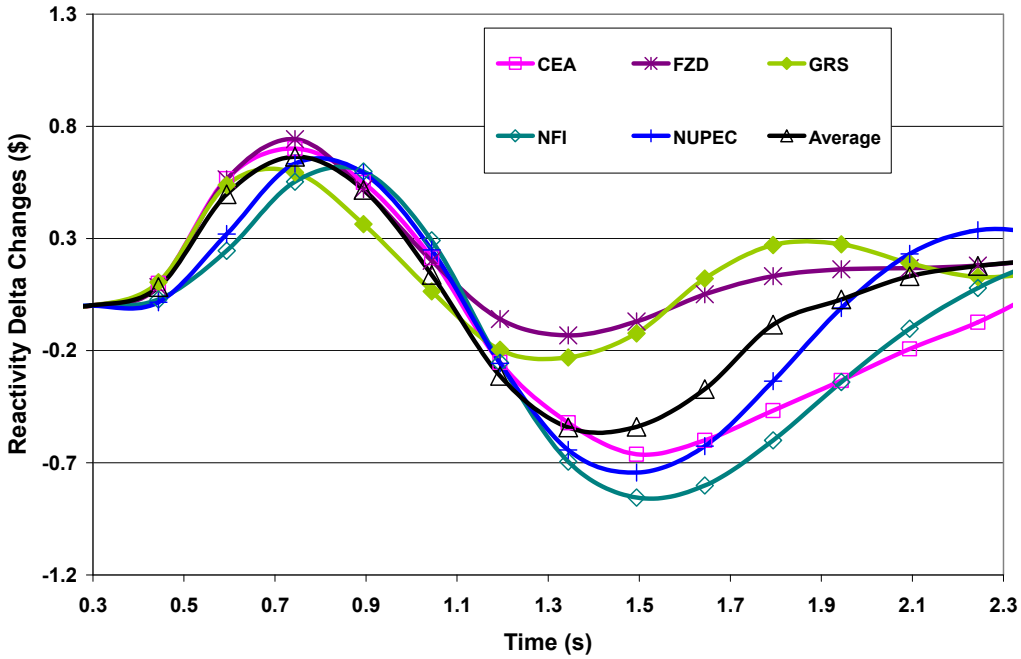

Figure 4-124: Extreme Scenario 2 – total reactivity (Group 2)

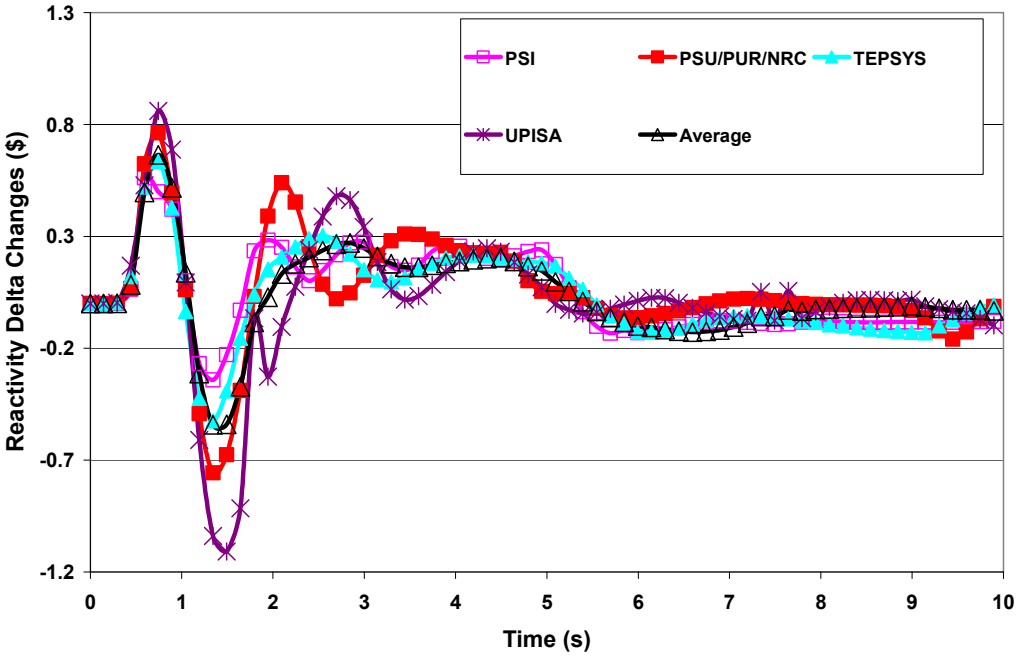

Figure 4-125: Extreme Scenario 2 – total reactivity (Group 2 – zoom)

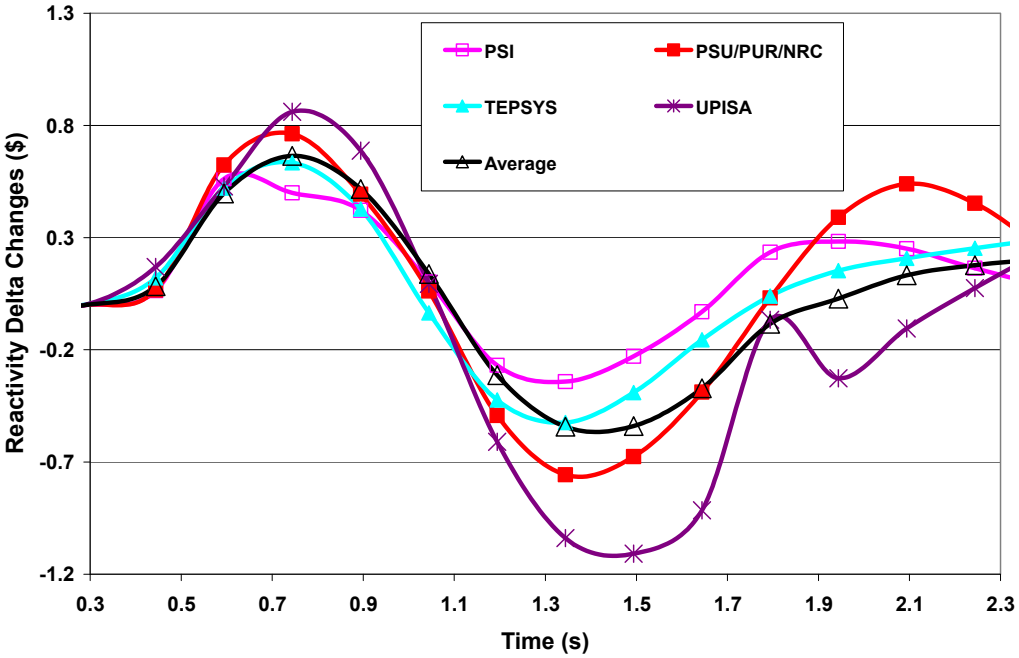

Table 4-43: Extreme Scenario 2 – total reactivity, figure of merit

Participant	D'Auria FFT	Mean error, ME
CEA	0.6192	0.9949
FZD	0.5449	0.9856
GRS	0.5854	0.9845
NFI	0.5812	0.9881
NUPEC	0.6346	0.9934
PSI	0.6072	0.9931
PSU/PUR/NRC	0.5964	0.9829
TEPSYS	0.6552	0.9983
UPISA	0.3625	0.9771

Figure 4-126: Extreme Scenario 2 – Doppler reactivity

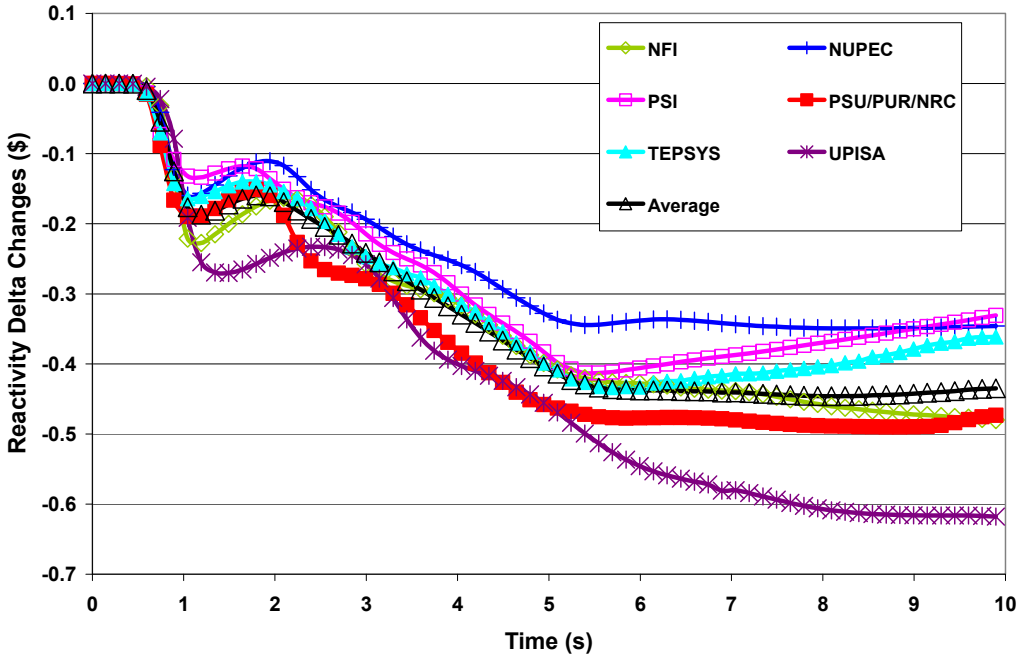

Figure 4-127: Extreme Scenario 2 – Doppler reactivity (zoom)

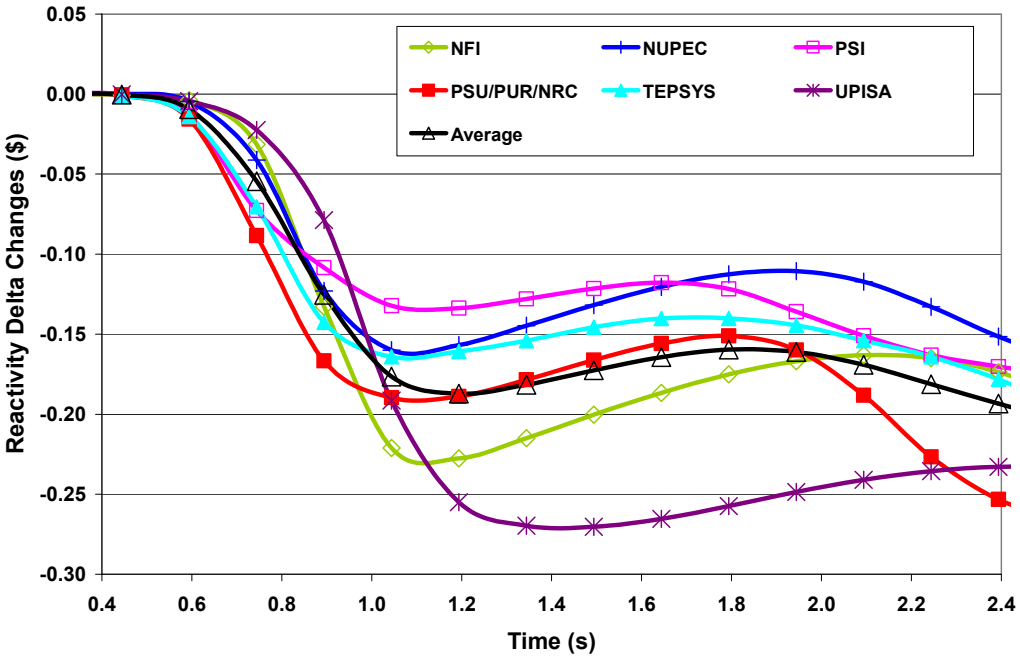

Table 4-44: Extreme Scenario 2 – Doppler reactivity, figure of merit

Participant	D'Auria FFT	Mean error, ME
NFI	0.8056	0.9878
NUPEC	0.7507	0.8862
PSI	0.7657	0.9245
PSU/PUR/NRC	0.7221	0.9362
TEPSYS	0.7937	0.9603
UPISA	0.5807	0.8540

Figure 4-128: Extreme Scenario 2 – void reactivity

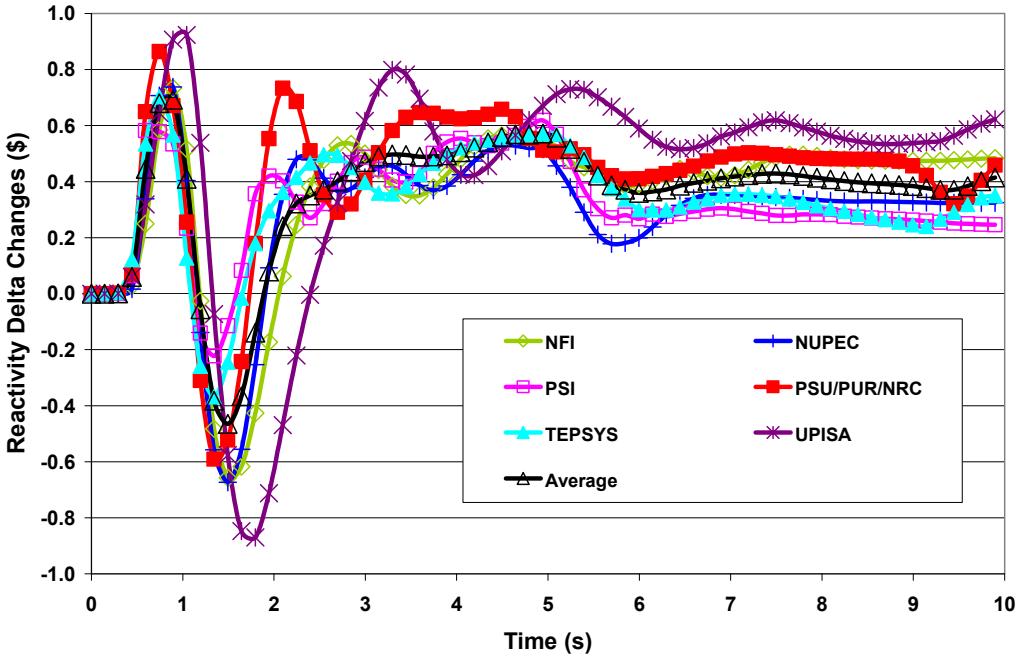

Figure 4-129: Extreme Scenario 2 – void reactivity (zoom)

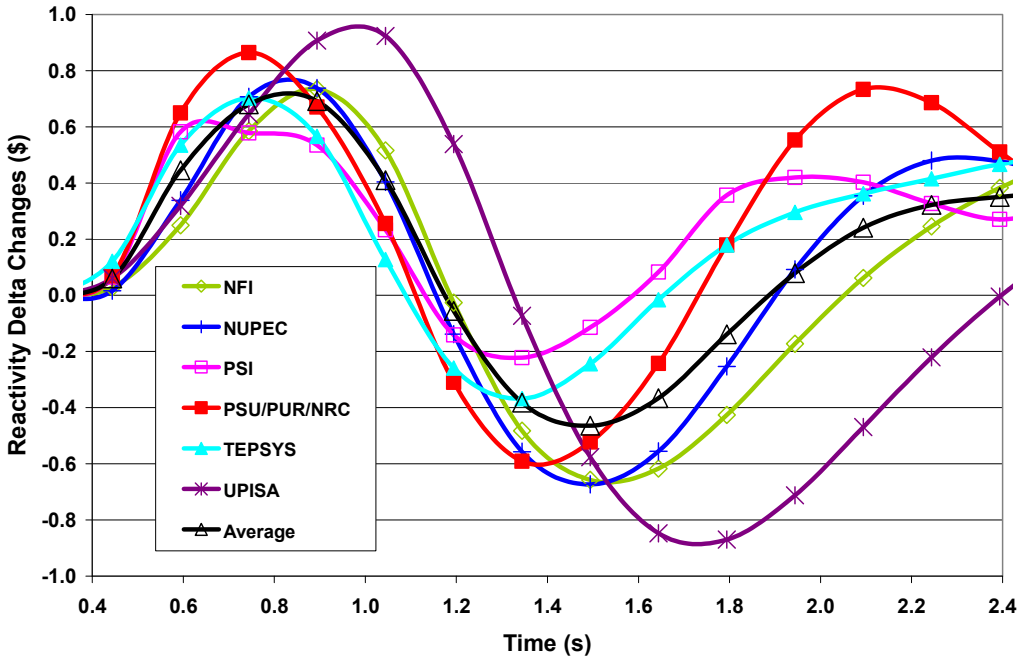

Table 4-45: Extreme Scenario 2 – void reactivity, figure of merit

Participant	D'Auria FFT	Mean error, ME
NFI	0.7460	0.9991
NUPEC	0.7386	0.9481
PSI	0.6762	0.9709
PSU/PUR/NRC	0.6912	0.9525
TEPSYS	0.7201	0.9798
UPISA	0.5538	0.9467

Figure 4-130: Extreme Scenario 2 – LPRM-A

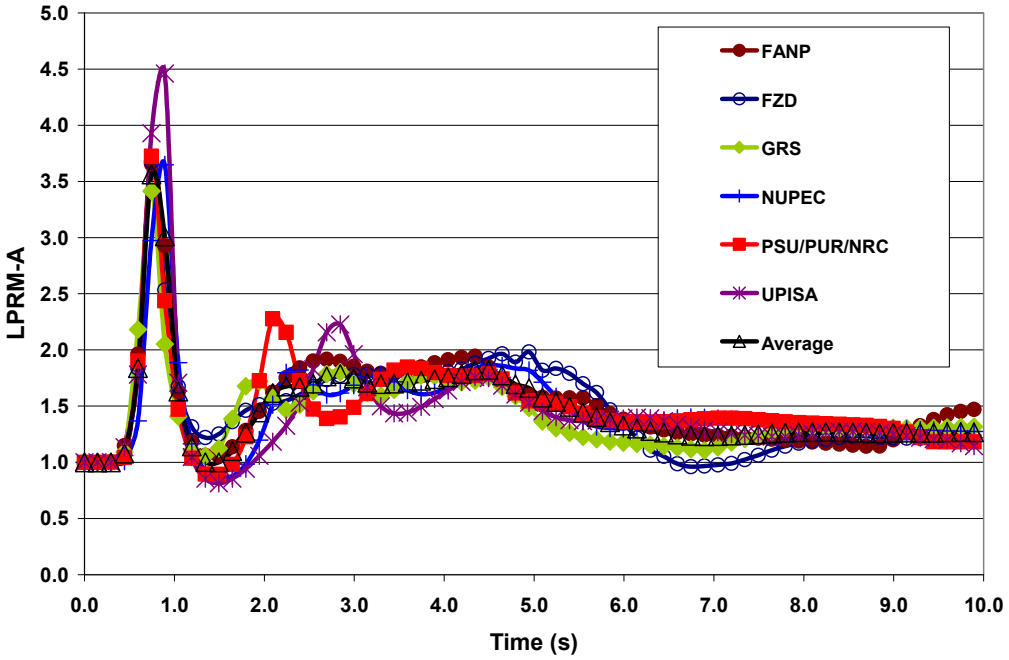

Figure 4-131: Extreme Scenario 2 – LPRM-A (zoom)

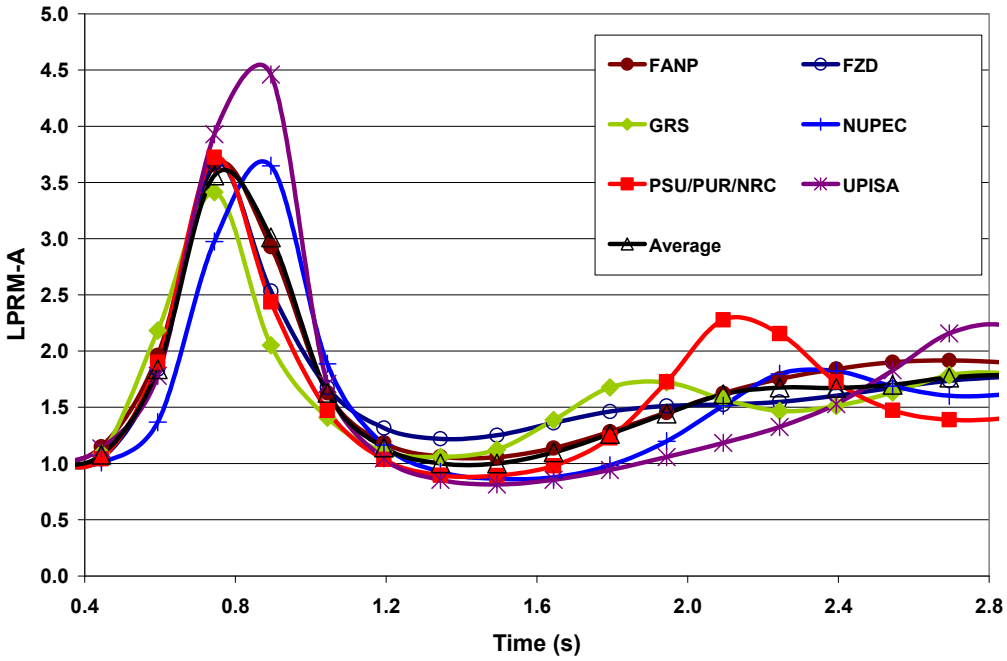

Table 4-46: Extreme Scenario 2 – normalised LPRM-A power, figure of merit

Participant	D'Auria FFT	Mean error, ME
FANP	0.8620	0.9856
FZD	0.8012	0.9991
GRS	0.7522	0.9845
NUPEC	0.7894	0.9965
PSU/PUR/NRC	0.7355	0.9956
UPISA	0.7039	0.9926

Figure 4-132: Extreme Scenario 2 – LPRM-B

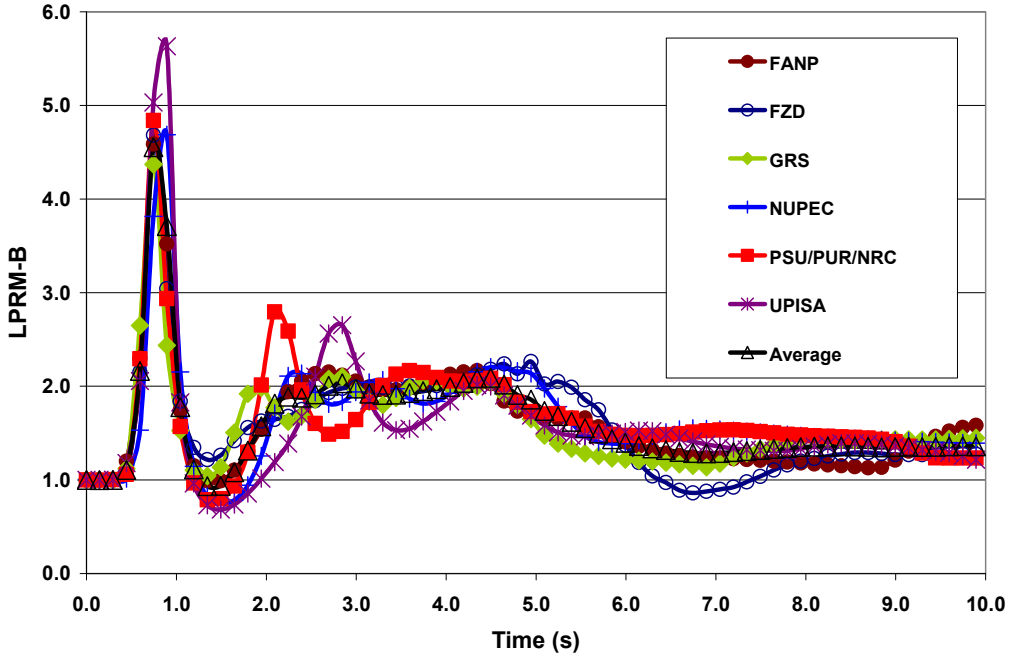

Figure 4-133: Extreme Scenario 2 – LPRM-B (zoom)

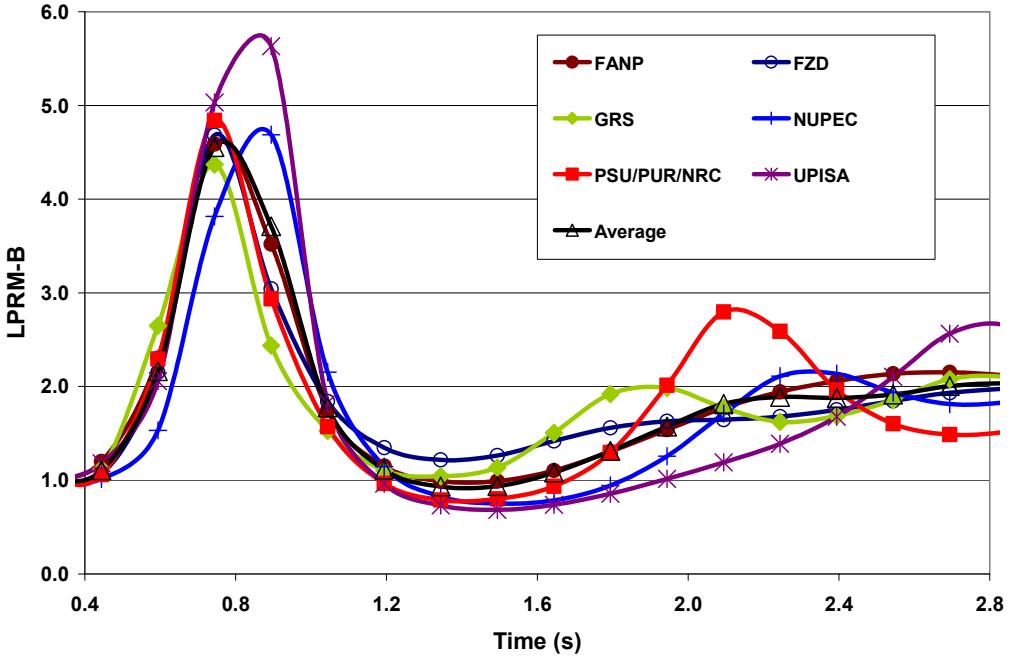

Table 4-47: Extreme Scenario 2 – normalised LPRM-B power, figure of merit

Participant	D'Auria FFT	Mean error, ME
FANP	0.8603	0.9988
FZD	0.7543	0.9930
GRS	0.7215	0.9921
NUPEC	0.7366	0.9887
PSU/PUR/NRC	0.7455	0.9898
UPISA	0.6742	0.9946

Figure 4-134: Extreme Scenario 2 – LPRM-C

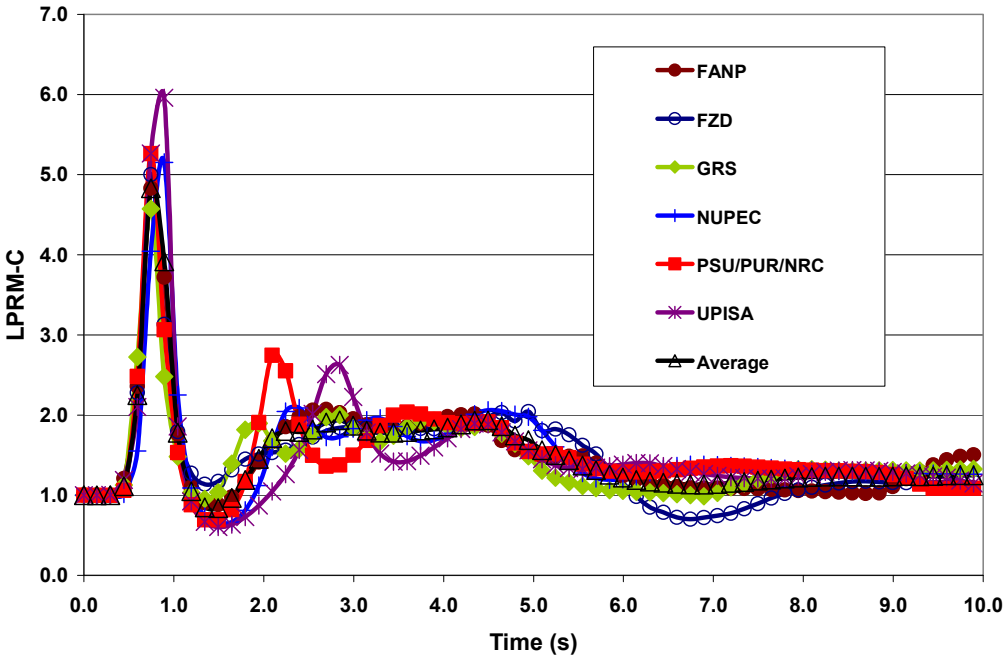

Figure 4-135: Extreme Scenario 2 – LPRM-C (zoom)

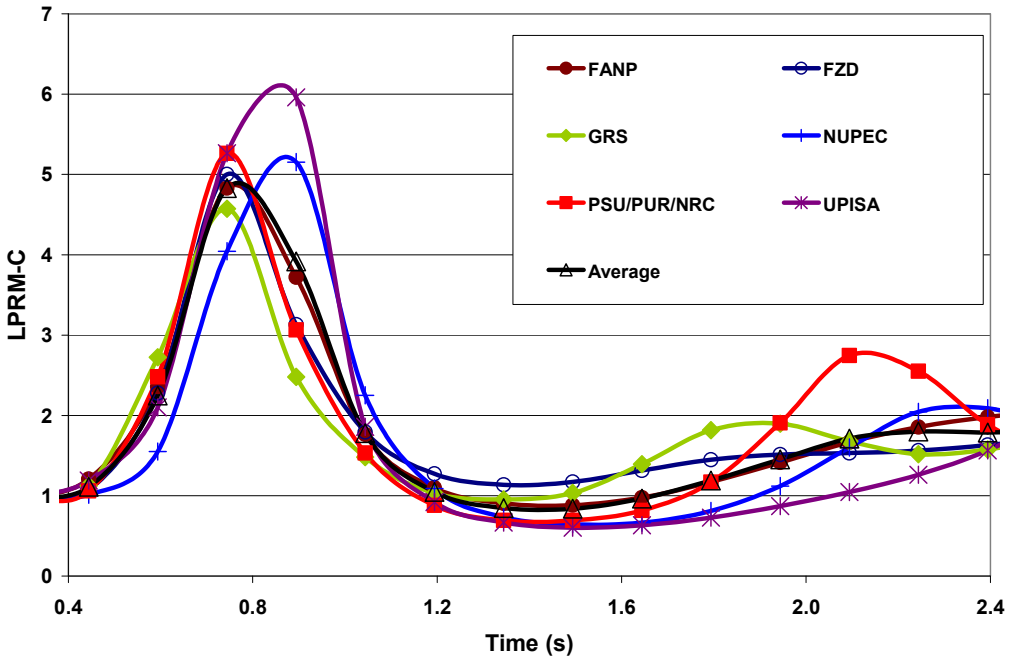

Table 4-48: Extreme Scenario 2 – normalised LPRM-C power, figure of merit

Participant	D'Auria FFT	Mean error, ME
FANP	0.8592	0.9997
FZD	0.7427	0.9893
GRS	0.7086	0.9924
NUPEC	0.7187	0.9903
PSU/PUR/NRC	0.7343	0.9935
UPISA	0.6650	0.9981

Figure 4-136: Extreme Scenario 2 – LPRM-D

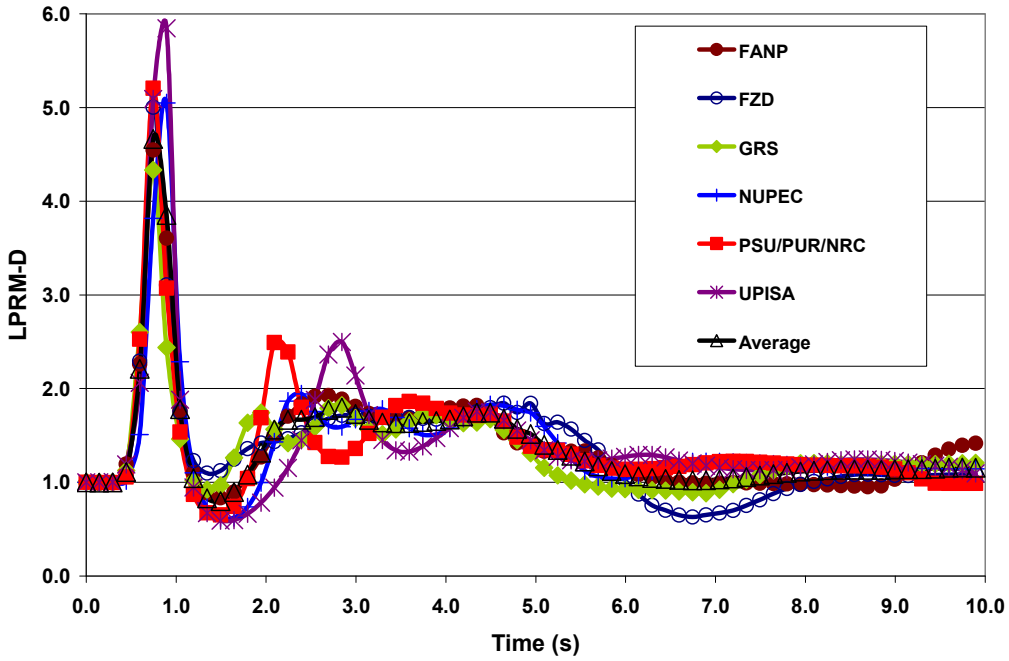

Figure 4-137: Extreme Scenario 2 – LPRM-D (zoom)

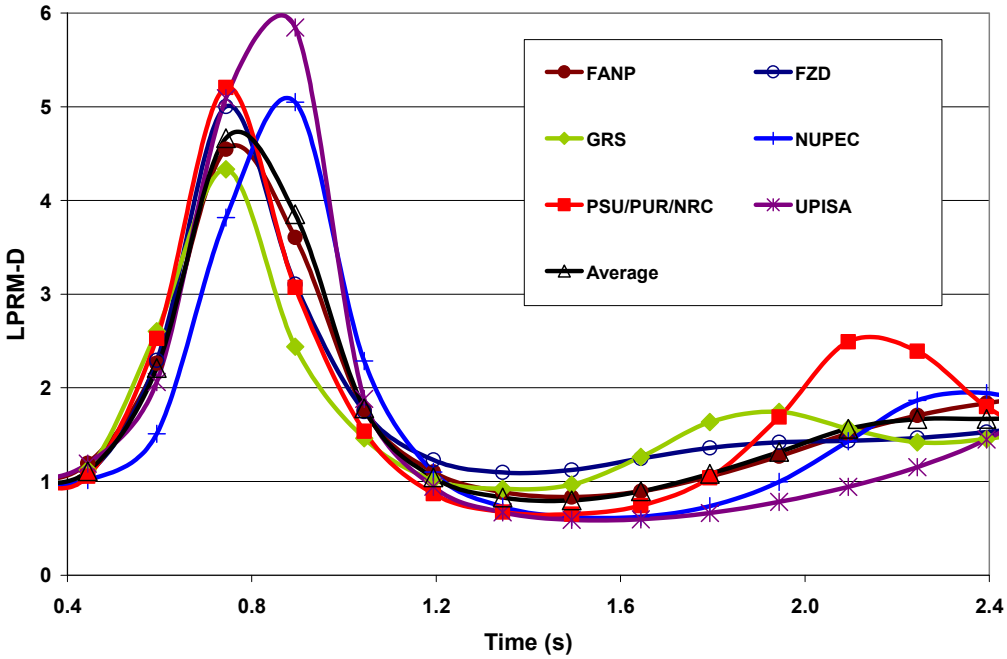

Table 4-49: Extreme Scenario 2 – normalised LPRM-D power, figure of merit

Participant	D'Auria FFT	Mean error, ME
FANP	0.8577	0.9992
FZD	0.7440	0.9920
GRS	0.7059	0.9887
NUPEC	0.7202	0.9956
PSU/PUR/NRC	0.7364	0.9953
UPISA	0.6562	0.9904

4.5 Transient results of Extreme Scenario 3

A combined scenario, turbine trip (TT) with steam bypass relief system failure and without reactor scram event is simulated in Exercise 3 Extreme Scenario 3. The following simulation results of the participants are presented in this subsection:

- core power;
- dome pressure;
- core exit pressure;
- S/RV pressure;
- total reactivity;
- Doppler reactivity;
- void reactivity;
- power of LPRM-A;
- power of LPRM-B;
- power of LPRM-C;
- power of LPRM-D.

Please note that the participants performed sensitivity studies on temporal coupling schemes and time step sizes in advance so as to obtain converged solutions. The results in this section should be considered together with Tables 4-50 and 4-51 since all of the models given in the table are important for the transient calculations.

The plots and tables in this section provide a comparison of the participants' results for the parameters that have the greatest effect on the Exercise 3 Extreme Scenario 3 analysis. For this reason core (averaged and local) and system time histories were requested from the participants to be submitted. These histories are: core-averaged (core power, total reactivity, Doppler reactivity and void reactivity), core local (powers of LPRM A, B, C and D) and system (dome pressure, core exit pressure and S/RV pressure). Similar to the Exercise 3 best-estimate scenario, in order to minimise the impact of the deviations in code predictions at the initial steady-state conditions (which already have been analysed in Section 4.1) and to focus on the deviations in transient calculations, the comparisons of the predictions of time evolutions of the above parameters are performed not on the absolute values of the parameters but on the delta changes of the parameters as compared to the values at the initial steady state.

Table 4-50: Number of channels used and power submitted by the participants – Extreme Scenario 3

Participant	Number of channels	Power submitted
CEA	33	Fission
FANP	33	Fission
FZD	764	Total
GRS	33	Fission
NFI	33	Total
NUPEC	33	Fission
PSI	34	Fission
PSU/PURDUE/NRC	33	Total
TEPSYS	33	Total
UPISA	33	Total
UPV (NOKIN)	33	Total
WESTINGHOUSE	764	Total

Table 4-51: Models used in Extreme Scenario 3

Participant	XENON	ADF	BYPASS	DECAY
CEA	No	No	Yes	Yes
FANP	Yes	Yes	Yes	Yes
FZD	Yes	Yes	Yes	Yes
GRS	Yes	No	Yes	Yes
NFI	Yes	No	Yes	Yes
NUPEC	Yes	Yes	No	Yes
PSI	Yes	Yes	Yes	No
PSU/PURDUE/NRC	Yes	Yes	Yes	Yes
TEPSYS	Yes	Yes	Yes	Yes
UPISA	No	Yes	Yes	Yes
UPV	Yes	Yes	Yes	Yes
WESTINGHOUSE	No	Yes	Yes	Yes

The mean time histories are provided in this section as well as in Appendix C. The figures of merit are presented in the tables of this section. Additionally, the participants' deviations and figures of merit are presented in Appendix D, and are listed in the same order as the reference solutions. Appendices C and D are provided upon request on CD-ROM.

In each case the figures (Figures 4-138 through 4-163) graphically illustrate the agreement or disagreement of participants' predictions. Statistical evaluation is employed to generate a mean solution, which is also shown in the plots.

Participants' sequences of events in Extreme Scenario 2 are given in Table 4-52.

Core power time evolutions are presented in two groups (fission or total) depending on the submitted core power type. Comparisons of the predictions of fission power evolution and the total power evolution calculated by each code throughout the transient (up to 10 seconds) are shown in Figures 4-138 and 4-140 while Figures 4-139 and 4-141 zoom on the first few seconds of the transient. Table 4-53 provides figure of merit (FOM) for two different methods, D'Auria FFT and Mean Error.

When analysing the power history results it should be taken into account that in Extreme Scenario 3 the same phenomena take place as in the actual TT2 test (best-estimate scenario), with the difference that a turbine trip with steam bypass relief system failure and without scram leads to a higher first power peak (as in Extreme Scenario 1) and continuing power oscillations throughout the transient with subsequent smaller power peaks (as in Extreme Scenario 2 but more pronounced because of the failure of steam bypass relief system). This power response in terms of timing and magnitude of power peaks during the transient as predicted by different codes is a function of the total reactivity time evolution. In Figure 4-112 (the fission power group), the NUPEC result differs from the cluster around the mean solution. In the total power group (Figure 4-114), all of the codes' predictions (except UPV and UPISA for the first peak as well as PSU/PUR/NRC for the subsequent peaks) form a cluster around the mean solution. In general, the power history results are in a good agreement.

System parameter (dome pressure, core exit pressure and S/RV pressure) time evolutions are presented in two groups (Group 1 and Group 2) in order to visualise them clearly. Comparisons of the predictions of these parameters calculated by each code throughout the transient (up to 10 seconds) are shown in Figures 4-142 through 4-147 while Tables 4-54 through 4-56 provide figure of merit (FOM) for two different methods, D'Auria FFT and Mean Error. It is important to note that for the S/RV pressure time history plots the three safety relief set points are provided to show which valves open and when for different participants' simulations.

Figures 4-148 through 4-155 show comparisons of the predictions of the total, Doppler and void reactivity throughout the transient (up to 10 seconds) and zoom of the beginning of transient. Larger deviations from mean solutions are observed after the first power peak for some participants for the total reactivity (FZD, GRS and UPISA), moderator density (void) reactivity (UPISA and PSU/PUR/NRC) and Doppler feedback reactivity (UPISA and NUPEC) time histories.

Core local parameter time evolutions such as LPRM A, B, C and D power time histories are presented through three types of comparisons. Comparisons of the predictions of local parameter time evolutions calculated by each code throughout the transient (up to 10 seconds) are shown in Figures 4-156, 4-158, 4-160 and 4-162. Figures 4-157, 4-159, 4-161 and 4-163 zoom on the first few seconds of the transient. Tables 4-60 through 4-62 provide figure of merit (FOM) for two different methods, D'Auria FFT and Mean Error. It is important to note that for the four LPRM power time histories the average (mean) of participants' predictions is used as reference solution.

Table 4-52: Sequence of events in Extreme Scenario 3

Participant	Event* (msec)				
	TSVC	DPIR	CEPIR	S/RVO	S/RVC
CEA	0.096	0.390	0.384	2.123	None
FANP	0.096	0.396	0.390	2.130	None
FZD	0.096	0.382	0.402	2.650	None
GRS	0.096	0.372	0.378	2.250	None
NFI	0.096	0.414	0.414	2.907	None
NUPEC	0.096	0.438	0.456	2.982	None
PSI	0.096	0.438	0.444	2.724	None
PSU/PUR/NRC	0.096	0.402	0.402	2.100	None
TEPSYS	0.096	0.366	0.360	2.255	None
UPISA	0.096	0.348	0.324	1.800	None
UPV	0.000	0.384	0.390	2.200	None
WES	0.870	0.396	0.444	3.036	None

* Description of the events: TSVC – turbine stop valve closed, DPIR – vessel dome pressure initial response (0.78% increased over initial value), CEPIR – core exit pressure initial response (0.27% increased over initial value), S/RVO – first safety/relief valve begins opening (refer to valve with lowest opening set-point), S/RVC – last safety/relief valve fully closed (refer to valve with lowest closing set-point).

Figure 4-138: Extreme Scenario 3 – transient power (fission)

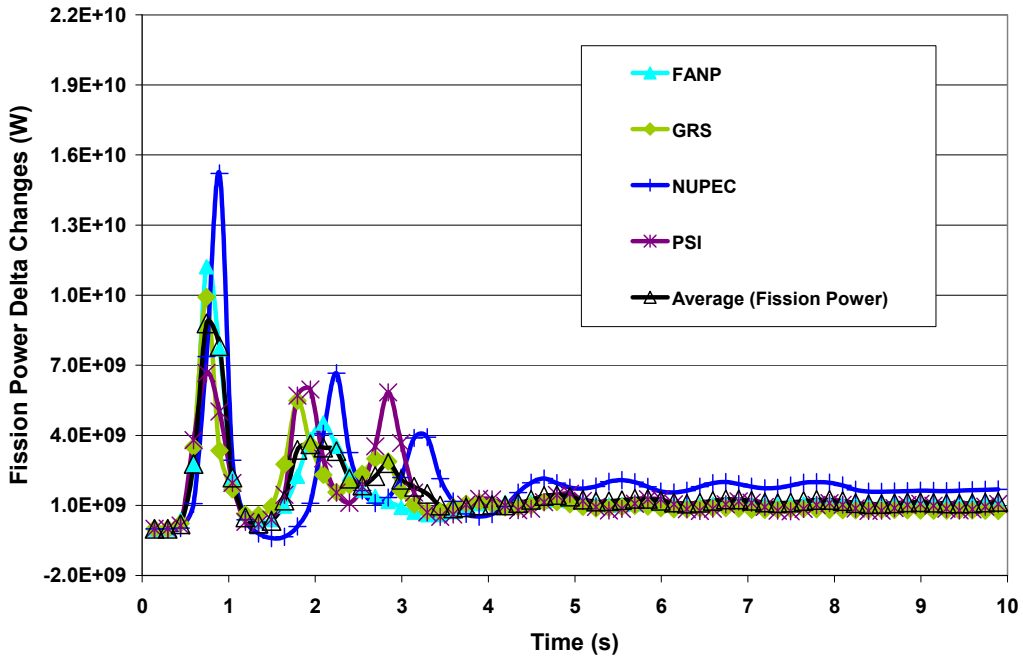

Figure 4-139: Extreme Scenario 3 – transient power (fission – zoom)

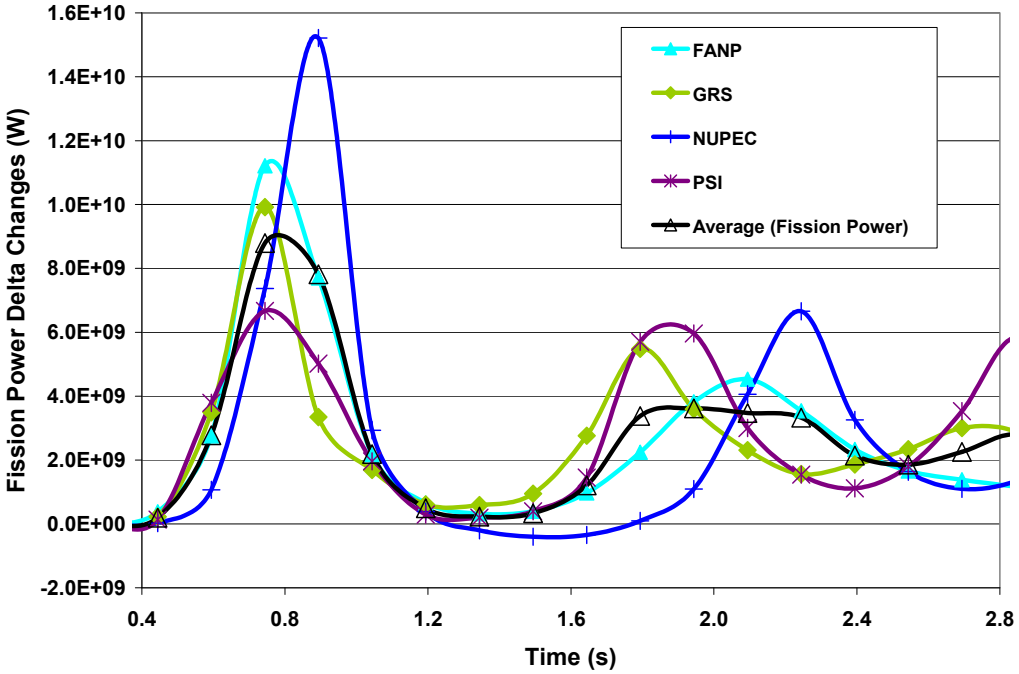

Figure 4-140: Extreme Scenario 3 – transient power (total)

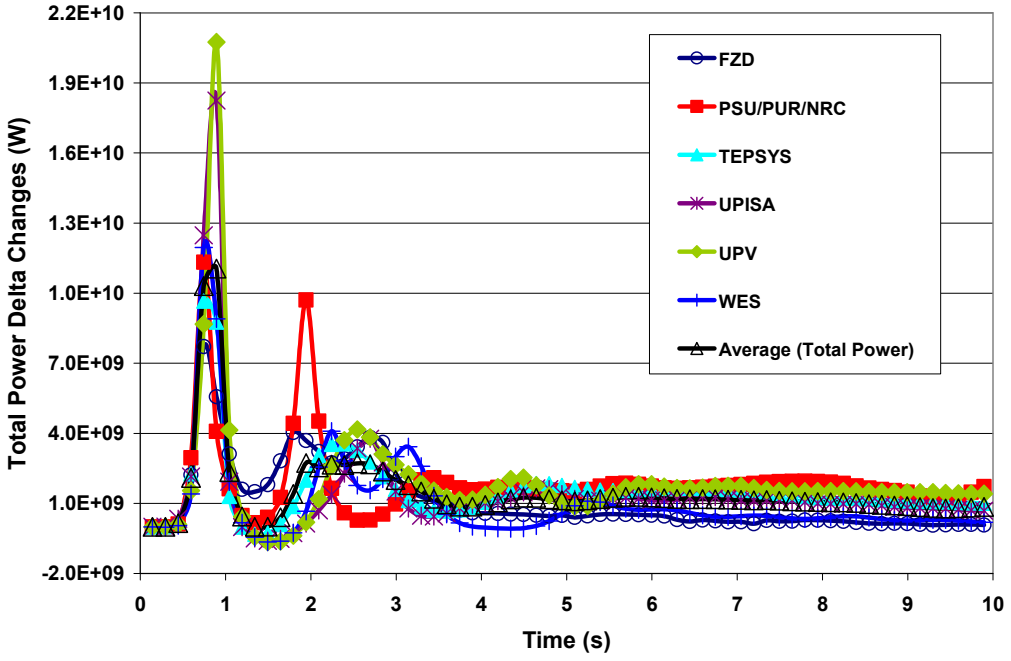

Figure 4-141: Extreme Scenario 3 – transient power (total – zoom)

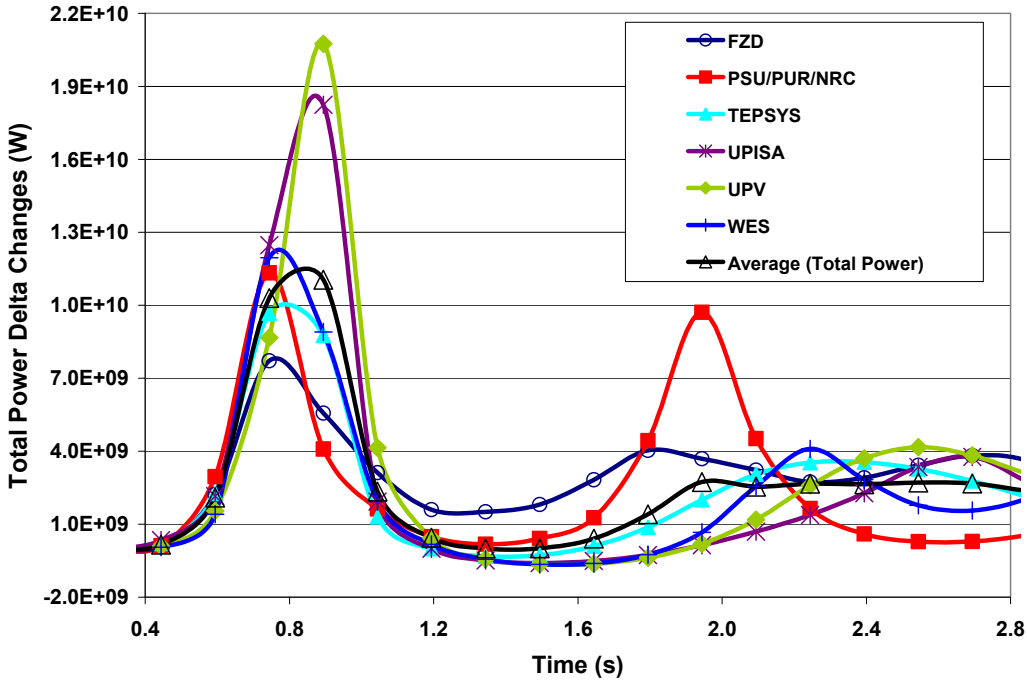

Table 4-53: Extreme Scenario 3 – transient power, figure of merit

Fission power submitted			Total power submitted		
Participant	**D'Auria FFT**	**Mean error, ME**	**Participant**	**D'Auria FFT**	**Mean error, ME**
FANP	0.6745	0.9896	FZD	0.5907	0.9754
GRS	0.6203	0.9765	PSU/PUR/NRC	0.5422	0.9763
NUPEC	0.5232	0.9595	TEPSYS	0.7594	0.9925
PSI	0.6016	0.9925	UPISA	0.5593	0.9991
			UPV	0.5784	0.9739
			WES	0.6561	0.9686

Figure 4-142: Extreme Scenario 3 – transient dome pressure (Group 1)

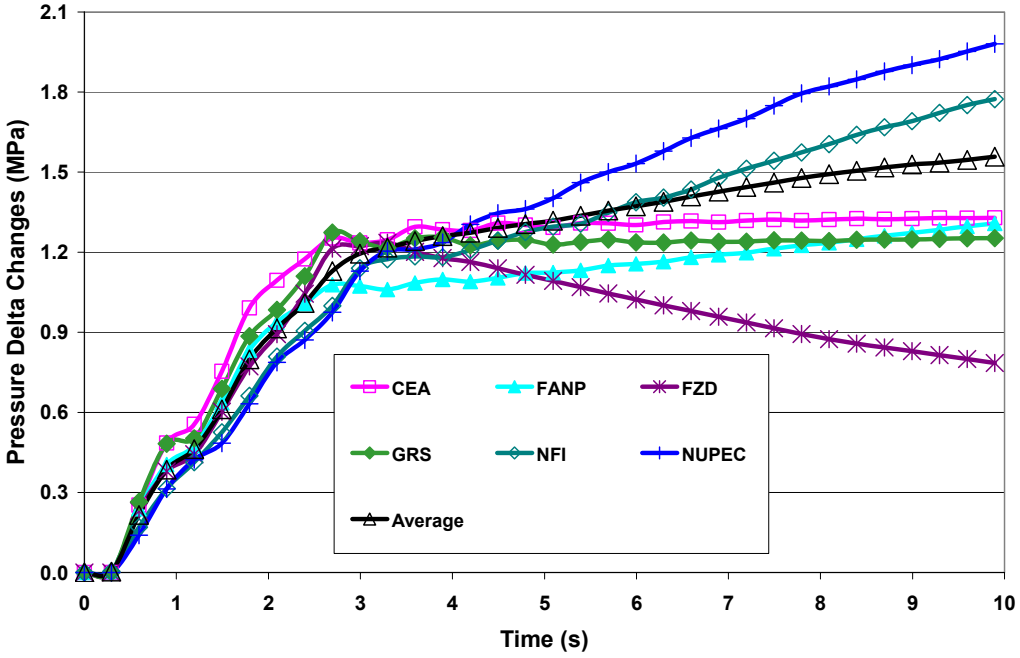

Figure 4-143: Extreme Scenario 3 – transient dome pressure (Group 2)

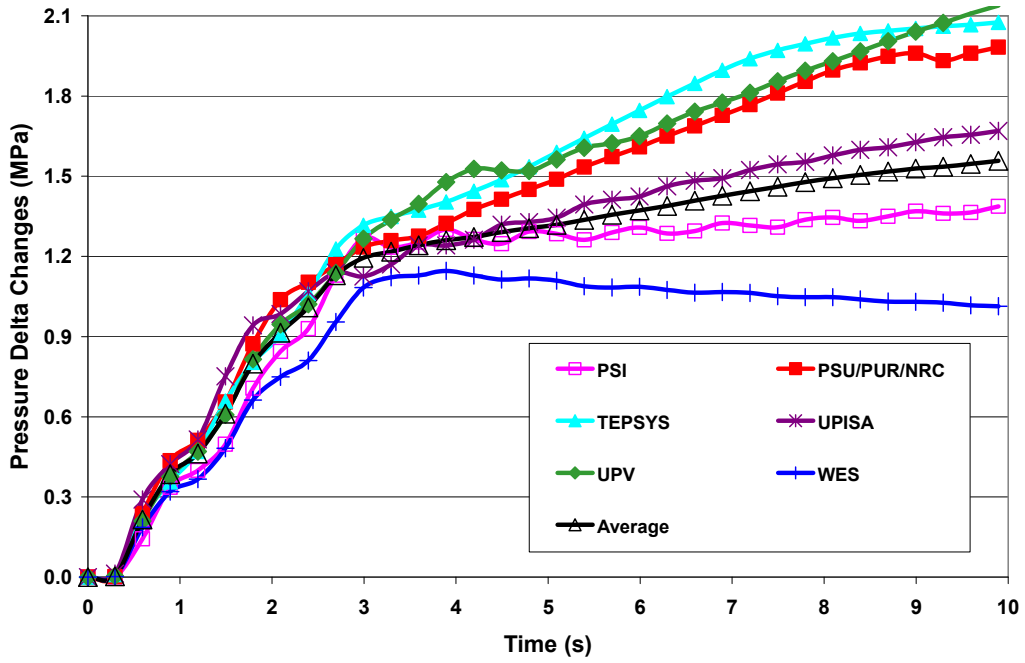

Table 4-54: Extreme Scenario 3 – transient dome pressure, figure of merit

Participant	D'Auria FFT	Mean error, ME
CEA	0.8580	0.9804
FANP	0.8223	0.9113
FZD	0.7207	0.8482
GRS	0.8348	0.9460
NFI	0.8746	0.9937
NUPEC	0.8052	0.9339
PSI	0.8182	0.9523
PSU/PUR/NRC	0.7969	0.8870
TEPSYS	0.7620	0.8519
UPISA	0.8825	0.9658
UPV	0.7607	0.8660
WES	0.7672	0.8585

Figure 4-144: Extreme Scenario 3 – transient core exit pressure (Group 1)

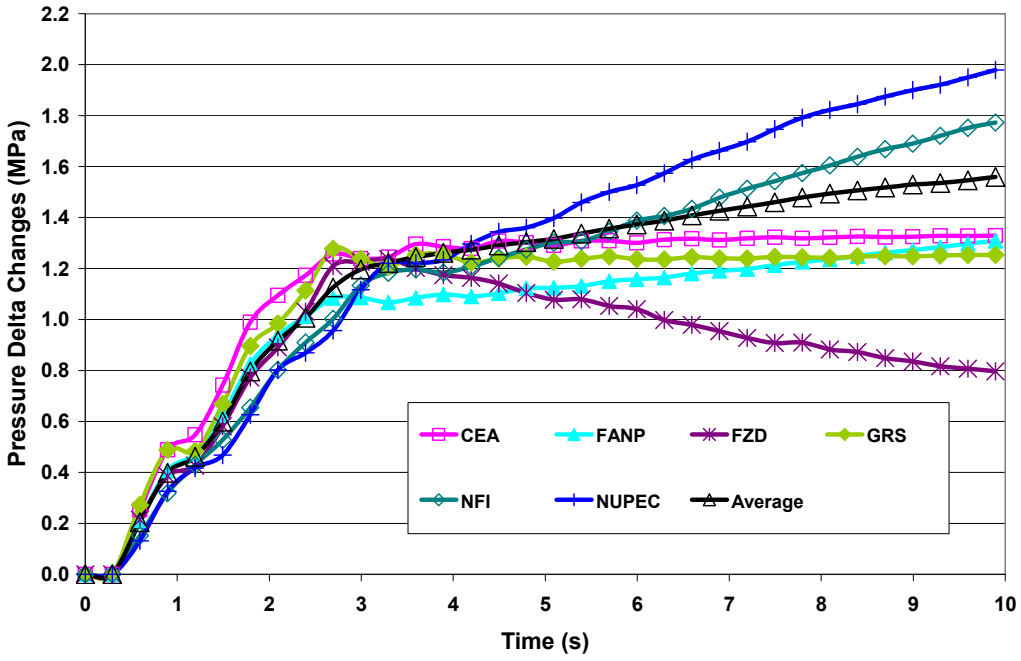

Figure 4-145: Extreme Scenario 3 – transient core exit pressure (Group 2)

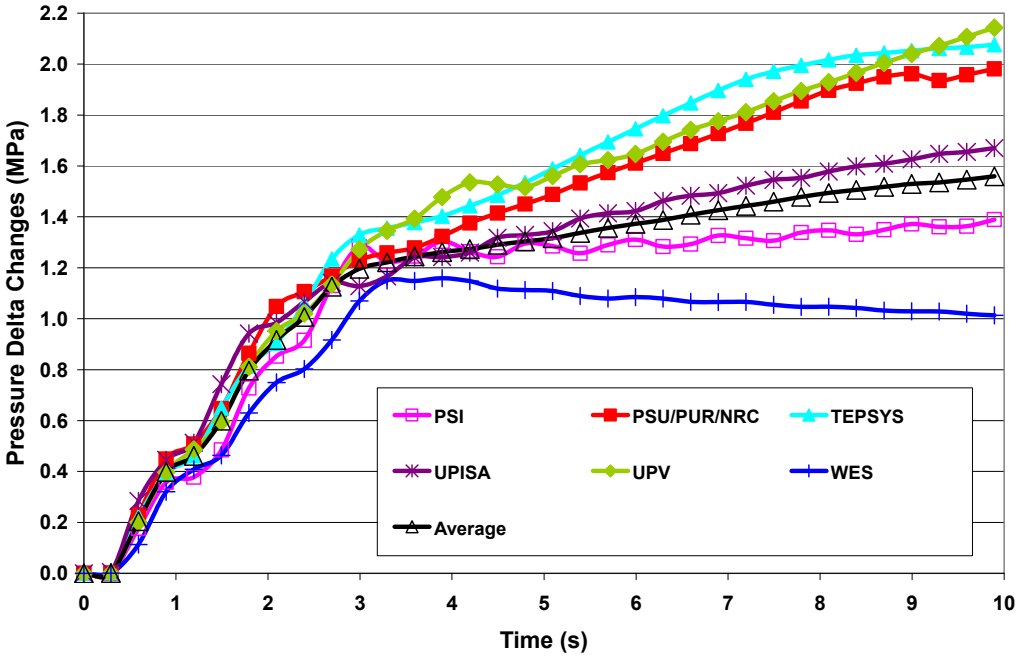

Table 4-55: Extreme Scenario 3 – transient core exit pressure, figure of merit

Participant	D'Auria FFT	Mean error, ME
CEA	0.8261	0.9805
FANP	0.7981	0.9114
FZD	0.7136	0.8480
GRS	0.8056	0.9465
NFI	0.8092	0.9929
NUPEC	0.7518	0.9347
PSI	0.8167	0.9527
PSU/PUR/NRC	0.7974	0.8869
TEPSYS	0.7620	0.8513
UPISA	0.8785	0.9657
UPV	0.7598	0.8657
WES	0.7661	0.8578

Figure 4-146: Extreme Scenario 3 – transient S/RV pressure (Group 1)

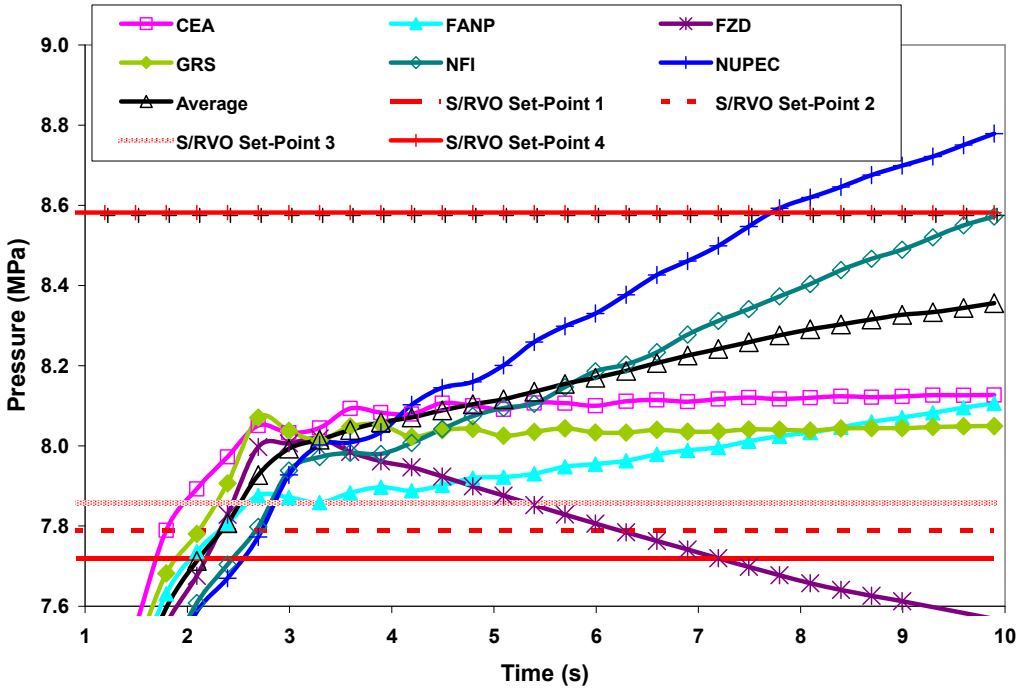

Figure 4-147: Extreme Scenario 3 – transient S/RV pressure (Group 2)

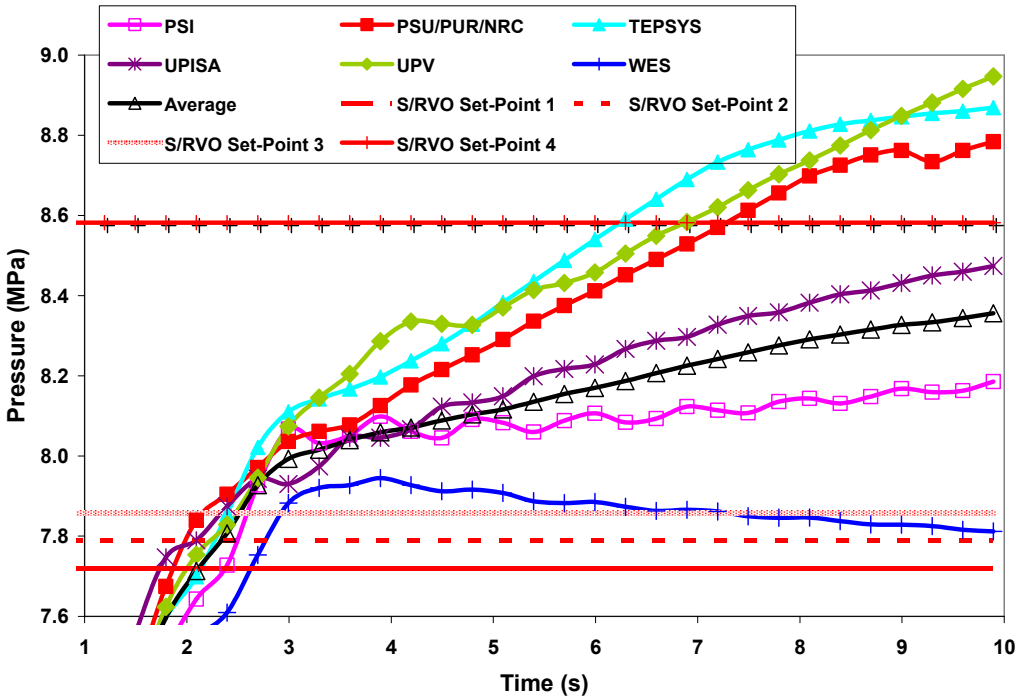

Table 4-56: Extreme Scenario 3 – transient S/RV pressure, figure of merit

Participant	D'Auria FFT	Mean error, ME
CEA	0.8449	0.9838
FANP	0.8130	0.9145
FZD	0.7196	0.8510
GRS	0.8230	0.9495
NFI	0.8448	0.9967
NUPEC	0.7812	0.9375
PSI	0.8202	0.9557
PSU/PUR/NRC	0.7999	0.8900
TEPSYS	0.7646	0.8545
UPISA	0.8835	0.9690
UPV	0.7628	0.8688
WES	0.7693	0.8611

Figure 4-148: Extreme Scenario 3 – total reactivity (Group 1)

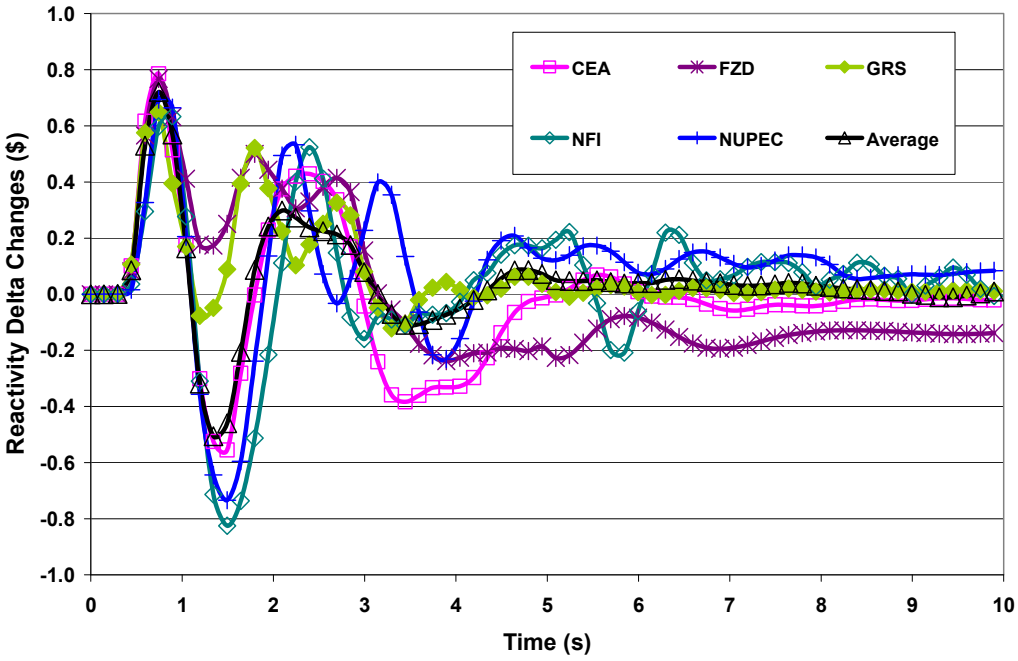

Figure 4-149: Extreme Scenario 3 – total reactivity (Group 1 – zoom)

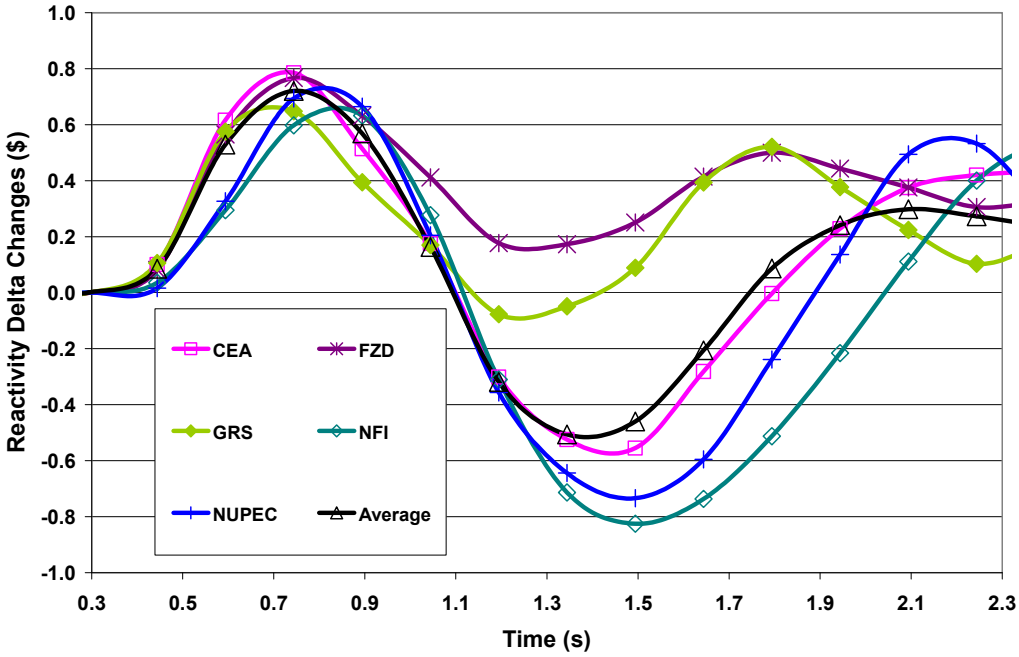

Figure 4-150: Extreme Scenario 3 – total reactivity (Group 2)

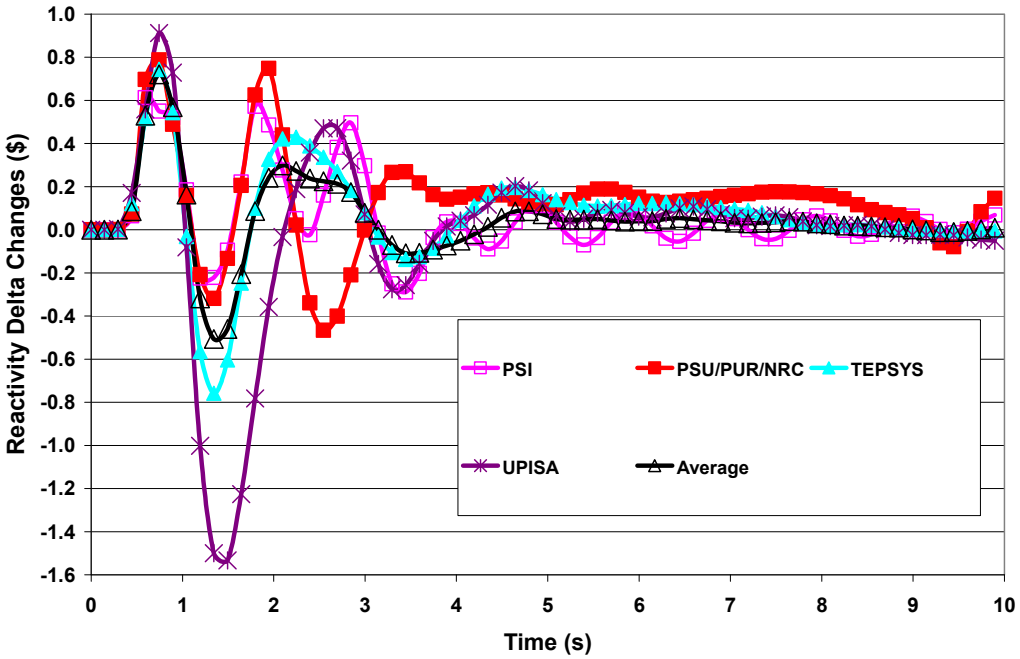

Figure 4-151: Extreme Scenario 3 – total reactivity (Group 2 – zoom)

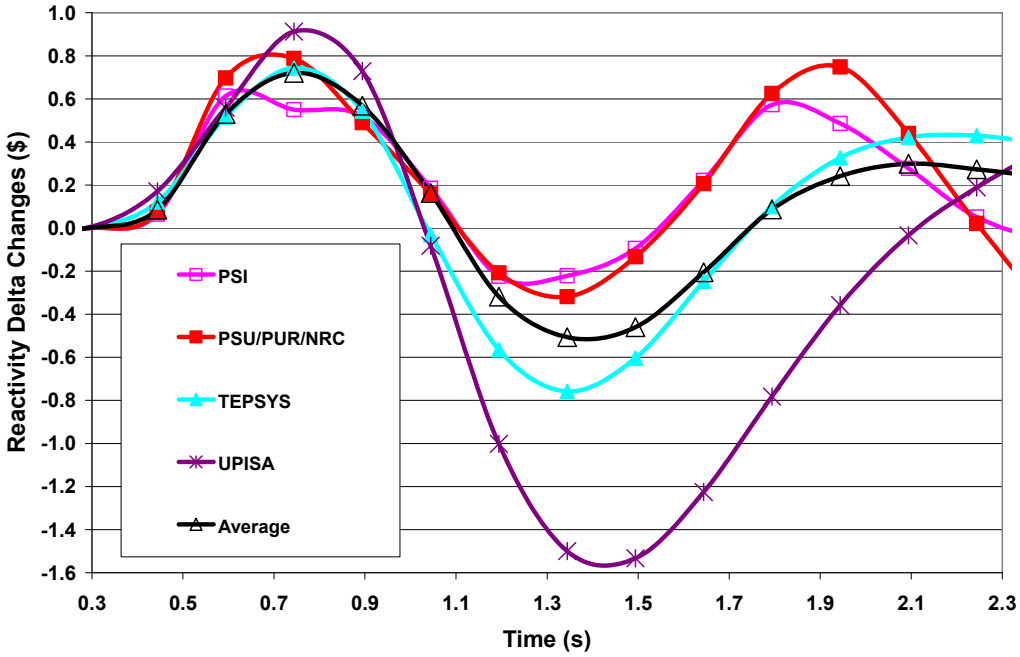

Table 4-57: Extreme Scenario 3 – total reactivity, figure of merit

Participant	D'Auria FFT	Mean error, ME
CEA	0.5679	0.9434
FANP	0.4914	0.9464
FZD	0.5302	0.9459
GRS	0.2201	0.9555
NFI	0.5564	0.9976
NUPEC	0.5356	0.9659
PSI	0.4901	0.9490
PSU/PUR/NRC	0.6143	0.9860
TEPSYS	0.4334	0.9026
UPISA	0.5679	0.9434
UPV	0.4914	0.9464
WES	0.5302	0.9459

Figure 4-152: Extreme Scenario 3 – Doppler reactivity

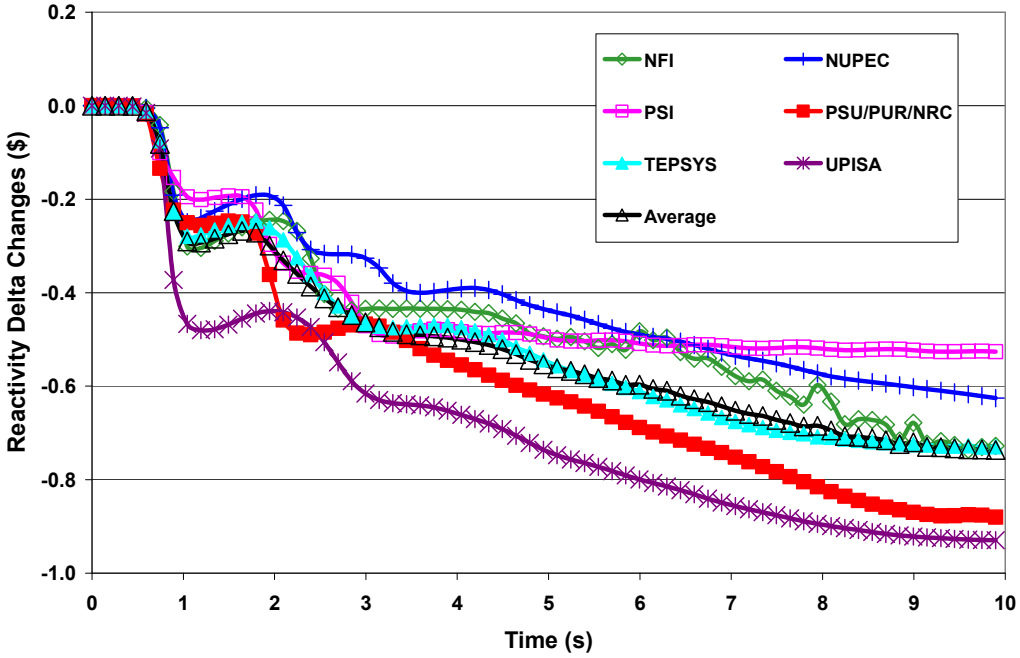

Figure 4-153: Extreme Scenario 3 – Doppler reactivity (zoom)

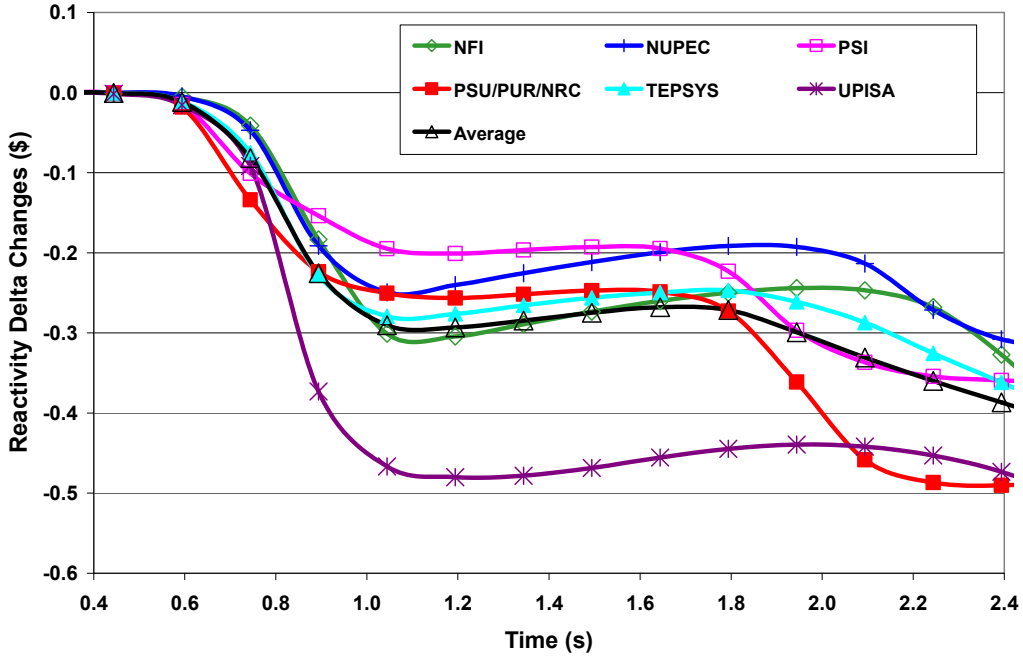

Table 4-58: Extreme Scenario 3 – Doppler reactivity, figure of merit

Participant	D'Auria FFT	Mean error, ME
NFI	0.7936	0.9433
NUPEC	0.8125	0.8817
PSI	0.7825	0.8941
PSU/PUR/NRC	0.8074	0.9122
TEPSYS	0.9300	0.9960
UPISA	0.7394	0.8193

Figure 4-154: Extreme Scenario 3 – void reactivity

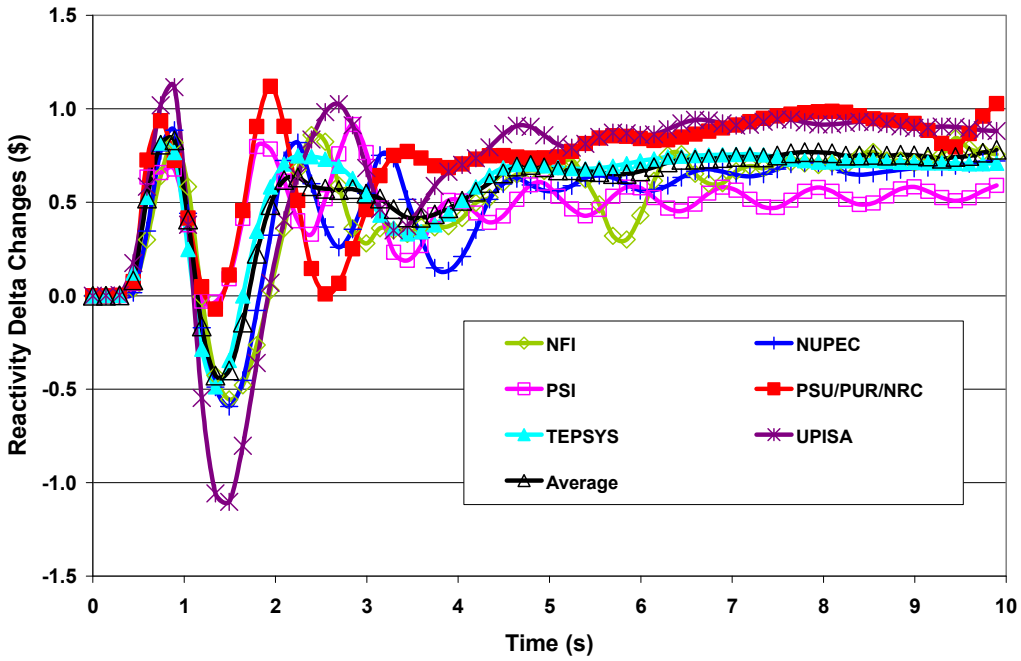

Figure 4-155: Extreme Scenario 3 – void reactivity (zoom)

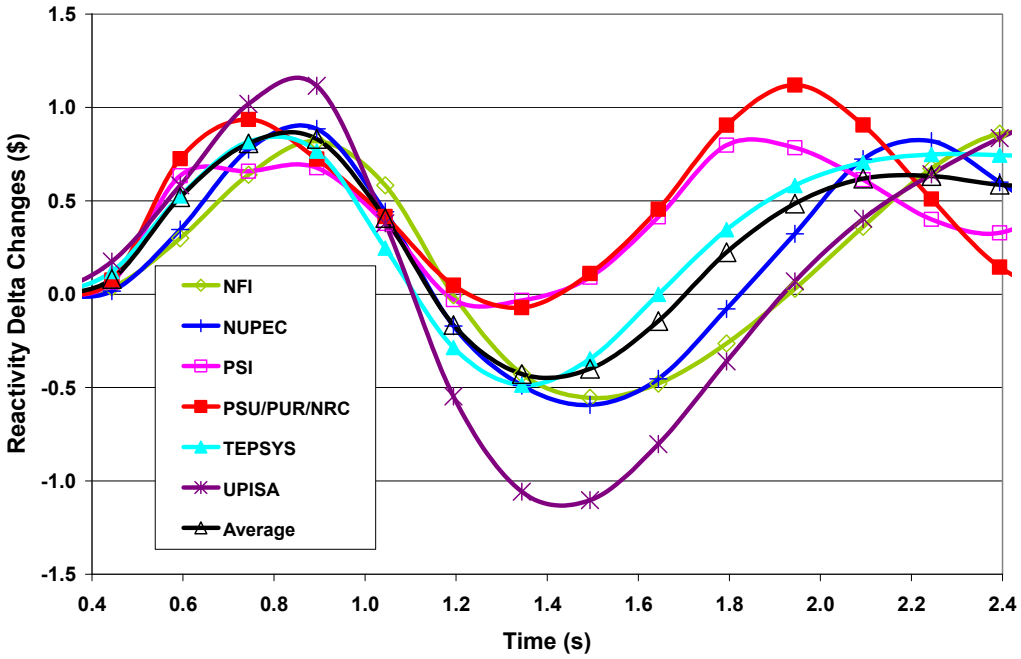

Table 4-59: Extreme Scenario 3 – void reactivity, figure of merit

Participant	D'Auria FFT	Mean error, ME
NFI	0.5901	0.9686
NUPEC	0.6819	0.9597
PSI	0.6294	0.9543
PSU/PUR/NRC	0.6156	0.9302
TEPSYS	0.7339	0.9990
UPISA	0.6207	0.9559

Figure 4-156: Extreme Scenario 3 – LPRM-A

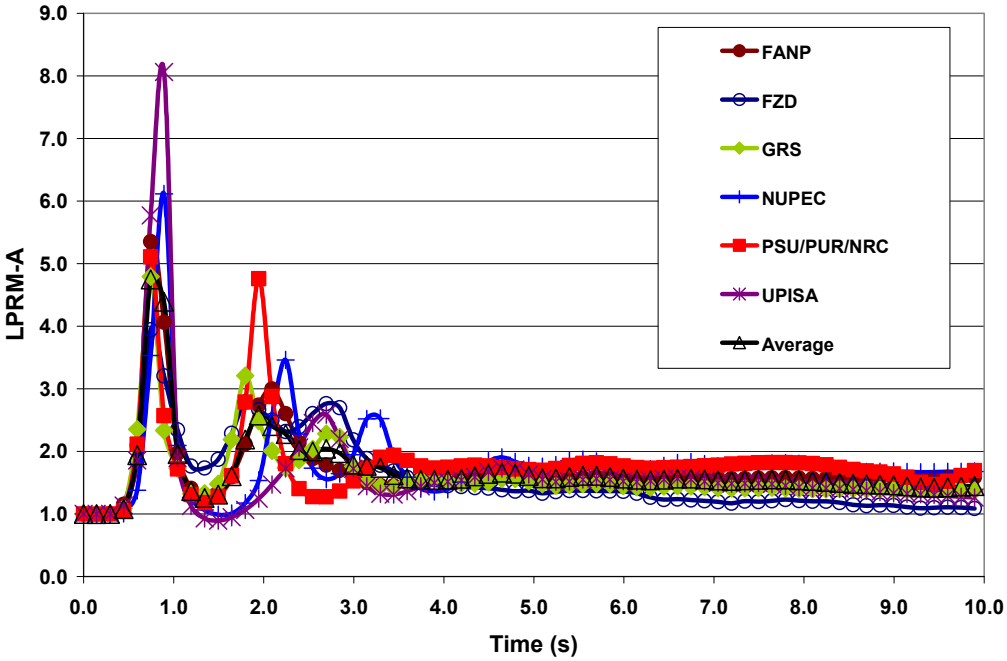

Figure 4-157: Extreme Scenario 3 – LPRM-A (zoom)

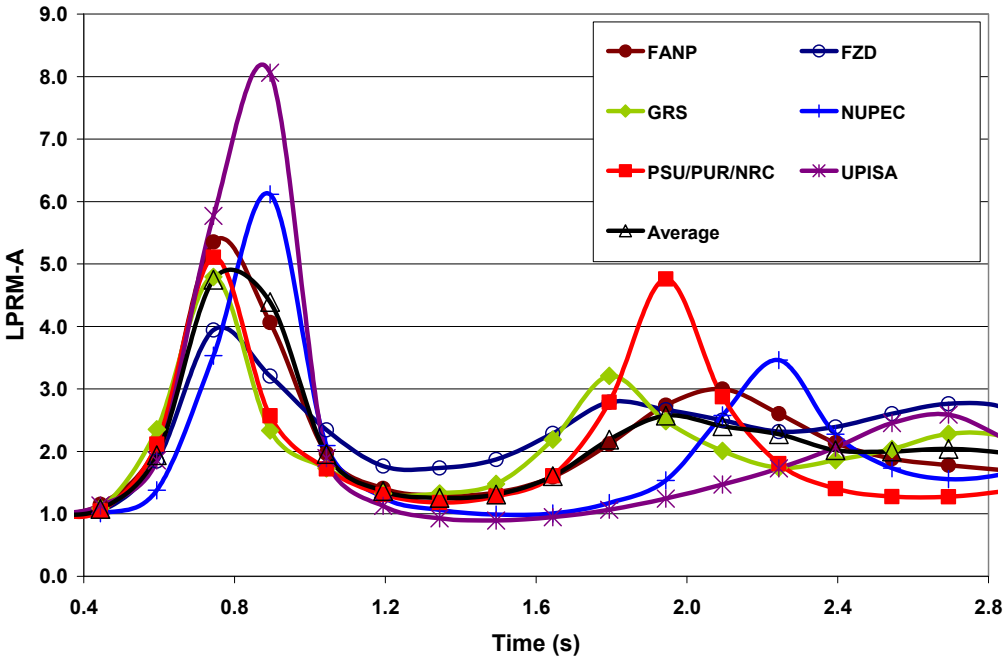

Table 4-60: Extreme Scenario 3 – normalised LPRM-A power, figure of merit

Participant	D'Auria FFT	Mean error, ME
FANP	0.7851	0.9914
FZD	0.6948	0.9753
GRS	0.6622	0.9810
NUPEC	0.6535	0.9772
PSU/PUR/NRC	0.6384	0.9773
UPISA	0.5462	0.9896

Figure 4-158: Extreme Scenario 3 – LPRM-B

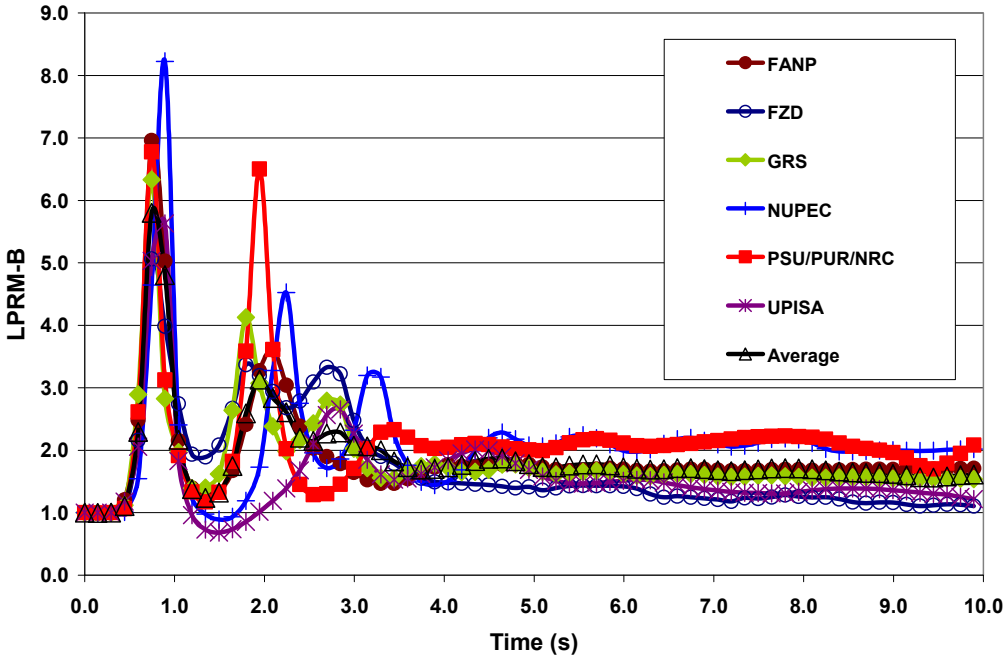

Figure 4-159: Extreme Scenario 3 – LPRM-B (zoom)

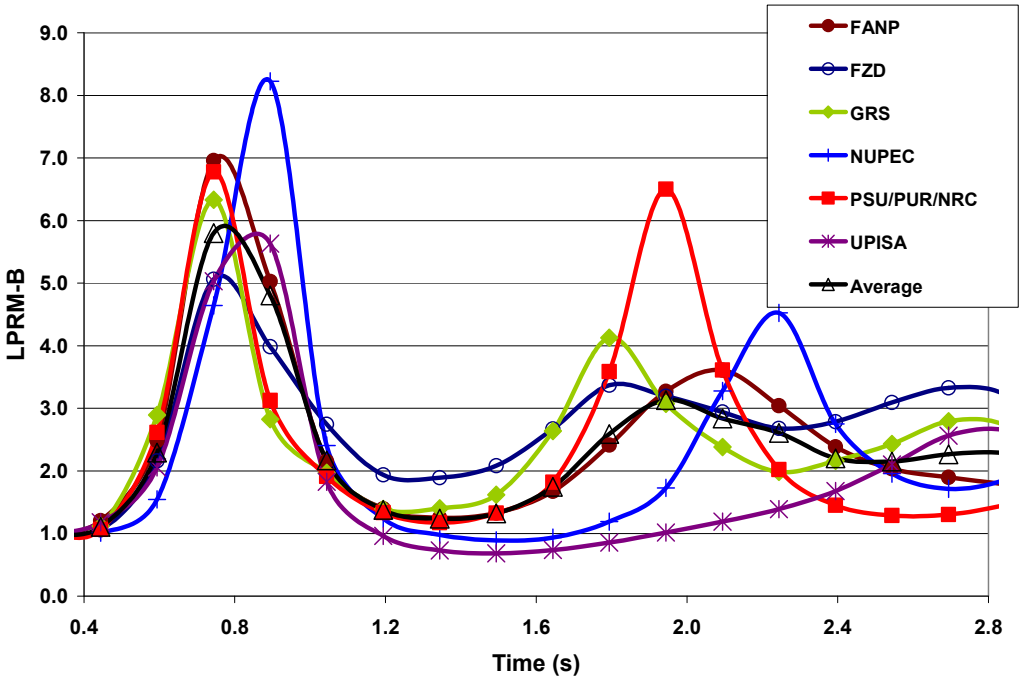

Table 4-61: Extreme Scenario 3 – normalised LPRM-B power, figure of merit

Participant	D'Auria FFT	Mean error, ME
FANP	0.7255	0.9989
FZD	0.7085	0.9690
GRS	0.6664	0.9912
NUPEC	0.5870	0.9542
PSU/PUR/NRC	0.6074	0.9517
UPISA	0.6590	0.9445

Figure 4-160: Extreme Scenario 3 – LPRM-C

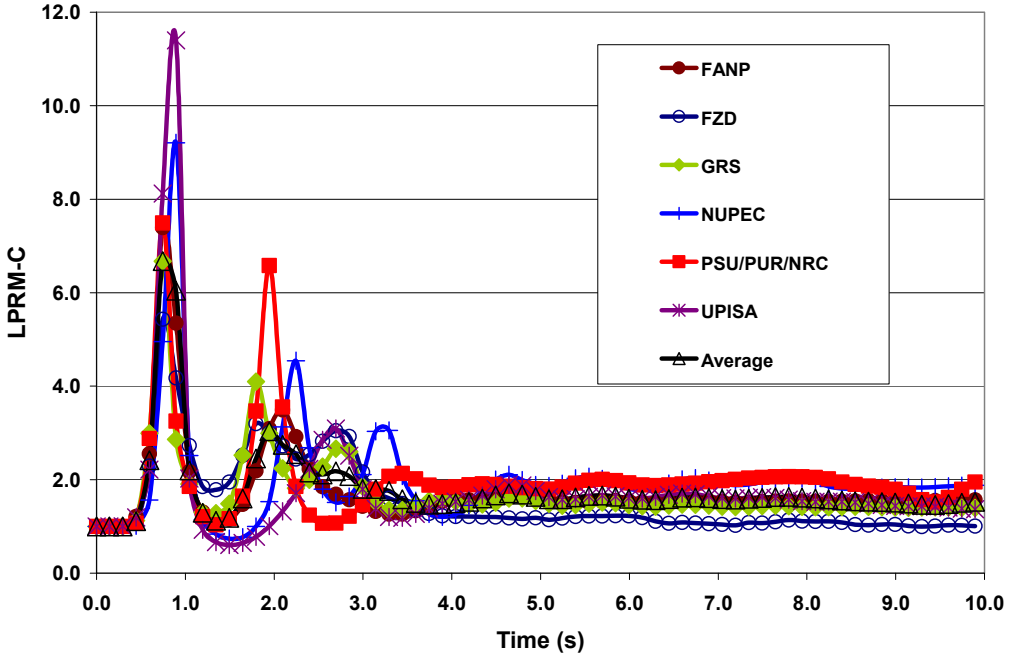

Figure 4-161: Extreme Scenario 3 – LPRM-C (zoom)

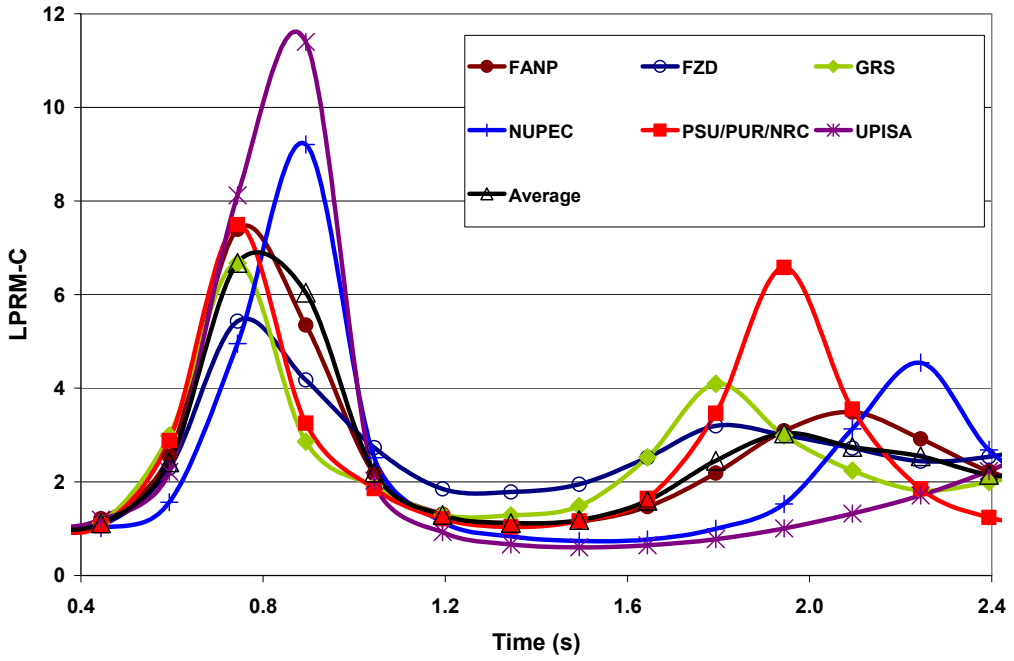

Table 4-62: Extreme Scenario 3 – normalised LPRM-C power, figure of merit

Participant	D'Auria FFT	Mean error, ME
FANP	0.7681	0.9935
FZD	0.6645	0.9654
GRS	0.6301	0.9861
NUPEC	0.6130	0.9724
PSU/PUR/NRC	0.5988	0.9717
UPISA	0.5183	0.9992

Figure 4-162: Extreme Scenario 3 – LPRM-D

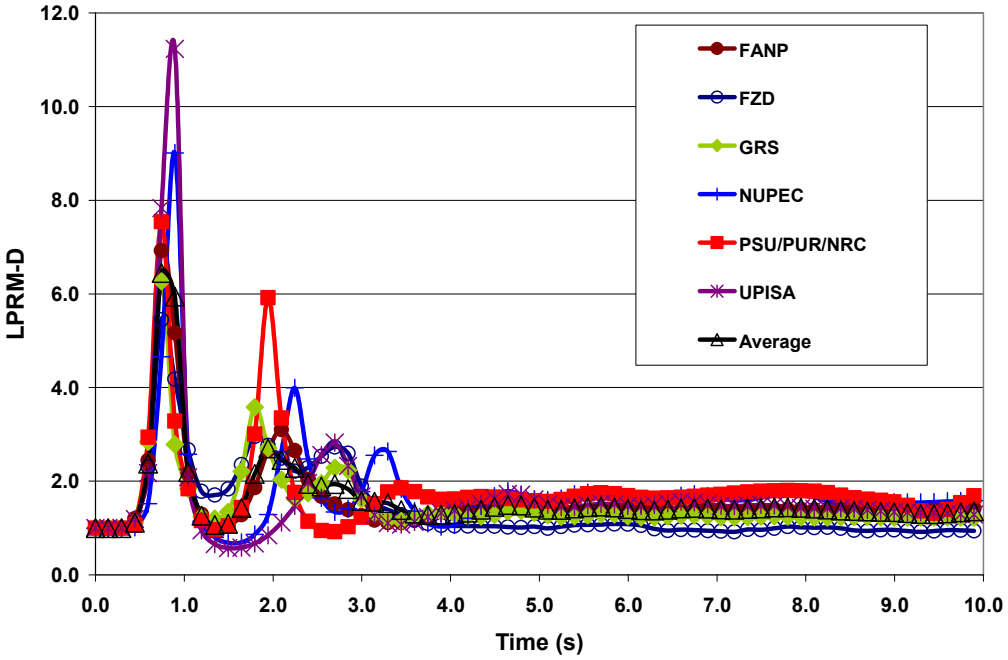

Figure 4-163: Extreme Scenario 3 – LPRM-D (zoom)

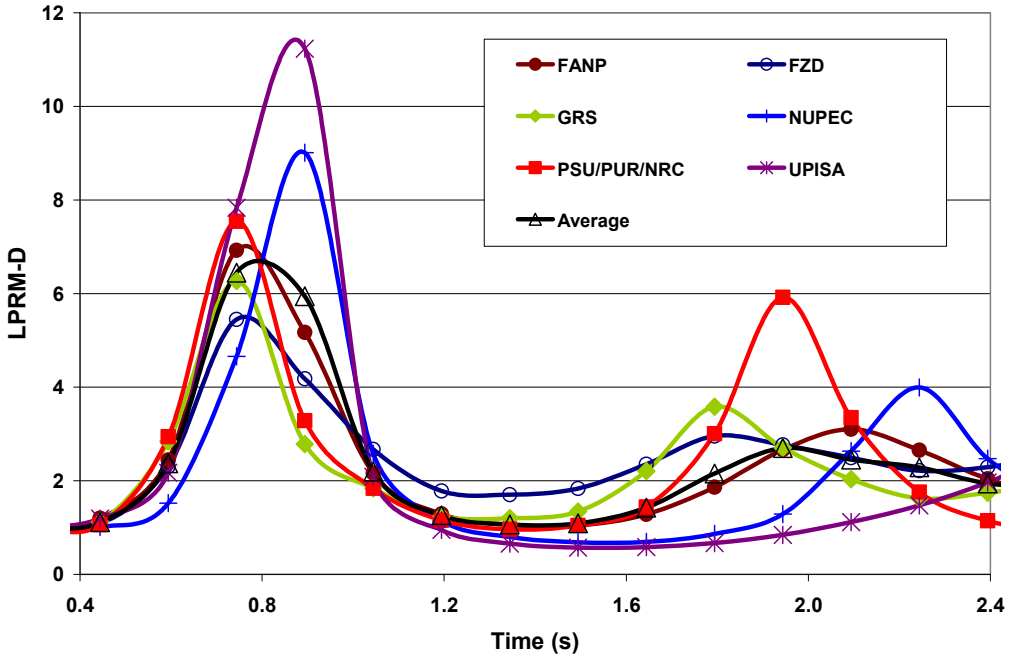

Table 4-63: Extreme Scenario 3 – normalised LPRM-D power, figure of merit

Participant	D'Auria FFT	Mean error, ME
FANP	0.7805	0.9963
FZD	0.6675	0.9709
GRS	0.6280	0.9823
NUPEC	0.6188	0.9818
PSU/PUR/NRC	0.5970	0.9750
UPISA	0.5103	0.9925

4.6 Transient results of Extreme Scenario 4

Turbine trip (TT) with steam bypass system failure, without scram and without safety relief valves opening event is simulated in Exercise 3 Extreme Scenario 4. The following simulation results of the participants are presented in this subsection.

- Time histories:
  - core power;
  - dome pressure;
  - core exit pressure;
  - total reactivity;
  - Doppler reactivity;
  - void reactivity;
  - power of LPRM-A;
  - power of LPRM-B;
  - power of LPRM-C;
  - power of LPRM-D.

The fourth extreme scenario provides both a basis for a better comparison of the physical models of the participants' codes without external perturbations since there is no need to model SRVs and their location, and the possibility to determine the eigen-frequency of the system. Extreme Scenario 4 (without bypass system relief opening, without scram, and without opening of safety relief valves) considers the coincidence of three independent failures, which are extremely unlikely from a safety perspective, while they help with the understanding of the short time dynamics of the reactor system. Hence, Extreme Scenario 4 serves as clear comparison of physical models of the participants' codes. It should be reminded that no comparison with measured data is possible for the extreme cases since they are hypothetical scenarios. Therefore, submitted extreme scenario results are compared with an ''average'' of the results of the benchmark participants.

Please note that the participants performed sensitivity studies on temporal coupling schemes and time step sizes in advance so as to obtain converged solutions. The results in this section should be considered together with Tables 4-64 and 4-65 since all of the models given in the table are important for the transient calculations.

Table 4-64: Number of channels used and power submitted by the participants – Extreme Scenario 4

Participant	No. of channels	Power submitted
CEA	33	Fission
FANP	33	Fission
FZD	764	Total
GRS	33	Fission
NFI	33	Total
NUPEC	33	Fission
PSI	34	Fission
PSU/PURDUE/NRC	33	Total
TEPSYS	33	Total
UPISA	33	Total
UPV (NOKIN)	33	Total
WESTINGHOUSE	764	Total

Table 4-65: Models used in Extreme Scenario 4

Participant	XENON	ADF	BYPASS	DECAY
CEA	No	No	Yes	Yes
FANP	Yes	Yes	Yes	Yes
FZD	Yes	Yes	Yes	Yes
GRS	Yes	No	Yes	Yes
NFI	Yes	No	Yes	Yes
NUPEC	Yes	Yes	No	Yes
PSI	Yes	Yes	Yes	No
PSU/PURDUE/NRC	Yes	Yes	Yes	Yes
TEPSYS	Yes	Yes	Yes	Yes
UPISA	No	Yes	Yes	Yes
UPV	Yes	Yes	Yes	Yes
WESTINGHOUSE	No	Yes	Yes	Yes

The plots and tables in this section provide a comparison of the participants' results for the parameters that have the greatest effect on the Exercise 3 Extreme Scenario 4 analysis. For this reason participants were requested to submit core (averaged and local) and system time histories. These histories are: core averaged (core power, total reactivity, Doppler reactivity and void reactivity), core local (powers of LPRM A, B, C and D) and system (dome pressure and core exit pressure). Similar to the Exercise 3 best-estimate scenario, in order to minimise the impact of the deviations in code predictions at the initial steady-state conditions (which were analysed in Section 4.1) and to focus on the deviations in transient calculations, the comparisons of the predictions of time evolutions of the above parameters are performed not on the absolute values of the parameters but on the delta changes of the parameters as compared to the values at the initial steady state.

The mean time histories are provided in this section as well as in Appendix C. The figures of merit are presented in the tables of this section. Additionally, the participant deviations and figures of merit are presented in Appendix D, and are listed in the same order as the reference solutions. Appendices C and D are provided upon request on CD-ROM.

In each case the figures (Figures 4-164 through 4-187) graphically illustrate the agreement or disagreement of participants' predictions. Statistical evaluation is employed to generate a mean solution, which is also shown in the plots.

Participants' sequences of events in Extreme Scenario 4 are given in Table 4-66.

Core power time evolutions are presented in two groups (fission or total) depending on the submitted core power type. Comparisons of the predictions of fission power evolution and the total power evolution calculated by each code throughout the transient (up to 10 seconds) are shown in Figures 4-164 and 4-166 while Figures 4-165 and 4-167 zoom on the first few seconds of the transient. Table 4-67 provides figure of merit (FOM) for two different methods, D'Auria FFT and Mean Error.

When analysing the power history results it should be taken into account that Extreme Scenario 4 is a turbine trip with no scram, no bypass system and no activation of SRV. It provides both a basis for better comparison of the physical models of the participants' codes without external perturbations and a possibility to determine the eigen-frequency of the system. In Exercise 3 the calculations of Extreme Scenarios 2, 3 and 4 indicated that the core power shows in-phase oscillations. While in Scenarios 2 and 3 the dynamics of physical interactions between power and feedback mechanisms is interrupted by opening of the bypass valve and/or SRV, in Scenario 4 the power oscillatory behaviour continues until the end of the calculation. This power response in terms of timing and magnitude of power peaks during the transient as predicted by different codes is a function of the total reactivity time evolution. In Figure 4-164 (the fission power group), the NUPEC result differs from the cluster around the mean solution. In the total power group (Figure 4-166), all of the codes' predictions (except UPV and UPISA for the first peak as well as PSU/PUR/NRC for the subsequent peaks) form a cluster around the mean solution. In general, the power history results are in a good agreement.

System parameter (dome pressure and core exit pressure) time evolutions are presented in two groups (Group 1 and Group 2) in order to visualise them clearly. Comparisons of the predictions of these parameters calculated by each code throughout the transient (up to 10 seconds) are shown in

Figures 4-168 through 4-171 while Tables 4-68 and 4-69 provide figure of merit (FOM) for two different methods, D'Auria FFT and Mean Error.

Figures 4-172 through 4-179 show comparisons of the predictions of the total, Doppler and void reactivity throughout the transient (up to 10 seconds) and zoom of the beginning of transient. Larger deviations from mean solutions are observed after the first power peak for some participants for the total reactivity (FZD, GRS, PSU/PUR/NRC and UPISA), moderator density (void) reactivity (UPISA and PSU/PUR/NRC) and Doppler feedback reactivity (UPISA and NUPEC) time histories.

Core local parameter time evolutions such as LPRM A, B, C and D power time histories are presented through three types of comparisons. Comparisons of the predictions of local parameter time evolutions calculated by each code throughout the transient (up to 10 seconds) are shown in Figures 4-180, 4-182, 4-184 and 4-186. Figures 4-181, 4-183, 4-185 and 4-187 zoom on the first few seconds of the transient. Tables 4-73 through 4.76 provide figure of merit (FOM) for two different methods, D'Auria FFT and Mean Error. It is important to note that for the four LPRM power time histories the average (mean) of participants' predictions is used as a reference solution.

Table 4-66: Sequence of events in Extreme Scenario 4

Participant	Event* (msec)		
	TSVC	DPIR	CEPIR
CEA	0.096	0.390	0.384
FANP	0.096	0.396	0.390
FZD	0.096	0.382	0.402
GRS	0.096	0.372	0.378
NFI	0.096	0.414	0.408
NUPEC	0.096	0.438	0.456
PSI	0.096	0.438	0.444
PSU/PURDUE/NRC	0.096	0.408	0.402
TEPSYS	0.096	0.366	0.360
UPISA	0.096	0.348	0.324
UPV	0.000	0.414	0.408
WESTINGHOUSE	0.087	0.396	0.444

* Description of the events: TSVC – turbine stop valve closed, DPIR – vessel dome pressure initial response (0.78% increased over initial value), CEPIR – core exit pressure initial response (0.27% increased over initial value).

Figure 4-164: Extreme Scenario 4 – transient power (fission)

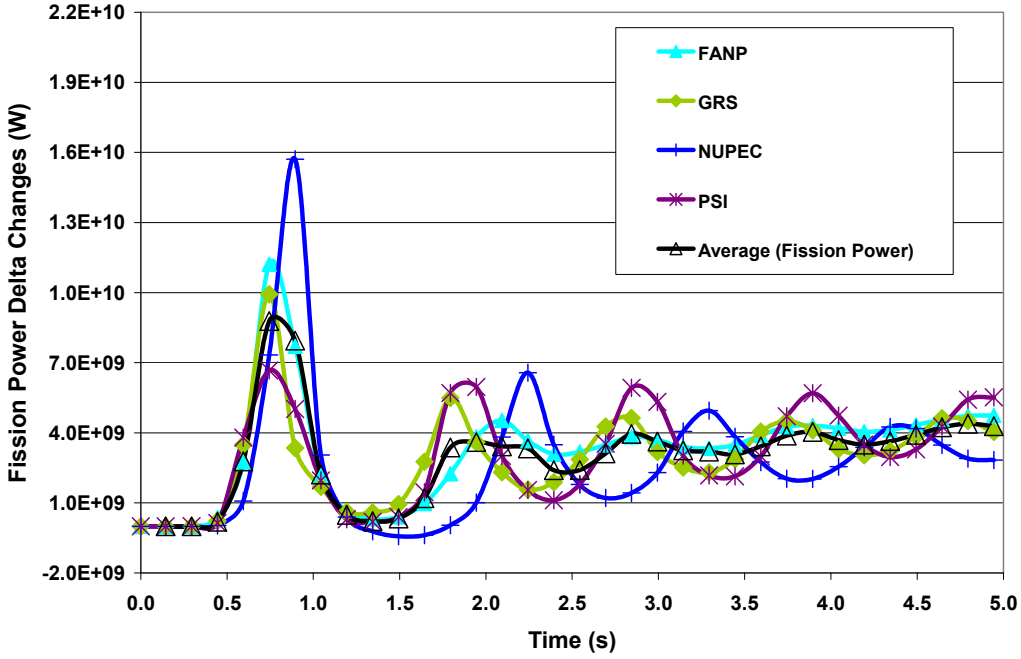

Figure 4-165: Extreme Scenario 4 – transient power (fission – zoom)

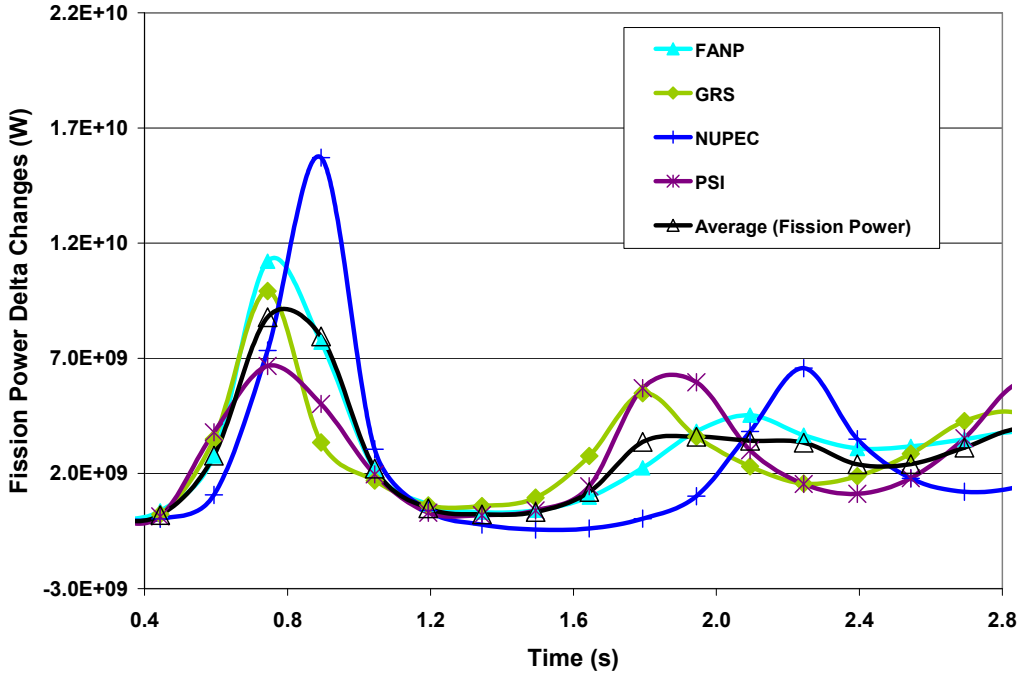

Figure 4-166: Extreme Scenario 4 – transient power (total)

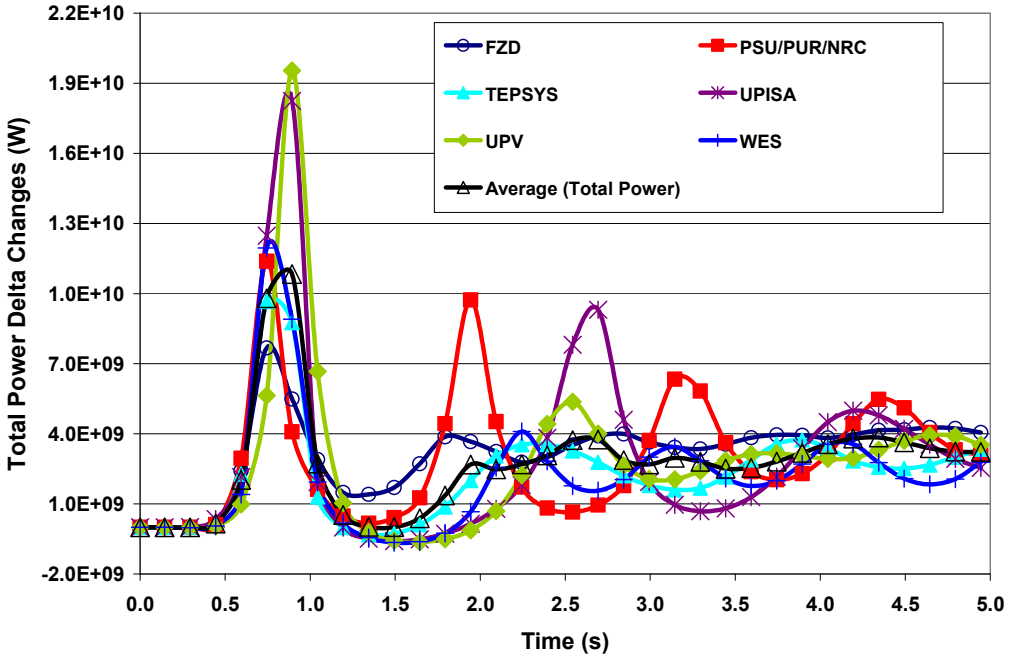

Figure 4-167: Extreme Scenario 4 – transient power (total – zoom)

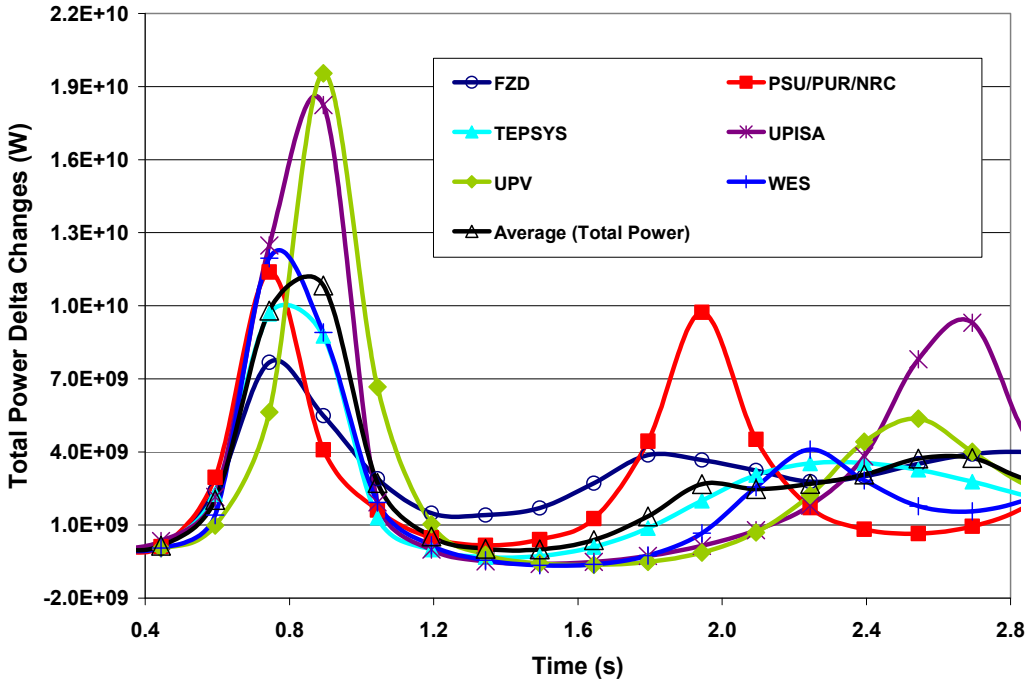

Table 4-67: Extreme Scenario 4 – transient power, figure of merit

Fission power submitted			Total power submitted		
Participant	**D'Auria FFT**	**Mean error, ME**	**Participant**	**D'Auria FFT**	**Mean error, ME**
FANP	0.7275	0.9687	FZD	0.6406	0.9683
GRS	0.6683	0.9934	PSU/PUR/NRC	0.5677	0.9834
NUPEC	0.5783	0.9657	TEPSYS	0.7667	0.9726
PSI	0.6582	0.9901	UPISA	0.5460	0.9829
			UPV	0.5834	0.9994
			WES	0.6685	0.9621

Figure 4-168: Extreme Scenario 4 – transient dome pressure (Group 1)

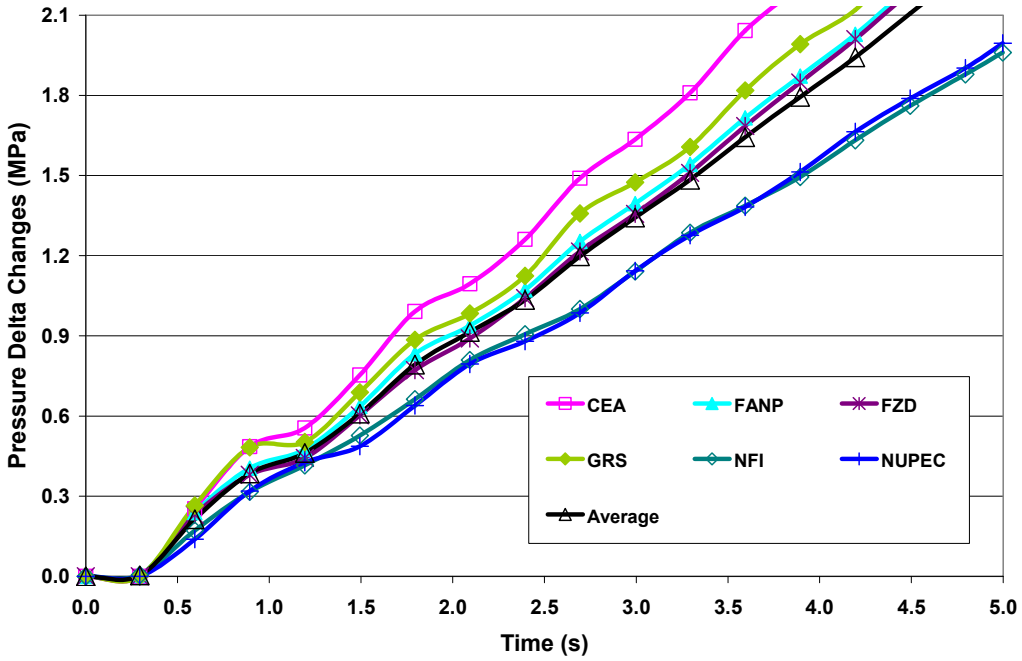

Figure 4-169: Extreme Scenario 4 – transient dome pressure (Group 2)

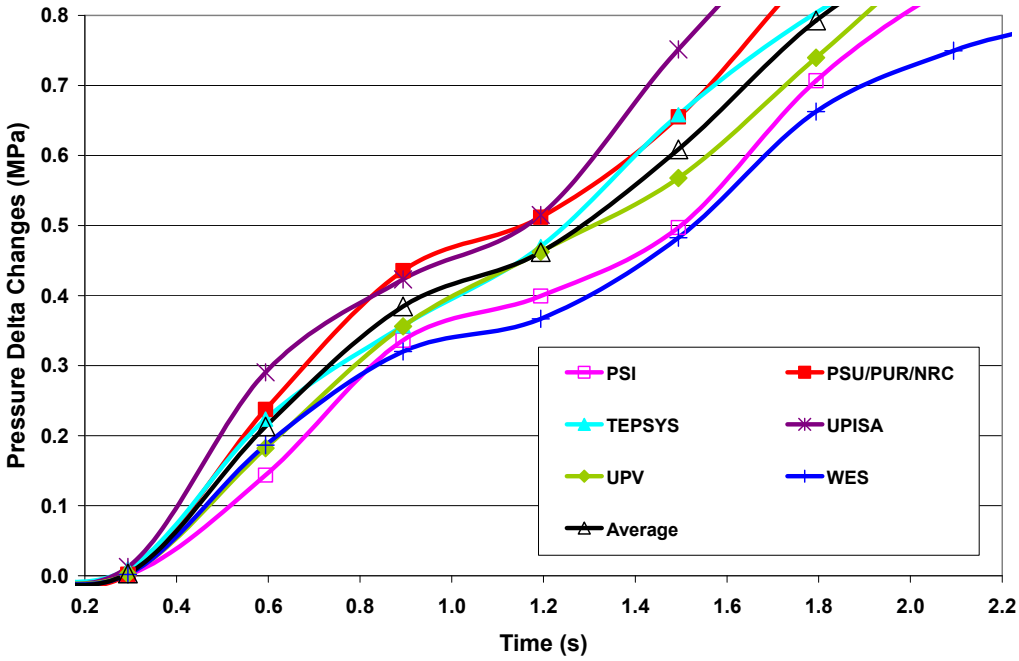

Table 4-68: Extreme Scenario 4 – transient dome pressure, figure of merit

Participant	D'Auria FFT	Mean error, ME
CEA	0.7924	0.9026
FANP	0.9139	0.9795
FZD	0.9235	0.9909
GRS	0.8661	0.9527
NFI	0.8315	0.9321
NUPEC	0.8351	0.9311
PSI	0.9053	0.9840
PSU/PUR/NRC	0.8721	0.9555
TEPSYS	0.9491	0.9952
UPISA	0.8699	0.9512
UPV	0.8949	0.9719
WES	0.7999	0.9102

Figure 4-170: Extreme Scenario 4 – transient core exit pressure (Group 1)

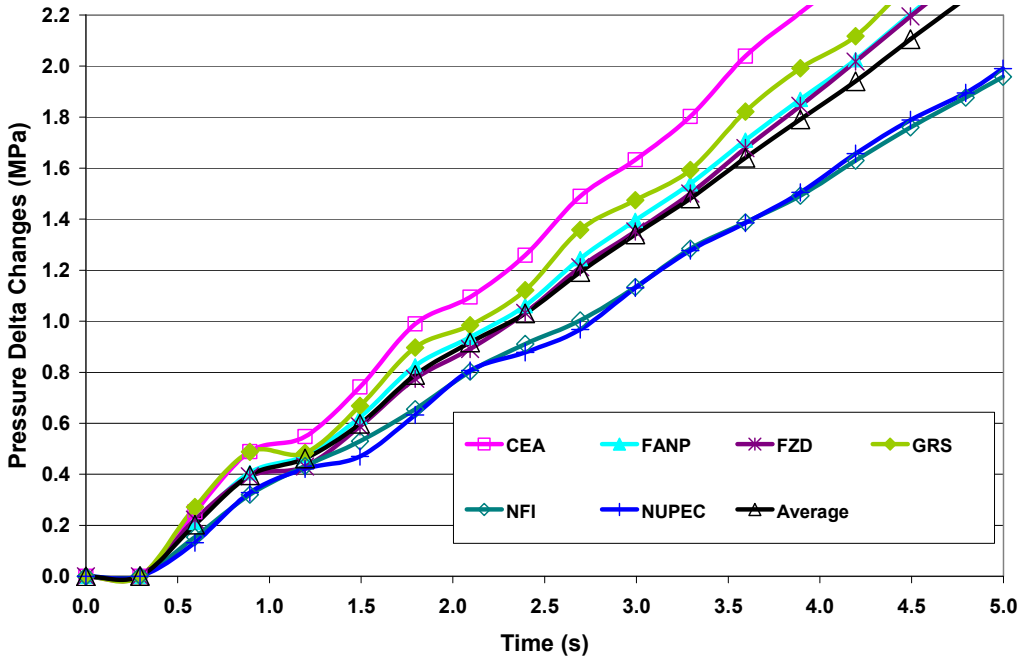

Figure 4-171: Extreme Scenario 4 – transient core exit pressure (Group 2)

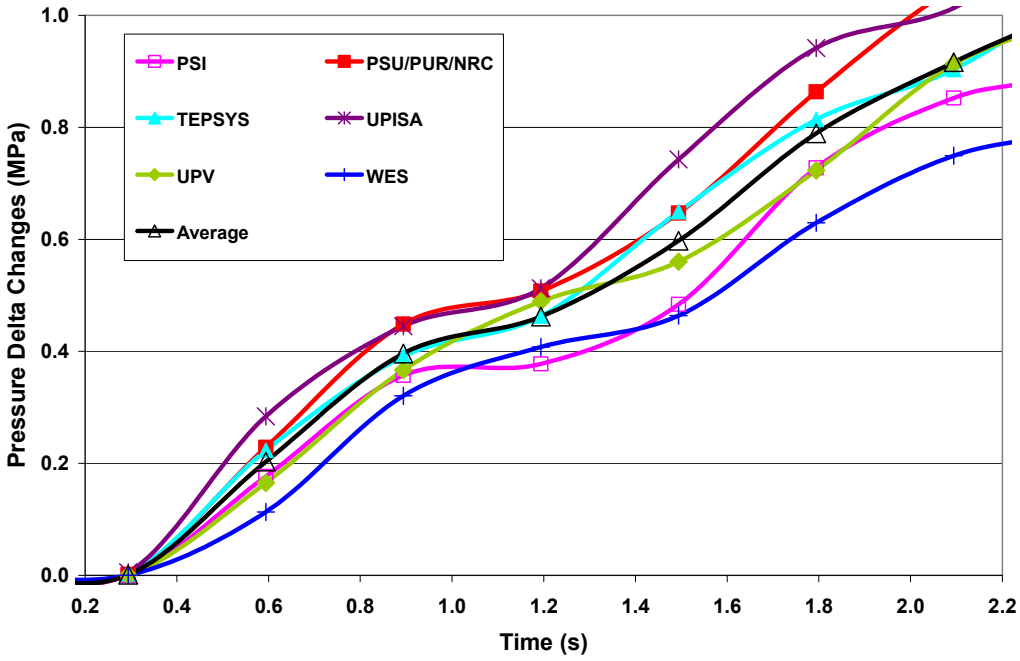

Table 4-69: Extreme Scenario 4 – transient core exit pressure, figure of merit

Participant	D'Auria FFT	Mean error, ME
CEA	0.7928	0.9025
FANP	0.9147	0.9807
FZD	0.9141	0.9904
GRS	0.8661	0.9517
NFI	0.8313	0.9325
NUPEC	0.8351	0.9304
PSI	0.9047	0.9854
PSU/PUR/NRC	0.8717	0.9551
TEPSYS	0.9463	0.9940
UPISA	0.8686	0.9505
UPV	0.8936	0.9730
WES	0.7950	0.9062

Figure 4-172: Extreme Scenario 4 – total reactivity (Group 1)

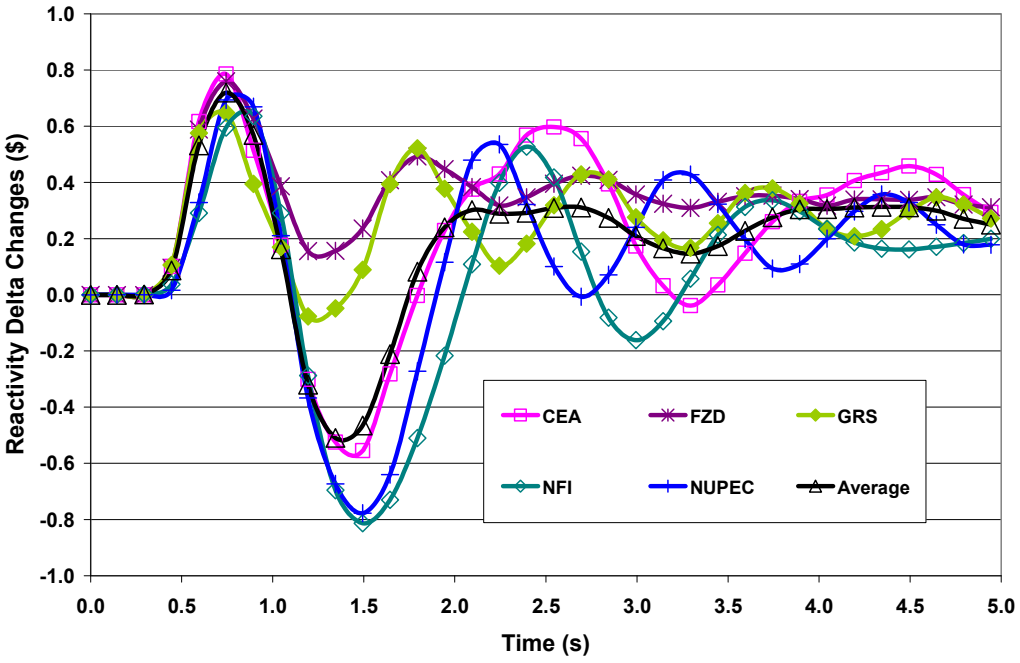

Figure 4-173: Extreme Scenario 4 – total reactivity (Group 1 – zoom)

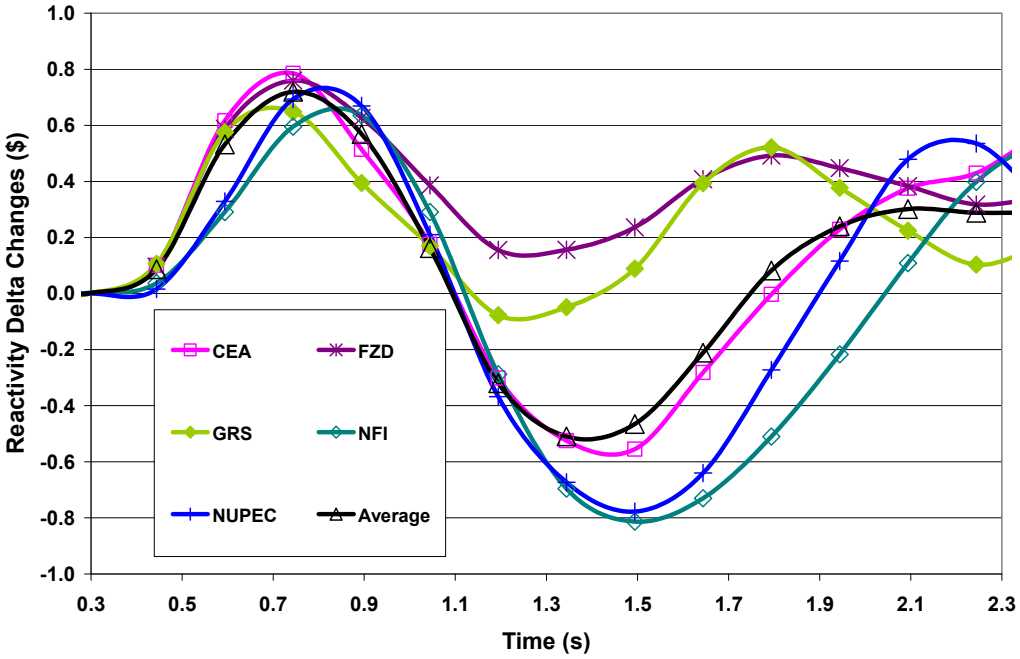

Figure 4-174: Extreme Scenario 4 – total reactivity (Group 2)

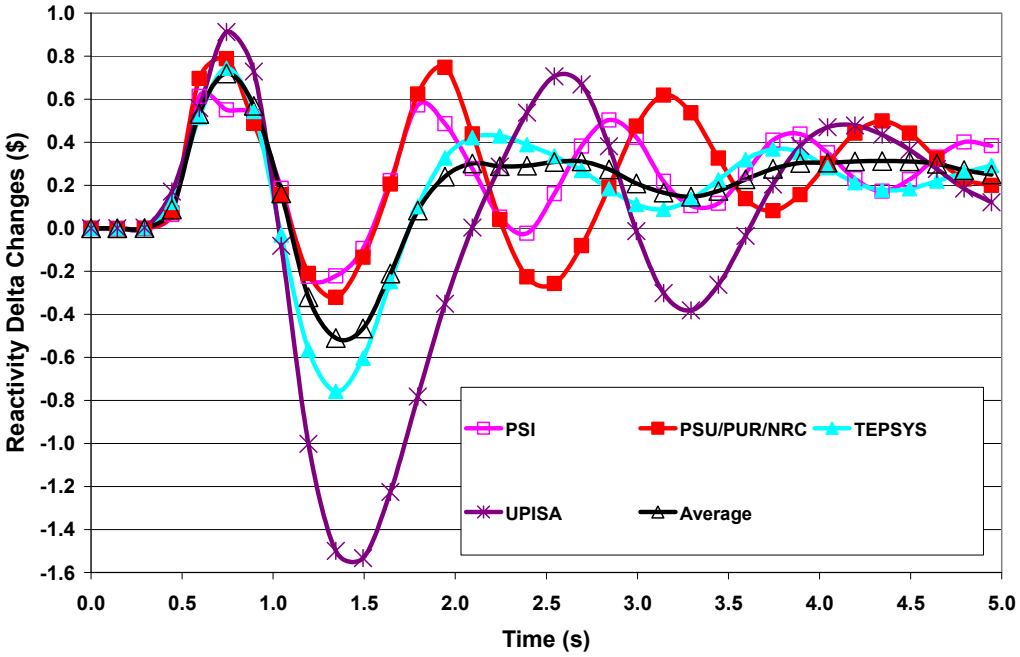

Figure 4-175: Extreme Scenario 4 – total reactivity (Group 2 – zoom)

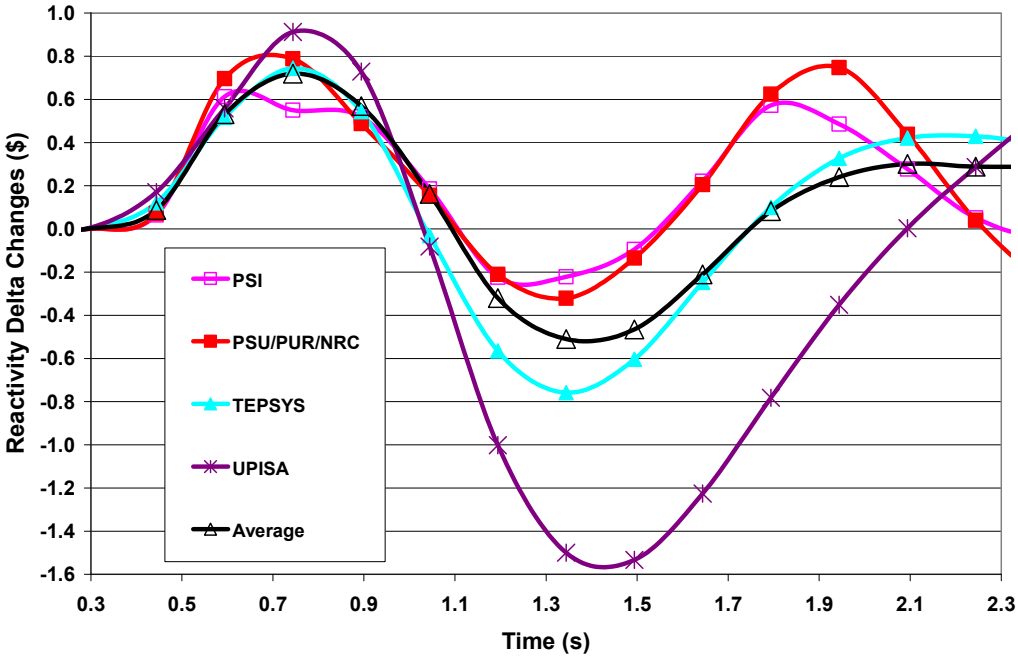

Table 4-70: Extreme Scenario 4 – total reactivity, figure of merit

Participant	D'Auria FFT	Mean error, ME
CEA	0.6757	0.9739
FZD	0.5600	0.8910
GRS	0.5915	0.9430
NFI	0.5764	0.9151
NUPEC	0.6192	0.9577
PSI	0.6007	0.9574
PSU/PUR/NRC	0.5541	0.9591
TEPSYS	0.7314	0.9807
UPISA	0.4527	0.8771

Figure 4-176: Extreme Scenario 4 – Doppler reactivity

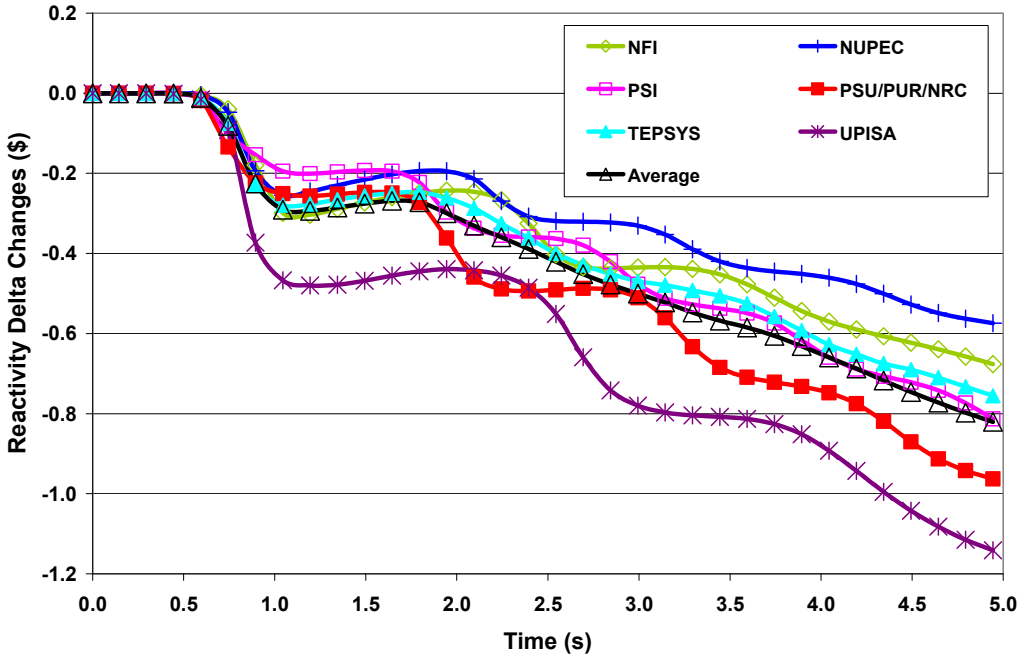

Figure 4-177: Extreme Scenario 4 – Doppler reactivity (zoom)

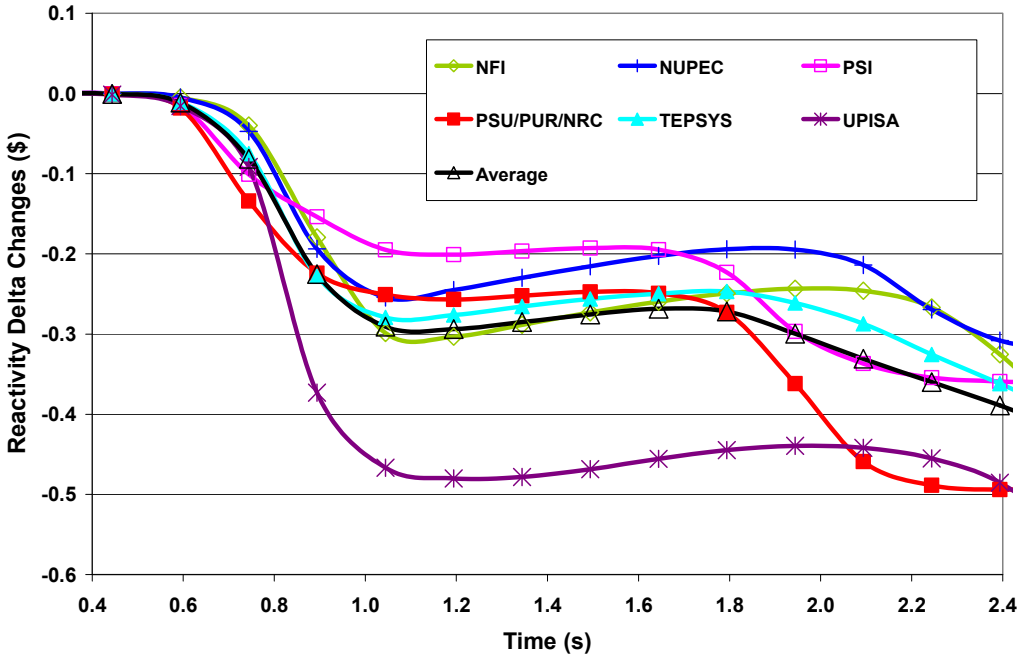

Table 4-71: Extreme Scenario 4 – Doppler reactivity, figure of merit

Participant	D'Auria FFT	Mean error, ME
NFI	0.8206	0.9335
NUPEC	0.7567	0.8777
PSI	0.8201	0.9647
PSU/PUR/NRC	0.8028	0.9373
TEPSYS	0.8619	0.9643
UPISA	0.6858	0.8216

Figure 4-178: Extreme Scenario 4 – void reactivity

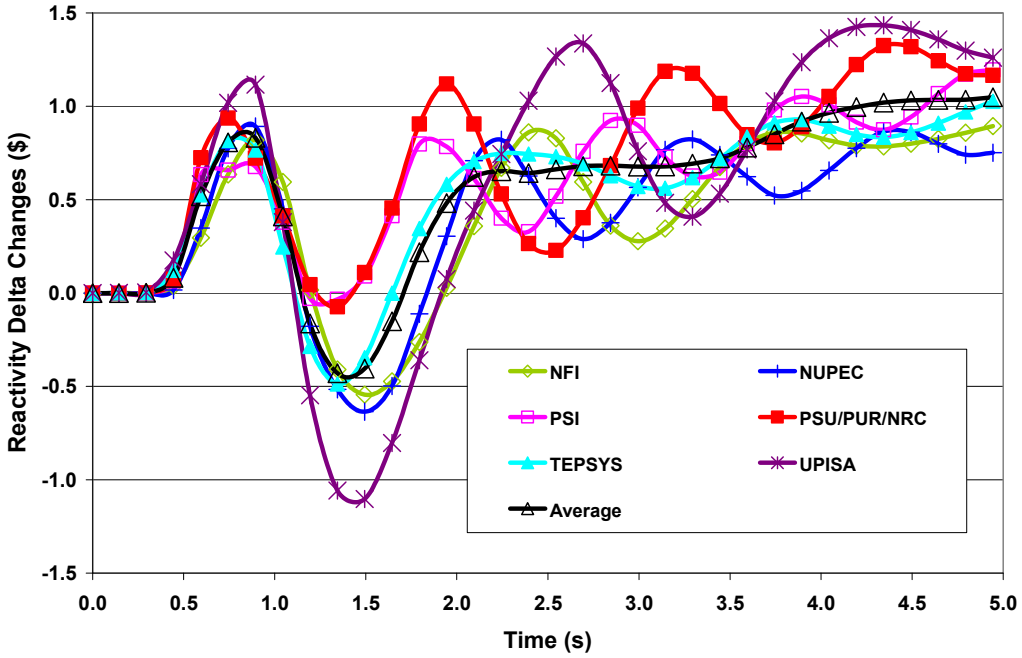

Figure 4-179: Extreme Scenario 4 – void reactivity (zoom)

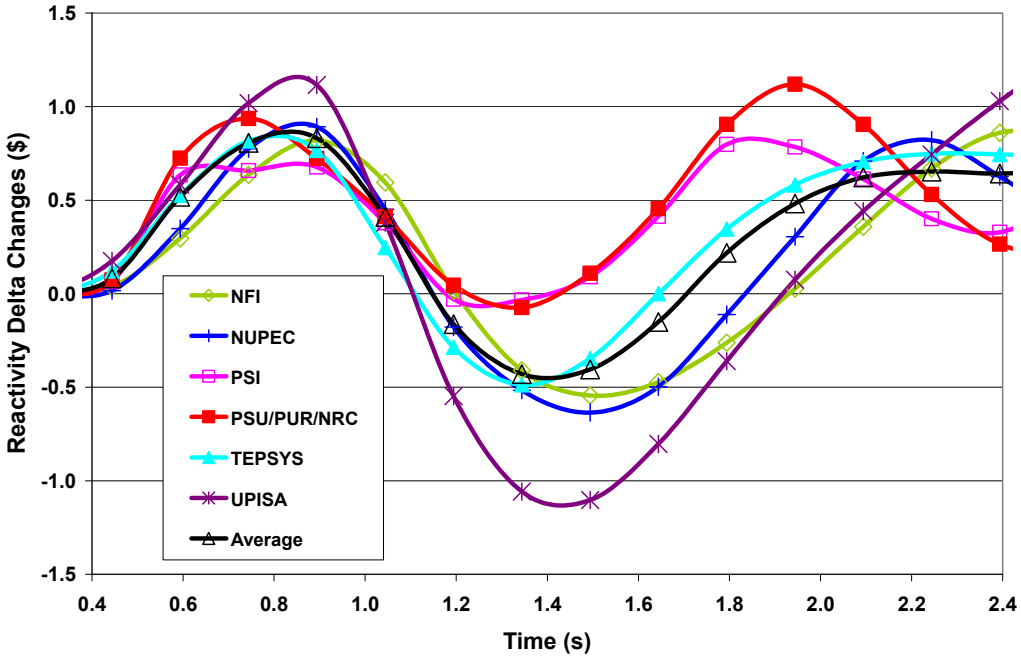

Table 4-72: Extreme Scenario 4 – void reactivity, figure of merit

Participant	D'Auria FFT	Mean error, ME
NFI	0.7287	0.9247
NUPEC	0.7330	0.9185
PSI	0.6911	0.9567
PSU/PUR/NRC	0.6625	0.9053
TEPSYS	0.6919	0.9891
UPISA	0.6635	0.9697

Figure 4-180: Extreme Scenario 4 – LPRM-A

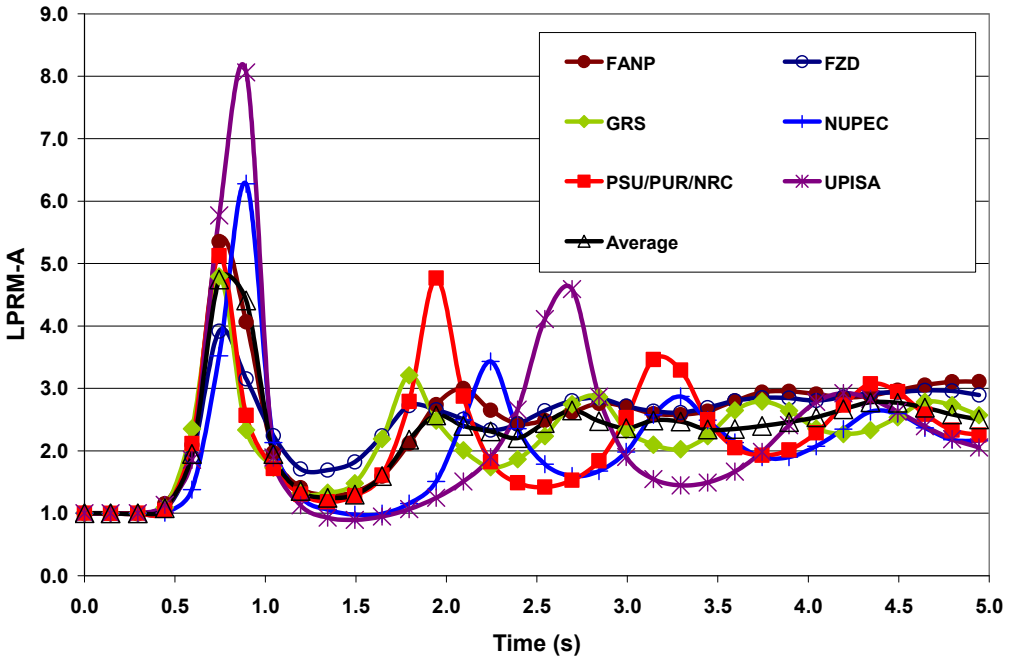

Figure 4-181: Extreme Scenario 4 – LPRM-A (zoom)

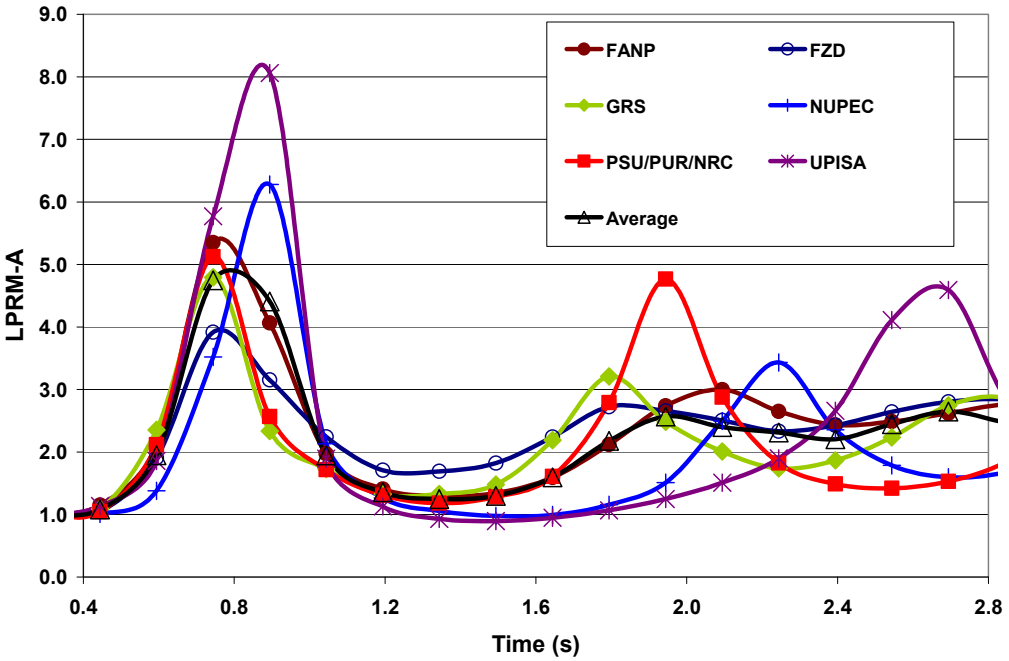

Table 4-73: Extreme Scenario 4 – normalised LPRM-A power, figure of merit

Participant	D'Auria FFT	Mean error, ME
FANP	0.7931	0.9546
FZD	0.7340	0.9612
GRS	0.6835	0.9844
NUPEC	0.6837	0.9508
PSU/PUR/NRC	0.6685	0.9866
UPISA	0.5742	0.9933

Figure 4-182: Extreme Scenario 4 – LPRM-B

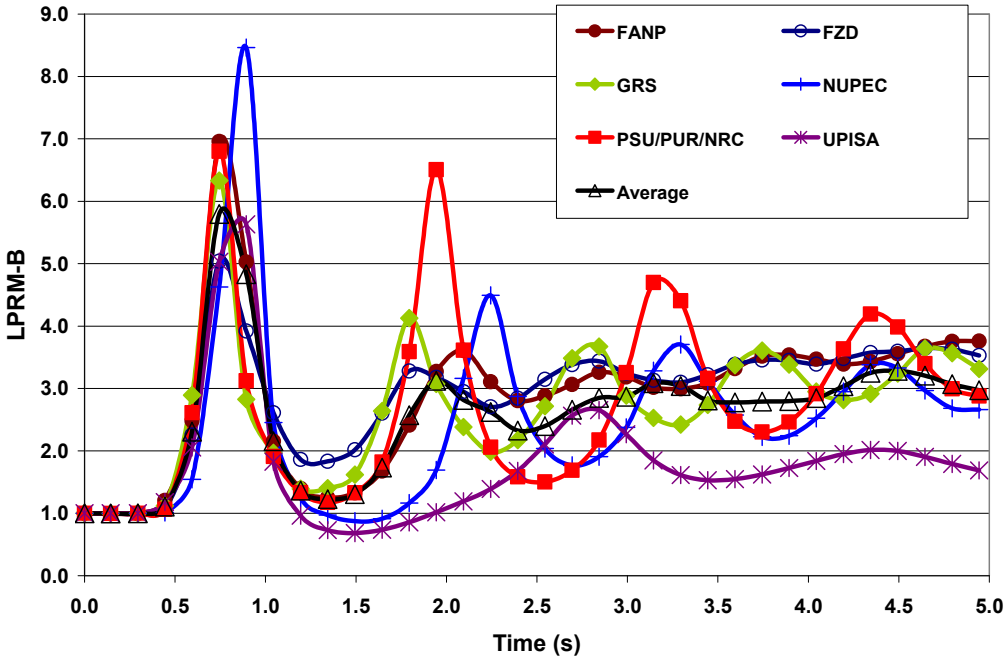

Figure 4-183: Extreme Scenario 4 – LPRM-B (zoom)

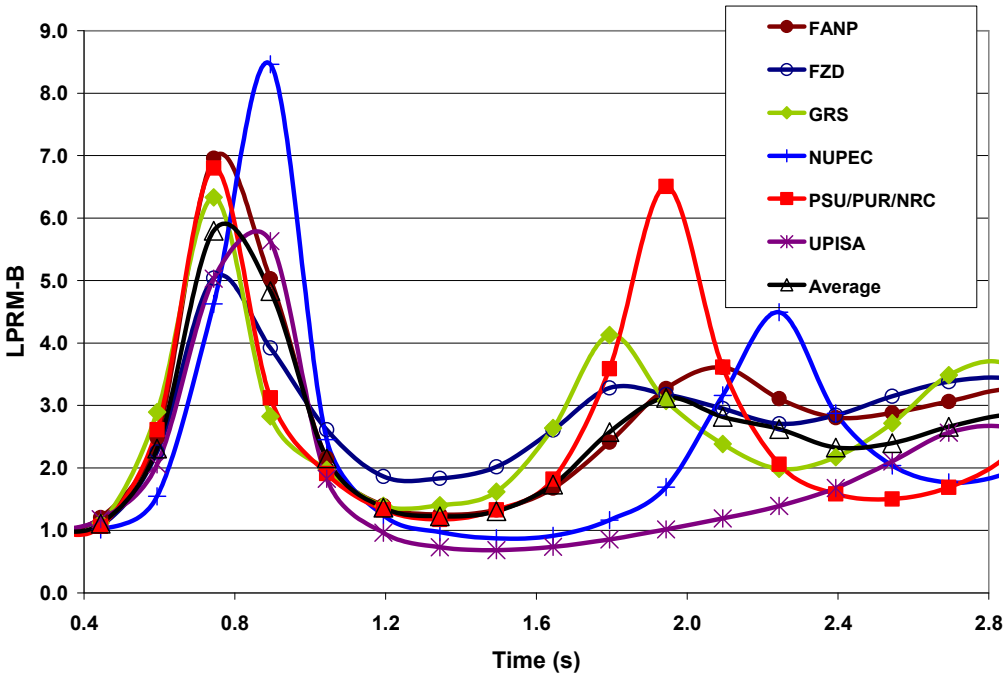

Table 4-74: Extreme Scenario 4 – normalised LPRM-B power, figure of merit

Participant	D'Auria FFT	Mean error, ME
FANP	0.7926	0.9931
FZD	0.8101	0.9957
GRS	0.8300	0.9879
NUPEC	0.7101	0.9986
PSU/PUR/NRC	0.8211	0.9920
UPISA	0.7426	0.9911

Figure 4-184: Extreme Scenario 4 – LPRM-C

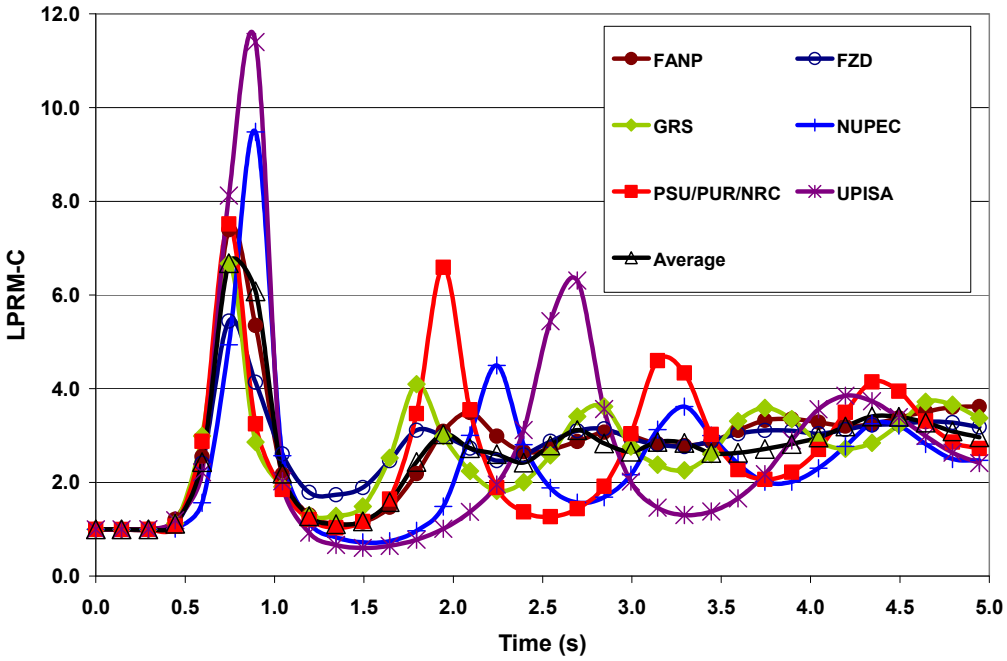

Figure 4-185: Extreme Scenario 4 – LPRM-C (zoom)

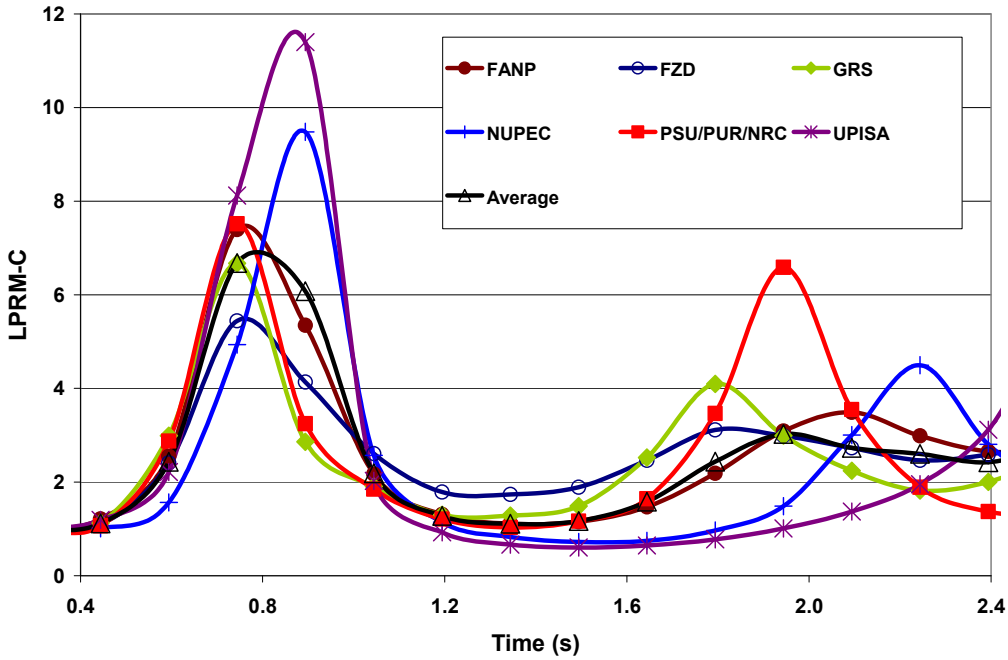

Table 4-75: Extreme Scenario 4 – normalised LPRM-C power, figure of merit

Participant	D'Auria FFT	Mean error, ME
FANP	0.7994	0.9782
FZD	0.7301	0.9882
GRS	0.6655	0.9991
NUPEC	0.6502	0.9620
PSU/PUR/NRC	0.6350	0.9979
UPISA	0.5445	0.9978

Figure 4-186: Extreme Scenario 4 – LPRM-D

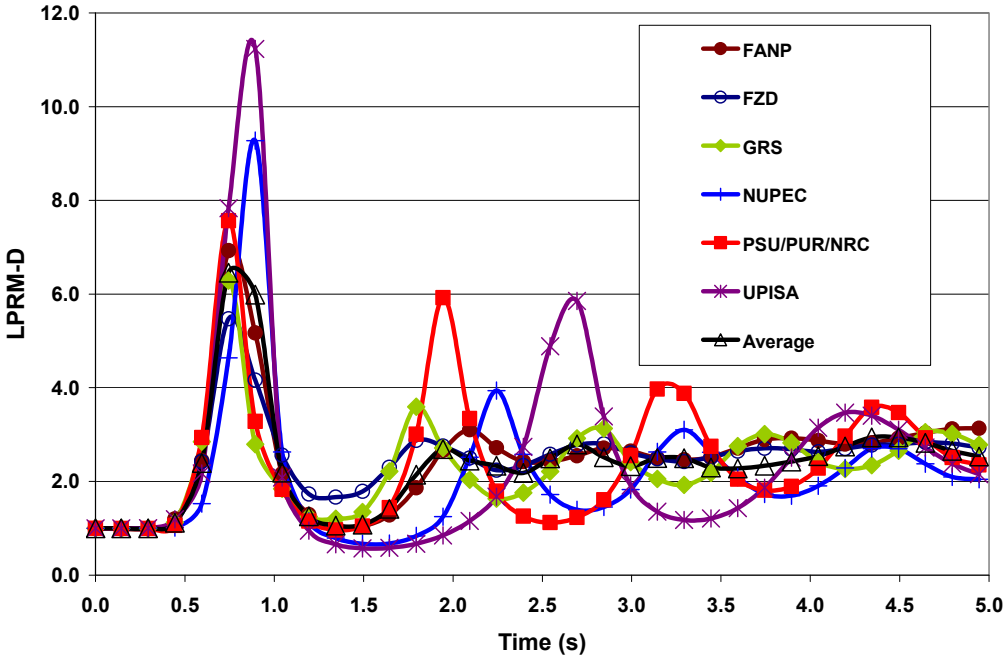

Figure 4-187: Extreme Scenario 4 – LPRM-D (zoom)

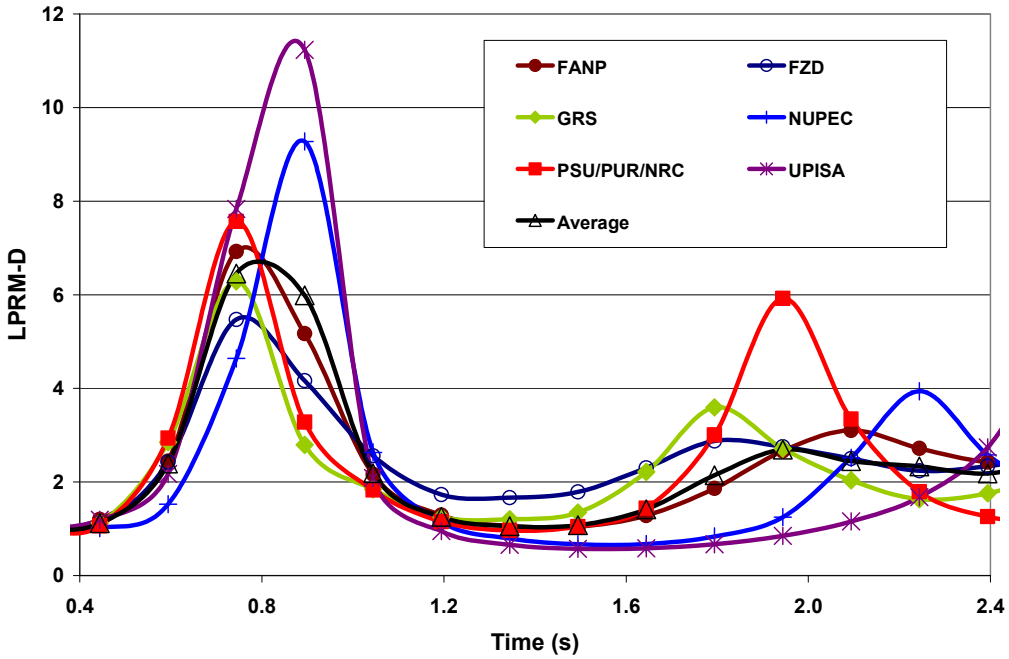

Table 4-76: Extreme Scenario 4 – normalised LPRM-D power, figure of merit

Participant	D'Auria FFT	Mean error, ME
FANP	0.7989	0.9810
FZD	0.7236	0.9855
GRS	0.6545	0.9905
NUPEC	0.6449	0.9606
PSU/PUR/NRC	0.6266	0.9956
UPISA	0.5315	0.9879

Chapter 5: Conclusions

The developed multi-level methodology is employed to perform a validation of coupled codes for BWR transient analysis. For this purpose, the application of three exercises was performed in the BWR TT benchmark. These exercises include the evaluation of different steady states and simulation of different transient scenarios. In this volume, Exercise 3 of the OECD/NRC BWR TT benchmark was discussed in detail in order to meet the objectives of the validation of best-estimate coupled codes.

The third exercise consists of performing a coupled 3-D kinetics/T-H calculation for the core and 1-D thermal-hydraulics modelling for the balance of the plant. There are five transient scenarios – the best-estimate scenario (the real test with available measured data) and four extreme versions. The extreme scenarios were introduced to provide the opportunity to better test the coupling and feedback modelling since they represent challenges for modelling the existing strong interactions between neutronics and thermal-hydraulics:

- Turbine trip without bypass system relief opening, which increases the peak pressure and thus the power peak, and provides enough pressurisation for safety/relief valve opening.
- Turbine trip without scram, which produces secondary power peaks that are of particular relevance for testing the coupled code predictions.
- Combined extreme scenario – turbine trip with bypass system relief failure and without reactor scram. This is a very challenging case for code-to-code comparisons.Turbine trip with no scram, no bypass system and no activation of safety relief valves (SRV). This extreme scenario provides both a basis for better comparison of the physical models of the participants' codes without external perturbations since there is no need to model SRV and their location, and the possibility to determine the eigen-frequency of the system.

The participants are provided with three-dimensional two-group macroscopic cross-section libraries. The expected ranges of the initial steady-state, best-estimate and extreme transient scenarios are covered by the selection of adequate ranges for the independent instantaneous variables (moderator density and fuel temperature) of cross-section modelling.

Exercise 3 of the OECD/NRC BWR TT benchmark has been well accepted internationally, with 13 participants representing 8 countries. CEA submitted two sets of results using coarse core T-H nodalisation with 33 channels and fine core T-H nodalisation with 764 core channels – one T-H channel per neutronics assembly. UPV submitted two sets of results with TRAC-BF1 coupled with two different neutronics codes – MODKIN and NOKIN-3D. The results submitted by the participants are used to make code-to-data and code-to-code comparisons and a subsequent statistical analysis. The results encompass several types of data for both thermal-hydraulic and neutronics parameters at the initial steady-state conditions and throughout the TT transient, including integral parameters, 1-D axial distributions, 2-D radial distributions and time histories.

Detailed assessments of the differences between the calculated results submitted by the participants for this exercise were presented in Chapter 4 of this volume. Overall, the participants' results for integral parameters, core-averaged axial distributions and core-averaged time histories are in good agreement, considering some of the shortcomings in participants' current models, uncertainties of some system parameters, and difficulties in interpreting some of the measured responses.

An important modelling issue for correct prediction of radial power distribution of initial steady-state and transient snapshots was the number of thermal-hydraulic channels and spatial mapping schemes with the neutronics core model. The basic 33-channel mapping that has mostly been used for the turbine trip benchmark may be adequate to provide global core behaviour during

the TT transient since it is predominantly a 1-D event. However, detailed information about the local power distribution during the transient would require a larger number of channels, which was demonstrated by the two sets of CEA results.

The most challenging part of the BWR initial steady-state analysis is the prediction of the void fraction distribution. The comparative analysis performed within the framework of this benchmark indicated that the most of differences between the participants' codes in the void modelling are in terms of sub-cooled boiling and vapour slip. As a result, investigation of more accurate predictions of void fraction by core thermal-hydraulics models was identified as area of future research.

The accurate prediction of void feedback during the TT transient depends on the modelling of the pressure wave propagation in the vessel. Although the OECD/NRC BWR TT benchmark does not cover all the safety analyses needed, it did provide an indication of successful modelling of pressure wave propagation by the participants' codes via comparisons of participants' results and measured data of dome pressure time history. The participants' results compared very satisfactorily with measured data for the parameters of dome pressure and power time histories for the best-estimate scenario. These results increased the trustworthiness of the current coupled code capabilities.

The coupled code simulations of the specially designed TT transient extreme scenarios demonstrated that the bypass system relief and SRV are sufficient to stabilise the power of the reactors. It should also be noted that the observed power peaks in TT transient simulations are not challenging for the fuel integrity. In this regard the important parameter for safety evaluation is the enthalpy or energy released to the fuel. Future work should include analysis of the energy released to the fuel, which can be carried out separately.

During the comparative analysis of the participants' results and through the performance of sensitivity studies the following sources (effects and parameters) of modelling uncertainties were identified:

- Thermal-hydraulic modelling issues – turbine bypass line modelling; nodalisation of vessel, steam line and steam separator region; the TSV position and steam mass flow modelling; thermal-hydraulic model – number of equations; void fraction model; steam-separator inertia; jet-pump modelling; SRV modelling.
- Thermal-hydraulic key parameters – feedwater temperature; jet pump parameters; void fraction in the bulk water (carry-under); the core outlet pressure; the active core pressure loss; the core inlet temperature; the core inlet mass flow without bypass flow; sub-cooling; void generation rate; gas gap conductance.
- Time step size – fixed time step of 6 ms vs. using a variable time step algorithm with a maximum time step size imposed.
- Cross-section modelling – cross-section history dependencies modelling, which is important for the initial steady state; instantaneous cross-section density dependence (void coefficient) – important for the transient modelling; xenon and bypass density correction in cross-section tables; ADF modelling; refinement of cross-section library.
- Neutronics and coupling modelling – different neutronics methods; spatial coupling schemes between core neutronics and thermal-hydraulics in terms of the number of the T-H channels; direct moderator heating; temporal coupling schemes and time step sizes; scram initialisation.

The PB TT2 test has previously been analysed elsewhere with different codes and models (Hornyik, 1979; Moberg, 1981). These analyses involved not only point kinetics and 1-D kinetics system simulations but also 3-D kinetics/core thermal-hydraulics boundary conditions calculations. Each of the organisations performing these separate analyses generated their own point kinetics parameters, 1-D cross-sections and 3-D cross-section libraries. In this way it was not possible to directly compare the results of different organisations, especially for the parameters where the measured data is not available. In most of the 3-D core boundary conditions analyses the cross-section functionalisation for instantaneous dependencies was done either by using polynomial fitting procedure or the procedure using multi-level tables with base and partial cross-sections. In both cases the instantaneous cross-term effects (which are important for the transient analysis) are not modelled completely, leading to a different degree of underestimation of the void feedback (void coefficient) depending on the procedure used.

The OECD/NRC BWR TT benchmark is designed to provide a validation basis for the new generation best-estimate codes – coupled 3-D kinetics system thermal-hydraulic codes. Based on the previous experience, three benchmark exercises were defined in order to develop and verify, in a consistent manner, the thermal-hydraulic system model, the coupled core model and the coupled core/system modelling. The three defined exercises also helped to identify the key parameters for modelling a turbine trip transient. This in turn allowed the evaluation of these key parameters, through the performance of sensitivity studies, which allowed the benchmark team to assist the participants in the most efficient way. The participants use the cross-section library generated by the benchmark team which removes the uncertainties introduced with using different cross-section generation and modelling procedures. The defined benchmark cross-section modelling approach is a direct interpolation in multi-dimensional tables with complete representation of the instantaneous cross-section cross-term dependencies. Developing a more in-depth knowledge of the coupled computer code systems is important because 3-D kinetic/thermal-hydraulic codes will play a critical role in the future of nuclear analysis. It is anticipated that the results of this benchmark problem will assist in the understanding of the behaviour of the next generation of coupled computer codes.

This benchmark has also stimulated follow-up developments and benchmark activities such as the OECD/NRC BFBT benchmark (NEA, 2005) and the OECD LWR Uncertainty in Modelling (UAM) benchmark (NEA, 2007). The need for more accurate prediction of void fraction identified in the OECD/NRC BWR TT benchmark led to establishing the BFBT benchmark, and the need for systematic integration of uncertainty and sensitivity analysis with simulations for safety analysis led to establishing the OECD LWR UAM benchmark.

References

Ambrosini, W., R. Bovalini, F. D'Auria (1990), "Evaluation of Accuracy of Thermal-hydraulics Code Calculations", *Energia Nucleare*, Vol. 7, No. 2.

Borkowski, J., N. Wade (1992), *TRAC-BF1/MOD1 – Model Description,* NUREG/CR-4356 EGG-2626 Vol. 1, Idaho National Engineering Laboratory, EG&G Idaho, Inc., August.

Carmichael, L., R. Niemi (1978), *Transient and Stability Tests at Peach Bottom Atomic Power Station Unit 2 at End of Cycle 2*, EPRI NP-564, June.

Hornyik, K., J. Naser (1979), *RETRAN Analysis of the Turbine Trip Tests at Peach Bottom Atomic Power Station Unit 2 at the End of Cycle 2*, EPRI NP-1076-SR Special Report, April.

Ivanov, K., *et al*. (2001), *OECD/NRC BWR TT Benchmark: A Core Boundary Condition Model Approach*, TANSAO 85, 275-277.

Kuntz, R., G. Kasmala, J. Mahaffy (1998), *Automated Code Assessment Program: Technique Selection and Mathematical Prescription*, Letter Report 3, Applied Research Laboratory, The Pennsylvania State University, April.

Larsen, N. (1978), *Core Design and Operating Data for Cycles 1 and 2 of Peach Bottom 2*, EPRI NP-563, June.

Moberg, L. *et al*. (1981), *RAMONA Analysis of the Peach Bottom-2 Turbine Trip Transients*, EPRI NP-1869, June.

Nuclear Energy Agency (NEA) (1999), *Pressurised Water Reactor Main Steam Line Break (MSLB) Benchmark, Volume I: Final Specifications*, NEA/NSC/DOC(99)8, OECD/NEA, Paris, April.

NEA (2001), *Boiling Water Reactor Turbine Trip (TT) Benchmark, Volume I: Final Specifications*, NEA/NSC/DOC(2001)1, OECD/NEA, Paris.

NEA (2004), *BWR TT Benchmark, Volume II: Summary Results of Exercise 1*, NEA/NSC/DOC(2004)21, OECD/NEA, Paris.

NEA (2005), *NUPEC BWR Full-size Fine-mesh Bundle Test (BFBT) Benchmark – Volume I: Specifications*, NEA/NSC/DOC (2005)5, OECD/NEA, Paris.

NEA (2006), *Boiling Water Reactor Turbine Trip (TT) Benchmark, Volume III: Summary Results of Exercise 2,* NEA/NSC/DOC(2006)23, November.

NEA (2007), *Benchmark for Uncertainty Analysis in Modelling (UAM) for Design, Operation and Safety Analysis of LWRs – Phase I Specifications and Support Data for the Neutronics Cases (Phase I)*, NEA/NSC/DOC(2007)23, OECD/NEA, Paris.

Nuclear Science and Engineering (NSE) (2004), "OECD/NRC BWR Turbine Trip Benchmark Special Issue", *Nuclear Science and Engineering*, Vol. 148, No. 2, October.

Olson, A.M. (1988), *Methods for Performing BWR System Transient Analysis*, Topical Report PECo-FMS-0004-A, Philadelphia Electric Company.

SRS1 Software (2003), *Cubic Spline for Excel Workbook*, February, available at *www.srs1software.com*.

Steinke, R., *et al*. (2001), *TRAC-M/FORTRAN 90 (Version 3.0) User's Manual*, NUREG/CR-6722, pp. 2-1, 2-2, May.

Appendix A: Description of the computer codes used for analysis in Exercise 3 of the NEA-NRC BWR TT benchmark

CATHARE/CRONOS2/FLICA4 (CEA, France)

CATHARE

CATHARE is a system thermal-hydraulics code developed by CEA, IRSN, EDF and Framatome for PWR safety analysis, and used for different kind of reactors (BWR, VVER, gas-cooled reactors). The code is modular (component modules) and based on a six-equation two-fluid model. CATHARE provides a set of physical closure laws validated against a large experimental database (current version is V1.5_1).

Reference

Geffraye, G., B. Brun (1999), "Validation of the CATHARE 2 V1.5 Revision 6 Code For Nuclear Safety", *Proceedings of the 4th Symposium on Multiphase Flow and Heat Transfer*, Xi'an China, 22-24 August.

CRONOS2

CRONOS2 is a 3-D neutronics code designed to provide all the computational means needed for diffusion and transport core calculations, including design, fuel management, operation and accidents. It allows steady-state, burn-up and kinetic multi-group calculations of power distribution taking into account the thermal-hydraulic feedback effects (performed either by FLICA4 or by a simplified 1-D model), including sensitivity analysis thanks to the generalised perturbation theory. Either eigenvalue or source calculations can be performed.

Reference

Lautard, J.J., D. Schneider, A.M. Baudron (1999), "Mixed Dual Methods for Neutronic Reactor Core Calculations in the CRONOS System", *Proceedings of M&C*, Madrid, 27-30 September.

FLICA4

FLICA4 is a 3-D thermal-hydraulics code used for many reactor types (PWR, BWR, experimental reactors, gas-cooled reactors...). The two-phase compressible flow is modelled by a set of four equations: mass, momentum, energy conservation for the two-phase mixture and mass conservation for the vapour. The velocity disequilibrium is taken into account by a drift flux correlation. A 1-D thermal module is also used to solve the conduction in solids (fuel). For neutronics, either the coupling with CRONOS2 (3-D solver) or the internal point kinetics model is used.

Reference

Aniel, Sylvie, *et al.* (2005), "FLICA4: Status of Numerical and Physical Models and Overview of Applications", *Proceedings of NURETH11*, Avignon, 2-6 October.

S-RELAP5/RAMONA5-2.1 (FANP, Germany)

For the simulation of a BWR vessel thermal-hydraulic and the related neutronic, the code S-RELAP5 is coupled with RAMONA5.

S-RELAP5 is the standard tool for the investigation of accident scenarios in nuclear power plants, both PWR and BWR. The range of applications covers LBLOCA on the one hand and reactor transients on the other hand. S-RELAP5 includes all features of the RELAP5 code family. It is a highly modular code in a sense that the user defines the granularity of the analysis by defining an appropriate node scheme. The hydraulic part of such a node scheme is a concatenation of hydraulic volumes being connected by junctions. In case of a two-phase state in the hydraulic volume, thermal non-equilibrium is assumed. The two-phase flow between the volumes is non-homogeneous, the corresponding phase velocities are determined by solving momentum equations. This approach requires the definition of a local static pressure, with the pressure gradient being the source of the movement of each phase. Thermal properties as densities or internal energies are locally defined. In S-RELAP5, flow maps and heat transfer models are defined. They allow constitutive relations as inter-phase shear or heat transfer coefficients, depending on them to be applied. A highly sophisticated numerical solution scheme allows hydraulic systems with up to 500 hydraulic volumes to be considered. S-RELAP5 has a fully developed fuel model; the neutronics representation is based on a point kinetics model.

RAMONA5 represents the highest current level of the RAMONA code series, developed by BNL and Scandpower especially for the needs of BWR analysis. RAMONA is a “hard-wired” code. A fixed set of components is used in the code with a fixed arrangement. For example, a component called “Lower Plenum 2” is connected with a core component. “Lower Plenum 2” is always upwardly oriented. The core component has one pre-defined bypass channel and an arbitrary number of channels, typically representing a fuel element. For the core component, the user can define the number of channels and axial noding. Within the standard thermal-hydraulic model, two-phase flow is modelled by a partial thermal non-equilibrium, with the vapour phase always being saturated. Thermal properties are evaluated with respect to a system pressure, being equal in each component. Phase velocities are evaluated by considering an integrated momentum equation of each flow path. A drift-flux model is applied to describe the relative motion of liquid and steam, and approximations are made which allow a formulation for the momentum of each component as a function of the inlet velocities. The thermal-hydraulic models in RAMONA are based on various approximations that nonetheless allow a detailed nodalisation in the core area. Each fuel element can be modelled separately. This fine granularity of spatial hydraulic modelling is a perfect environment for the application of a 3-D kinetic. For many BWR applications, the use of a 3-D kinetic model is mandatory, and it is of course – in conjunction with a suited core hydraulic – the most important argument for using RAMONA.

The coupling of S-RELAP5 and RAMONA5 takes advantage of different code capabilities depending on different objectives. Through coupling, the advanced features of each code are activated. The most relevant model of RAMONA5 is the three-dimensional neutronic modelling, whereas in S-RELAP5 the non-equilibrium non-homogeneous two-fluid model is most suited for simulation of the overall plant behaviour during a reactor transient. The coupling is realised by forcing RAMONA to apply the core boundary conditions (core inlet flow, core inlet enthalpy, steam dome pressure) of S-RELAP5. On the other hand, RAMONA provides the power produced in the core to S-RELAP5. The coupling scheme is drawn in the figure below.

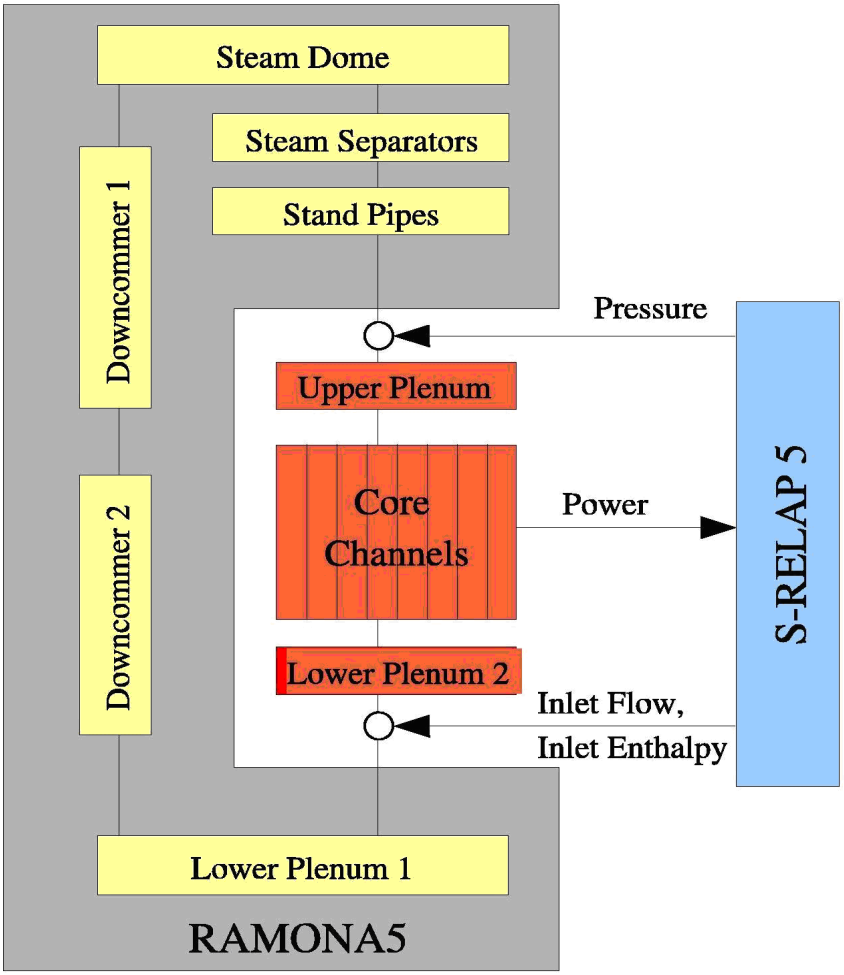
Steam Dome
Steam Separators
Stand Pipes
Downcommer 1
Downcommer 2
Pressure
Upper Plenum
Core
Channels
Power
Lower Plenum 2
Inlet Flow,
Inlet Enthalpy
S-RELAP 5
Lower Plenum 1
RAMONA5

DYN3D/ATHLET (FZD, Germany)

The core model: DYN3D

Capabilities

DYN3D is a three-dimensional core model for dynamic and depletion calculations in light water reactor cores with quadratic or hexagonal fuel assembly geometry. The two-group neutron diffusion equation is solved by nodal methods. A thermal-hydraulic model of the reactor core and a fuel rod model are implemented in DYN3D. The reactor core is modelled by parallel coolant channels which can describe one or more fuel elements. Starting from the critical state (k_{eff} value, critical boron concentration or critical power) the code allows to simulate the neutronic and thermal-hydraulic core response to reactivity changes caused by control rod movements and/or changes of the coolant core inlet conditions. Depletion calculations can be performed to determine the starting point of the transient. Steady-state concentrations of the reactor poisons can be calculated. The transient behaviour of Xe and Sm can be analysed. The decay heat is taken into account based on power history and during the transient. Hot channels can be investigated by using the nodal flux reconstruction in assemblies and the pin powers of the cell calculations. Cross-section libraries generated by different cell codes for different reactor types are linked with DYN3D. Macroscopic cross-section libraries created within the common software platform can easily be linked to DYN3D.

Methods of solution

Neutron kinetics

The neutron kinetic model is based on the solution of the three-dimensional two-group neutron diffusion equations by nodal expansion methods. Different methods are used for quadratic and hexagonal fuel assembly geometry. It is assumed that the macroscopic cross-sections are spatially constant in a node being the part of a fuel assembly. In the case of Cartesian geometry, the three-dimensional diffusion equation of each node is transformed into one-dimensional equations in each direction x, y, z by transversal integrations. The equations are coupled by the transversal leakage term. In each energy group, the one-dimensional equations are solved with the help of flux expansions in polynomials up to second order and exponential functions being the solutions of the homogeneous equation. The fission source in the fast group and the scattering source in the thermal group as well as the leakage terms are approximated by the polynomials. In the case of hexagonal fuel assemblies, the diffusion equation in the node is transformed into a two-dimensional equation in the hexagonal plane and a one-dimensional equation in the axial direction. The two equations are coupled by the transverse leakage terms which are approximated by polynomials up to the second order. Considering the two-dimensional equation in the hexagonal plane, the side-averaged values (HEXNEM1) or the side-averaged and the corner point values (HEXNEM2) of flux and current are used for the approximate solution of the diffusion equation. The method used for the one-dimensional equations of the Cartesian geometry is applied for the axial direction. It is extended to two dimensions in the HEXNEM1 and HEXNEM2 methods. In the steady state, the homogeneous eigenvalue problem or the heterogeneous problem with given source is solved. An inner and outer iteration strategy is applied. The outer iteration (fission source iteration) is accelerated by Chebychev extrapolation.

The steady-state iteration technique is applied for the calculation of the initial critical state, the depletion calculations and the Xe and Sm dynamics. Concerning reactivity transients an implicit difference scheme with exponential transformation is used for the time integration over the neutronic time step. The exponents in each node are calculated from the previous time step or during the iteration process. The precursor equations are analytically solved, assuming the fission rate behaves exponentially over the time step. The heterogeneous equations obtained for each time step are solved by an inner and outer iteration technique similar to the steady state.

Thermal-hydraulics

The parallel channels are coupled hydraulically by the condition of equal pressure drop over all core channels. Additionally, the so-called hot channels can be considered for the investigation of hot spots and uncertainties in power density, coolant temperature or mass flow rate. Thermo-hydraulic boundary conditions for the core like coolant inlet temperature, pressure and coolant mass flow rate

or pressure drop must be given as input for DYN3D. The module FLOCAL comprises a one- or two-phase coolant flow model on the basis of four differential balance equations for mass, energy and momentum of the two-phase mixture and the mass balance for the vapour phase allowing the description of thermodynamic non-equilibrium between the phases, a heat transfer regime map from one-phase liquid up to post-critical heat transfer regimes and superheated steam. A fuel rod model for the calculation of fuel and cladding temperatures is implemented. A thermo-mechanical fuel rod model allows the estimation of the relevant heat transfer behaviour of the gas gap during transients and the determination of some parameters for fuel rod failure estimation. The two-phase flow model is closed by constitutive laws for heat mass and momentum transfer, *e.g.* vapour generation at the heated walls, condensation in the sub-cooled liquid, phase slip ratio, pressure drop at single flow resistances and due to friction along the flow channels as well as heat transfer correlations. Different packages of water and steam thermo-physical properties presentation can be used.

Coupling neutron kinetics/thermal-hydraulics

A two-time-step scheme consisting of thermal-hydraulic and neutron kinetic time steps is used for the transient integration. One or several neutron kinetic steps are used within a thermal-hydraulic step. Iterations between neutron kinetics and thermal-hydraulics are carried out in the steady state as well as for each thermal-hydraulic time step. Based on the changes of the main physical parameters of the transient process the time step size is controlled during the calculation.

Outstanding features

The assembly discontinuity factors (ADF) can be considered in the two geometries, Cartesian and hexagonal. The pin-wise flux reconstruction can be used for hot channel calculation during the DYN3D run. A decay heat model based on the power history or the initial power distribution can be taken into account during the transient. The decay heat model integrated in the code is based on the four fissionable isotopes ^{235}U, ^{238}U, ^{239}Pu and ^{241}Pu, the contributions from the decay of actinides resulting from the neutron capture and the contributions from the decay of nuclides formed by neutron capture in fission products. Based on perturbation theory, the reactivity contributions due to control rod motions, changes of moderator properties and fuel temperatures are calculated.

A model for description of the mixing of coolant from different primary loops in the downcomer and lower plenum of VVER-440 type reactors is implemented. It is based on the special feature of VVER-440 type reactors, that the coolant flow in the downcomer is nearly parallel without large re-circulation vortexes as they are known from Western-type PWR. Thus the flow can be well described in the potential flow approximation, where the Navier-Stokes equations can be solved analytically for the 2-D flow in the downcomer. The velocity gradient in the radial direction was neglected. In the lower control rod chamber a parallel flow with constant velocity was assumed. With this approximation of the velocity field the diffusion equation for the temperature is solved. The solution is presented as a closed analytical expression based on series of orthogonal eigenfunctions. The turbulence was taken into account by constant scalar turbulent Peclet numbers individually defined for the downcomer and the lower control rod chamber. The turbulent Peclet numbers describe the intensity of turbulent diffusion and were adapted to experimental data. For the validation of the model, measured values from an air-operated 1:5 scaled VVER-440 model were used. Temperature measurements were taken at the end of the downcomer and at the inlet of the reactor core. Further, the model was validated against measured operational data from NPP with VVER-440 and CFD calculations.

Concerning the transport of boron gradients into the core at low velocities a particle-in-cell model for avoiding the numerical diffusion can be applied in DYN3D. An integrated fuel rod model allows considering dynamic changes in heat transfer conditions (gap behaviour) and fuel rod failure limits estimation on-line during transient calculations.

Validation

DYN3D is validated by numerous benchmarks (including experimental results) for two geometries, Cartesian and hexagonal fuel element geometry.

The thermal-hydraulic system code: ATHLET

The thermal-hydraulic computer code ATHLET (Analysis of Thermal-hydraulics of Leaks and Transients) is developed by the Gesellschaft für Anlagen- und Reaktorsicherheit (GRS) for the analysis of anticipated and abnormal plant transients, small and intermediate leaks as well as large breaks in light water reactors. The aim of the code development is to cover the whole spectrum of design basis and beyond design basis accidents (without core degradation) for PWR and BWR with only one code. The main code features are: advanced thermal-hydraulics, modular code architecture, separation between physical models and numerical methods, pre- and post-processing tools and portability. The code offers the possibility to choose between models for the simulation of fluid dynamics. The first option is a five-equation model with separate conservation equations for liquid and vapour mass and energy, and a mixture equation, accounting for the thermal and mechanical non-equilibrium, and including a mixture-level tracking capability. Further, a complete two-fluid model with separate conservation equations for liquid and vapour mass, energy and momentum is available. Moreover, both fluid dynamic options allow for the simulation of non-condensable gases on the basis of the ideal gas formulation. Additional mass conservation equations can be included for the description of boron transport within a coolant system as well as of the transport and release of nitrogen dissolved in the liquid phase of the coolant. The time integration of the thermal fluid dynamics is performed with a general solver for ordinary differential equations called FEBE (forward-Euler, backward-Euler).

For the simulation of heat conduction a one-dimensional heat conductor module (HECU) is available. This model can simulate the one-dimensional temperature profile and heat conduction in plates, hollow and full cylinders in radial direction. The created heat conduction objects can be coupled on the left and/or right side of thermal fluid objects by consideration of the energy transport between the heat conductor surface and the surrounding fluid. A heat transfer package which covers a wide range of single-phase and two-phase flow conditions is available inside the module. Correlations for critical heat flux and minimum film boiling temperature are included; evaporation and condensation are calculated directly at the heating surfaces. A quench front model for bottom and top reflooding is also available.

Code development is accompanied by a systematic and comprehensive validation programme. A large number of integral experiments and separate effect tests, including the major International Standard Problems, have been calculated by GRS and by independent organisations. The range of applicability has been extended to the Russian reactor types VVER and RBMK in co-operation with foreign partner organisations. ATHLET is being applied by numerous institutions in Germany and abroad.

Coupling of the core model DYN3D with the system code ATHLET

Three different ways of coupling based on so-called “external”, “internal” and “parallel” coupling options have been realised at FZR for the integration of the ATHLET and DYN3D codes into the DYN3D/ATHLET code system.

The external coupling option means that both the neutron kinetics and thermal-hydraulics of the core are simulated with the code of 3-D neutron kinetics, and the system code calculates thermal-hydraulic conditions outside the core (see Figure 1). For this option the DYN3D-calculated data passed to ATHLET include mass flow rates at the core inlet/outlet (G_{in}/G_{out}) and a core outlet coolant enthalpy (h_{out}). The ATHLET-calculated data passed to DYN3D include core inlet/outlet pressures (P_{in}/P_{out}) as well as an enthalpy (h_{in}) and boron concentration ($C_{b,in}$) at the core inlet.

Using the internal coupling option, the core thermal-hydraulics are calculated by the system code ATHLET, and only the neutron kinetics part of DYN3D is employed in this case. The cross-sections are updated using the feedback from the system code thermal-hydraulics. For this coupling option the DYN3D-calculated data passed to the system code include a distribution of the core power [P(r)] only. The data calculated by the system code and passed to DYN3D include core distributions of fuel and moderator temperatures [$T_f(r)$, $T_m(r)$], moderator density [$\rho_m(r)$] and boron concentration [$C_b(r)$].

With the parallel coupling option, the core thermal-hydraulics are calculated by the coupled code within the same run of the code system (see Figure 1). The core inlet and outlet boundary conditions (G_{in}, h_{in}, $C_{b,in}$, P_{out}) are calculated by the ATHLET-code and passed to DYN3D. Based on these data,

DYN3D recalculates the core thermal-hydraulics and uses these results to update the core power distribution. The parallel coupling option has been used for the calculation of the BWR TT benchmark.

DYN3D is also coupled with the system code RELAP5.

Figure 1: Coupling scheme of the parallel coupling between DYN3D and ATHLET

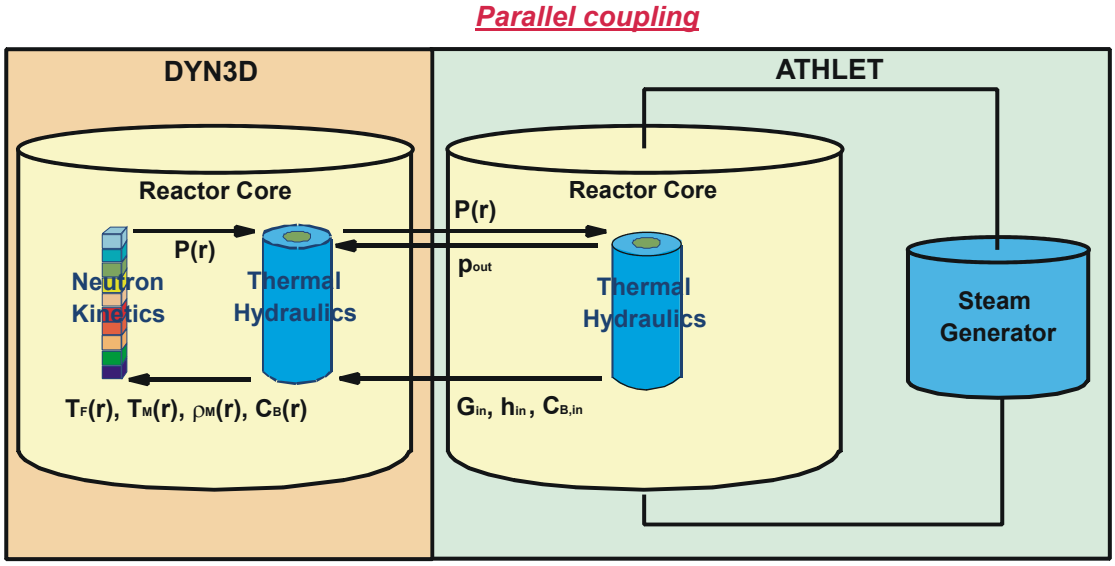

References

Grundmann, U., U. Rohde, S. Mittag (2000), "DYN3D – Three-dimensional Core Model for Steady-state and Transient Analysis of Thermal Reactors", *Proceedings of the 2000 ANS International Topical Meeting on Advances in Reactor Physics and Mathematics and Computation into the Next Millennium*, Pittsburgh (USA), 7-11 May.

Grundmann, U., U. Rohde, S. Mittag, S. Kliem (2005), *DYN3D Version 3.2 – Code for Calculation of Transients in Light Water Reactors (LWR) with Hexagonal or Quadratic Fuel Elements – Description of Models and Methods*, Scientific-Technical Report FZR-434, Forschungszentrum Rossendorf, August.

Manera, A., U. Rohde, H-M. Prasser, T.H.J.J. van der Hagen (2005), "Modeling of Flashing-induced Instabilities in the Start-up Phase of Natural-circulation BWRs Using the Code FLOCAL", *Nucl. Eng. Design*, Vol. 235, pp. 1517-1535.

Grundmann, U., D. Lucas, U. Rohde (1995), "Coupling of the Thermohydraulic Code ATHLET with the Neutron Kinetic Core Model DYN3D", *Int. Conf. on Mathematics and Computations, Physics and Environmental Analysis*, Portland, Oregon (USA), 30 April-5 May, Proc. Vol. 1, pp. 257-263.

Teschendorff, V., H. Austregesilo, G. Lerchl (1996), "Methodology, Status and Plans for Development and Assessment of the Code ATHLET", *Proceedings of the OECD/CSNI Workshop on Transient Thermal-hydraulic and Neutronic Codes Requirements*, Annapolis, USA, 5-8 November, Proc. pp. 112-128.

QUABOX/CUBBOX-ATHLET (GRS, Germany)

The thermal-hydraulic system code ATHLET (Analysis of Thermal-hydraulics of Leaks and Transients) is being developed by the Gesellschaft für Anlagen- und Reaktorsicherheit (GRS) mbH for the analysis of the whole spectrum of leaks and transients in PWR and BWR. The code is applicable for Western LWR designs as well as for Russian VVER and RBMK reactors. The main code features are the advanced thermal-hydraulics, the modular code architecture, especially the separation between physical models and numerical methods, the pre- and post-processing tools, and the portability to the prevalent computer platforms.

ATHLET is composed of several basic modules for the simulation of the different phenomena involved in the operation of a light water reactor: thermo-fluid dynamics (TFD), heat transfer and heat conduction (HECU), neutron kinetics (NEUKIN), and control and balance-of-plant (GCSM), together with the fully implicit numerical time integration method FEBE. Other independent modules (*e.g.* 3-D neutron kinetics or containment modules) can be coupled by means of a general interface.

The TFD module is based on a five-equation system (mixture momentum equation with drift) as well as on a six-equation two-fluid model, additionally enabling the simulation of several non-condensable gases, dissolved nitrogen and of boron transport. The reactor coolant system is modelled just by connecting basic fluid dynamic elements, called thermo-fluid objects (TFO), allowing for cross-flow between parallel channels.

The 3-D reactor core behaviour is described by QUABOX/CUBBOX. This code solves the neutron diffusion equations with two prompt neutron groups and up to six groups of delayed neutron precursors. The coarse mesh method is based on a polynomial expansion of neutron flux in each energy group. The time-integration is performed by a matrix-splitting method which decomposes the solution into implicit one-dimensional steps for each spatial direction. The reactivity feedback is taken into account by dependence of homogenised cross-section on feedback parameters, the functional dependence can be defined in a very general and flexible manner.

The coupling approach for 3-D neutronics models implemented in ATHLET is based on a general interface, which separates data structures from neutronics and thermo-fluid dynamic code and performs the data exchange in both directions. The internal coupling method has the following features: the fluid dynamic equations for the primary circuit and the flow channels in the reactor core region are completely modelled and numerically solved by ATHLET methods. Time integration in the neutronics code QUABOX/CUBBOX is performed separately. Thus, both codes maintain their capabilities.

TRAC-BF1/COS3D (NFI, Japan)

The code system used by NFI for this benchmark is TRAC-BF1/COS3D. COS3D, based on a modified one-group neutronics model is a three-dimensional core simulator. TRAC-BF1 is a plant simulator based on a two-fluid model. TRAC-BF1/COS3D is a coupled system of both codes, which are connected using a parallel computing tool.

COS3D is a 3-D BWR core simulator used for designing and licensing analyses and core management of commercial BWR plants in Japan. The neutronics model deals with three-dimensional geometry of rectangular co-ordinates. The characteristics of COS3D neutron kinetics model are as follows:

- modified one-group time-dependent diffusion equation derived from three-group diffusion equation;
- six delayed neutron precursor groups;
- direct consideration of feedback effect due to changes of moderator density, fuel temperature and control rod movement.

TRAC-BF1 includes a full non-homogeneous, non-equilibrium, two-fluid thermal-hydraulic model of two-phase flow. This also includes detailed modelling of a fuel bundle, thermal equilibrium critical flow model and so on. RPV is treated as three-dimensional nodalisation, and the other components are one-dimensional. The fundamental equations of thermal-hydraulics consist of mass, energy and momentum for each phase.

Instantaneous variables, namely, moderator density and fuel temperature are calculated at each CHAN component of TRAC-BF1. Those variables are transferred from TRAC-BF1 to COS3D via parallel virtual machine (PVM). After COS3D calculates the neutronic condition according to those variables, it returns the power distribution data to TRAC-BF1, which then calculates thermal-hydraulic condition in the plant based on the power distribution. Such a data transfer is executed by turns at every time step on UNIX or Linux environments.

TRAC-BF1/SKETCH-INS (NUPEC, Japan)

NUPEC used the SKETCH-INS/TRAC-BF1 coupled code system in the second exercise. The coupled code system was originally developed in Japan Atomic Energy Research Institute (JAERI) through a coupling of the best-estimate BWR transient analysis code TRAC-BF1 with the three-dimensional neutron kinetics code SKETCH-N. The coupling between the codes is organised using an interface module based on the message-passing library called parallel virtual machine (PVM).

TRAC-BF1 is the latest public domain BWR version of TRAC, which deals with thermal-hydraulics, fuel heat transfer and plant system. Thermal-hydraulics utilises the two-fluid model that solves six balance equations of mass, momentum and energy for liquid and vapour phases. Two-phase flow in the core region is treated as one-dimensional parallel vertical flows. A heat transfer model solves one-dimensional radial heat conduction equations. A standard finite differential method with staggered mesh is used for space integration of both fluid flow and heat conduction. Time integration of the fluid flow equations is performed by the semi-implicit scheme with the stability-enhanced two-step (SETS) method.

The SKETCH-INS code is a modification of the SKETCH-N code that was originally developed at JAERI. The SKETCH-INS code deals with neutron kinetics, which solves time-dependent diffusion equations in three-dimensional Cartesian co-ordinates. The code treats two neutron energy groups and six groups of delayed neutron precursors. In order to improve the spatial resolution accuracy, an assembly discontinuity factor (ADF) has been implemented in the code based upon the original one. Reactivity feedback is taken into account with moderator density, fuel temperature, control rod motion and reactor scram. The ANS-1979 standard decay heat model has been implemented in the code. Direct gamma heating is taken into account for the in-channel active coolant flow. Numerical methods for the neutronic calculations are as follows: polynomial and semi-analytical nodal method based on the non-linear iteration procedure is used for spatial integration of diffusion equations, time integration of the neutron kinetics equations is performed by the fully implicit scheme.

RETRAN-3D and CORETRAN (PSI, Switzerland)

Within the STARS project at PSI, the code environment for the coupled 3-D reactor-kinetics/ thermal-hydraulics transient analyses of the Swiss LWR is based principally on RETRAN-3D and CORETRAN, for both PWR and BWR systems. (It should be noted that the TRACE code has recently become increasingly important within our project and that other codes are used for specific applications: *e.g.* RAMONA for BWR stability.) Both codes play distinct roles in this environment: RETRAN-3D (Paulsen, 2001) is used for the analysis of coupled 3-D core/plant system transients, while CORETRAN (Eisenhart, 2000) is used for core-only dynamic analysis. An important aspect is that both codes are based on an identical neutronics algorithm, allowing the use of CORETRAN as an interface code to help prepare the 3-D core model for RETRAN-3D. This approach forms the basis of the PSI 3-D transient analysis methodology.

Participation in the OECD/NRC Peach Bottom 2 (PB2) Turbine Trip (TT) benchmark was prompted by the following considerations. First, the PSI methodology has thus far only been assessed for neutronically driven transients, and for a PWR system transient. Since the benchmark addresses a BWR transient driven by system thermal-hydraulic perturbations, it extends the range of the code's assessment. Secondly, the benchmark incorporates three different phases, which are, from the PSI point of view, well suited to a comprehensive assessment of all the participating codes. Consequently, PSI participated in all three phases of the benchmark.

RETRAN-3D MOD003.1, which is used in all three phases of the benchmark, is developed by EPRI to perform licensing and best-estimate transient thermal-hydraulic analyses of light water reactors and it is maintained by CSA/USA. RETRAN-3D is used to analyse thermal-hydraulic transients and requires numerical input data that completely describe the components and geometry of the system being analysed. The input data include fluid volume sizes, initial flow, pump features, power generation, heat exchanger properties and material compositions. RETRAN-3D can calculate a steady-state initialisation from a minimal amount of information. The steady-state option computes volume enthalpies from a steady-state energy balance, with the restriction that generally only one enthalpy may be supplied per flow system. The range of applications of RETRAN-3D also contains the spatial kinetics behaviour of multi-dimensional reactor cores. RETRAN-3D also permits the analysis of systems with non-equilibrium thermodynamic conditions and allows for the presence of non-condensable gases in the fluid stream.

References

Paulsen, M.P., *et al.* (2001), *RETRAN-3D – A Program for Transient Thermal-hydraulic Analysis of Complex Fluid Flow Systems, Volume 1: Theory and Numerics*, EPRI Report NP-7450(A), Volume 1, Revision 5, July, EPRI, Palo Alto, California, USA.

Eisenhart, L.D (2000), *CORETRAN-01: A Three-dimensional Program for Reactor Core Physics and Thermal-hydraulics Analysis. Volume 1: Theory and Numerical Analysis*, EPRI Report WO-3574, Revision 3, November, EPRI, Palo Alto, California, USA.

TRAC-M/PARCS (PSU/PURDUE/NRC, United States)

TRAC-M

TRAC-M performs best-estimate analyses of loss-of-coolant accidents (LOCA) and other accident and operational transients in pressurised light water reactors (LWR), as well as neutronics/thermal-hydraulic experiments in reduced-scale facilities. Models used include multi-dimensional two-phase flow, non-equilibrium thermo-dynamics, generalised heat transfer, reflood and reactor kinetics. Automatic steady-state and dump/restart capabilities are also provided.

The partial differential equations that describe two-phase flow and heat transfer are solved by finite differences. The heat-transfer equations are evaluated using a semi-implicit time-differencing technique. The fluid-dynamics equations in the spatial 1-D, 2-D and 3-D components use a multi-step time-differencing procedure that allows the material Courant-limit condition to be exceeded. The finite-difference equations for hydrodynamic phenomena form a system of coupled, non-linear equations that are solved by the Newton-Raphson iteration method. The resulting linearised equations are solved by direct matrix inversion. For the 1-D network matrix, this is done by a direct full-matrix solver; for the multiple-vessel matrix, this is done by the capacitance-matrix method using a direct banded-matrix solver.

The number of reactor components in the problem and the manner in which they are coupled are arbitrary. Reactor hydraulic components in TRAC-M include PIPE, PLENUM, PRIZER (pressurisers), PUMP, TEE, VALVE and VESSEL with associated internals. HSTR (heat structure), SLAB and ROD components are available to compute 2-D conduction and surface-convection heat transfer in Cartesian and cylindrical geometries, respectively. FILL and BREAK components are used to apply the desired coolant flow and pressure boundary conditions, respectively, for TRAC-M steady-state and transient calculations. There are also SEPD (separator) and TURB (turbine, TRAC-M/F77 only) components, which are to be replaced in future TRAC-M/F90 development. The current status of the SEPD and TURB is indicated at appropriate places in this document. Additional component models that are under development are indicated later in this section.

The TRAC-M computer execution time is highly problem-dependent and is a function of the total number of mesh cells, the maximum allowable time step size, and the rate of the neutronics/thermal-hydraulic phenomena being evaluated. For TRAC-PF1 and later versions, stability-enhancing two-step (SETS) numerics in 1-D hydraulic components allowed the material Courant limit to be exceeded. This allowed very large time steps to be used in slow transients when only 1-D hydraulic components are modelled. In TRAC-PF1/MOD2 and later versions, SETS numerics have also been applied to the multi-dimensional VESSEL component to allow the material Courant limit to be exceeded and very large time steps to be used for all system models. This allows significant speed-ups of one or two orders of magnitude for slow-accident and operational transients when multi-dimensional VESSEL components need to be modelled.

Reference

Steinke, R.G., *et al.* (2001), *TRAC-M/FORTRAN 90 (Version 3.0) User's Manual*, NUREG/CR-6722, pp. 2-1, 2-2, May.

PARCS

Purdue Advanced Reactor Core Simulator (PARCS) is a three-dimensional (3-D) reactor core simulator which solves the steady-state and time-dependent, multi-group neutron diffusion and SP_3 transport equations in orthogonal and non-orthogonal geometries in order to predict the eigenvalue and the dynamic response of the reactor to reactivity perturbations such as control rod movements or changes in the temperature/fluid conditions in the reactor core (Downar, 2004; Maggini, 2004).

The highlights of PARCS features can be listed as in the following (Downar, 2004):

- PARCS is coupled directly to the thermal-hydraulics system code, TRAC/RELAP Advanced Computational Engine (TRACE) (Odar, 2003; Spore, 2003), which provides the temperature and flow field information to PARCS during the transient calculations via the few group cross-sections (Miller, 1999).
- PARCS has ability to perform eigenvalue calculations, transient (kinetics) calculations, xenon transient calculations, decay heat calculations, pin power calculations and adjoint calculations for commercial LWR.
- Although PARCS has the capability to calculate 3-D models of realistic physical reactor cores, it has various 1-D modelling features that support faster simulations for a group of transients in which the dominant variation of the flux is in the axial direction, as for example in several BWR applications.
- The coarse mesh finite difference (CMFD) formulation is employed in PARCS to solve for the neutron fluxes in the homogenised nodes. The CMFD formulation provides a means of performing a fast core transient calculation by employing a non-linear iteration with local nodal calculation. The solution of the CMFD linear system is obtained using a Krylov subspace method.
- A transient fixed source problem is formed and solved at each time point in the transient.
- For spatial discretisation, a variety of solution kernels are available to include the most popular LWR two-group nodal methods, Advanced Nodal Method (ANM) and Nodal Expansion Method (NEM). NEM is also available in multi-group calculations.

References

Downar, T., *et al.* (2004), *PARCS v2.6 U.S. NRC Core Neutronics Simulator Theory Manual*, *https://engineering.purdue.edu/PARCS/Code/Manual/Theory/PDF/PARCS_TheoryManual.pdf* (2004).

Maggini, F. (2004), "*Contributions to Study Instability in BWR: Application to Peach Bottom-2 NPP*", Thesis of Bachelor, University of Pisa, May.

Miller, R.M., T.J. Downar (1999), *Completion Report for the Coupled TRAC-M/PARCS Code*, August.

Odar, F., C. Murray (2003), *et al.*, *TRACE V4.0 User's Manual*, May.

Spore, J.W., *et al.* (2003), *TRAC-M/FORTRAN 90 (Version 3.0) Theory Manual*, July.

TRAC-M/PARCS coupling

TRAC-M/PARCS coupling is performed using a general interface (GI), which was implemented using parallel virtual machine (PVM). Overall controls of the coupled transient such as convergence checks and trip initiation are handled by TRAC-M. For fast steady-state initialisation, a neutronic calculation skipping strategy is used, *i.e.* a PARCS calculation was performed only once per every 20 time advances in TRAC-M. In this benchmark, the reflector nodes in PARCS are not mapped to thermal-hydraulic channels since the reflector thermal-hydraulic properties are fixed. Minor modifications were made to the GI module in order to treat the fixed reflector nodes, as well as to handle the method specified for treating the moderator bypass density correction.

Reference

Lee, D., *et al.* (2004), "Analysis of the OECD/NRC BWR TT Benchmark with Coupled Neutronics and Thermal-hydraulics Code TRAC-M/PARCS", *Nuclear Science and Engineering*, 148, 2004.

TRAC-BF1/ENTRÉE (TEPSYS, Japan)

TRAC/BF1-ENTRÉE is a parallel coupling system between the highly accurate three-dimensional neutron kinetic code ENTRÉE and the versatile BWR simulator, TRAC/BF1. ENTRÉE solves the two-energy group three-dimensional diffusion equation based on the transverse integrated nodal expansion method. The inside bundle flux is expanded either with the Legendre polynomial functions or the Legendre semi-analytical functions. Due to its high accuracy, the non-linear iteration method with the Legendre semi-analytical functions will be applied to this study. A parallel processing between two codes will be realised by the parallel virtual machine (PVM) protocols that enable synchronisation of data sending and receiving calls in two processes.

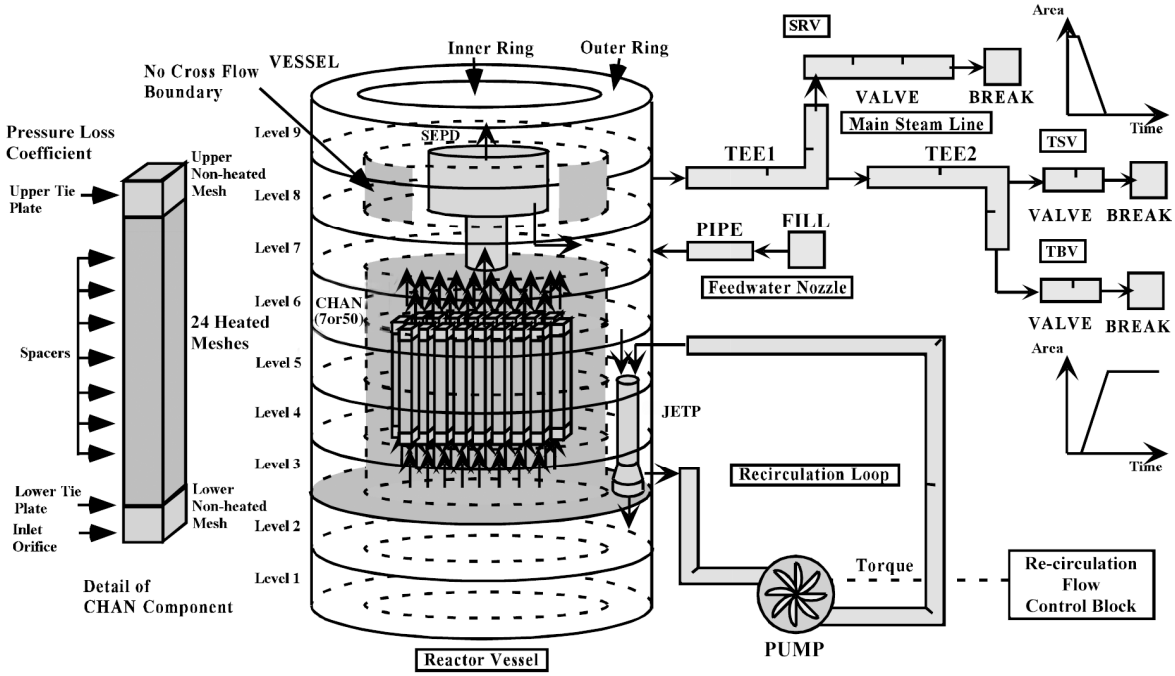

RELAP5/PARCS (UPISA, Italy)

RELAP5

The RELAP5 code was developed to perform best-estimate transient simulation of light water reactor coolant systems during postulated accidents and operational transients. It is capable of simulating many generic component models including pumps, valves, pipes, heat releasing or absorbing structures, electric heaters, jet pumps, turbines, separators, accumulators and control system components.

The RELAP5 hydrodynamic model is based upon a one-dimensional, transient, two-fluid model formulated in terms of volume and time-averaged parameters of the flow. Phenomena that depend upon transverse gradients, such as friction and heat transfer, are formulated in terms of the bulk properties using empirical transfer coefficient formulations. The basic field equations for the two-fluid non-equilibrium model consist of two phasic mass continuity equations, two phasic momentum equations and two phasic energy equations. The system model is solved numerically using a semi-implicit finite-difference technique, which basically means that mass, energy and even momentum flux are conducted explicitly. But the pressure equation is solved implicitly for all the cells simultaneously.

PARCS

PARCS/2.4 code solves the neutron kinetics diffusion equations using a nodal, two-energy-groups approach. The major calculation features of the code include its ability to perform eigenvalue calculations (k_{eff}), transient flux calculations, xenon transient calculations, decay heat calculations, adjoint calculations and ADF correction.

POLCA-T (Westinghouse, Sweden)

POLCA-T is a coupled 3-D core neutron-kinetics and system thermal-hydraulics computer code (Panayotov, 2003b, 2004a, 2005) that integrates Westinghouse BWR core simulator POLCA7 (Lindahl, 1996) and the most advanced features of company's BWR thermal-hydraulic system transient codes in a single software product. Moreover, the code utilises models of other Westinghouse BWR tools, such as fuel performance code (Zhou, 2005), steam lines models and plant control models (Wijkström, 2000).

Code features

The codes multi-physics models can be summarised as follows:

1. Reactor physics models consist of 3-D two-group neutron diffusion nodal core simulator POLCA7 (neutronics) and associated 3-D neutron kinetics equations.
2. Core and plant thermal-hydraulics are described by five-equation system with drift flux model. The thermal-hydraulics model is used for all plant systems: reactor pressure vessel (RPV), main steam lines (MSL), recirculation loops, auxiliary systems, etc. Additional dry-out (DO) and critical power ratio (CPR) correlations, boiling transition and post-dry-out heat transfer models are implemented in the code. Special models for steam separators and dryers, jet pumps, etc. have been developed as well.
3. Thermal mechanical behaviour is predicted by two-dimensional thermal conduction model that describes the processes in both fuel rods and plant hardware as follows:
   - Fuel, gas gap and cladding behaviour models are based on power, exposure and fission product (gas release) dependencies. The models account for the pellet swelling, densification, relocation and thermal expansion, cladding creep and elastic deformations, and thermal expansion. These models are consistent with the models used in our BWR fuel performance code (Zhou, 2005).
   - Heat structures depict the fuel assemblies (FA) boxes, water rods, water channels (crosses, wings), all RPV internals and vessel, external pump loops, MSL, steam bypass system, etc.
4. Chemistry features cover the boron transport and non-condensable gases transport with their solution and dissolution.
5. Balance of plant describes protection, control and safety systems. Models to simulate the I&C systems, feedwater systems, emergency core cooling systems (ECCS), MSL and steam bypass systems, plant protection and control systems, turbine, generator, pumps, controllers, safety and relief valves, piping to containment are available.

Other features of the code worth mention include:

1. The code is an internal coupled code of neutron kinetics and thermal-hydraulics. The coupling is based on the use of the very same thermal-hydraulics equations for core and plant system models. Proper drift flux correlation are specified for each model, and if required for any of its fluid nodes.
2. The code also integrates a multi-scale geometrical flexibility. On the micro level there are models in the core: fuel, gas gap, cladding, fuel assemblies, pin power, DO, CPR, core bypass, etc. At a macro level, it covers the RPV, recirculation loops, MSL, steam bypass lines and other plant models. This geometrical flexibility allows the code's application to a wide range of plant designs as well as to separate test facilities.
3. The code allows applying a comprehensive approach to core and plant analyses with full consistency between the core design and safety analyses, and between the steady-state and transient simulations. Both are achieved by means of the integration of the steady-state core simulator POLCA7 in the code.

Scope and status of application

The practical applications of POLCA-T mainly concern three areas:

- BWR steady-state core design: stability and POLCA7 steady-state capabilities;
- BWR safety analysis;
- modelling of separate test facilities.

Applications for core design are covered by POLCA7's wide range of capabilities. Applications for safety analysis include operational transient, stability, reactivity initiated accidents (RIA), anticipated transients without scram (ATWS), and loss of coolant accidents (LOCA). During its validation, the code was applied for pre- and post-test calculations of experiments performed at several facilities such as FRIGG, FIX-II, SPERT, BWR90+ core catcher, etc.

The POLCA-T code is well adapted to analyse scenarios with a number of failing control rods and boron shutdown scenarios.

POLCA-T has already been used for several specific applications with highly satisfactory results. Some examples of applications are the analysis of:

- stability analyses of Ringhals 1, Forsmark and KKL plants;
- nuclear heating events in BWR;
- hydraulic loads in piping due to pipe break and valve closure;
- natural circulation in BWR90+ core catcher test facility;
- Forsmark plant: different failing control rods, ATWS and boron system scenarios.

Overview of the validation

The validation matrix of POLCA-T ranges from simple available analytical solutions over small scale basic and component tests known also as separate tests, to full scale BWR bundle tests, to integral thermal-hydraulic tests, and finally to recorded reactor plant events and transients. The verification and validation activities are pursued in the same order.

Some examples of code validation against separate and integral tests, as well against plant recorded tests and events are the analysis of:

- void, single- and two-phase pressure drop, steady-state and transient dry-out measurements at FRIGG loop;
- INEL one-sixth and full size jet pump tests;
- main circulation (centrifugal) pump tests;
- steam separator tests "Snorre";
- FIX II: power and flow DO transients;
- integral steady-state tests: Peach Bottom 2 (PB2) end of cycle (EOC) 2 TIP and LPRM (Panayotov, 2005), KKL cycle 19 TIP;
- stability analyses of measurements performed at Ringhals 1 International Stability Benchmark (cycles 14-17), KKL (cycles 7, 10, 13, 19), Forsmark 2 (cycles 15-20), and PB2 EOC2 (Panayotov, 2003a);
- TVO unit 1 begin of cycle (BOC) 1 pump trip test 406 recorded on 17 October 1978;
- OECD NEACRP-L-335 rod ejection benchmark;
- SPERT-IIIE RIA experiments;

- OECD/NRC BWR turbine trip benchmark including four extreme scenarios (Panayotov, 2002, 2004a, 2004b);
- PB2 EOC2 three turbine trip TT1, TT2, TT3 tests (Panayotov, 2005);
- Forsmark 2 turbine trip with pump run down recorded on 10 November 2002;
- Forsmark 3 CR insertion at full power, "Pancake" core recorded on 15 June 1994.

The validation work continues with connection to development and qualification of more plant models and the codes applications.

References

Lindahl, S-Ö., E. Müller (1996), "Status of ABB Atom's Core Simulator POLCA", *Int. Conf. PHYSOR96*, Mito, Japan, 16-20 September.

Panayotov, D. (2002), "OECD/NRC BWR Turbine Trip Benchmark: Simulation by POLCA-T Code", *PHYSOR-2002 International Conference on the New Frontiers of Nuclear Technology: Reactor Physics, Safety and High-performance Computing*, Seoul, Korea, 7-10 October, Track H-2, Paper 3C-02.

Panayotov, D., M. Thunman (2003a), "POLCA-T Code Validation against Peach Bottom 2 End of Cycle 2 Low-flow Stability Tests", *Mathematics and Computation (M&C 2003) Conference*, Gatlinburg, TN, USA, 6-10 April.

Panayotov, D., U. Bredolt, P. Jerfsten (2003b), "POLCA-T – Consistent BWR Core and Systems Modelling", *ANS/AESJ/ENS Int. Conf. Top Fuel 2003*, Paper 410, Wurzburg (G), 16-19 March.

Panayotov, D. (2004a), "OECD/NRC BWR Turbine Trip Benchmark: Simulation by POLCA-T Code", *Nuclear Science and Engineering*, Volume 148, pp. 247-255, October.

Panayotov, D. (2004b), "POLCA-T Simulation of OECD/NRC BWR Turbine Trip Benchmark Exercise 3 Best Estimate Scenario TT2 Test and Four Extreme Scenarios", *PHYSOR-2004 Reactor Physics Topical Meeting*, Chicago, Illinois, USA, 25-29 April, Session: 6B "Nuclear Safety".

Panayotov, D., U. Bredolt, H. Lindgren (2005), "POLCA-T – A Coupled Multi-physics Tool for Design and Safety Analyses", *M&C Topical Meeting: Supercomputing, Reactor Physics and Nuclear and Biological Applications*, Technical Session on Multi-physics Coupled Code Systems for Nuclear Reactor Design and Safety, Avignon, France, 12-15 September.

Wijkström, H. (2000), "ABB Atom's New Code for 3D Static and Transient Analysis", *Proceedings of the German Nuclear Society Workshop on Thermal and Fluid Dynamics, Reactor Physics and Computing Methods*, Rossendorf, Germany, 31 January-1 February.

Zhou, G., *et al.* (2005), "Westinghouse Advanced UO_2 Fuel Behaviors During Power Transients", *Water Reactor Fuel Performance Meeting 2005*, Kyoto, Japan, 2-6 October, paper no. 1059, track #5.

Appendix B: Questionnaire for Exercise 3 of the NEA-NRC BWR TT benchmark

I. Thermal-hydraulic model

a) Core thermal-hydraulic (T-H) model and nodalisation (1-D, 3-D and number of channels or cells with schematic if possible). How are channels/T-H cells chosen?

b) How core bypass flow was modelled?

c) Number of heat structures (fuel rods) modelled?

d) Please provide with more detail the nodalisation of the steam line.

e) How are the jet pumps modelled?

f) How are the steam separators and dryers modelled?

g) How are the turbine stop valves closing phenomena and steam bypass system modelled?

h) How are the safety and relief valves modelled?

i) What are the difficulties encountered during the component modelling?

j) Which core thermal-hydraulic initial and transient boundary conditions are used and how?

k) Radial and axial heat structure (fuel rod) nodalisation?

l) Used correlations for fuel properties vs. temperature?

II. Core neutronics model

a) Number of radial nodes per assembly?

b) Axial nodalisation?

c) Radial and axial reflector modelling?

d) Cross-section interpolation procedure used?

e) Used method to get a critical reactor at the beginning of transient?

f) How is the xenon effect modelled?

g) How is assembly discontinuity factor (ADF) modelled?

h) Is bypass density correction used? If so, how it is modelled?

i) How is decay heat modelling modelled?

III. Coupling schemes

a) Hydraulics/heat structure spatial mesh overlays (mapping schemes in radial and axial plane)?

b) Hydraulics/neutronics spatial mesh overlays (mapping schemes in radial and axial plane)?

c) Heat structure/neutronics spatial mesh overlays mapping schemes in radial and axial plane)?

d) Temporal coupling scheme?

e) Coupling numerics for steady state and transient – explicit, semi-implicit or implicit? Please also provide time step size, convergence criteria, courant number etc.

f) Coupling method – external or internal?

g) Coupling design – serial integration or parallel processing?

IV. General

a) User assumptions?

b) What are the code's limitations that affect the results?

c) Specific features of the used codes?

d) Number of solutions submitted per participant? If more than one please provide comments and brief analysis on the solutions.

e) If your results are significantly different than the reference results, are there any explanations for these differences? Please explain each significant difference.

CATHARE/CRONOS2/FLICA4 (CEA, France)

I. Thermal-hydraulic model

a) Core thermal-hydraulic (T-H) model and nodalisation (1-D, 3-D, and number of channels or cells with schematic if possible). How are channels/T-H cells chosen?

3-D with one channel per assembly (*i.e.* 764).

b) How core bypass flow was modelled?

One additional channel models the bypass.

c) Number of heat structures (fuel rods) modelled?

One heat structure per assembly (or channel).

d) Please provide with more detail the nodalisation of the steam line.

300 meshes for the steam line.

e) How are the jet pumps modelled?

Jet pumps are modelled by 1-D and Tee modules of CATHARE.

f) How are the steam separators and dryers modelled?

The separator and the dryer are respectively modelled by 0-D (volume) and 1-D modules of CATHARE.

g) How are the turbine stop valves closing phenomena and steam bypass system modelled?

They are modelled by the VALVE module of CATHARE.

h) How are the safety and relief valves modelled?

They are modelled by the VALVE module of CATHARE.

i) What are the difficulties encountered during the component modelling?

j) Which core thermal-hydraulic initial and transient boundary conditions are used and how?

Initial conditions are obtained from the specifications: mass flow, inlet temperature, outlet pressure. There are no boundary conditions for the core in Exercise 3.

k) Radial and axial heat structure (fuel rod) nodalisation?

20 axial nodes and 10 radial nodes for each heat structure.

l) Used correlations for fuel properties vs. temperature?

Obtained from the specifications.

II. Core neutronics model

a) Number of radial nodes per assembly?

One radial node per assembly.

b) Axial nodalisation?

26 axial nodes (refer to specifications): 24 for core + 2 for reflector.

c) Radial and axial reflector modelling?

One radial ring and 2 axial nodes.

d) Cross-section interpolation procedure used?

Linear interpolation (standard module of CRONOS2).

e) Used method to get a critical reactor at the beginning of transient?

Normalisation of the fission operator: nu*Sigma_fission/k_eff.

f) How is the xenon effect modelled?

No specific model.

g) How is assembly discontinuity factor (ADF) modelled?

Not taken into account.

h) Is bypass density correction used? If it is used, how it is modelled?

Yes it is used. The density is obtained by combining the fuel assembly channels on one hand and the bypass channel on the other hand.

i) How is decay heat modelling modelled?

We use the time evolution provided in the specifications.

III. Coupling schemes

a) Hydraulics/heat structure spatial mesh overlays (mapping schemes in radial and axial plane)?

Same axial nodalisation. One heat structure per hydraulic channel.

b) Hydraulics/neutronics spatial mesh overlays (mapping schemes in radial and axial plane)?

Same radial nodalisation. Linear interpolation in axial direction.

c) Heat structure/neutronics spatial mesh overlays mapping schemes in radial and axial plane)?

Same radial nodalisation (one heat structure per neutronic radial node). Linear interpolation in axial direction.

d) Temporal coupling scheme?

Synchronism of CATHARE, CRONOS2 and FLICA4 at each time step of coupling.

e) Coupling numerics for steady state and transient – explicit, semi-implicit or implicit? Please also provide time step size, convergence criteria, courant number etc.

Semi-implicit time scheme for the coupling. Variable time step during the transient (in the range 10^{-3} to 10^{-2} s).

f) Coupling method – external or internal?

External coupling (ISAS software).

g) Coupling design – serial integration or parallel processing?

Parallel processing (one CPU per code).

IV. General

a) User assumptions?

b) What are the code's limitations that affect the results?

c) Specific features of the used codes?

d) Number of solutions submitted per participant? If more than one please provide comments and brief analysis on the solutions.

Two main solutions. The main one is described above. The second one is based on a limited number of channels in the core (33 to 100).

e) If your results are significantly different than the reference results, are there any explanations for these differences? Please explain each significant difference.

S-RELAP5/RAMONA5-2.1 (FANP, Germany)

I. Thermal-hydraulic model

a) Core thermal-hydraulic (T-H) model and nodalisation (1-D, 3-D and number of channels or cells with schematic if possible). How are channels/T-H cells chosen?

See nodalisation scheme below.

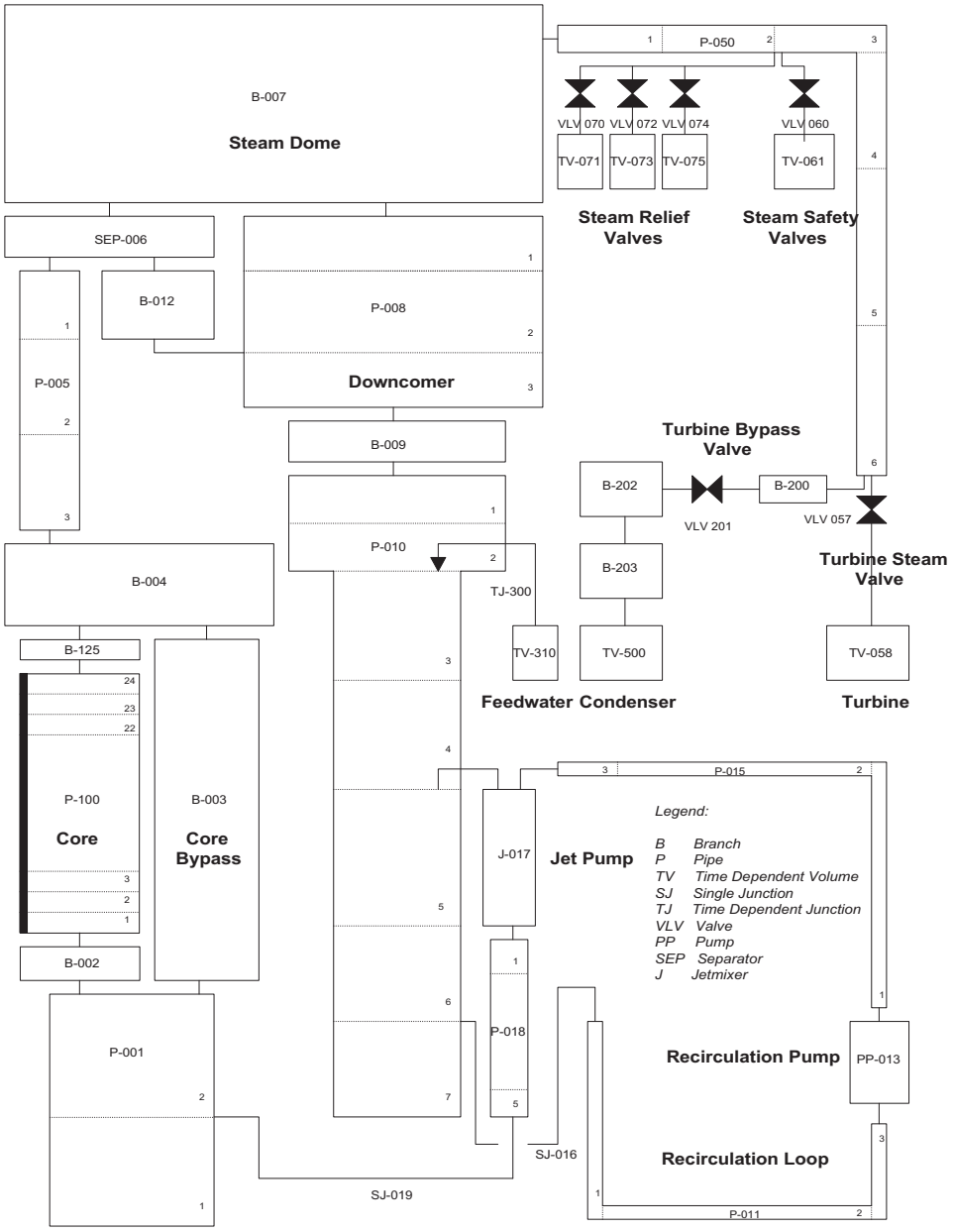

b) How core bypass flow was modelled?

One channel that summarises the core bypass.

c) *Number of heat structures (fuel rods) modelled?*

Three types of fuel rods.

d) *Please provide with more detail the nodalisation of the steam line.*

See attached nodalisation scheme.

e) *How are the jet pumps modelled?*

S-RELAP5 standard component.

f) *How are the steam separators and dryers modelled?*

S-RELAP5 standard component.

g) *How are the turbine stop valves closing phenomena and steam bypass system modelled?*

Turbine stop valve: linear closure within 96 ms. Steam bypass system: this was modelled in such a way that the steam outflow value of RETRAN (provided by the benchmark team) resulted.

h) *How are the safety and relief valves modelled?*

S-RELAP5 standard component; set-points according to benchmark specifications.

i) *What are the difficulties encountered during the component modelling?*

j) *Which core thermal-hydraulic initial and transient boundary conditions are used and how?*

Imposed according to benchmark specifications.

k) *Radial and axial heat structure (fuel rod) nodalisation?*

24 axial/10 radial nodes.

l) *Used correlations for fuel properties vs. temperature?*

AREVA standard correlation.

II. Core neutronics model

a) *Number of radial nodes per assembly?*

Each fuel assembly is represented by one radial node.

b) *Axial nodalisation?*

The active core is modelled with 24 axial nodes.

c) *Radial and axial reflector modelling?*

The reflector is explicitly modelled in axial direction by an additional node at the bottom and at the top of the active core and in radial direction by an additional row of reflector assemblies.

d) *Cross-section interpolation procedure used?*

The nodal cross-sections have been calculated based on linear interpolation in the provided cross-sections tables.

e) Used method to get a critical reactor at the beginning of transient?

The steady-state solution of RAMONA5 has been calculated based on the initial conditions of the PBTT. In RAMONA5 it is assumed that the initial state is just critical.

f) How is the xenon effect modelled?

The xenon effect has been modelled in the thermal absorption cross-section. The nodal thermal absorption cross-section has been corrected by subtracting the macroscopic xenon cross-section and adding the product of microscopic xenon cross-sections and nodal xenon concentration.

g) How is assembly discontinuity factor (ADF) modelled?

The provided ADF has been used to calculate the transverse leakage in the nodal expansion method.

h) Is bypass density correction used? If so, how it is modelled?

A bypass density has been determined for each axial node based on one common bypass channel. The effective nodal moderator density used in the cross-section calculations is then given by the area-weighted average of the nodal active moderator density and the nodal bypass moderator density.

i) How is decay heat modelling modelled?

The decay heat standard model ANS-79 has been used.

III. Coupling schemes

a) Hydraulics/heat structure spatial mesh overlays (mapping schemes in radial and axial plane)?

33 hydraulic channels/17 different types of fuel conditions.

b) Hydraulics/neutronics spatial mesh overlays (mapping schemes in radial and axial plane)?

33 hydraulic channels/888 fuel assemblies. 24 axial nodes (neutronics: one additional reflector node at bottom and at top). The radial mapping of the thermal-hydraulic channels as specified in the final specification has been used.

c) Heat structure/neutronics spatial mesh overlays mapping schemes in radial and axial plane)?

17 different types of fuel conditions/888 fuel assemblies.

d) Temporal coupling scheme?

e) Coupling numerics for steady state and transient – explicit, semi-implicit or implicit? Please also provide time step size, convergence criteria, courant number etc.

Explicit coupling, 6 ms time step.

f) Coupling method – external or internal?

External.

g) Coupling design – serial integration or parallel processing?

Serial integration.

IV. General

a) User assumptions?

b) What are the code's limitations that affect the results?

c) Specific features of the used codes?

d) Number of solutions submitted per participant? If more than one please provide comments and brief analysis on the solutions.

e) If your results are significantly different than the reference results, are there any explanations for these differences? Please explain each significant difference.

DYN3D/ATHLET (FZD, Germany)

I. Thermal-hydraulic model

a) Core thermal-hydraulic (T-H) model and nodalisation (1-D, 3-D and number of channels or cells with schematic if possible). How are channels/T-H cells chosen?

1-D model with one T-H channel/fuel assembly.

b) How core bypass flow was modelled?

One average T-H channel for the bypass in the core.

c) Number of heat structures (fuel rods) modelled?

One average fuel rod/T-H channel.

d) Please provide with more detail the nodalisation of the steam line.

The steam line is divided into 30 nodes according to Figure 1.

Figure 1: Modelling of the steam line including dryer and bypass line in the DYN3D/ATHLET calculation

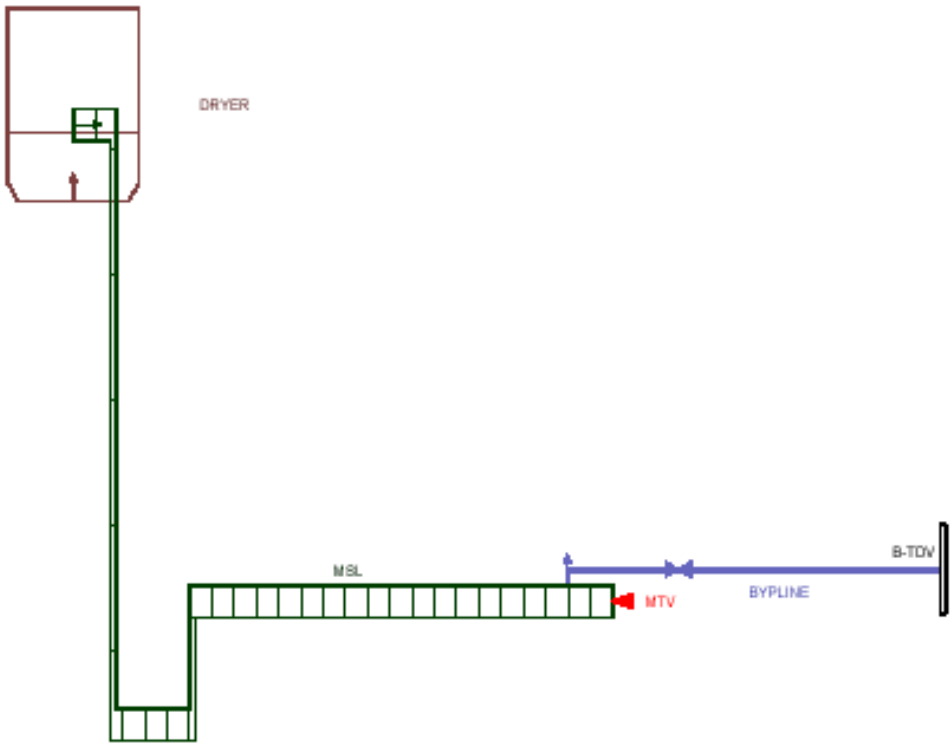

e) How are the jet pumps modelled?

Two jet pumps were completely modelled including the diffuser part (see Figure 2).

Figure 2: DYN3D/ATHLET calculation scheme with the nodalisation of the reactor pressure vessel and the recirculation loops

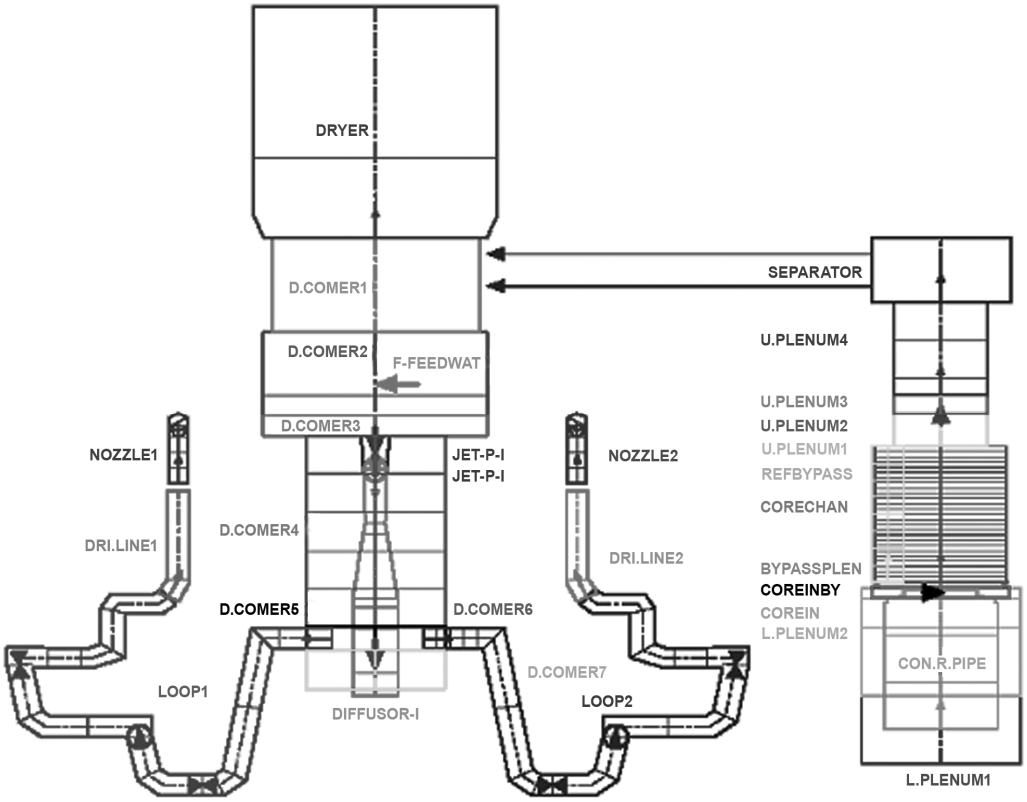

f) How are the steam separators and dryers modelled?

ATHLET contains a special separator model, which was used for the modelling of the steam separator. The steam dryer was modelled with the main geometrical details (see Figure 2).

g) How are the turbine stop valves closing phenomena and steam bypass system modelled?

The modelling of the bypass line is shown in Figure 1, the turbine stop valve was modelled as a typical valve with the specified closing characteristics.

h) How are the safety and relief valves modelled?

Safety and relief valves were modelled according to the specification.

i) What are the difficulties encountered during the component modelling?

The ATHLET part of the calculation scheme was delivered by GRS Germany. No additional difficulties appeared during the core modelling.

j) Which core thermal-hydraulic initial and transient boundary conditions are used and how?

In the coupled core/plant calculation no specific core boundary conditions are specified, the data calculated for the thermal-hydraulic objects below and above the core are used.

k) Radial and axial heat structure (fuel rod) nodalisation?

10 radial and 24 axial nodes of equal height are used.

l) *Used correlations for fuel properties vs. temperature?*

As specified.

II. Core neutronics model

a) *Number of radial nodes per assembly?*

One node/assembly.

b) *Axial nodalisation?*

24 axial nodes of equal height for the active core.

c) *Radial and axial reflector modelling?*

Two layers for the axial reflectors each with a height of 15.24 cm, radial reflector modelled by assemblies.

d) *Cross-section interpolation procedure used?*

Yes.

e) *Used method to get a critical reactor at the beginning of transient?*

Eigenvalue k_{eff}.

f) *How is the xenon effect modelled?*

Given Xe concentration.

g) *How is assembly discontinuity factor (ADF) modelled?*

Explicitly.

h) *Is bypass density correction used? If so, how it is modelled?*

Bypass densities were taken into account by using the specified formula of cross-section calculation.

i) *How is decay heat modelling modelled?*

The decay heat model of DYN3D was used by assuming an infinite state with the initial power distribution.

III. Coupling schemes

a) *Hydraulics/heat structure spatial mesh overlays (mapping schemes in radial and axial plane)?*

Identical mapping in hydraulics and heat structures.

b) *Hydraulics/neutronics spatial mesh overlays (mapping schemes in radial and axial plane)?*

Identical mapping in hydraulics and neutronics.

c) *Heat structure/neutronics spatial mesh overlays mapping schemes in radial and axial plane)?*

Identical mapping in neutronics and heat structures.

d) Temporal coupling scheme?

Several neutron time steps per T-H time steps, the concrete number depends on the convergence performance.

e) Coupling numerics for steady state and transient – explicit, semi-implicit or implicit? Please also provide time step size, convergence criteria, courant number etc.

Explicit with iteration between core thermal-hydraulics and neutron kinetics. No iteration between ATHLET model and the thermal-hydraulic core model of DYN3D, the core model (thermal-hydraulic and neutron kinetic) is calculated at the end of the ATHLET time step.

f) Coupling method – external or internal?

Parallel, the core is modelled in the system code and in the core model, the calculated reactor power is transferred to both models.

g) Coupling design – serial integration or parallel processing?

Serial integration.

IV. General

a) User assumptions?

Use of the Molochnikov boiling model.

b) What are the code's limitations that affect the results?

No.

c) Specific features of the used codes?

No.

d) Number of solutions submitted per participant? If more than one please provide comments and brief analysis on the solutions.

One.

e) If your results are significantly different than the reference results, are there any explanations for these differences? Please explain each significant difference.

No.

QUABOX/CUBBOX-ATHLET (GRS, Germany)

I. Thermal-hydraulic model

a) Core thermal-hydraulic (T-H) model and nodalisation (1-D, 3-D and number of channels or cells with schematic if possible). How are channels/T-H cells chosen?

In the ATHLET model the flow in the reactor vessel is described by two lower plena, 33 thermal-hydraulic channels in the core region with two types of fuel assemblies, a parallel bypass channel with two additional plena, and four layers of the upper plenum. The thermal-hydraulic channels are divided into 26 axial nodes.

b) How core bypass flow was modelled?

The bypass flow begins in the lowest layer of the lower plenum, it passes two additional volumes and continues parallel to the core channel and flows into the lower layer of the upper plenum stand pipes. The bypass channel has in the core region also 26 axial nodes as the core channels.

c) Number of heat structures (fuel rods) modelled?

Each thermal-hydraulic channel of the active core has assigned a heat structure modelling the fuel rods of the 7×7 or 8×8 fuel assembly types.

d) Please provide with more detail the nodalisation of the steam line.

The steam line of 133 m length has at the end the turbine stop valve (TSV). The steam line is divided into 30 nodes. The bypass line, 74.8 m long, divided into 20 nodes, is connected to the 28^{th} node of the steam line.

e) How are the jet pumps modelled?

The jet pumps in the ATHLET code are modelled by a pipe system consisting of four parts: the part of the downcomer, the riser pipe with the nozzle, a pipe with the mixing region and the diffuser. At the end of the diffuser an additional pump is applied to obtain the needed pressure difference.

f) How are the steam separators and dryers modelled?

The steam separator and the dryers are built by pipes. The separator is connected over two junction pipes with a branch with a mixture level. In the upper junction, the carry over junction, flows steam with water droplets, and in the lower junction, the carry under junction, flows water with bubbles. The separation depends on the quality in the water and steam region of the separator, which are functions of the mass flow and the quality at the separator inlet and the height of the mixture level in the mixture branch.

g) How are the turbine stop valves closing phenomena and steam bypass system modelled?

The turbine stop valve TSV is modelled as standard valve and the turbine bypass valve is modelled as discharge valve. In the TSV model the cross-sectional area, CSA, decreases during the closure of the valve. The relative valve form loss coefficient is determined as a function of the CSA. The form loss coefficient increases with decreasing CSA. The mass flow in the steam line depends on the location. At the outlet, the mass flow is reduced rapidly due to the closure of the TSV. This reduction also takes place at the inlet of the bypass line. Because of the opening of the MTV, the mass flow reaches a value of about 600 kg/s. The MTV is modelled as discharge valve where the flow at outlet is limited by the critical flow. The critical flow is modelled with the Moody model.

h) How are the safety and relief valves modelled?

The set points for valve opening and closure are specified. The capacity is defined by the cross-sectional area.

i) What are the difficulties encountered during the component modelling?

The simplified modelling of jet pumps.

j) Which core thermal-hydraulic initial and transient boundary conditions are used and how?

A complete model of the primary thermal-hydraulic circuit is applied.

k) Radial and axial heat structure (fuel rod) nodalisation?

The fuel pellet is described with six radial layers and the cladding is described with two radial layers. In axial direction 24 nodes are used for the heated length.

l) Used correlations for fuel properties vs. temperature?

The dependency of the material temperature for the specific heat capacity, the heat conductivity and the density of the fuel and the cladding is considered by tables in very good agreement with the proposed correlations of the specification.

II. Core neutronics model

a) Number of radial nodes per assembly?

One node per assembly.

b) Axial nodalisation?

24 nodes for the active core and 2 for the reflectors, 26 in total.

c) Radial and axial reflector modelling?

Radial reflector is modelled adding additional reflector assemblies at the core boundary. Axial reflectors are modelled adding one layer at the top and one at the bottom of the core, each one with a height of 30 cm.

d) Cross-section interpolation procedure used?

Yes, that specified (lint4d subroutine).

e) Used method to get a critical reactor at the beginning of transient?

The core was critical after the steady-state calculations (performing the criticality K_{eff} search option of the code).

f) How is the xenon effect modelled?

The effect of Xe was taken into account applying the proposed specified corrections of the cross-sections.

g) How is assembly discontinuity factor (ADF) modelled?

It is not modelled due to the specific solution method applied in the core model QUABOX/CUBBOX.

h) Is bypass density correction used? If so, how it is modelled?

Yes, it is used. The assumption is made that there is no boiling in the bypass and the coolant density is axially linear decreasing from the core inlet value to the corresponding saturation density value at core outlet.

i) How is decay heat modelling modelled?

The provided table of the decay heat rate is applied.

III. Coupling schemes

a) Hydraulics/heat structure spatial mesh overlays (mapping schemes in radial and axial plane)?

The number in axial and radial directions of the hydraulics structures in the active core equals the number of the heat structures. Axial nodes are 24. Radial objects are 33.

b) Hydraulics/neutronics spatial mesh overlays (mapping schemes in radial and axial plane)?

In radial plane the core is neutronically modelled with one node per assembly, 764 in total. These assemblies are distributed in 33 T-H channels. Axially the neutronics and hydraulics meshes are the same – 26 (2 of them are reflector nodes).

c) Heat structure/neutronics spatial mesh overlays mapping schemes in radial and axial plane)?

The heat structures follow the hydraulic structures in the active core, *i.e.* radially their number is 33. Radially the mapping with the neutronics is the same as in question I.k). Axially the neutronics and heat structure meshes for the active core are also the same – 24.

d) Temporal coupling scheme?

A specific time synchronisation schema is applied where the leading role of the time step determination has the ATHLET code, *i.e.* the solving of the thermal-hydraulic equations and after that the time step for neutronics in QUABOX/CUBBOX is automatically adapted.

e) Coupling numerics for steady state and transient – explicit, semi-implicit or implicit? Please also provide time step size, convergence criteria, courant number etc.

For the steady-state calculations iterations between the two codes are made till a specific aim function (axial power distribution deviation less than 1.10^{-3}) is fulfilled or a maximum number of iterations is reached.

f) Coupling method – external or internal?

Internal.

g) Coupling design – serial integration or parallel processing?

Serial.

IV. General

a) User assumptions?

No important user assumptions.

b) What are the code's limitations that affect the results?

There are no limitations for this transient.

c) *Specific features of the used codes?*

ATHLET applies the six-equation model for the thermal-hydraulic calculations.

d) *Number of solutions submitted per participant? If more than one please provide comments and brief analysis on the solutions.*

One.

e) *If your results are significantly different than the reference results, are there any explanations for these differences? Please explain each significant difference.*

No significant differences.

TRAC-BF1/SKETCH-INS (NUPEC, Japan)

I. Thermal-hydraulic model

a) Core thermal-hydraulic (T-H) model and nodalisation (1-D, 3-D and number of channels or cells with schematic if possible). How are channels/T-H cells chosen?

Core thermal-hydraulic (T-H) model is the two-fluid model with 6 equations. The reactor pressure vessel is modelled in 3-D cylindrical co-ordinates with 2 radial rings and 15 axial levels as shown in Figure 1. Thermal-hydraulic channels were treated as 1-D, 33 parallel channels (same as the final specifications).

b) How core bypass flow was modelled?

The reactor vessel simulated core bypass region. The core bypass flow was simulated with a leak path model from T-H channel to the vessel (core bypass) region. Gamma heating in the bypass region was neglected.

c) Number of heat structures (fuel rods) modelled?

33 heat structures, *i.e.* one heat structure for one T-H channel.

d) Please provide with more detail the nodalisation of the steam line.

See figure below.

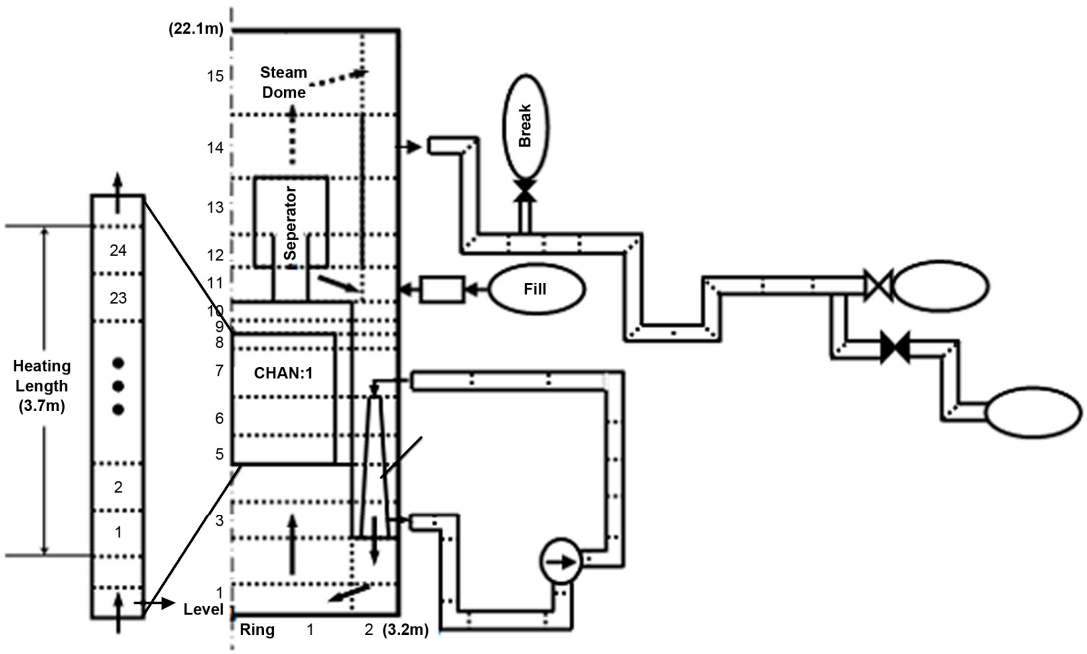

e) How are the jet pumps modelled?

The jet pumps were modelled with JETP component of TRAC-BF1 following Table 3.1.2.2 and Figure 3.1.2.1 in the final specifications.

f) How are the steam separators and dryers modelled?

The steam separators were modelled with SEPD component using a mechanistic model of TRAC-BF1. The defaults of the code were used.

g) How are the turbine stop valves closing phenomena and steam bypass system modelled?

The turbine stop valve and steam bypass valve were modelled with VALVE component of TRAC-BF1. The valve movements were given by timetables.

h) How are the safety and relief valves modelled?

The safety and relief valves were modelled with VALVE component of TRAC-BF1 with the specified set points.

i) What are the difficulties encountered during the component modelling?

Simulation of inertia of the steam separators.

j) Which core thermal-hydraulic initial and transient boundary conditions are used and how?

Table 5.2.1 in the final specifications was used for the initial condition. TSV closure, TBV open and CRD scram given by Tables 5.3.1-5.3.5 in the final specifications was used for the transient boundary condition.

k) Radial and axial heat structure (fuel rod) nodalisation?

Radial: pellet 10 rings, gap 1 ring, crud 2 rings; axial: 24 nodes.

l) Used correlations for fuel properties vs. temperature?

MATPRO in TRAC-BF1 was used, which is consistent with the final specifications.

II. Core neutronics model

a) Number of radial nodes per assembly?

One node.

b) Axial nodalisation?

24 nodes.

c) Radial and axial reflector modelling?

Radial: 1 node (Figure 2.4.2); axial: bottom 2 nodes, top 1 node.

d) Cross-section interpolation procedure used?

Cross-section was fitted as a pronominal function of coolant density and fuel temperature.

e) Used method to get a critical reactor at the beginning of transient?

K_{eff} was set at 1 at the beginning of transient.

f) How is the xenon effect modelled?

Xenon absorption is excluded at HZP. Absorption cross-section with xenon was used at HFP and transient.

g) How is assembly discontinuity factor (ADF) modelled?

Same as the Code Smith model.

h) Is bypass density correction used? If so, how it is modelled?

No.

i) How is decay heat modelling modelled?

Same as ANS-1979.

III. Coupling schemes

a) Hydraulics/heat structure spatial mesh overlays (mapping schemes in radial and axial plane)?

Radial: 1 heat structure per 1 T-H channel; axial: same noding.

b) Hydraulics/neutronics spatial mesh overlays (mapping schemes in radial and axial plane)?

Radial: 33 T-H channels/764 neutronic channels, axial: same noding.

c) Heat structure/neutronics spatial mesh overlays mapping schemes in radial and axial plane)?

Radial: 33 heat structure/764 neutronic channels, axial: same noding.

d) Temporal coupling scheme?

PVM coupling scheme.

e) Coupling numerics for steady state and transient – explicit, semi-implicit or implicit? Please also provide time step size, convergence criteria, courant number etc.

Explicit.

f) Coupling method – external or internal?

External.

g) Coupling design – serial integration or parallel processing?

Parallel processing.

IV. General

a) User assumptions?

None.

b) What are the code's limitations that affect the results?

c) Specific features of the used codes?

Polynomial and semi-analytical nodal method based on the non-linear iteration procedure (Zimin, *et al.*, 1998) is used for spatial integration of diffusion equations. Time integration of the neutron kinetics equations is performed by the fully implicit scheme.

Zimin, V.G., H. Ninokata and L. Pogosbekyan, L., 1998, Polynomial and Semi-Analytic Nodal Methods for Nonlinear Iteration Procedure, *Proc. ANS Int. Conf. on the Physics of Nuclear Science and Technology (PHYSOR)*, Long Island, New York, 5-8 October 1998, vol. 2, pp. 994-1002.

d) Number of solutions submitted per participant? If more than one please provide comments and brief analysis on the solutions.

One.

e) If your results are significantly different than the reference results, are there any explanations for these differences? Please explain each significant difference.

RETRAN-3D (PSI, Switzerland)

I. Thermal-hydraulic model

a) Core thermal-hydraulic (T-H) model and nodalisation (1-D, 3-D and number of channels or cells with schematic if possible). How are channels/T-H cells chosen?

In the core region, the flow from the lower plenum is mainly to the core inlet volume, with a small fraction of the total core flow flowing through the core bypass volume. From the core inlet volume, most of the coolant flows into the core, while again a small amount enters the core bypass volume, see Figure 1. The core region is represented by 34 thermal-hydraulic channels, each with 24 axial nodes, and the flow through each channel corresponds to the combined flow through a certain number of fuel assemblies. The steam/water mixture flowing out of the top of the core channels flows into a single core exit volume and from there into the upper plenum, where it mixes with the core bypass flow.

Figure 1: Nodalisation of the core region

It consists of the core, the core inlet volume, the core exit volume and the core bypass volume. 34 thermal-hydraulic channels represent the core itself, where each channel consists of 24 axially stacked volumes levels.

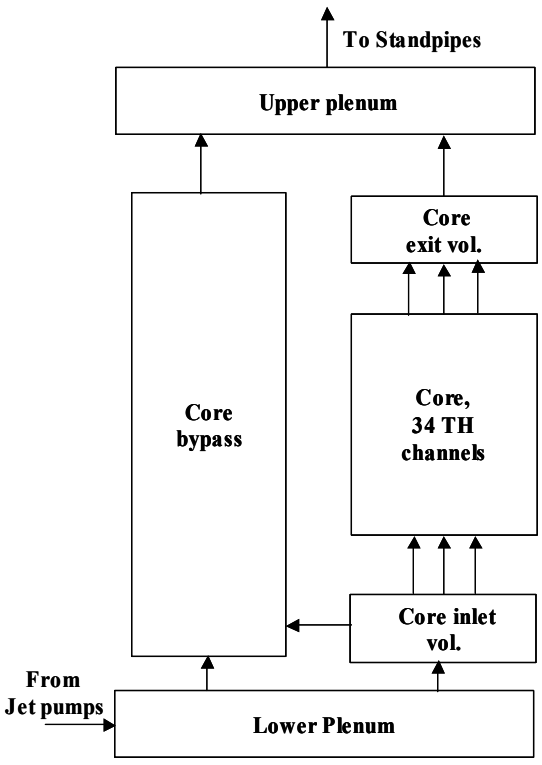

In the PSI methodology, the input required for RETRAN-3D to perform a 3-D core calculation consists of three separate input files, two of which are prepared by CORETRAN, and the remaining one forms part of the normal RETRAN-3D input structure. The two files prepared by CORETRAN consist of a transient cross-section (tcs) file, and a file containing geometric information for all the individual fuel assemblies (cdi or CORETRAN Data Interface file). The additional information contained within the standard RETRAN input includes a "map" which allocates each reactor fuel assembly to a given RETRAN core hydraulic channel (a total of 34 such channels were used in the present analysis, see below). Thus, prior to the RETRAN-3D calculation, a CORETRAN static calculation of Phase II (core only boundary condition model) was performed to provide well-founded parameters for the 3-D core.

Accordingly, in the benchmark Phase II and III calculations, the neutronics parameters of each of the 764 fuel assemblies have been entered at 24 axial levels. The combining, or "lumping", of the flow through these assemblies into the 34 thermal-hydraulic channels is that suggested in the benchmark specification (see Figure 3.2.2 in NEA, 2001), except that since RETRAN-3D will not combine assembly types with different numbers of fuel rods within the same hydraulic channel, Channel 26 in Figure 3.2.2 (NEA, 2001) was subdivided into two separate channels: Number 26 (for the 4 outermost fuel assemblies with Assembly Design 5 (see Figure 2.4.2 in NEA, 2001), and Number 34 (for the 4 innermost fuel assemblies with Assembly Design 4). See the radial channel map in Figure 2.

Figure 2: Thermal-hydraulic channel radial map, with channels 10, 34 highlighted. The + symbols represent differently inserted control rods.

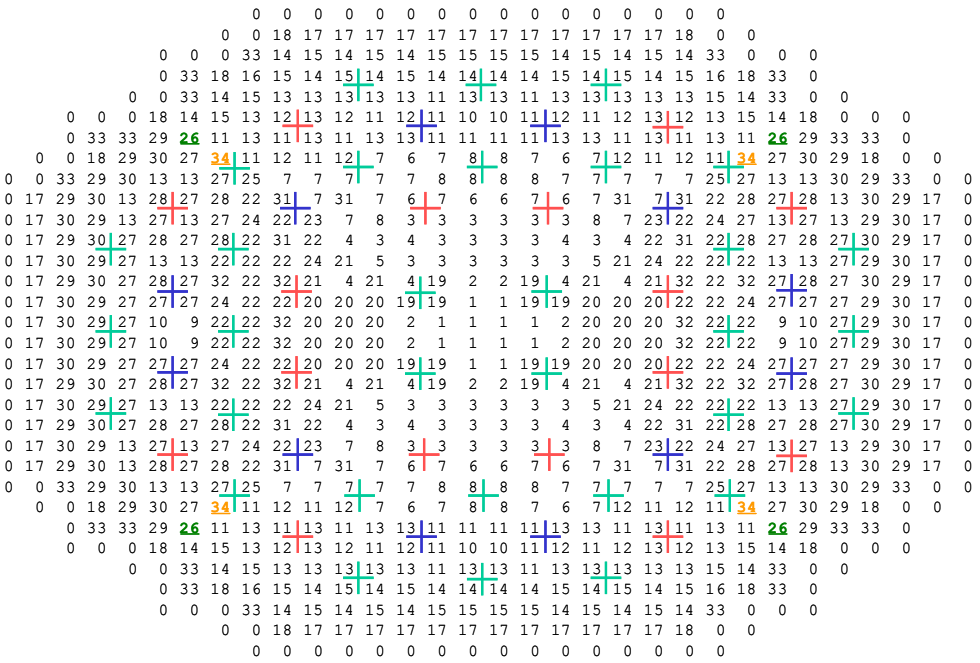

b) How core bypass flow was modelled?

The core bypass (as in the Phase I calculation) is modelled as a RETRAN-3D volume, which is connected to the lower plenum, core inlet and upper plenum volumes. For the coupling of the thermal-hydraulics with the neutronics calculations in the core, the RETRAN-3D code separates the core bypass volume into 24 axially stacked volumes.

c) Number of heat structures (fuel rods) modelled?

The flow in the core is lumped into 34 thermal-hydraulic channels at 24 axial levels and an additional bypass channel and the same number heat structures (34*24) are modelled by RETRAN-3D. Bypass heating is taken into account.

d) Please provide with more detail the nodalisation of the steam line.

See Figure 3.

e) How are the jet pumps modelled?

The jet pumps are modelled using a RETRAN-3D pump model.

Figure 3: Detailed nodalisation of the steam line

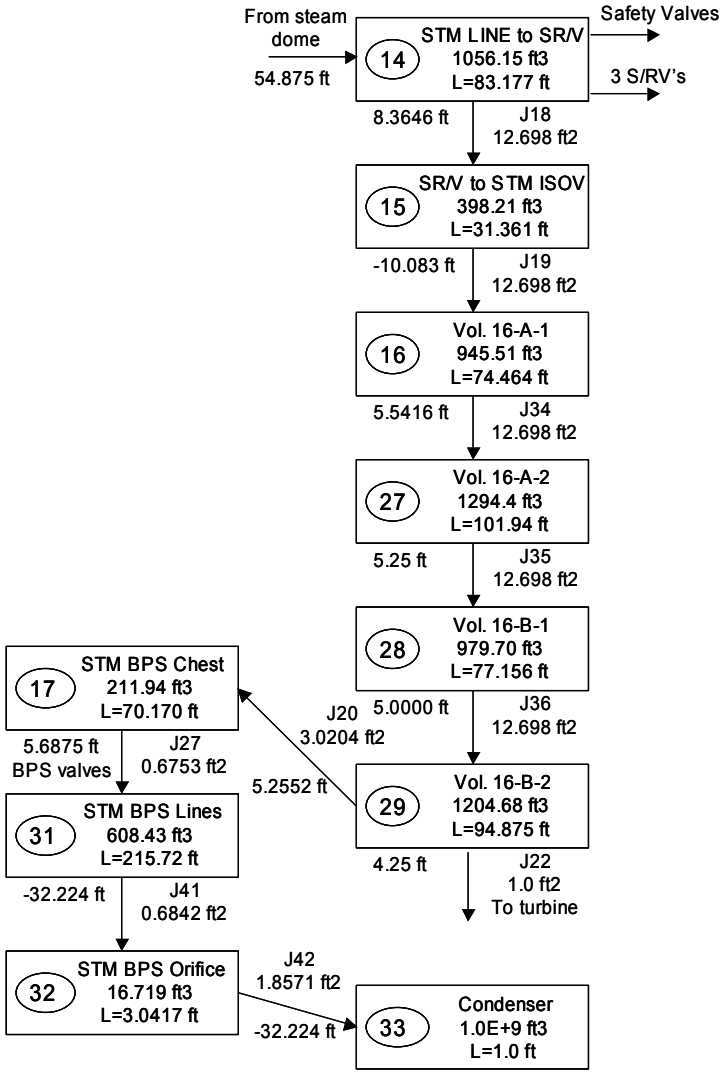

f) How are the steam separators and dryers modelled?

In order to determine the distribution of the steam flow it is important to follow the flow of steam through the separators into the steam dome. In the reactor, two-phase flow from the core region passes through the standpipes and then enters the steam separators. In each separator, the steam-water mixture passes turning vanes, which impart a spin to establish a vortex, which separates the water from the steam. The denser liquid is thrown radially outward by centrifugal force forming a continuous film on the inside wall of the inner pipe. The separator water exits from under the separator cap and flows out between the standpipes, draining into the downcomer. Steam with a quality of at least 90% exits from the top of the separator and rises to the dryers. The dryers force the wet steam to be directed horizontally through the dryer panels. The steam flow makes a series of rapid changes in direction while traversing the panels. During these direction changes the heavier drops of entrained moisture are forced to the outer walls where moisture collection hooks catch and drain the liquid to collection troughs, then through tubes into the vessel downcomer, so that the steam dryer assembly increases the quality of the steam to more than 99.9%. This dry steam flows into the steam dome and into the steam lines.

This behaviour is approximated in the RETRAN-3D model by control volumes (CV 1-5 in Figure 4), which was developed from an early RETRAN-02 model for Turbine Trip 1 by Hornyik and Naser (1979). Two-phase flow from the core region flows into the steam separator volume (CV 1). In this volume a liquid level is defined below which two-phase flow is established, while above the level there is only steam flow. In this volume (CV 1) the RETRAN-3D bubble rise model option is used. The steam flow is upwards to the lower dryer volume (CV 2) and continues to the steam dome volume (CV 3) and into the steam line.

Figure 4: Nodalisation of the steam separator region

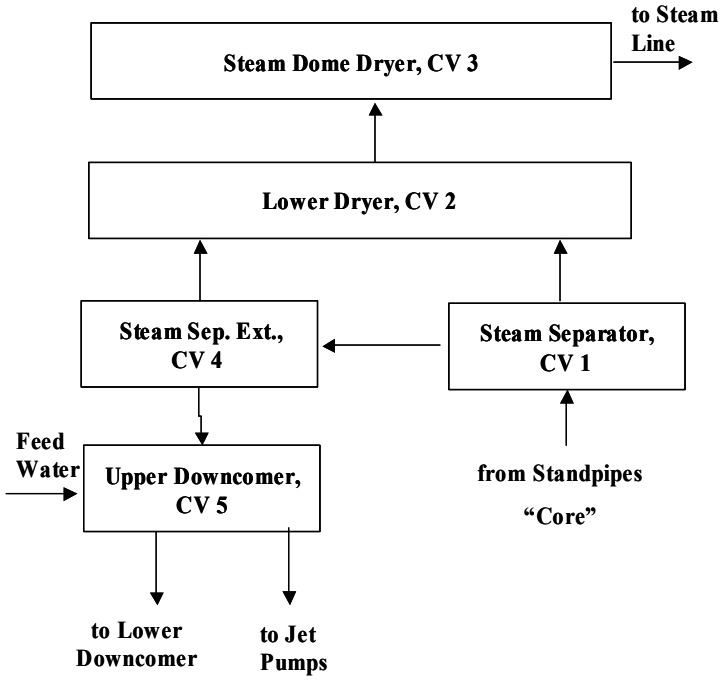

Two-phase flow consisting of water with some vapour carry-under flows from the steam separator volume to the steam separator external volume (CV 4). The junction between these two control volumes is below the liquid level in CV 1. In the steam separator external (CV 4) a liquid level develops with a steam phase above the liquid level and a two-phase region below the level. The RETRAN-3D bubble rise model is again used to describe this phenomenon. At t = 0 there is a very small steam flow from the steam separator external to the lower dryer volume (CV 2), while the main flow is water down into the upper downcomer (CV 5). The feedwater also flows into the upper downcomer volume. From there, water flows to the lower downcomer and the jet pumps and from there back into the core.

Since the RETRAN-3D code option used in this analysis is that of the 4-equation model (*i.e.* full thermal equilibrium), the volume of water in the steam separator (CV 1) and steam separator external (CV 4) two-phase control volumes is in equilibrium with the steam, and this strongly influences the pressure increase per unit of steam generated in the core. For this reason in Benchmark Phase I a sensitivity study a re-nodalisation of the separator/downcomer region was performed, which gave a pressure increase equal to the measured one at about 1 sec. In order to achieve this, the volumes of the steam separator and the steam separator external control volumes were reduced in this sensitivity test, while the volume of the upper downcomer control volume was increased to preserve the total volume of water.

The main effect of the re-nodalisation is a reduction in the energy transfer from the steam to the liquid, because the volume in which thermal equilibrium is established is smaller. Thus there is less condensation of the vapour as the pressure increases. To obtain the measured pressure increase it was necessary to approximately half the volume of the steam separator and the steam separator external control volumes.

Another RETRAN-3D code option that can be used to obtain a reduced energy transfer between the liquid and the vapour is the "two-region non-equilibrium model". (Note this model was used in conjunction with the RETRAN-3D bubble rise model to obtain the submitted results.) This model divides the fluid in the control volume at the liquid level interface into two regions, where each region is in internal thermal equilibrium, but the two regions are not necessarily in equilibrium with each other. The "liquid" region below the interface and the "vapour" region above the interface have the same pressure, but in general have different temperatures, *i.e.* in the vapour region for example we may have superheated steam. The application of this model (in the steam separator volume and the steam separator external volume, CV 1 and CV 4 in Figure 4) also produced an increased pressure rise at about 1 sec. A sensitivity study showed that the effect in the steam separator volume is negligible and the increased pressure rise at 1 sec comes mostly from the steam separator external volume. The reason for this is as follows: after 0.3 sec in the steam separator external volume the pressure increase leads to an increase in the steam temperature in the "vapour" region, but because of the non-equilibrium model the energy transfer between the "vapour" region and the "liquid" region is reduced so maintaining the superheated steam in the "vapour" and dryer regions. In the steam separator region, however, there is a transfer of vapour from the liquid region at the level interface, because of the rising bubbles through the liquid region, and relative to this the reduction of the energy transfer across the interface due to the non-equilibrium model gives only a small effect.

g) How are the turbine stop valves closing phenomena and steam bypass system modelled?

The turbine stop valve closing is described by a negative fill junction model, which is combined with a valve where the area versus time is specified. This defines the flow rate to the turbine.

The steam bypass system is modelled using four RETRAN-3D control volumes: the steam bypass chest volume connected via the bypass valves to the steam bypass lines volume connected to the steam bypass orifice volume connected to the condenser. In the turbine bypass valve between the steam bypass chest volume and the steam bypass lines volume the area versus time is defined to approximately get the specified flow through the turbine bypass. Choked flow through the bypass valve is assumed.

h) How are the safety and relief valves modelled?

According to the benchmark specifications three groups of safety relief valves (SRV) are modelled. "SRV 1" means a group of four safety relief valves. "SRV 2" means a different group of four safety relief valves and "SRV 3" means a further group of three safety relief valves. The set points and delay times are specified according to the benchmark specifications and the capacities of the valve are adjusted accordingly, see Table 1. Choked flow through the safety relief valves is assumed.

Table 1: Safety relief valve set points

Safety relief valve bank	No. of valves	Opening set point (pressure) [MPa]	Capacity per valve at 103% of opening pressure [kg/s]	Opening delay time [s]	Closure set point (pressure) [MPa]	Closure delay time [s]
SRV 1	4	7.720	103.19	0.4	7.496	0.0
SRV 2	4	7.789	104.20	0.4	7.555	0.0
SRV 3	3	7.858	105.08	0.4	7.622	0.0

i) What are the difficulties encountered during the component modelling?

j) Which core thermal-hydraulic initial and transient boundary conditions are used and how?

A steady-state initialisation is performed using the respective RETRAN-3D code option in order to calculate the core thermal-hydraulic initial conditions. No boundary conditions to the core thermal-hydraulic components are necessary as they are provided by the adjacent components.

k) Radial and axial heat structure (fuel rod) nodalisation?

The heat structure (fuel rod) nodalisation has been chosen according to the lumping of the fuel rods 34 thermal-hydraulic channels with 24 axial nodes each, see also (a).

l) Used correlations for fuel properties vs. temperature?

All specified correlations for fuel and cladding properties have been used.

II. Core neutronics model

a) Number of radial nodes per assembly?

A 1 × 1 radial assembly mesh is used (*i.e.* 1 radial node per assembly).

b) Axial nodalisation?

The neutronics model contains 24 active nodes and two reflector nodes (bottom and top). All nodes have equal size.

c) Radial and axial reflector modelling?

Both radial reflectors and axial reflectors are explicitly modelled. The geometry and nodalisation for the radial reflectors is identical to the one used for the active fuel assemblies and contains hence 26 axial nodes (*i.e.* 24 + 2 reflector nodes).

d) Cross-section interpolation procedure used?

The specified cross-section tables and the provided interpolation routine have been implemented and used.

e) Used method to get a critical reactor at the beginning of transient?

Normalisation of the fission cross-section with the initial (steady-state) K_{eff} value.

f) How is the xenon effect modelled?

A SIMULATE summary file containing the nodal xenon number density distributions was provided by the benchmark organisers and used to define a CORETRAN restart file containing only the xenon nodal distributions (*i.e.* all other distributions set to zero). Then, a two-step procedure was used for the xenon correction during the cross-section evaluation.

- *Step 1*. Evaluate the thermal macroscopic absorption cross-section with no xenon as:

$$\Sigma_{a,2}^{NoXe} = \Sigma_{a,2} - \Sigma_{Xe}$$

where $\Sigma_{a,2}$ is the thermal absorption cross-section (interpolated from the specified cross-section data tables) and Σ_{Xe} is the macroscopic xenon cross-section (interpolated from the specified cross-section data tables).

- *Step 2*. Compute the corrected thermal absorption macroscopic cross-section as:

$$\Sigma_{a,2}^{Corr} = \Sigma_{a,2}^{NoXe} + n_{Xe} \cdot \sigma_{Xe}$$

where n_{Xe} is the (nodal) xenon number density read from the restart file, σ_{Xe} is the xenon microscopic cross-section (interpolated from the specified cross-section data tables) and $\Sigma_{a,2}^{NoXe}$ is the nodal macroscopic thermal absorption cross-section with no xenon (obtained from Step 1).

These xenon number distributions are read from an additional RETRAN-3D input file.

g) *How is assembly discontinuity factor (ADF) modelled?*

The ADF are modelled to correct for heterogeneous flux condition at the interfaces. They are treated as all other specified cross-sections (*i.e.* tables and interpolation procedure).

h) *Is bypass density correction used? If so, how it is modelled?*

The bypass density correction is applied with a two-step procedure.

- *Step 1*. First, the nodal moderator density (for an active fuel node) obtained from the T-H solution is corrected to take into account bypass density changes as follows:

$$\rho_{act}^{eff} = \rho_{act} + \frac{A_{Byp}}{A_{act}} \cdot \left(\rho_{byp} - \rho_{sat}\right)$$

where ρ_{act} is the nodal density calculated by RETRAN-3D, ρ_{byp} and ρ_{sat} are the bypass actual and saturation density, respectively, and $\frac{A_{Byp}}{A_{act}}$ is the ratio of the bypass flow area to the active flow area.

- *Step 2*. The corrected moderator density of Step 1 is then used by the neutronic module to evaluate the cross-sections (*i.e.* by interpolation from specified tables). An approximation is made by using a uniform bypass-to-active area ratio $\frac{A_{Byp}}{A_{act}}$ for all active nodes based on the observation that fuel type designs 2 and 3 were the predominant assembly types. Hence, the geometry of these bundles was considered significantly representative for all fuel channels. The geometry for the fuel design type 2 is shown in Figure 5 below.

Figure 5: Geometry of Fuel Type 2 with surrounding bypass water

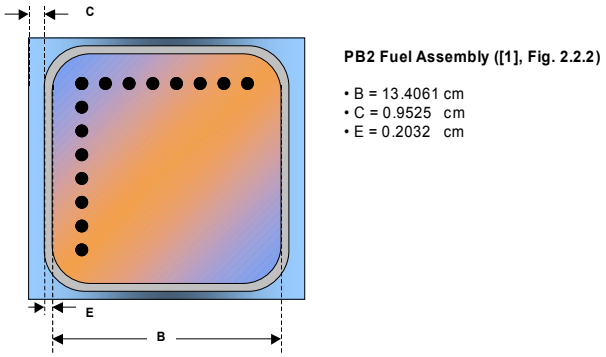

To derive the ratio based on the geometry above, a constant gap between fuel channels was assumed and the eventual presence of control rod blades was neglected. The assumed gap was chosen as D = 2*C. Thereafter, the ratio used for all fuel nodes is evaluated as:

$$A_{Ratio} = \frac{A_{byp}}{A_{act}} = \frac{\left(B + 2 \cdot C + 2 \cdot E\right)^2 - \left(B + 2E\right)^2}{FA} \approx 0.56141$$

where FA is the active fuel channel area which for simplicity was defined as constant for all channels with the value FA = 100 cm^2.

The bypass heating (1.7%) is taken into account, and the bypass conditions are calculated using the non-conducting heat exchanger option in RETRAN-3D.

i) *How is decay heat modelling modelled?*

The RETRAN-3D decay heat model used is based on the 1979 ANS standard.

III. Coupling schemes

a) Hydraulics/heat structure spatial mesh overlays (mapping schemes in radial and axial plane)?

A total of 34 heat structures are used to model an average fuel pin in each of the 34 heated thermal-hydraulic channels (see next question). The radial distribution of the fuel pins hence corresponds to the thermal-hydraulic channel representation. For the axial nodalisation, each fuel pin is discretised in a similar manner as the corresponding thermal-hydraulic channel, *i.e.* 24 axial volumes.

b) Hydraulics/neutronics spatial mesh overlays (mapping schemes in radial and axial plane)?

All of the 764 fuel assemblies are modelled as single neutronic channels mapped on 34 thermal-hydraulic channels. For the axial nodalisation, 24 uniform volumes nodes are consistently used in the neutronic and thermal-hydraulic representation of the active fuel part.

c) Heat structure/neutronics spatial mesh overlays mapping schemes in radial and axial plane)?

Same as above, see a) and b).

d) Temporal coupling scheme?

The complete mathematical model used in RETRAN-3D consists of a very large system of differential and algebraic equations that describe the numerous physical phenomena that occur in complex thermal-hydraulic systems. A variety of numerical methods are required due to the nature of the equations that make up the complete RETRAN-3D model and the wide range of analyses for which the code is used. The differential equation models in RETRAN-3D include:

- mass, momentum and energy equations for the coolant fluid;
- conduction equation for heat transfer in solids;
- multidimensional (3-D) kinetics for power generation in the core;
- model equations for some equipment components and special physical processes.

In general, these equations are coupled in the following manner. The neutron kinetics equations give the power generated in the fuel rods, which provides the internal volumetric heat generation rate for the conduction equations for the fuel rods. In this application the Coarse Mesh Finite Difference (CMFD) non-linear iteration procedure is used, where the local two-node problems are solved using a Nodal Expansion Method (NEM). The coupling between the kinetics and the heat conduction equations is explicit. The heat conduction solution uses implicit coupling between the heat transfer correlations and the source term for the energy equations. Feedback between the thermal-hydraulic equations and the kinetics equations is also treated explicitly in this application.

e) Coupling numerics for steady state and transient – explicit, semi-implicit or implicit? Please also provide time step size, convergence criteria, courant number etc.

Explicit coupling is used, see also answer to d). The minimum time step size between 0 and 1.2 s is 0.001 s and 0.006 s after 1.2 s. A sensitivity study showed, however, that the effect of choosing an overall minimum time step of 0.006 s would have only a negligible effect on the results. For the time step control the default values are used.

f) Coupling method – external or internal?

Explicit coupling, see also answer to d).

g) Coupling design – serial integration or parallel processing?

Serial integration.

IV. General

a) User assumptions?

For the benchmark calculation the same bypass density correction has been implemented in RETRAN-3D as for the PSI CORETRAN calculation and consequently also a uniform flow area ratio is assumed.

b) What are the code's limitations that affect the results?

For the core bypass heating the non-conducting heat exchanger option in RETRAN-3D is used. An effective core bypass density correction is implemented according to the benchmark specifications in RETRAN-3D as in CORETRAN, which is non-standard for both codes. The same thermal fuel and cladding properties as before in CORETRAN have been entered in RETRAN-3D using tables. An algebraic slip equation based on drift flux model of Chexal-Lellouche (recommended option) is used for the thermal-hydraulic calculation, which therefore is based on a four-equation model. The neutron void reactivity is calculated from profile fit equation.

c) Specific features of the used codes?

d) Number of solutions submitted per participant? If more than one please provide comments and brief analysis on the solutions.

For each case one solution has been submitted, see Barten (2004, 2006) for more details. The parameters for each case have been chosen consistently so that for instance Extreme Scenario 2 coincides exactly with the base case until the time of the SCRAM. Extreme Scenarios 3 and 4 also coincide with Extreme Scenario 1 until the time of the SCRAM, and Extreme Scenario 4 coincides with Extreme Scenario 3 until the SRV are initiated.

e) If your results are significantly different than the reference results, are there any explanations for these differences? Please explain each significant difference.

References

Barten, W., H. Ferroukhi, P. Coddington (2004), "Peach Bottom BWR Turbine Trip Benchmark Analyses with RETRAN-3D and CORETRAN", *Nuclear Science and Engineering*, 148, 306-324.

Barten, W., P. Coddington, H. Ferroukhi (2006), "RETRAN-3D Analysis of the Base Case and the Four Extreme Cases of the OECD/NRC Peach Bottom 2 Turbine Trip Benchmark", *Annals of Nuclear Energy*, 33, 99-118.

Hornyik, K., J.A. Naser (1979), *RETRAN Analysis of the Turbine Trip Tests at Peach Bottom Atomic Power Station Unit 2 at the End of Cycle 2*, EPRI Special Report, NP-1076-SR, EPRI, Palo Alto, California, USA.

Nuclear Energy Agency (NEA) (2001), *Boiling Water Reactor Turbine Trip (TT) Benchmark, Volume I: Final Specifications*, NEA/NSC/DOC(2001)1, OECD/NEA, Paris, June.

TRAC-M/PARCS (PSU/PURDUE/NRC, United States)

I. Thermal-hydraulic model

a) Core thermal-hydraulic (T-H) model and nodalisation (1-D, 3-D and number of channels or cells with schematic if possible). How are channels/T-H cells chosen?

3-D nodalisation for VESSEL and 1-D nodalisation for other components. As shown in Figure 1, the developed TRAC-M Peach Bottom model consists of 67 components. The reactor is modelled using the vessel component with 4 radial rings and 14 axial levels.

Figure 1: TRAC-M thermal hydraulics model for PB2 TT2

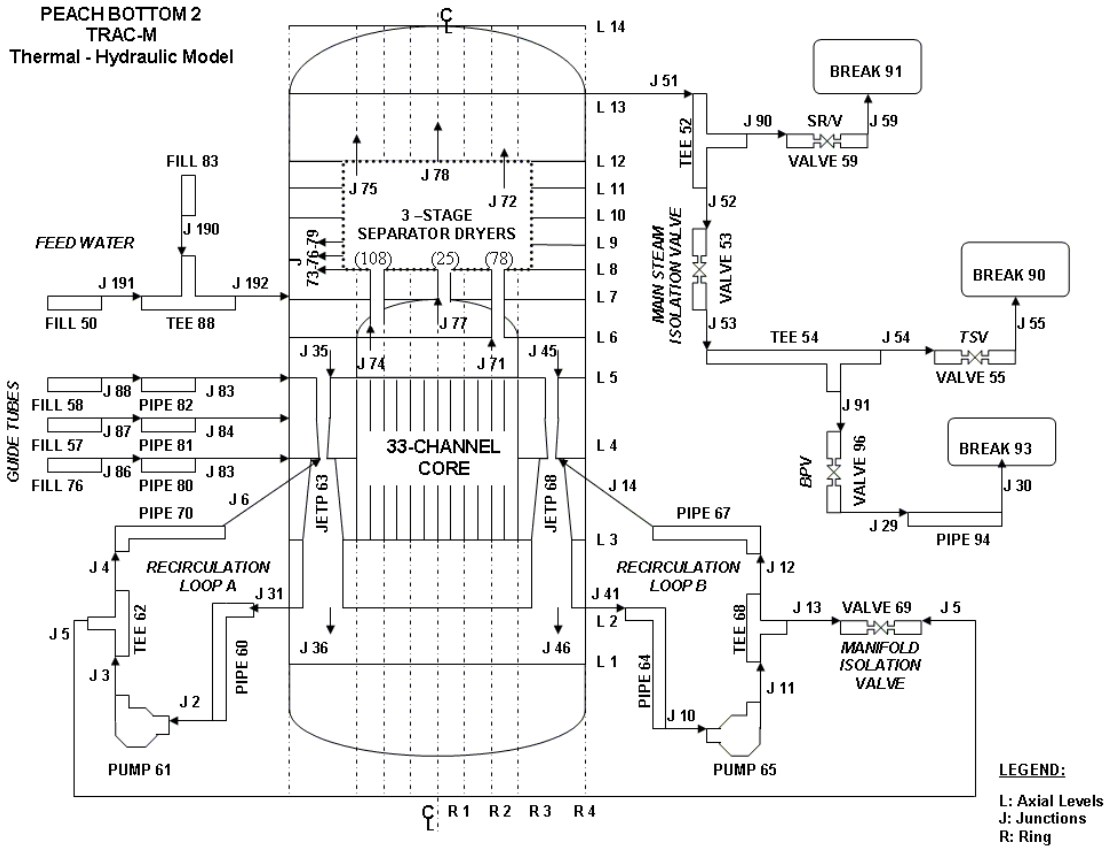

b) How core bypass flow was modelled?

No bypass channel is used. Instead of bypass channels, channel leak path flow model of TRAC-M is used for the in-channel bypass flow. Core bypass flow through the core shroud is modelled by setting orifice at the core plate.

c) Number of heat structures (fuel rods) modelled?

The 33 CHAN components provided the hydraulic simulation of the actual core channels. In addition, through the power card input settings the channels are heated and the code automatically spawns 33 heat structure associated to the channels.

d) Please provide with more detail the nodalisation of the steam line.

The steam line is modelled using 2 TEE components and 3 VALVE components. Figure 1 shows detailed nodalisation of the steam line.

e) How are the jet pumps modelled?

The reactor vessel downcomer region and jet pump component (levels 3 and 4) are modelled in Ring 4. The standard jet pump model of TRAC-M is given in Figure 2.

Figure 2: TRAC-M jet pump nodalisation

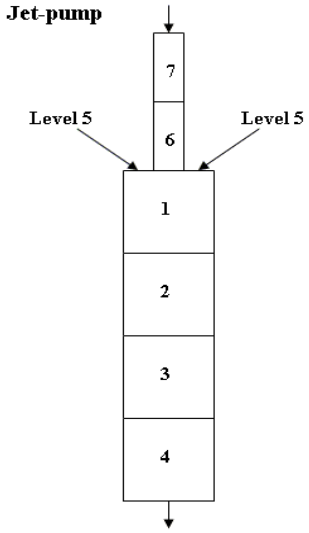

f) How are the steam separators and dryers modelled?

The vessel model uses 3 SEPD components using the TRAC-M mechanistic separator option. At mechanistic separator model, the user supplies geometric parameters that describe the physical separator. The coding that supports this option was written by General Electric Company (GE), and it assumes a design similar to that used in a GE BWR steam/water separator. A simple nodalisation diagram of separators is shown in Figure 3.

Figure 3: Separator/standpipe nodalisation

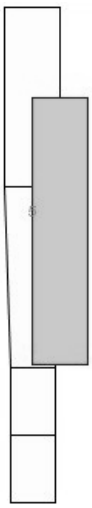

g) How are the turbine stop valves closing phenomena and steam bypass system modelled?

There four steam lines in total, and each has a flow-limiting nozzle, main steam isolation valves (MSIV), safety relief valves (SRV) and a turbine stop valve (TSV). The steam bypass system consists of nine bypass valves (BPV) mounted on a common header, which is connected to each of the four steam lines. The data and models given in the specifications were strictly applied in TRAC-M PB2 model.

h) How are the safety and relief valves modelled?

The safety relief valve (SRV) modelling plays an important role in Extreme Scenarios 1, 2 and 3. In the SRV model used here, the pressure at the first cell of TEE 52 is used as the reference pressure. This TEE represents a steam line as indicated in the nodalisation diagram of Figure 1 and its pressure is almost the same as the dome pressure. In this model, one valve simulates the relief valve group #1 (4 valves), the relief valve group #2 (4 valves), the relief valve group #3 (4 valves), and the safety valve group #4 (2 valves), respectively. Opening and closing pressure set points are modelled as specified and TRAC-M allows SRV modelling through valve component.

i) What are the difficulties encountered during the component modelling?

None.

j) Which core thermal-hydraulic initial and transient boundary conditions are used and how?

Clean steady-state initialisation is performed for stand-alone TRAC-M and coupled TRAC-M/PARCS respectively. Coupled TRAC-M/PARCS transient calculation is started after 10 s null transient to avoid transient numerical initialisation problems. No boundary conditions to the core thermal-hydraulic components are necessary as they are provided by the adjacent components.

k) Radial and axial heat structure (fuel rod) nodalisation?

9 radial rings and 24 axial nodes.

l) Used correlations for fuel properties vs. temperature?

TRAC-M correlations which are consistent with the final specifications are used.

II. Core neutronics model

a) Number of radial nodes per assembly?

The PARCS model represents each of the 764 fuel assemblies as a single neutronics node. Full core geometry is modelled for the benchmark since the core is not symmetric due to the radial burn-up distribution asymmetry.

b) Axial nodalisation?

The active core height is 365.76 cm, which is modelled in PARCS with 24 axial layers. The thickness of the axial layers is 15.24 cm.

c) Radial and axial reflector modelling?

At the top and bottom of the active core, there are 15.24 cm-thick axial reflector regions. Radial reflector region is indicated with the number "0" in Figure 4.

d) Cross-section interpolation procedure used?

Linear interpolation with regard to independent instantaneous variables. The benchmark specifications provide a cross-section library with 432 sets of cross-sections in the fuel region

and 3 sets for reflector region (bottom, top and radial reflector). The group constants for each set consist of two types of macroscopic cross-section data, one for rodded and one for unrodded fuel assemblies. In the cross-section library, the microscopic fission cross-sections are provided for the fissile material of the fission chambers, as well as the assembly detector factors, which are the ratio between the flux in the detector location and the average flux of the neutronic cell.

e) Used method to get a critical reactor at the beginning of transient?

The eigenvalue problem was solved prior to the fixed source problem.

f) How is the xenon effect modelled?

Production of microscopic Xe cross-sections from the final specifications and Xe number density (also given in the final specifications).

g) How is assembly discontinuity factor (ADF) modelled?

Values from cross-section libraries were used. Those libraries were provided by benchmark team.

h) Is bypass density correction used? If so, how it is modelled?

Yes. Methodology is consistent with the final specifications.

i) How is decay heat modelling modelled?

ANS-1979 standard.

III. Coupling schemes

a) Hydraulics/heat structure spatial mesh overlays (mapping schemes in radial and axial plane)?

One by one mapping.

b) Hydraulics/neutronics spatial mesh overlays (mapping schemes in radial and axial plane)?

Were done according to the methodology specified in the final specification. Fuel assemblies are mapped into 33 thermal-hydraulic channels as shown in Figure 4. The numbers indicate the channel assignments of the fuel assemblies and "0" corresponds to the reflector region. A thermal-hydraulic channel was not assigned to the reflector so that fixed reflector properties were used as provided in the final specifications. The reflector nodes in PARCS are not mapped to thermal-hydraulic channels since the reflector thermal-hydraulic properties are fixed.

c) Heat structure/neutronics spatial mesh overlays mapping schemes in radial and axial plane)?

Same as one applied for hydraulics/neutronics spatial mesh overlays.

d) Temporal coupling scheme?

T-H state variables of previous step were fixed.

e) Coupling numerics for steady state and transient – explicit, semi-implicit or implicit? Please also provide time step size, convergence criteria, courant number etc.

For fast steady-state initialisation, a neutronic calculation skipping strategy is used, *i.e.* PARCS calculation was done only once per every 20 time advances in TRAC-M. SETS numeric scheme is used for steady-state calculations while semi-implicit is used for the transient calculations. Maximum time step size is usually of the order of 10^{-3}during the coupled calculations.

Figure 4: Thermal-hydraulic channel mapping for PB2 TT2

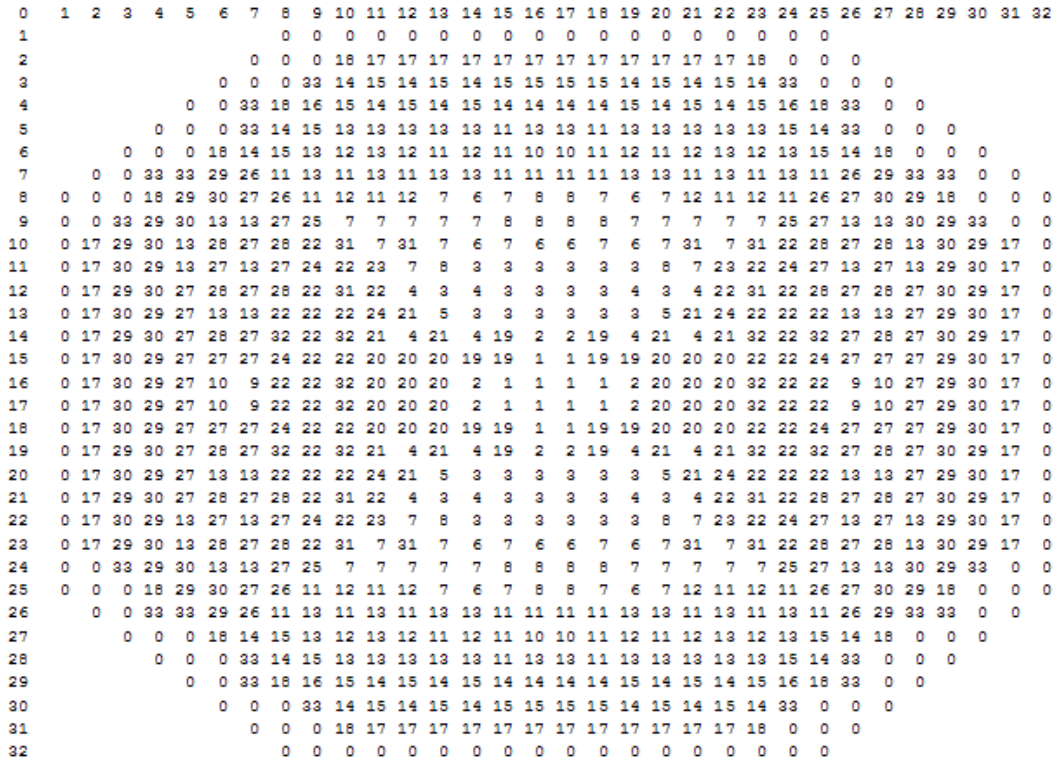

f) Coupling method – external or internal?

TRAC-M/PARCS coupling is performed using a general interface, which was implemented using parallel virtual machine (PVM). Overall controls of the coupled transient such as convergence checks and trip initiation are handled by TRAC-M.

g) Coupling design – serial integration or parallel processing?

Parallel virtual machine (PVM) is utilised for the coupling design.

IV. General

a) User assumptions?

Minor modifications were made to the GI module in order to treat the fixed reflector nodes, as well as to handle the method specified for treating the moderator bypass density correction. The feedwater mass flow equals the steam lines' mass flow rate (steady state and no control rods' water supply is considered). It was assumed that the flow area of the leak path from a channel to the core bypass of the vessel is the same for all the modelled channels.

b) What are the code's limitations that affect the results?

N/A

c) Specific features of the used codes?

General features of the codes are given in Appendix A. In particular, specific SRV option of TRAC-M VALVE component was the key issue for Extreme Scenarios 1, 2 and 3.

d) Number of solutions submitted per participant? If more than one please provide comments and brief analysis on the solutions.

One set of solution was submitted for the best-estimate case and the extreme scenarios.

e) If your results are significantly different than the reference results, are there any explanations for these differences? Please explain each significant difference.

N/A

TRAC-BF1/ENTRÉE (TEPSYS, Japan)

I. Thermal-hydraulic model

a) Core thermal-hydraulic (T-H) model and nodalisation (1-D, 3-D and number of channels or cells with schematic if possible). How are channels/T-H cells chosen?

Basically, the T-H region strategy depends on phenomena, power distribution and other core configurations. In this study, the T-H region map was specified.

b) How core bypass flow was modelled?

Flow paths are considered for the lower plenum, the bypass region and the channel (the core bypass).

c) Number of heat structures (fuel rods) modelled?

One rod for each channel.

d) Please provide with more detail the nodalisation of the steam line.

See the attached figure*.

e) How are the jet pumps modelled?

See the attached figure*.

f) How are the steam separators and dryers modelled?

See the attached figure*.

g) How are the turbine stop valves closing phenomena and steam bypass system modelled?

Closing and opening time tables are given.

h) How are the safety and relief valves modelled?

SRV upper and lower activation pressures are given.

i) What are the difficulties encountered during the component modelling?

The existent TRAC nodalisation was applied in this study. Hence, no significant difficulty was encountered.

j) Which core thermal-hydraulic initial and transient boundary conditions are used and how?

Core flow distribution was solved in TRAC/BF1. The transient core boundary conditions are also solved in this code.

k) Radial and axial heat structure (fuel rod) nodalisation?

7 radial rings and 24 axial nodes.

l) Used correlations for fuel properties vs. temperature?

Those implemented in TRAC/BF1 and other from MATPRO.

* The figure in question can be found on page 224.

II. Core neutronics model

a) Number of radial nodes per assembly?

One.

b) Axial nodalisation?

Twenty-six (24 heated nodes and 2 unheated nodes).

c) Radial and axial reflector modelling?

One node for both radial and axial reflectors.

d) Cross-section interpolation procedure used?

Given by specification.

e) Used method to get a critical reactor at the beginning of transient?

The eigenvalue problem was solved first. The result was transferred to the fixed source problem.

f) How is the xenon effect modelled?

The transient xenon concentration was given by the specification. A treatment in the cross-section was given by the specification.

g) How is assembly discontinuity factor (ADF) modelled?

It was modelled according to the method of the assembly discontinuity factor of SIMULATE3.

h) Is bypass density correction used? If so, how it is modelled?

Yes. According to the specification.

i) How is decay heat modelling modelled?

ANS-1979.

III. Coupling schemes

a) Hydraulics/heat structure spatial mesh overlays (mapping schemes in radial and axial plane)?

One fuel rod per one T-H region. 24 axial nodes are mapped to the corresponding nodes in CHAN components.

b) Hydraulics/neutronics spatial mesh overlays (mapping schemes in radial and axial plane)?

Given by the specification.

c) Heat structure/neutronics spatial mesh overlays mapping schemes in radial and axial plane)?

Same as b).

d) Temporal coupling scheme?

Explicit.

e) Coupling numerics for steady state and transient – explicit, semi-implicit or implicit? Please also provide time step size, convergence criteria, courant number etc.

Semi-implicit/Courant number = 0.999.

f) Coupling method – external or internal?

External.

g) Coupling design – serial integration or parallel processing?

Serial.

IV. General

a) User assumptions?

Ambiguous question.

b) What are the code's limitations that affect the results?

Maximum number of components is limited within 99. A numerical damping is significant.

c) Specific features of the used codes?

Two-fluid model. Three-dimensional vessel flow field.

d) Number of solutions submitted per participant? If more than one please provide comments and brief analysis on the solutions.

One reference solution per one exercise. + Several sensitivity study results were presented in the workshop.

e) If your results are significantly different than the reference results, are there any explanations for these differences? Please explain each significant difference.

The pressure wave in the steam line may be much damped in comparison with RELAP or RETRAN. This is due to the strong numerical damping effect in TRAC/BF1 solution scheme.

RELAP5/PARCS (U. PISA, Italy)

I. Thermal-hydraulic model

a) Core thermal-hydraulic (T-H) model and nodalisation (1-D, 3-D and number of channels or cells with schematic if possible). How are channels/T-H cells chosen?

The core model is based upon 1-D approach. Thirty-three (33) parallel thermal-hydraulic channels are chosen as shown in the figures below.

Figure 1: Map of the adopted 33 channels repartition into the core

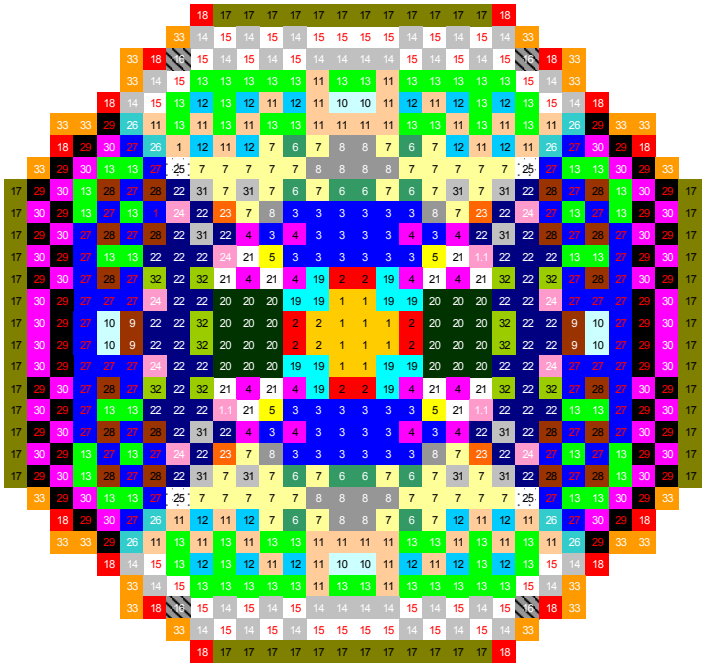

Figure 2: Thirty-three (33) channel core nodalisation for RELAP5 code

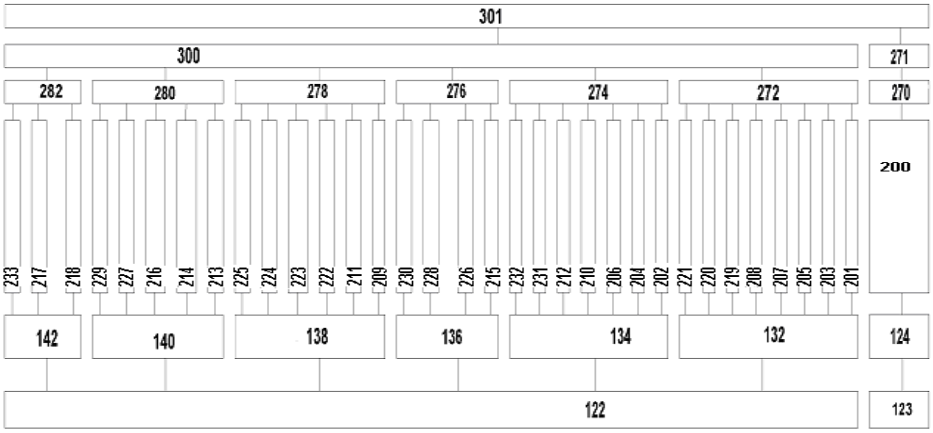

b) How core bypass flow was modelled?

The core bypass is modelled as one channel (see Figure 2) and represents the sum of the entire gap regions located between the fuel assemblies for which the associated flow is normally subcooled. The bypass is introduced as a simple core parallel flow path radially interconnected with the heated channels at the bottom and in the top core zones.

c) Number of heat structures (fuel rods) modelled?

Thirty-three (33) heated structures are used.

d) Please provide with more detail the nodalisation of the steam line.

A special care was devoted to the steam line nodalisation in order to avoid a rapid attenuation of the acoustic phenomena (water hammer) which is the predominant phenomenon of the current study. In addition to the consideration of a short time step, the node size was judiciously calculated. In the adopted nodalisation a compromise is made between these two parameters. The steam lines were modelled in such a way that most of the meshes have the same dimensions. One meter is chosen as the base mesh size, which represents nearly 1/140 of the total SL length. Furthermore, and in order to take into account the difference in the steam line lengths, 2 steam lines were modelled.

e) How are the jet pumps modelled?

The adopted model consists of lumping the 20 jet pumps into 2 equivalent ones. The jet pump model is made up of a side tube with 2 cells; the driveline and the nozzle suction. The primary tube is divided into 4 cells (throat, diffuser and discharge).

f) How are the steam separators and dryers modelled?

The three stages of the steam separator are simulated utilising a very basic model with prescribed void fraction limits for determining ideal separation functionality.

g) How are the turbine stop valves closing phenomena and steam bypass system modelled?

Linear closure and opening model is used for the turbine stop valve and the steam bypass valve, respectively.

h) How are the safety and relief valves modelled?

Three relief valves and one safety valve are considered. They open and close automatically when the pressure rises above a certain prescribed limit.

i) What are the difficulties encountered during the component modelling?

None in particular.

j) Which core thermal-hydraulic initial and transient boundary conditions are used and how?

No core boundary conditions are used.

k) Radial and axial heat structure (fuel rod) nodalisation?

Each heated channel is divided radially in 8 nodes in the fuel, 1 node for the gap and 4 nodes for the cladding. Axially, 24 nodes are considered.

l) Used correlations for fuel properties vs. temperature?

The material thermodynamic heat properties are derived through tables.

II. Core neutronics model

a) Number of radial nodes per assembly?

The core is discretised into nodes where the nuclear properties are supposed to be constant. Hence, radially, 18 fuel types are defined.

b) Axial nodalisation?

Axially, the core is subdivided into 24 axial nodes.

c) Radial and axial reflector modelling?

One radial reflector node, and one lower and one upper core nodes are considered.

d) Cross-section interpolation procedure used?

Bilinear interpolation.

e) Used method to get a critical reactor at the beginning of transient?

The criticality is obtained according to the convergence criteria of the K-effective.

f) How is the xenon effect modelled?

The xenon effect is considered implicitly in the cross-section look-up table.

g) How is assembly discontinuity factor (ADF) modelled?

The ADF are provided in the cross-section look-up table.

h) Is bypass density correction used? If so, how it is modelled?

No.

i) How is decay heat modelling modelled?

The RELAP5 ANS-79 model is used.

III. Coupling schemes

a) Hydraulics/heat structure spatial mesh overlays (mapping schemes in radial and axial plane)?

Yes.

b) Hydraulics/neutronics spatial mesh overlays (mapping schemes in radial and axial plane)?

Yes.

c) Heat structure/neutronics spatial mesh overlays mapping schemes in radial and axial plane)?

Yes.

d) Temporal coupling scheme?

Yes.

e) Coupling numerics for steady state and transient – explicit, semi-implicit or implicit? Please also provide time step size, convergence criteria, courant number etc.

Explicit coupling numerics for steady state and transient are used. The maximal time step size is 0.01 s. The convergence criteria is 0.001.

f) Coupling method – external or internal?

Internal.

g) Coupling design – serial integration or parallel processing?

Parallel processing.

IV. General

a) User assumptions?

The turbine stop valve flow area is considered to be the same as the steam line pipe flow area.

b) What are the code's limitations that affect the results?

The one-dimensional approach seems to be not very suitable to model the pressure wave reflections in the steam dome. A 3-D approach should be considered.

c) Specific features of the used codes?

Good prediction of the pressure wave propagation and amplitude in the steam lines.

d) Number of solutions submitted per participant? If more than one please provide comments and brief analysis on the solutions.

One.

e) If your results are significantly different than the reference results, are there any explanations for these differences? Please explain each significant difference.

None.

POLCA-T (Westinghouse, Sweden)

I. Thermal-hydraulic model

a) Core thermal-hydraulic (T-H) model and nodalisation (1-D, 3-D and number of channels or cells with schematic if possible). How are channels/T-H cells chosen?

3-D nodalisation with 764 T-H channels, 24 axial fuel assembly nodes and 2 nodes for bottom and top reflector in each channel. One T-H channel per fuel assembly and 122 radial reflector channels.

b) How core bypass flow was modelled?

Explicitly by one core bypass channel.

c) Number of heat structures (fuel rods) modelled?

One average fuel rod per fuel assembly.

d) Please provide with more detail the nodalisation of the steam line.

Main steam lines are modelled by steam lines, safety and relieve valves, turbine stop valves, and steam head with total of 65 nodes and 5 valves.

e) How are the jet pumps modelled?

By POLCA-T jet-pumps model, which is validated against full and 1/6 scale test facility data, the model has nodalisation similar to that used in TRAC-M calculations.

f) How are the steam separators and dryers modelled?

By POLCA-T steam separator model, which is validated against the data from Westinghouse test facility.

g) How are the turbine stop valves closing phenomena and steam bypass system modelled?

The turbine stop valve closing is modelled by signal activated by turbine pressure controller, the controller's set-point versus time table is given as a boundary condition, bypass valve position versus time is given as a boundary condition, steam bypass system model covers: the bypass chest, bypass valves, lines and orifice, and steam condenser with total of 51 nodes and 1 valve.

h) How are the safety and relief valves modelled?

Safety and relieve valves are modelled by one valve per group, *i.e.* totally by 4 valves and controlled by POLCA-T balance of plant model using in-house SAFIR code.

i) What are the difficulties encountered during the component modelling?

There were no difficulties encountered during the component design modelling. However, in order to set up the correct plant model there was a need for sensitivity study of some of the parameters, such as caryunder and caryover, the turbine stop valve closing linear or non-linear model, jet pump model to work along the M-N curve, etc.

j) Which core thermal-hydraulic initial and transient boundary conditions are used and how?

Turbine pressure controller set-point versus time, bypass valve position versus time and feedwater mass flow. All are controlled by POLCA-T balance of plant model.

k) Radial and axial heat structure (fuel rod) nodalisation?

One average fuel rod per fuel assembly has following the fuel assembly axial nodalisation, *i.e.* 24 nodes. Radially the fuel rod was modelled by 9 nodes for fuel pellet, 1 node for gas gap and 2 nodes for cladding – total 12 nodes in each fuel rod.

l) Used correlations for fuel properties vs. temperature?

Those provided in the benchmark specification.

II. Core neutronics model

a) Number of radial nodes per assembly?

One.

b) Axial nodalisation?

24 fuel nodes.

c) Radial and axial reflector modelling?

122 radial channels and 2 axial (bottom and top) reflectors.

d) Cross-section interpolation procedure used?

Standard cross-section interpolation procedure in in-house core simulator POLCA7 was used with quadratic interpolation.

e) Used method to get a critical reactor at the beginning of transient?

Not required.

f) How is the xenon effect modelled?

Equilibrium xenon has been assumed for the initial steady-state and obtained nodal xenon distribution was kept constant during the transient.

g) How is assembly discontinuity factor (ADF) modelled?

Standard ADF model used in in-house core simulator POLCA7.

h) Is bypass density correction used? If so, how it is modelled?

Yes, as provided by the benchmark specification.

i) How is decay heat modelling modelled?

By tables provided by the benchmark team/specification.

III. Coupling schemes

a) Hydraulics/heat structure spatial mesh overlays (mapping schemes in radial and axial plane)?

Each hydraulic channel that models the fuel assembly had one heat structure for the fuel rod, one for the water channels (if any are presented) and one for assembly box.

b) Hydraulics/neutronics spatial mesh overlays (mapping schemes in radial and axial plane)?

One to one mapping both in radial and axial planes.

c) *Heat structure/neutronics spatial mesh overlays mapping schemes in radial and axial plane)?*

See the answers to questions III.a) and III.b).

d) *Temporal coupling scheme?*

One T-H time step per each neutronics step, *i.e.* at each time both T-H and neutronics solutions are obtained.

e) *Coupling numerics for steady state and transient – explicit, semi-implicit or implicit? Please also provide time step size, convergence criteria, courant number etc.*

Semi-implicit second order numerics are used. Constant time step as given in the specifications – 0.006 seconds.

f) *Coupling method – external or internal?*

Internal.

g) *Coupling design – serial integration or parallel processing?*

Serial integration.

IV. General

a) *User assumptions?*

Used only those described in the benchmark specifications.

b) *What are the code's limitations that affect the results?*

None.

c) *Specific features of the used codes?*

- Description given in the input data of our core simulator POLCA7.
- POLCA-T qualified steam separator model.
- POLCA-T qualified jet pump model.
- Control rod speed and position controller.
- Scram controller.
- Jet pump drive flow controller.
- Feedwater controller.
- RPV water level controller.
- Turbine pressure controller.
- SRV controller and balance of plant SAFIR code.

d) *Number of solutions submitted per participant? If more than one please provide comments and brief analysis on the solutions.*

One (1) solution for each scenario with and without the decay heat modelling.

e) *If your results are significantly different than the reference results, are there any explanations for these differences? Please explain each significant difference.*

They are not.

OECD PUBLICATIONS, 2 rue André-Pascal, 75775 PARIS CEDEX 16
PRINTED IN FRANCE